Diplomarbeit

Construction of Discrete Surfaces, Conformal Reparametrisation, and Applications to the Gradient Flow of the Willmore Functional

Carla Cederbaum

Mathematisches Institut
Albert-Ludwigs-Universität Freiburg

Vorgelegt am 24. Juli 2006
Betreuung: Prof. Dr. E. Kuwert, Abteilung für Reine Mathematik,
Prof. Dr. G. Dziuk, Abteilung für Angewandte Mathematik,
Mathematisches Institut, Fakultät für Mathematik und Physik,
Albert-Ludwigs-Universität Freiburg im Breisgau

Name:
Rafaela Carla Deborah Cederbaum

Geboren:
23. September 1980 in Heidelberg

Anschrift:
Merzhauser Str. 8, Whg 457
79100 Freiburg

Erklärung zur Diplomarbeit

Hiermit versichere ich, dass die von mir vorgelegte Diplomarbeit mit dem Titel "Construction of Discrete Surfaces, Conformal Reparametrisation, and Applications to the Gradient Flow of the Willmore Functional"

- von mir selbstständig verfasst und andere als die von mir angegebenen Quellen und Hilfsmittel nicht benutzt wurden
- noch nicht anderweitig als Diplomarbeit eingereicht wurde.

Freiburg, der 24. Juli 2006,

_____

Carla Cederbaum

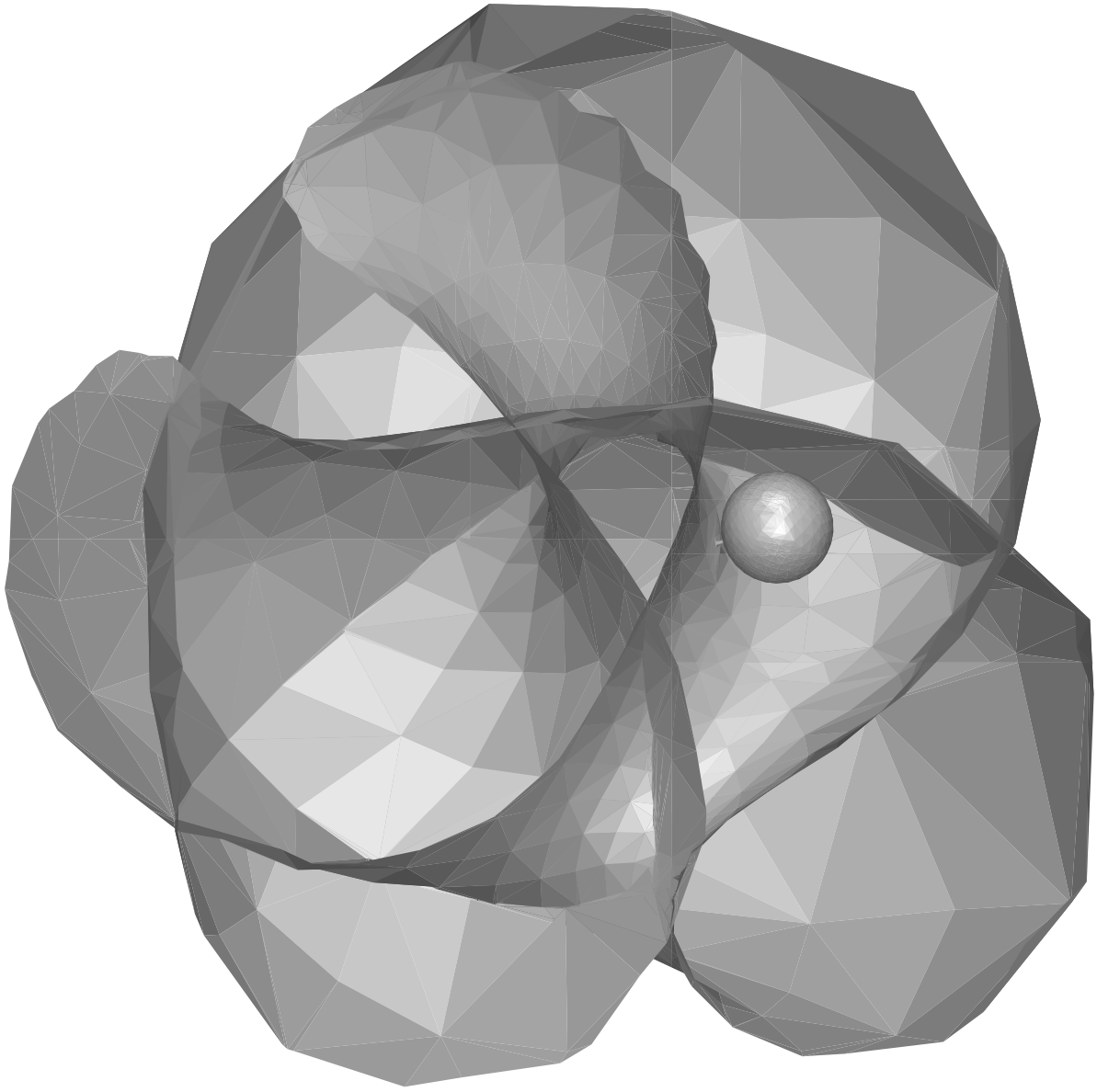

Contents

0 Introduction

The Willmore energy or elastic bending energy of a surface immersed into $\mathbb{R}^3$ is given as half of the integral over its squared mean curvature vector. It measures the deviation from local sphericity. Immersions of surfaces which are critical points of this energy have been studied since 1929[1] and are called Willmore surfaces. They are of interest in several areas such as conformal geometry[2], elastic membrane physics[3], and biology of red blood cells[4].

Since 2002, the gradient flow of the Willmore functional has been an object of active research, both theoretically[5] and numerically[6]. Most of the research has been dedicated to immersions of the sphere $\mathbb{S}^2$. In this diploma thesis, a scheme for the construction of discrete surfaces of arbitrary genera is introduced. The behaviour of these surfaces under the discretised gradient flow of the Willmore functional is studied.

The scheme we will present is based on an existence result for surfaces minimising the Willmore energy by M. Bauer and E. Kuwert[7]. Imitating the glueing procedure they use to prove this result, we construct higher genus surfaces by glueing together surfaces of lower genera. Knowing that the gradient flow of the Willmore energy converges to the round sphere if the starting point is chosen appropriately[8], we are interested in finding out to what surfaces the glued surfaces might converge.

As U. Clarenz and G. Dziuk have shown[9], the discretised gradient flow drives the mesh of a discrete surface to degeneration. They have presented an algorithm for mesh improvement relying on the existence of conformal parameters which has proven to stabilise the mesh of a spherical surface during the flow. We will study the applicability of their mesh improvement trick to glued surfaces in chapter 6. In chapter 5, we provide evidence for the existence of such global conformal parameters in a smooth setting. Our proof simplifies a proof of J. Jost[10].

I would like to thank my supervisors Prof. Dr. E. Kuwert and Prof. Dr. G. Dziuk for introducing me to this fascinating topic and for giving me advice. I would also like to

[1] cf. [Bla29].
[2] cf. [Wil91].
[3] cf. [LH92].
[4] Canham-Helfrich model, cf. [Can70, Hel73].
[5] cf. [KS02].
[6] cf. [Rus, DDE05].
[7] cf. [BK03].
[8] cf. [Sim01, KS04].
[9] cf. [CD03].
[10] cf. [Jos90].

thank Dr. C.-J. Heine, Dr. M. Fried, Dipl.-Math. S. Suhr, Dipl.-Math. Th. Albrecht, Dipl.-Math. C. Eilks and B. Link for their helpful answers to many questions may they be of mathematical or technical nature.

The code of the discretised gradient flow of the Willmore functional has been provided by G. Dziuk, M. Fried, and A. Schmidt. It is written in FORTRAN 77[11]. The digital images in this thesis have been processed with the help of the Graphics Programming Environment GRAPE[12], the sketches and flow charts have been manufactured with the aid of the Gnu Image Manipulation Program GIMP[13]. The thesis has been typeset with LaTeX.

[11] cf. [Hei91].
[12] see *www.mathematik.uni-freiburg.de/IAM/Research/grape/GENERAL/*
[13] see *www.gimp.org*

1 Mathematical Setting

In this chapter, we will briefly study the mathematical framework for the glueing construction and for conformal reparametrisation. Proofs will only be given where they are either central for understanding or refer to not very well-known facts. All notations and definitions are listed in the index. Section 1.1 introduces some notations and is based on [Alt91]. Section 1.2 gives a very concise overview over the topological notions of genus, orientability and Euler characteristic of a surface, introduces concepts from differential geometry and quotes a topological as well as a geometric variant of the surface classification theorem. These concepts are needed to describe Willmore surfaces, cf. chapter 2. Also, curvature and conformality concepts are introduced. The concept of mean curvature is needed to formulate Willmore energy, conformality is important both for the theoretic and the numerical treatment of Willmore energy as well as for the topic of conformal reparametrisation (cf. chapter 5). Section 1.2 is based on [Hir91, Lee03, Soe04, Jos91]. Section 1.3 concisely treats Sobolev spaces on manifolds based on [Wlo82].

1.1 Analysis in $\mathbb{R}^n$

Let us first of all agree on some basic notations. Let $\mathbb{N}$ denote the set of natural numbers (without 0), $\mathbb{N}_0 := \mathbb{N} \cup \{0\}$. Let $\mathbb{Z}, \mathbb{Q}, \mathbb{R}$ and $\mathbb{C}$ denote the sets of integer, rational, real, and complex numbers respectively.

Definition 1.1.1 (Euclidean $\mathbb{R}^n$). For any $n \in \mathbb{N}_0$ let $\mathbb{R}^n$ denote the n-dimensional Euclidean space. Its standard inner product will be denoted by $x \cdot y$, its norm by $|x|$ for all $x, y \in \mathbb{R}^n$. If $\Lambda \subset \mathbb{R}^n$ is any subset, let $\partial\Lambda$ denote its topological boundary, $\overline{\Lambda}$ its closure and $\operatorname{int}\Lambda$ its interior. Ω usually denotes an open subset of $\mathbb{R}^n$, in symbols $\Omega \subset_o \mathbb{R}^n$.

Definition 1.1.2 (Continuous Function Spaces C^0 and $C^{0,1}$). Let $\Omega \subset_o \mathbb{R}^n$. We say $f \in C^0(\Omega)$ if $f : \Omega \to \mathbb{R}$ is continuous. If $f : \overline{\Omega} \to \mathbb{R}$ is continuous, we say $f \in C^0(\overline{\Omega})$. Any $f \in C^0(\Omega)$ (or $C^0(\overline{\Omega})$) is said to be *Lipschitz continuous*, in symbols $f \in C^{0,1}(\Omega)$ ($C^{0,1}(\overline{\Omega})$), if there is a constant $C > 0$ such that

$$|f(x) - f(y)| \leq C|x - y| \quad \text{for all} \quad x, y \in \Omega \ (\overline{\Omega}).$$

It is said to be *Hölder continuous with exponent* $\alpha \in (0, 1)$, in symbols $f \in C^{0,\alpha}(\Omega)$ ($C^{0,\alpha}(\overline{\Omega})$), if for a constant $C > 0$

$$|f(x) - f(y)| \leq C|x - y|^\alpha \quad \text{for all} \quad x, y \in \Omega \ (\overline{\Omega}).$$

If Ω is bounded, $C^0(\overline{\Omega})$ is a Banach space if equipped with the norm

$$\|f\|_{C^0} := \sup_{x\in\overline{\Omega}}|f(x)| \quad \text{for} \quad f \in C^0(\overline{\Omega}).$$

Definition 1.1.3 (Derivatives, C^k-Spaces, $C^{k,\alpha}$-Spaces). Let $\Omega \subset_o \mathbb{R}^n$. Then $C^k(\Omega)$ denotes the space of k times continuously differentiable maps $f : \Omega \to \mathbb{R}$, $C^{k,\alpha}(\Omega)$ denotes the subspace of $C^k(\Omega)$ consisting of all maps where the highest (k-th) order derivative is Hölder-continuous for $\alpha \in (0,1)$ or Lipschitz-continuous ($\alpha = 1$). $C^\infty(\Omega) := \bigcap_{m\in\mathbb{N}} C^m(\Omega)$ is called the space of *infinitely differentiable* or *smooth maps*.

We say $f : \Omega \to \mathbb{R}$ *is of class* C^k *(*$C^{k,\alpha}$*)* if $f \in C^k(\Omega)$ ($f \in C^{k,\alpha}(\Omega)$) for $k \in \mathbb{N}_0$. If $f : \Omega \to \mathbb{R}$ is of class C^1, $\partial_i f = \nabla_i f = D_i f$ denote the partial i-th derivatives, $\operatorname{grad} f = \nabla f = df$ the gradient, and $\triangle f = \operatorname{div}\cdot\operatorname{grad} f$ the Laplacian of $f \in C^1(\Omega)$. We will frequently use all common rules for differentiation, especially the chain and product rules.

Definition 1.1.4 (Test Functions, $C_0^\infty(\Omega)$). The space $C_0^\infty(\Omega)$ contains all functions $\varphi : \Omega \to \mathbb{R}$ that are infinitely differentiable and that have compact support. This means that $\operatorname{supp}(\varphi) := \overline{\{x \in \Omega \,|\, \varphi(x) = 0\}} \subset\subset \Omega$. Functions in $C_0^\infty(\Omega)$ are called *test functions*.

Definition 1.1.5 (L^p-Spaces). A map $f : \Omega \to \mathbb{R}$, Ω being an open subset of $\mathbb{R}^n$, is called *measurable* if the pre-images of all open subsets of $\mathbb{R}$ are measurable with respect to the n-dimensional Lebesgue-measure λ^n on Ω. If, for such an f and any $p \in [1,\infty)$, the Lebesgue-integral $\int_\Omega |f(x)|^p d\lambda^n(x)$ is finite, we say $f \in \mathcal{L}^p(\Omega)$. If $p = \infty$, we say $f \in \mathcal{L}^\infty(\Omega)$ if the essential supremum $\operatorname{ess\,sup}_{x\in\Omega}|f(x)|$ is finite. We factor $\mathcal{L}^p(\Omega)$ through the equivalence relation of being identical outside a set of measure zero and get $L^p(\Omega)$. We use L^p as a shorthand for $L^p(\Omega)$ for $p \in [1,\infty]$. In the usual way, L^p-spaces are Banach spaces when equipped with the natural norms

$$\|f\|_{L^p} := \Big(\int_\Omega |f(x)|^p d\lambda^n(x)\Big)^{\frac{1}{p}} \quad \text{for} \quad p \in [1,\infty), \quad \text{and} \quad \|f\|_{L^\infty} := \operatorname{ess\,sup}_{x\in\Omega}|f(x)|.$$

$L^2(\Omega)$ is a Hilbert space with the well-known inner product

$$\langle f, g\rangle_{L^2} := \int_\Omega f(x)g(x)\, d\lambda^n(x) \quad \text{for} \quad f, g \in L^2(\Omega).$$

Definition 1.1.6 (Sobolev Spaces $H^{m,p}$). Let $\Omega \subset_o \mathbb{R}^n$, $m \in \mathbb{N}_0$, $p \in [1,\infty]$, $f \in L^p(\Omega)$, α a multi-index of length m. f is said to have a *weak partial α-th derivative* if there is a map $g_\alpha \in L^p(\Omega)$ satisfying

$$\int_\Omega \partial_\alpha \varphi f = (-1)^m \int_\Omega \varphi g_\alpha \quad \text{for all} \quad \varphi \in C_0^\infty(\Omega).$$

g_α is necessarily unique up to changes on a set of Lebesgue measure zero and is usually denoted by $\partial_\alpha f$. If f has partial weak derivatives for all multi-indices α with $|\alpha| \le m$,

we write $f \in H^{m,p}(\Omega)$. The vector $\operatorname{grad} f = (\partial_1 f, \ldots, \partial_n f)$ is called the *weak gradient of* f. We write $H^{m,p}$ as a shorthand for $H^{m,p}(\Omega)$. Again, $H^{m,p}$ is a Banach space with norm given by

$$\|f\|_{H^{m,p}} := \sum_{|\alpha|=0}^{m} \|\partial_\alpha f\|_{L^p} \quad \text{for} \quad f \in H^{m,p}(\Omega) \quad (p \in [1,\infty]).$$

$H^m := H^{m,2}$ is a Hilbert space with the inner product

$$\langle f, g\rangle_{H^m} := \sum_{|\alpha|=0}^{m} \langle \partial_\alpha f, \partial_\alpha g\rangle_{L^2} \quad \forall f, g \in H^m(\Omega).$$

Remark. The function spaces $C^0(\Omega)$, $C^k(\Omega)$, $L^p(\Omega)$, and $H^{m,p}(\Omega)$ contain real valued functions by definition. By $(C^0(\Omega))^n = C^0(\Omega, \mathbb{R}^n)$, $C^k(\Omega)^n = C^k(\Omega, \mathbb{R}^n)$ etc., we understand the spaces of all functions $f : \Omega \to \mathbb{R}^n$ that have components in $C^0(\Omega)$, $C^k(\Omega)$ etc., respectively. The norms (or inner products) on these spaces arise canonically from the norms of the $\mathbb{R}$-valued spaces.

Proposition 1.1.7 (Sobolev Chain and Product Rule). [1] *Let $\Omega \subset_o \mathbb{R}^n$ be an open subset, $m \in \mathbb{N}$, $p, q \in [1,\infty]$, $f \in H^{m,p}(\Omega)$, $g \in H^{m,q}(\Omega)$, $\frac{1}{p} + \frac{1}{q} = 1$. Then $f \cdot g \in H^{m,1}(\Omega)$ can be differentiated by the product rule. Also, if $h : \tilde{\Omega} \to \Omega$ is bijective and if h and its inverse are of class C^1 with bounded differentials, $f \in H^{1,p}(\Omega)$, then $f \circ h \in H^{1,p}(\tilde{\Omega})$ and the weak derivatives of $f \circ h$ can be calculated by the chain rule.*

Proposition 1.1.8 (Density of Smooth Functions). [2] *Let $\Omega \subset_o \mathbb{R}^n$ be an open subset, $m \in \mathbb{N}$, $p \in [1,\infty)$. Then $C^\infty \cap H^{m,p}(\Omega)$ is dense in $H^{m,p}(\Omega)$.*

Definition 1.1.9 (Boundary Values in $H^{m,p}$). We define $\mathring{H}^{m,p}(\Omega)$ as the closure of $C_0^\infty(\Omega) \subset H^{m,p}(\Omega)$ with respect to $\|.\|_{H^{m,p}}$. $f \in H^{m,p}(\Omega)$ then has *boundary values* 0 if $f \in \mathring{H}^{m,p}(\Omega)$. $f, g \in H^{m,p}(\Omega)$ *have the same boundary values* if $(f - g) \in \mathring{H}^{m,p}(\Omega)$.

Remarks. There are several different definitions of $H^{m,p}(\Omega)$ (as well as several names). If Ω has a sufficiently smooth boundary, they all agree. There are different ways of defining boundary values for maps $f \in H^{m,p}(\Omega)$, too.

We use the same notation for weak and classical derivatives. One can show that no confusion arises since, if both derivatives globally exist, they agree outside a set of Lebesgue measure zero, cf. e. g. [GT70].

[1] cf. [Alt91], pp. 109.
[2] cf. [Alt91], pp. 108.

1.2 Topology and Geometry of Surfaces

In this section, we will give some important definitions from the topology of surfaces and quote a classification theorem. We will then describe how this classification carries over to a geometrical setting.

1.2.1 Topological Surfaces

Definition 1.2.1 (Topological Surfaces). A topological second countable Hausdorff space Σ is called an *n-dimensional topological manifold* if for every $p \in \Sigma$ there is an open neighbourhood $U \subset \Sigma$ homeomorphic to an open subset $V \subset \mathbb{R}^n$. Such a homeomorphism $\varphi : U \to V$ is called a *(coordinate) chart* of Σ, $\varphi(p) = (x^1(p), \dots, x^n(p))$ are called *(local) coordinates* on U. We also write $\varphi : U \to \mathbb{R}^n$ instead of $\varphi : U \to V$. The inverse of φ is called a *local parametrisation* of U. A topological manifold of dimension 2 is called a *topological surface*. A manifold is called *closed* if it is compact. Any set $\mathcal{A} = \{\varphi : U_\varphi \to \mathbb{R}^n\}$ of charts of Σ satisfying that for every $p \in \Sigma$ there is a chart $\varphi \in \mathcal{A}$ with $p \in U_\varphi$ is called an *atlas of* Σ. An atlas $\mathcal{B}$ is said to be *subordinate* to $\mathcal{A}$ if for every chart $\varphi : U \to \mathbb{R}^2$ in $\mathcal{B}$ there exists a chart $\hat{\varphi} : V \to \mathbb{R}^2$ in $\mathcal{A}$ such that $U \subset V$ and $\varphi \equiv \hat{\varphi}|_U$.

Remarks. The dimension of Σ is uniquely determined. A topological surface is usually required to be connected. The notion of closed manifolds arises in the context of manifolds with boundaries where it describes a manifold with empty boundary that is compact. Here, as we only treat manifolds without boundaries to start with, both notions coincide. Clearly, on every closed manifold we can find a finite atlas. The standard examples of topological surfaces are the sphere $\mathbb{S}^2$, the torus $\mathbb{T}^2$, and the projective plane $\mathbb{RP}^2$.

We will later need the notion of compact charts in order to generalise Sobolev spaces to manifolds.

Definition 1.2.2 (Compact Charts and Atlases). Let Σ be a manifold. A chart $\varphi : U \to \mathbb{R}^n$ is called *compact* if there are a compact set K and an open set V satisfying $U \subset K \subset V$ and φ can be extended to V, i. e. there is a chart $\hat{\varphi} : V \to \mathbb{R}^n$ that is identical to φ on U. An atlas consisting of compact charts only is called *compact*.

Lemma 1.2.3 (Existence of Compact Atlases). *Let Σ be any closed manifold. Then there exists a finite atlas of compact charts, a compact atlas on Σ. In particular, if $\mathcal{A}$ is any finite atlas on Σ, there is a finite compact atlas subordinate to $\mathcal{A}$.*

Proof. Let $\mathcal{A} = \{\varphi_k : U_k \to \mathbb{R}^n\}_{k=1}^K$ be any finite atlas of Σ (exists by compactness). As each φ_k is a local homeomorphism into $\mathbb{R}^n$, every $p \in \Sigma$ has an open neighbourhood V_p the closure of which lies inside of some $U_{k(p)}$. By compactness of Σ, there are $p_1, \dots, p_L$ such that the set of restricted charts $\mathcal{B} := \{\varphi_{k(p_l)}|_{V_{p_l}} : V_{p_l} \to \mathbb{R}^n\}_{l=1}^L$ is an atlas of Σ. By construction, $\mathcal{B}$ is finite and compact as well as subordinate to $\mathcal{A}$. □

We will now introduce the notion of a disk in a surface. Then, we will quote the connected sum construction which allows us to formulate a theorem that classifies all closed connected topological surfaces.

Definition 1.2.4 (Disks). Let Σ be a closed connected surface. A *disk* D in Σ is a subset $D \subset U_\varphi \subset \Sigma$ of the domain U_φ of a coordinate chart φ, the image of which is the unit disk $D^2 := \{x \in \mathbb{R}^2 | \, |x| \leq 1\}$, in symbols $\varphi(D) = D^2$.

Proposition 1.2.5 (Connected Sum). *Let Σ_1, Σ_2 be closed connected surfaces, D_1, D_2 disks in Σ_1, Σ_2 respectively, $h : \partial D_1 \to \partial D_2$ a homeomorphism. Then the* connected sum of Σ_1, Σ_2, $\Sigma_1 \# \Sigma_2$, *is defined as the union $(\Sigma_1 \setminus \mathrm{int}(D_1)) \cup (\Sigma_2 \setminus \mathrm{int}(D_2))$ modulo identification via h. The connected sum is a topological surface. It is known that this surface is in fact independent (with respect to homeomorphy) of the identification homeomorphism. $\#$ is a commutative and associative binary operator on the homeomorphy classes of closed connected surfaces with unique neutral element $[\mathbb{S}^2]$.*

Theorem 1.2.6 (Topological Classification of Closed Connected Surfaces). [3] *Any closed connected surface is homeomorphic to the sphere, a (finite) connected sum of tori or a (finite) connected sum of projective planes. The number of addenda (tori or projective planes) in such a connected sum is unique. The surfaces in this list are all distinct. The* topological type *of a closed connected surface Σ is the (unique) surface in this list to which Σ is homeomorphic.*

Next, we will introduce the notions of orientability, genus, and Euler characteristic. The approach chosen here is somewhat misleading, since one would usually use these notions in the proof of 1.2.6. Also, the definitions are not easy to verify for a given surface, since its homeomorphic image in the above list has to be found out first. However, we will follow this path for simplicity. See e. g. M. Hirsch's book [Hir91] for more information.

Definition 1.2.7 (Orientable Surfaces). A closed connected surface Σ is called *orientable* if it is homeomorphic to either the sphere or a connected sum of tori. Otherwise, Σ is called *non-orientable*.

Definition 1.2.8 (Genus). To each closed connected surface Σ we assign a natural number $g(\Sigma)$, the *genus* of Σ, as follows: If Σ is homeomorphic to the sphere, $g(\Sigma) := 0$. If Σ is homeomorphic to a connected sum of n tori, then $g(\Sigma) := n$. If Σ is homeomorphic to a connected sum of n projective planes, then also $g(\Sigma) := n$.

Definition 1.2.9 (Euler Characteristic). The *Euler characteristic* $\chi(\Sigma)$ of a closed connected orientable surface is defined as $\chi(\Sigma) = 2 - 2g(\Sigma)$. It is defined as $\chi(\Sigma) = 2 - g(\Sigma)$ if Σ is non-orientable.

Remark. The Euler characteristic of a surface can be calculated directly via triangulations: It can be shown[4] that every closed connected surface Σ can be topologically triangulated,

[3] cf. [ST80, Soe04].
[4] cf. [Rad25].

which means it is homeomorphic to a simplicial complex that is a surface in its own right. If, for any triangulation, one counts the number of vertices f_0, the number of edges f_1, and the number of faces (triangles) f_2, then $\chi(\Sigma) = f_0 - f_1 + f_2$[5]. We can also calculate the genus of Σ from the Euler characteristic if we know whether it is orientable or not. Thus, we can determine the Euler characteristic very easily if we are given an oriented triangulated surface as will be shown in chapter 3. Indeed, we make use of it for a verification test in the glueing scheme.

Proposition 1.2.10 (Properties of #). *Let Σ_1, Σ_2 be closed connected surfaces. Their connected sum $\Sigma_1 \# \Sigma_2$ is orientable if and only if both Σ_1 and Σ_2 are orientable. If the surfaces are either both orientable or both non-orientable, then $g(\Sigma_1 \# \Sigma_2) = g(\Sigma_1) + g(\Sigma_2)$; if Σ_1 is non-orientable and Σ_2 is orientable we have $g(\Sigma_1 \# \Sigma_2) = g(\Sigma_1) + 2g(\Sigma_2)$, and in any case $\chi(\Sigma_1 \# \Sigma_2) = \chi(\Sigma_1) + \chi(\Sigma_2) - 2$.*

From this proposition and the classification theorem, we can derive

Corollary 1.2.11. *Two closed connected surfaces are homeomorphic if and only if they are both (non-)orientable and have the same Euler characteristic. This allows us to describe the topological type of Σ by specifying its genus or Euler characteristic and its orientability.*

1.2.2 Smooth Surfaces

In this section, we will carry over the topological notions introduced above to a differential geometry setting.

Definition 1.2.12 (C^k and $C^{k,\alpha}$-Manifolds). Let Σ be a topological manifold, let $\mathcal{A}$ be an atlas of Σ. Let $k \in \mathbb{N}$. If all *coordinate changes* $\varphi \circ \psi^{-1} : \psi(U \cap V) \to \mathbb{R}^2$ between charts $\varphi : U \to \mathbb{R}^n, \psi : V \to \mathbb{R}^n \in \mathcal{A}$ are of class C^k, we call $\mathcal{A}$ a *C^k-atlas* and $(\Sigma, \mathcal{A})$ a *C^k-manifold*. Similarly, let $k \in \mathbb{N}_0, \alpha \in (0, 1]$, and $\alpha = 1$ if $k = 0$. If all coordinate changes $\varphi \circ \psi^{-1} : \psi(U \cap V) \to \mathbb{R}^2$ between charts $\varphi : U \to \mathbb{R}^n, \psi : V \to \mathbb{R}^n \in \mathcal{A}$ are of class $C^{k,\alpha}$, we call $\mathcal{A}$ a *$C^{k,\alpha}$-atlas* and $(\Sigma, \mathcal{A})$ a *$C^{k,\alpha}$-manifold*. We usually don't mention the atlas which should be clear from context. We call two atlases *compatible* if they are of the same *regularity* C^k or $C^{k,\alpha}$ and if all coordinate changes between their respective charts are of this regularity. The union of all compatible atlases on a given manifold Σ is called its *differentiable structure*. If Σ is a surface, we call $(\Sigma, \mathcal{A})$ a *C^k- or $C^{k,\alpha}$-surface*, respectively. A manifold or surface is called *smooth* if it has a C^∞-atlas.

Let us agree on some notations for the following familiar notions. We use $T_p\Sigma$ to denote the tangent space of Σ in a point $p \in \Sigma$ and $T\Sigma$ to denote the tangent bundle. The cotangent bundle is denoted by $(T\Sigma)^*$. Let $f : \Sigma_1 \to \Sigma_2$ between differentiable manifolds Σ_1, Σ_2 (of any class) be a differentiable map defined in the usual way. Then, we denote its differential by $df : T\Sigma_1 \to T\Sigma_2$ and by $df_p : T_p\Sigma_1 \to T_{f(p)}\Sigma_2$ its differential in p. The usual rules for differentiation (chain, product rule) will be used frequently. Also, we will throughout use Einstein's summing convention wherever it seems helpful. Vector and tensor fields, local frames, pull backs etc. are defined as usual, cf. [Lee03], for example.

[5] cf. p. 139 in [ST80].

Definition 1.2.13 (Continuous Function Spaces C^k and $C^{k,\alpha}$). The function spaces $C^k(\Sigma_1, \Sigma_2)$ and $C^{k,\alpha}(\Sigma_1, \Sigma_2)$ are defined analogously to section 1.1.

Definition 1.2.14 (Immersion, Embedding). A differentiable map $f : \Sigma_1 \to \Sigma_2$ between the C^k-manifolds Σ_1, Σ_2 ($k \geq 1$) is called an *immersion* if its differential is injective at every point. An immersion $f : \Sigma_1 \to \Sigma_2$ is called an *embedding* if it is a homeomorphism onto its image $f(\Sigma_1) \subset \Sigma_2$.

We will mainly be interested in immersions (or embeddings) of surfaces into Euclidean $\mathbb{R}^3$. Next, we will now quote the geometric variant of 1.2.6:

Theorem 1.2.15 (Geometric Classification of Closed Connected Surfaces). [6] *Any closed connected smooth surface is diffeomorphic to the sphere, a (finite) connected sum of tori or a (finite) connected sum of projective planes.*

Orientation of differentiable manifolds is usually defined as follows:

Definition 1.2.16 (Orientation). [7] A vector space is called *oriented*, if we are given a specific basis to be positively oriented. A C^1-manifold is called *pointwise oriented* if we are given an orientation on each tangent space. A local frame is called *(positively) oriented* if it is a positively oriented basis at each point of its domain of definition. A pointwise oriented manifold is called *oriented* if every point lies in the domain of definition of a positively oriented frame. A manifold is called *orientable* if there exists an orientation for it, otherwise it is called *non-orientable*.

Proposition 1.2.17 (Orientation). *A closed connected C^1-surface is orientable in the sense of definition 1.2.16 if and only if it is orientable in the sense of definition 1.2.7.*

Proof. It is sufficient to show that proposition 1.2.10 remains valid for the geometric definition of orientability since it is known that both the sphere and the torus are orientable in both senses of the word whereas the projective plane is not. This can be found in [Hir91]. □

1.2.3 Surfaces and Curvature

This section intends to give the necessary background for the definition of mean curvature. As the Willmore energy is proportional to the integral over the squared mean curvature of a surface, we are getting to the heart of this chapter, here.

Definition 1.2.18 (Riemannian Metric). Let Σ be a C^1-manifold. A *(Riemannian) metric* g is a continuous symmetric positive definite 2-tensor field on the tangent bundle $T\Sigma$. The metric is called of class C^k or $C^{k,\alpha}$ for $k \in \mathbb{N}_0$ and $\alpha \in (0, 1]$, if its local representations are of this class (and the manifold is sufficiently smooth). The pairing $(T_p\Sigma, g_p)$ is a Euclidean space. We often write $\langle ., . \rangle$ instead of g_p if no confusion arises

[6] cf. chapter 9, [Hir91].
[7] cf. [Lee03], for example.

thereof. A manifold with a Riemannian metric is called a *Riemannian manifold*. A map $f : \Sigma_1 \to \Sigma_2$ between the Riemannian manifolds (Σ_1, g), $(\Sigma_2, \overline{g})$ is called *isometric* if $g_p(X,Y) = \overline{g}_{f(p)}(df_p(X), df_p(Y)) \quad \forall\, p \in \Sigma_1 \quad \forall\, X, Y \in T_p\Sigma_1$. An isometric diffeomorphism is called an *isometry*.

Remark. There also is a notion of *Riemann surfaces* in conformal geometry and a notion of *Riemannian surfaces* in the theory of complex functions. The first is going to play an implicit rôle in chapter 5 and will be defined below, the second will not appear in this text and will therefore not cause any confusion.

In the following, we will have a look at the curvature of a surface with a Riemannian metric. We will restrict ourselves to surfaces immersed in $\mathbb{R}^3$ for simplicity and since this will be the only case we need. For the rest of this section, let Σ be a C^2-surface, $f : \Sigma \to \mathbb{R}^3$ an immersion. We can define a Riemannian metric g on Σ by setting

$$g_p(X,Y) := \langle df_p X, df_p Y \rangle \quad \forall\, p \in \Sigma \quad \forall\, X, Y \in T_p\Sigma.$$

We sometimes call g the *first fundamental form of* Σ for historical reasons. The *area measure on* Σ is given by $d\mu_f = d\mu_g = \sqrt{\det g^\varphi}\, d\lambda^2 \circ \varphi$ in coordinates φ. It is clear that there exists a C^1 local unit-normal field on Σ, i. e. a C^1-section of the normal bundle $T_p\Sigma^\perp$ that has unit length everywhere in its domain of definition.

Definition 1.2.19 (Second Fundamental Form). Let $f : \Sigma \to \mathbb{R}^3$ be a C^2-immersion, $U \subset_o \Sigma$ an open subset with unit normal field $\nu : U \to (TU)^\perp$. Then the *second fundamental form of* f on U is the pointwise defined symmetric 2-tensor field

$$h_p(X,Y) := -\langle d\nu_p X, df_p Y \rangle \quad \forall\, p \in U \quad \forall\, X, Y \in T_p\Sigma.$$

One can show that h is continuous and that $h_p(X,Y) = \langle \nu(p), d^2 f(X,Y)|_p \rangle$. The sign of h depends on the choice of the normal field ν.

Remark. One could get rid of this dependency if Σ were assumed to be orientable. We could then choose a positively oriented atlas on Σ and define local unit normal fields by $\nu^\varphi = \frac{\partial_1^\varphi f \times \partial_2^\varphi f}{|\partial_1^\varphi f \times \partial_2^\varphi f|}$ for each chart φ. By positivity, these fields agree on the intersections of chart domains. As we want to include non-orientable surfaces, we will not do so. The dependency will not carry over to the Willmore energy integral, though, since we are integrating over the squared mean curvature there.

Definition 1.2.20 (Weingarten map). Let $f : \Sigma \to \mathbb{R}^3$ be a C^2-immersion, $U \subset_o \Sigma, \nu$ as above. Then we can associate a pointwise defined linear map $L_p : T_p\Sigma \to T_p\Sigma$ to the second fundamental form satisfying

$$g_p(L_p X, Y) = h_p(X,Y) \quad \forall\, p \in U \quad \forall\, X, Y \in T_p\Sigma.$$

L_p is called the *Weingarten map* of Σ in p. L also is continuous on U and its sign depends on the choice of the normal field. In addition, L_p is self-adjoint for all $p \in U$.

Definition 1.2.21 (Mean Curvature, Gaußian Curvature). Let the setting be as above. We define the *Gaußian curvature* $K_p(f)$ of Σ in $p \in U$ as the product of the (real) eigenvalues of L_p (the determinant of L_p), and the *mean curvature* $H_p(f)$ of Σ in $p \in U$ as their average (half the trace of L_p). Both curvatures $K(f), H(f)$ then are continuous on U. $K(f)$ is independent of the choice of the normal field, $H(f)$ depends on it. We also define the so-called *mean curvature vector* $\mathcal{H}(f)$ by $\mathcal{H}(f) := 2H(f)\nu$ which is independent of the choice of normal. The factor 2 is introduced for convenience.

It is possible to define the *gradient, divergence*, and *Laplacian* of a sufficiently smooth map on a differentiable surface just as in $\mathbb{R}^n$, see e. g. [Lee97]. Let grad_g denote the gradient, div_g the divergence and $\triangle_g$ the Laplace-Beltrami operator on Σ with g induced by an immersion $f : \Sigma \to \mathbb{R}^3$ of class C^2. In local coordinates, denoting by $\det(g)$ the Gram determinant of g, it is well-known that $\mathrm{grad}_g u = g^{ij}\partial_i u\, \partial_j$, $\mathrm{div}_g(X^i\partial_i) = \frac{1}{\sqrt{\det(g)}}\partial_i(X^i\sqrt{\det(g)})$ and $\triangle_g u = \frac{1}{\sqrt{\det(g)}}\partial_i(g^{ij}\sqrt{\det(g)}\,\partial_j u)$ for $u : \Sigma \to \mathbb{R}$, X a vector field on Σ, both smooth enough. We will often use the following fact.

Lemma 1.2.22. [8] *Let Σ be a C^2-surface and $f : \Sigma \to \mathbb{R}^3$ a C^2-immersion. Then*

$$\triangle_g f = \mathcal{H}(f).$$

Proof. By product rule, differentiating the identity, and the Weingarten equations[9] we get (choosing a unit normal ν and denoting the Christoffel symbols[10] of g by Γ^l_{ij})

$$\begin{aligned} \langle \triangle_g f, \partial_k f\rangle &= \partial_i g^{ij}\, g_{jk} + \frac{1}{2}g^{ij}\partial_k g_{ij} + g^{ij}\Gamma^l_{ij}g_{kl} = 0 \quad \text{and} \\ \langle \triangle_g f, \nu\rangle &= \frac{1}{\sqrt{\det(g)}}(\partial_i(g^{ij}\sqrt{\det(g)})\,\langle \partial_j f, \nu\rangle + \sqrt{\det(g)}\, g^{ij}h_{ij}) = 2H(f) \end{aligned}$$

for $k = 1, 2$ and thus the claim follows. □

Integrals of 2-forms over orientable surfaces are defined with the help of a partition of unity[11], as usual. On orientable surfaces with a Riemannian metric, we can define the integral of a continuous function $u : \Sigma \to \mathbb{R}$ by the integral of the 2-form $u\, d\mu_f$. Since the transformation laws for integrals and 2-forms possibly differ by a sign on non-oriented surfaces, we have to be more careful for those, see below. We will later need

Theorem 1.2.23 (Gauß-Bonnet). [12] *Let Σ be an oriented closed connected surface and $f : \Sigma \to \mathbb{R}^3$ a C^2-immersion. Then*

$$\int_\Sigma K(f)\, d\mu_f = 2\pi\chi(\Sigma).$$

[8] as found in [Kuw98].
[9] cf. [Lee97].
[10] cf. [Lee97].
[11] Existence and definition of partitions of unity subordinate to a given atlas can be found in J. M. Lee's book [Lee03], for example.
[12] cited from [Lee97].

If Σ is non-orientable, let $\mathcal{P} : \tilde{\Sigma} \to \Sigma$ be its orientation covering (cf. pp. 329 in [Lee03]). It is shown in the same text that $\tilde{\Sigma}$ is an oriented closed connected surface of the same regularity as Σ and that $\mathcal{P}$ is 2-sheeted. In section 2.2, we will frequently need

Lemma 1.2.24 (Lifting to Orientation Cover). *Let Σ be a non-orientable, closed, and connected surface, $f : \Sigma \to \mathbb{R}^3$ a C^2-immersion. Let $\mathcal{P} : \tilde{\Sigma} \to \Sigma$ be the orientation covering of Σ. Then $\tilde{f} := f \circ \mathcal{P}$ is an immersion of $\tilde{\Sigma}$ into $\mathbb{R}^3$. Let $\tilde{g}$, $\tilde{K}$, $\tilde{H}$, $\tilde{\mathcal{H}}$, and $\mu_{\tilde{f}}$ denote the Riemannian metric, the Gaußian curvature, the mean curvature, the mean curvature vector, and the surface measure of $\tilde{\Sigma}$ induced by $\tilde{g}$, respectively. Then*[13]

$$\tilde{g} = \mathcal{P}^* g, \quad \tilde{K} = K(f) \circ \mathcal{P}, \quad \tilde{H} = H(f) \circ \mathcal{P}, \quad \tilde{\mathcal{H}} = \mathcal{H}(f) \circ \mathcal{P}, \quad \text{and} \quad \mathcal{P}(\mu_{\tilde{f}}) = \mu_f.$$

Before we prove this lemma, we explain how, relying on it, we can define integrals over non-orientable surfaces. Let Σ be a closed, connected, and (possibly) non-orientable surface, embedded into $\mathbb{R}^3$ by $f : \Sigma \to \mathbb{R}^3$ of class C^2. let $\mathcal{P} : \tilde{\Sigma} \to \Sigma$ be its orientation covering, $\tilde{f}$ as in the lemma. If $u : \Sigma \to \mathbb{R}$ is continuous, we define $\int_\Sigma u \, d\mu_f := \frac{1}{2} \int_{\tilde{\Sigma}} u \circ \mathcal{P} \, d\mu_{\tilde{f}}$. By the factor $\frac{1}{2}$, we take into account that the orientation cover is 2-sheeted so that this definition agrees with the one given before in case Σ is orientable.[14]

Proof. The orientation covering is a local diffeomorphism (cf. p. 40 in [Lee03]), so $\tilde{f}$ is both locally injective and as regular as f, i. e. an immersion whence all geometrical properties mentioned in the lemma are well-defined. The metric $\tilde{\boldsymbol{g}}$ induced on $\tilde{\Sigma}$ by $\tilde{f}$ clearly **agrees with $\boldsymbol{\mathcal{P}^* g}$** and makes $\mathcal{P}$ a local isometry. It follows from the transformation behaviour of measures[15] and from $\det(\tilde{g}) = \det(d\mathcal{P})^2 \det(g) \circ \mathcal{P}$ that $\boldsymbol{\mathcal{P}(\mu_{\tilde{f}}) = \mu_f}$. Let $\tilde{\nu}$ be a unit normal on $\tilde{\Sigma}$. Let $\tilde{U} \subset_o \tilde{\Sigma}$ be such that $\mathcal{P}|_{\tilde{U}}$ is a diffeomorphism onto its image U. On U, let $\nu := \tilde{\nu} \circ (\mathcal{P}|_{\tilde{U}})^{-1}$. Then ν is a unit normal field on U as unit length is measured by the surrounding $\mathbb{R}^3$ and $\langle \nu, df(X) \rangle \circ \mathcal{P} = \langle \tilde{\nu}, d\tilde{f} \, (d\mathcal{P})^{-1} X|_{\mathcal{P}} \rangle \equiv 0$ for all vector fields X on Σ.

All arguments in the next paragraph are local on $\tilde{U}$. Let $\tilde{X}, \tilde{Y}$ be two arbitrary smooth vector fields on $\tilde{U}$, set $X := d\mathcal{P}\tilde{X}|_{\mathcal{P}}, Y := d\mathcal{P}\tilde{Y}|_{\mathcal{P}}$. For the second fundamental form, we get $\tilde{h}(\tilde{X}, \tilde{Y}) = \langle \tilde{\nu}, d^2\tilde{f}(\tilde{X}, \tilde{Y}) \rangle = \langle \nu \circ \mathcal{P}, d^2 f|_{\mathcal{P}}(d\mathcal{P}\tilde{X}, d\mathcal{P}\tilde{Y}) \rangle = \langle \nu, d^2 f(X, Y) \rangle|_{\mathcal{P}} = h(X, Y) \circ \mathcal{P}$ by product rule, or $\boldsymbol{\tilde{h} = \mathcal{P}^* h}$. Consequently, for the Weingarten map $\tilde{L}$, $\tilde{L} = d\mathcal{P} L (d\mathcal{P})^{-1}$. Since $d\mathcal{P}_p$ is an isometry for $p \in \tilde{\Sigma}$, or, in the language of linear algebra, an orthogonal mapping, the trace and determinant of $\tilde{L}$ and $L \circ \mathcal{P}$ agree, thus $\boldsymbol{\tilde{K} = K(f) \circ \mathcal{P}}$ and $\boldsymbol{\tilde{H} = H(f) \circ \mathcal{P}}$. Also, $\tilde{\mathcal{H}} = 2\tilde{H}\tilde{\nu} = 2(H(f) \circ \mathcal{P}) \, (\nu \circ \mathcal{P}) = \mathcal{H}(f) \circ \mathcal{P}$ on $\tilde{U}$ and since every $p \in \tilde{\Sigma}$ has a diffeomorphy neighbourhood $\tilde{U}$, the lemma is proved. □

With this technical result, we conclude the section of surfaces with Riemannian metrics. We will come back to these facts in the following chapter, where we will use them to define the Willmore energy.

[13] cf. p. 87 in [Els00] for a definition and for the notation of pushed forward measures.

[14] We could alternatively use the Riemannian measure μ_f and integrate measurable functions on Σ on both orientable and non-orientable surfaces. The result would be the same, cf. [Lee97].

[15] cf. pp. 203 in [Els00].

1.2.4 Conformal Geometry

On Riemannian manifolds, we can define angles between intersecting curves as we are given an inner product on every tangent space. We can thus generalise a fundamental notion from Euclidean geometry, namely *similarity*, where angles are preserved. We will do so by introducing the concept of *conformal maps* which take the place of similarity transformations. Conformality is important for our treatment of Willmore energy as it turns out that this energy is invariant under conformal transformations. Also, conformal maps of $\mathbb{S}^2$ will play a key rôle in chapters 5 and 6 which discuss the theoretical and numerical background for mesh improvement in the Willmore flow.

In order to shorten our notation, we give the following definition:

Definition 1.2.25 (f-Compatible Charts / Atlases). Let Σ_1, Σ_2 be closed manifolds. Set $C^0(\Sigma_1, \Sigma_2) := \{f : \Sigma_1 \to \Sigma_2 \,|\, f \text{ is continuous}\}$. Let $f \in C^0(\Sigma_1, \Sigma_2)$. We call a pair of charts $\varphi : U \to \mathbb{R}^n$ of Σ_1 and $\psi : V \to \mathbb{R}^k$ of Σ_2 *f-compatible* if $f(\overline{U}) \subset V$. We call an atlas $\mathcal{A}_1$ on Σ_1 *f-compatible* to an atlas $\mathcal{A}_2$ on Σ_2 if for any chart $\varphi \in \mathcal{A}_1$ there is a chart $\psi \in \mathcal{A}_2$ such that φ, ψ are f-compatible. In that case, we also say that $\mathcal{A}_1$ and $\mathcal{A}_2$ are *f-compatible* atlases.

Lemma 1.2.26 (Existence of f-compatible Atlases). *If Σ_1, Σ_2 are closed manifolds, $f \in C^0(\Sigma_1, \Sigma_2)$, $\mathcal{A}_1$ is any atlas on Σ_1, and $\mathcal{A}_2$ is a finite compact atlas on Σ_2, then there is a finite compact atlas on Σ_1 which is f-compatible to $\mathcal{A}_2$ and subordinate to $\mathcal{A}_1$.*

Proof. Let $\tilde{\mathcal{A}}_1$ be any finite compact atlas on Σ_1 subordinate to $\mathcal{A}_1$ (exists by lemma 1.2.3). Since f is continuous, we know that $f^{-1}(V) \subset \Sigma_1$ is open for all chart domains $V \subset \Sigma_2$. We can thus refine $\mathcal{A}_1$ such that for any $\varphi \in \mathcal{A}_1$ with domain U satisfying $U \cap f^{-1}(V) \neq \emptyset$, we restrict φ to every open set W with $\overline{W} \subset U \cap f^{-1}(V)$. As f is defined on all of Σ_1, this refinement gives an atlas on Σ_1 of the same regularity as $\mathcal{A}_1$ and f-compatible to $\mathcal{A}_2$. By compactness of Σ_1, we can find a finite sub-atlas. Also, we can further refine this atlas in order to secure its compactness by lemma 1.2.3. □

Definition 1.2.27 (Conformal Maps, Conformal Metrics). Let Σ_1, Σ_2 be Riemannian manifolds with metrics $g, \overline{g}$, respectively. A map $f : \Sigma_1 \to \Sigma_2$ is called *conformal* if there is a smooth positive function $\lambda : \Sigma_1 \to \mathbb{R}^+$ s. t.

$$g_p(X, Y) = \lambda(p)\, \overline{g}_{f(p)}(df_p(X), df_p(Y)).$$

Σ_1, Σ_2 are called *conformally equivalent* if there is a conformal diffeomorphism $f : \Sigma_1 \to \Sigma_2$. A Riemannian metric on Σ_1 is called *conformal* if all charts on Σ_1 are conformal maps with respect to g and the canonical metric on $\mathbb{R}^n$.

Remark. As announced above, a map is conformal if and only if angles are preserved. Conformality is a weaker notion than isometry where lengths are preserved as well. Also, conformality induces an equivalence relation both on the Riemannian metrics on one manifold as well as on all Riemannian manifolds of a fixed dimension.

Definition 1.2.28 (Isothermal Coordinates, Conformal Charts). [16] Let Σ be a Riemannian manifold of class C^1 with metric g. We call a chart $\varphi : U \to \mathbb{R}^n$ of Σ *conformal with respect to* g, if there is a continuous map $\rho^\varphi : U \to \mathbb{R}^+$ such that

$$g^\varphi_{ij} = \rho^\varphi \, \delta_{ij} \text{ on } U.$$

It is clear that ρ^φ is as smooth as g if g has higher regularity. We call an atlas *conformal* if it consists of conformal charts. The coordinates associated to a conformal chart are called *isothermal*.

For the following, it will be useful to know

Theorem 1.2.29 (Existence of Isothermal Coordinates). [17] *Let Σ be a smooth closed surface, g a Riemannian metric of class C^∞ on Σ. Then there exists a finite conformal atlas $\mathcal{A}$ on Σ the charts of which are of class C^∞ and compatible with the given atlas. If, additionally, Σ is orientable, then $\mathcal{A}$ can be chosen to be oriented.*

Proof. It is well-known that the Gaußian curvature is an isometry invariant and that it can be defined for any smooth surface with Riemannian metric which need not be immersed into $\mathbb{R}^3$ whatsoever, see pp. 143 in [Lee97]. Let K be the Gaußian curvature of (Σ, g), then $K : \Sigma \to \mathbb{R}$ is smooth by the same result. It is well-known that the elliptic equation

$$-\triangle_g f = K \tag{1.1}$$

locally has smooth solutions $f : U \to \mathbb{R}$.

[In fact, for each $p \in \Sigma$, we can choose an open neighbourhood $U \subset \Sigma$ so that $\overline{U}$ is contained in the domain of a chart φ of Σ and that $\varphi(U) = D$, where D is the open unit disk in $\mathbb{R}^2$. In coordinates, the equation then reads

$$-(\frac{1}{\sqrt{\det(g)}} \partial^\varphi_i(\sqrt{\det(g)} g^{ij} \partial_j f)) \circ (\varphi|_D)^{-1} = K \circ (\varphi|_D)^{-1} \text{ on } D.$$

As the differential operator of this equation is strictly elliptic by smoothness of the g_{ij} and by compactness of $\overline{U}$, Corollary 6.9 in [GT70] tells us there is a (unique) solution of the above equation (with boundary values $\equiv 0$, for example). We can deduce the existence of local solutions of the Poisson equation on Σ.]

Let thus for every $p \in \Sigma$ $f : U \to \mathbb{R}$ be a smooth solution of 1.1 on an open neighbourhood U of p. Setting $\tilde{g} := e^{2f} g|_U$, we know that $\tilde{g}$ and $g|_U$ are conformally equivalent metrics on U as $e^{2f} : U \to \mathbb{R}^+$ is smooth. From [KP88], p. 72, we deduce that

$$K + \triangle_g f = e^{2f} \tilde{K}$$

on U, where $\tilde{K} : U \to \mathbb{R}$ is the Gaußian curvature of $\tilde{g}$ and whence by 1.1 $\tilde{K} \equiv 0$. As Σ is two-dimensional, it follows[18] that the Riemannian curvature tensor of $(U, \tilde{g})$ vanishes. In

[16] The notion of isothermal coordinates goes back to C. F. Gauß in the real analytic case, cf. [Beh95,KP88].
[17] Parts of this proof have been found in [KP88].
[18] cf. lemma 8.7 in [Lee97].

consequence[19], $(U, \tilde{g})$ is *flat*, i. e. locally isometric to $\mathbb{R}^2$. We deduce that there is an open neighbourhood $V \subset U$ of p and an isometry $\varphi : (V, \tilde{g}) \to (\varphi(V) \subset \mathbb{R}^2, \delta|_{\varphi(V)})$, where δ denotes the canonical metric on $\mathbb{R}^2$. In symbols, this means

$$\varphi^*(\delta|_{\varphi(V)}) = \tilde{g}|_V = e^{2f|_V} g|_V$$

or in other words, $\varphi : V \to \mathbb{R}^2$ is a conformal chart of (Σ, g) at p compatible with the given atlas. As p was arbitrary, we have shown that a conformal atlas of (Σ, g) exists.

Let Σ additionally be oriented. Then since $(\Sigma, \tilde{g})$ is locally flat, there exists an atlas $\tilde{\mathcal{A}}$ consisting of all local isometries compatible with the given atlas. As reflections are isometries of $\mathbb{R}^2$, we can choose an oriented atlas $\mathcal{A} \subset \tilde{\mathcal{A}}$, so that all charts in $\mathcal{A}$ are conformal with respect to g. □

Finally, we define holomorphy and Riemann surfaces.

Definition 1.2.30 (Holomorphic Functions). [20] Let $U \subset_o \mathbb{C}$ be an open subset, let $f = (f^1, f^2) : U \to \mathbb{C}$. Then f is called *holomorphic*, if it is complex differentiable, i. e. if the limit $\frac{df}{dz}(z) = \lim_{h\to 0} \frac{f(z+h)-f(z)}{h}$ exists for every $z \in U$. This is equivalent to f^1, f^2 being continously differentiable on U and satisfying the *Cauchy-Riemann equations*

$$\begin{aligned} \frac{\partial f^1}{\partial x^1} &= \frac{\partial f^2}{\partial x^2} \\ \frac{\partial f^1}{\partial x^2} &= -\frac{\partial f^2}{\partial x^1}, \end{aligned} \tag{1.2}$$

in all of U, where (x^1, x^2) are the (real) coordinates in U.

Remark. Holomorphic functions with non-vanishing derivative are conformal with respect to the standard Riemannian metric on $\mathbb{C}$ and have a positive Jacobian.[21]

Definition 1.2.31 (Riemann Surface). [22] A smooth surface is called a *Riemann surface*, if it possesses a complex-valued atlas with holomorphic chart transitions.

Corollary 1.2.32. [23] *Riemann surfaces are orientable.*

Definition 1.2.33 (Holomorphic Maps, Conformal Metrics). [24] Let Σ_1, Σ_2 be Riemann surfaces, $f : U \subset_o \Sigma_1 \to \Sigma_2$ continuous. Then f is called *holomorphic* on U if its coordinate representations $\psi \circ f \circ \varphi^{-1}$ with respect to all pairs of f-compatible charts φ, ψ are holomorphic. If g is a Riemannian metric on a Riemann surface Σ, we say that g *is conformal* if all charts are conformal with respect to g. This notion of conformality agrees with the one given before.

[19] cf. theorem 7.3 in [Lee97].
[20] cf. pp. 24 in [Ahl66].
[21] cf. pp. 74 in [Ahl66].
[22] cf. p. 19 in [Jos00].
[23] cf. p. 55 in [Jos00].
[24] cf. p. 19 in [Jos00].

Corollary 1.2.34. *Holomorphic maps between Riemann surfaces with non-vanishing complex derivative (i. e. with non-vanishing Jacobian) are conformal with respect to any conformal Riemannian metrics g_1, g_2 on Σ_1, Σ_2, respectively.*

Lemma 1.2.35 (Orientable Surfaces are Riemann). *Let Σ be a smooth closed orientable surface, g a Riemannian metric of class C^∞ on Σ. Then there exists a finite atlas on Σ the charts of which are compatible with the given atlas and have holomorphic chart transitions.*

Proof. By theorem 1.2.29, there exists an oriented atlas $\mathcal{A}$ compatible with the given atlas and consisting of charts conformal with respect to g. As conformality is transitive, all chart transitions $\varphi \circ \psi^{-1} : \psi(U_\psi \cap U_\varphi) \to \mathbb{R}^2$ can be understood as orientation-preserving conformal complex-valued functions on (open subsets of) $\mathbb{C}$. By complex analysis[25], they are holomorphic.

Corollary 1.2.36. *Let g be any smooth Riemannian metric on $\mathbb{S}^2$. Then $\mathbb{S}^2$ can be given a Riemann surface structure with respect to which g is a conformal metric.*

1.3 Analysis on Surfaces

In order to introduce Finite Elements on surfaces, we will need Sobolev spaces on surfaces. We will also use these spaces in chapter 5 to prove an existence theorem for conformal diffeomorphisms. As in the Euclidean setting, we define

Definition 1.3.1 (L^p-Spaces on a Surface). Let Σ be a closed surface immersed in $\mathbb{R}^n$, let $p \in [1, \infty)$, $f : \Sigma \to \mathbb{R}$ measurable with respect to the pulled back surface measure μ on Σ. Then f is said to lie in $\mathcal{L}^p(\Sigma)$ if the integral $\int_\Sigma |f|^p \, d\mu$ is finite. If $p = \infty$, we say $f \in \mathcal{L}^\infty(\Sigma)$, if $\operatorname{ess\,sup}_\Sigma |f|$ is finite. The spaces $L^p(\Sigma)$ are obtained by factorising $\mathcal{L}^p(\Sigma)$ through the equivalence relation of identity outside a set of measure zero. We use L^p as a shorthand for $L^p(\Sigma)$. In the usual way, L^p-spaces are Banach spaces when equipped with the natural norms

$$\|f\|_{L^p} := \left(\int_\Sigma |f|^p d\mu\right)^{\frac{1}{p}} \quad \text{for} \quad p \in [1, \infty), \quad \text{and} \quad \|f\|_{L^\infty} := \operatorname{ess\,sup}_\Sigma |f|.$$

$L^2(\Sigma)$ is a Hilbert space with the well-known inner product

$$\langle f, g \rangle_{L^2} := \int_\Sigma f \, g \, d\mu \quad \text{for} \quad f, g \in L^2(\Sigma).$$

[25] cf. pp. 74 in [Ahl66].

Definition 1.3.2 (Sobolev Space H^1 on a Surface). [26] Let Σ be a closed $C^{0,1}$-surface. We call $f : \Sigma \to \mathbb{R}$ a member of $H^1(\Sigma) := H^{1,2}(\Sigma)$, if for a given partition of unity $\{\eta_i\}$ subordinate to a (finite) atlas $\{\varphi_i : U_i \to \mathbb{R}^n\}$ of Σ, all maps of the form $(f\eta_i) \circ \varphi_i^{-1} : \varphi_i(U_i) \to \mathbb{R}$ belong to $\mathring{H}^1(\varphi_i(U_i))$. This definition is independent of the particular choice of atlas (as long as it belongs to the same differentiable structure) and of the partition of unity. $H^1(\Sigma)$ becomes a Hilbert space if it is equipped with the inner product $\langle f, g\rangle_{H^1(\Sigma)} := \sum_i \langle (f\eta_i) \circ \varphi_i^{-1}, (g\eta_i) \circ \varphi_i^{-1}\rangle_{\mathring{H}^1(\mathbb{R}^2)}$ for $f, g \in H^1(\Sigma)$.

Remark. As in the Euclidean case, the function spaces $C^0(\Sigma)$, $L^p(\Sigma)$, and $H^1(\Sigma)$ contain real valued functions by definition. By $C^0(\Sigma)^n = C^0(\Sigma, \mathbb{R}^n)$, $L^p(\Sigma)^n = L^p(\Sigma, \mathbb{R}^n)$ etc., we understand the spaces of all functions $f : \Sigma \to \mathbb{R}^n$ that have components in $C^0(\Sigma)$, $L^p(\Sigma)$ etc., respectively. Also, the norms (or inner products) on these spaces arise canonically from the norms of the $\mathbb{R}$-valued spaces.

Also, if Σ satisfies "further conditions" – which $\mathbb{S}^2$ satisfies –, strong (weak) $H^1(\Sigma)$-convergence implies strong (weak) $L^2(\Sigma)$-convergence on $H^1(\Sigma) \subset L^2(\Sigma)$.

Before we proceed to define $H^1(\Sigma_1, \Sigma_2)$, we remark

Lemma 1.3.3. *We have $f \in H^1(\Sigma)$ if and only if $f \circ \varphi^{-1} \in H^1(\varphi(U_\varphi))$ for all compact charts $\varphi : U_\varphi \to \mathbb{R}^n$ of Σ.*

Proof. Let $f \in H^1(\Sigma)$. Let $\{\varphi_i : U_i \to \mathbb{R}^2\}_{i=1}^I$ be a finite compact atlas of Σ, $V_i \subset_o \Sigma$ open and such that φ_i can be extended to V_i with $\overline{U_i} \subset V_i$ (exists by lemma 1.2.3). Then the set $\mathcal{A} := \{\varphi_i : V_i \to \mathbb{R}^2\}_{i=1}^I$ is another finite atlas of Σ belonging to the same differential structure. Choose $l \in \{1, \dots, I\}$. Let $\{\eta_i^l\}$ be a partition of unity subordinate to $\mathcal{A}$ satisfying $\eta_l^l \equiv 1$ on $\overline{U}_l$. Then, by definition, $(f\eta_i^l) \circ \varphi_i^{-1} \in \mathring{H}^1(\varphi_i(V_i))$ for all i and in particular $f \circ \varphi_l^{-1} \in H^1(\varphi_l(U_l))$.

On the other hand, let $f \circ \varphi^{-1} \in H^1(\varphi(U_\varphi))$ for all compact charts $\varphi : U_\varphi \to \mathbb{R}^2$. Let $\mathcal{A} := \{\varphi_i : U_i \to \mathbb{R}^2\}_{i=1}^I$ be any finite atlas of Σ, $\{\eta_i\}$ a subordinate partition of unity. Let next $\mathcal{B} = \{\psi_k : V_k \to \mathbb{R}^2\}_{k=1}^K$ be a compact atlas subordinate to $\mathcal{A}$ with the following property $(*)$: for all $i \in \{1, \dots, I\}$ and for all $x \in U_i$, there is a $k \in \{1, \dots, K\}$ with $x \in V_k$ and $\psi_k \equiv \varphi_{i_k}|_{V_k}$ (exists by lemma 1.2.3). We have $f \circ \psi_k^{-1} \in H^1(\psi_k(V_k))$ so that $(f\eta_{i_k}) \circ (\varphi_{i_k}|_{V_k})^{-1} = (f\eta_{i_k}) \circ \psi_k^{-1} \in H^1(\psi_k(V_k))$, as well. Thus, $(f\eta_i) \circ \varphi_i^{-1} \in H^1(\varphi_i(U_i))$ by $(*)$ and finiteness of the compact atlas $\mathcal{B}$. It remains to show that the boundary values of $(f\eta_i) \circ \varphi_i^{-1}$ in $\varphi_i(U_i)$ are zero which is immediate since η_i has compact support in U_i. □

Lemma 1.3.4 (Invariance under Diffeomorphisms). *Let $\Sigma_1, \Sigma_2 \subset \mathbb{R}^n$ be closed embedded surfaces of class at least C^1, $h : \Sigma_1 \to \Sigma_2$ a diffeomorphism. Let U be a bounded open subset of $\mathbb{R}^2$, $f : U \to \Sigma_1$. Then $f \in H^1(U)^n$ if and only if $h \circ f \in H^1(U)^n$.*

Proof. It suffices to show one direction since the other one follows from h^{-1} being a diffeomorphism, too. Thus, let $f \in H^1(U)^n$, i. e. $\partial_j f \in L^2(U)^n$ for all j and $f \in L^2(U)^n$. As h is bounded by its continuity and by compactness of Σ_1, $h \circ f$ clearly lies in $L^2(U)^n$ as it is clearly measurable. By the Sobolev chain rule (see proposition 1.1.7), we can

[26] See pp. 92 [Wlo82] for more information about this definition.

deduce that $\partial_j(h \circ f)^i = (\partial_k h^i \circ f) \cdot \partial_j f^k$. In this sum, all coefficients of the derivatives of f^k consist of derivatives of h and are thus clearly measurable. Since Σ_1 is compact and h is a diffeomorphism, the coefficients lie in $L^\infty(U)^n$. Taking all together, by the Hölder inequality $\partial_j(h \circ f)$ lies in $L^2(U)^n$. As j was arbitrary, $h \circ f \in H^1(U)^n$ and we are done. □

We now proceed to define $H^1(\Sigma_1, \Sigma_2)$. The Whitney embedding theorem[27] states that any closed smooth surface can be embedded into some $\mathbb{R}^n$. We can thus assume that Σ_2 is embedded into some $\mathbb{R}^n$.

Definition 1.3.5 (Sobolev Space $H^1(\Sigma_1, \Sigma_2)$). Let Σ_1, Σ_2 be closed C^1-surfaces and $e : \Sigma_2 \to \mathbb{R}^n$ an embedding. Then a map $f : \Sigma_1 \to \Sigma_2$ is said to belong to $H^1(\Sigma_1, \Sigma_2)$ if $e \circ f$ belongs to $H^1(\Sigma_1)^n$ as defined above. This definition is independent of the chosen embedding.

Proof. Let e_1, e_2 be two embeddings of Σ_2 into $\mathbb{R}^n, \mathbb{R}^k$ respectively. Then without loss of generality $k = n$, since $\mathbb{R}^k$ is canonically embedded in $\mathbb{R}^n$ for $k \leq n$. Thus $e_1(\Sigma_2), e_2(\Sigma_2)$ are two surfaces as needed for lemma 1.3.4 and $h := e_2 \circ (e_1^{-1})|_{e_1(\Sigma_2)}$ is a diffeomorphism. Choose a finite atlas $\mathcal{A} = \{\varphi_i : U_i \to \mathbb{R}^2\}$ on Σ_1 consisting of compact charts with $\varphi_i(U_i)$ having smooth boundary (its boundedness and openness being immediate). Thus for any i, $e_1 \circ f \circ \varphi_i^{-1} \in H^1(\varphi_i(U_i))^n$ if and only if $e_2 \circ f \circ \varphi_i^{-1} = h \circ e_1 \circ f \circ \varphi_i^{-1} \in H^1(\varphi_i(U_i))^n$ by the above lemma and since $\varphi_i(U_i)$ satisfies all necessary conditions. □

Proposition 1.3.6. *Let Σ_1, Σ_2 be closed surfaces of class C^1, Σ_2 embedded in some $\mathbb{R}^n$. If $f \in C^0(\Sigma_1, \Sigma_2)$, we have $f \in H^1(\Sigma_1, \Sigma_2)$ if and only if all its compact coordinate representations $\psi \circ f \circ \varphi^{-1}$ lie in $H^1(\varphi(U_\varphi \cap f^{-1}(U_\psi)))^2$.*

Proof. Let all compact coordinate representations of f belong to H^1. Let π_2 denote the projection onto the first two components of $\mathbb{R}^n$, π_{n-2} the projection onto the last $n-2$ components. Since Σ_2 is embedded into $\mathbb{R}^n$, there is a finite atlas $\mathcal{A}_2 = \{\overline{\psi}_k : U_{\overline{\psi}_k} \to \mathbb{R}^n\}$ of $\mathbb{R}^n$ consisting of *slice charts*[28], i. e. such that the projections $\{\psi_k := \pi_2 \circ \overline{\psi}_k|_{\Sigma_2 \cap U_{\overline{\psi}_k}}\}$ constitute a compact atlas of Σ_2 and such that $\pi_{n-2} \circ \overline{\psi}_k|_{\Sigma_2 \cap U_{\overline{\psi}_k}} \equiv 0$. Set $U_{\psi_k} := \Sigma_2 \cap U_{\overline{\psi}_k}$. By possibly refining the atlas $\mathcal{A}_2$, we find a finite compact atlas $\mathcal{A}_1 = \{\varphi_k : U_k \to \mathbb{R}^2\}$ on Σ_1 satisfying $f(U_k) = U_{\psi_k}$ by continuity as in lemma 1.2.26. We have to show that $f \in H^1(\Sigma_1)^n$, or, by lemma 1.3.3, that $\overline{\psi}_k \circ f \circ \varphi_k^{-1} \in H^1(\varphi_k(U_k))^n$ for all k. By construction, we know that $\pi_2 \circ \overline{\psi}_k \circ f \circ \varphi_k^{-1} = \psi_k \circ f \circ \varphi_k^{-1} \in H^1(\varphi_k(U_k))^2$ so that the first two coordinate functions of $\overline{\psi}_k \circ f \circ \varphi_k^{-1}$ lie in $H^1(\varphi_k(U_k))$. All other coordinate functions are zero anyway, so we have shown $f \in H^1(\Sigma_1)^n$ and thus $f \in H^1(\Sigma_1, \Sigma_2)$.

Let us now suppose that $f \in H^1(\Sigma_1, \Sigma_2)$. Let $\mathcal{A}_1$ be a compact atlas of Σ_1 f-compatible to a slice chart atlas $\mathcal{A}_2$ of Σ_2 as above (exists by lemma 1.2.26). It then follows that $\psi \circ f \circ \varphi^{-1} = \pi_2 \circ \overline{\psi} \circ f \circ \varphi^{-1} \in H^1(\varphi(U))^2$ from lemma 1.3.3 whenever $\psi \in \mathcal{A}_2$ is the restriction of a chart $\overline{\psi}$ of $\mathbb{R}^n$ to Σ_2, and $\varphi : U \to \mathbb{R}^2 \in \mathcal{A}_1$ such that φ, ψ are f-compatible. We have thus got the desired result. □

[27] cf. p. 251 in [Lee03].
[28] cf. [Lee03], pp. 174.

2 Willmore Surfaces

In this chapter, we will define the Willmore energy and study some of its properties. Section 2.1 introduces some concepts from the calculus of variations which will allow us to differentiate the Willmore energy in order to find minimisers. It is based on [Str96]. In section 2.2, we will give the definition and study some properties of the energy functional. Parts of this section are based on [Wil93].

2.1 Calculus of Variations

We will need a few basic definitions from the calculus of variations, such as the notion of the first variation of a functional, of Fréchet- and Gateaux differentiability.

Definition 2.1.1 (Gateaux Differentiability). A functional $\mathcal{F} : U \to \mathbb{R}$ on a subset U of a linear space X is called *Gateaux-differentiable in $x \in U$ in the direction $\phi \in X$* if there exists $\delta > 0$ such that $x + \varepsilon\phi \in U$ for all $\varepsilon \in (-\delta, \delta)$ and the limit

$$\lim_{\varepsilon \to 0} \frac{\mathcal{F}(x + \varepsilon\phi) - \mathcal{F}(x)}{\varepsilon} =: \delta\mathcal{F}(x)\phi \tag{2.1}$$

exists. In that case, we call $\delta\mathcal{F}(x)\phi$ the *first variation of $\mathcal{F}$ in x (in direction ϕ)*. If $\mathcal{F}$ is Gateaux-differentiable in x in all directions, we just say $\mathcal{F}$ is *Gateaux-differentiable in x*. In particular, if X is equipped with a norm and $U \subset_o X$ is open with respect to the induced topology, then $\mathcal{F}$ is Gateaux-differentiable in x (in direction ϕ) if the limit in 2.1 exists.

Definition 2.1.2 (Fréchet Differentiability). A functional $\mathcal{F} : U \to \mathbb{R}$ on an open subset U of a normed space X is called *Fréchet-differentiable in $x \in U$* if there exists a continuous linear functional $\delta\mathcal{F}(x) : X \to \mathbb{R}$ satisfying

$$\lim_{\|\phi\| \to 0} \frac{\|\mathcal{F}(x + \phi) - \mathcal{F}(x) - \delta\mathcal{F}(x)\phi\|}{\|\phi\|} = 0$$

for all $\phi \in X \backslash \{0\}$. $\delta\mathcal{F}(x)$ is called the *first variation of $\mathcal{F}$ in x*. If $\mathcal{F}$ is Fréchet-differentiable on an open set $U \subset X$ and its first variation is continuous (in the dual X^*), we say that $\mathcal{F}$ is *C^1-(Fréchet-differentiable)*.

The connection between Gateaux- and Fréchet differentiability is illuminated by

Proposition 2.1.3 (Fréchet Differentiability). [1] *If a functional $\mathcal{F} : U \to \mathbb{R}$ on an open subset U of a normed space X is Gateaux-differentiable on U and its first variation is continuous with respect to x (for fixed ϕ), then $\mathcal{F}$ is C^1-Fréchet-differentiable on U.*

Definition 2.1.4 (Critical Points, Euler-Lagrange Equations). Let $\mathcal{F} : U \to \mathbb{R}$ be Fréchet-differentiable on an open subset U of a normed space X. An element $x \in U$ is called a *critical point for* $\mathcal{F}$ if the first variation of $\mathcal{F}$ vanishes in x. The equations $\delta\mathcal{F}(x) = 0$ characterising critical points of $\mathcal{F}$ in U are called its *Euler-Lagrange equations.*

2.2 Definition of Willmore Energy

In this section, we will study some properties of the Willmore energy of a surface. It is also called the *classical bending energy* of this surface and measures the deviation of a surface from the round sphere $\mathbb{S}^2$. Examples will be given at the end of this section. For the whole section, let Σ be a closed connected sufficiently smooth surface.

Definition 2.2.1 (Willmore Energy). Let $f : \Sigma \to \mathbb{R}^3$ be a C^2-immersion. The *Willmore energy of f, $\mathcal{W}(f)$*, is defined by

$$\mathcal{W}(f) := \frac{1}{2} \int_\Sigma |\mathcal{H}(f)|^2 d\mu_f.$$

We define

$$\mathcal{W}(\Sigma) := \inf\{\mathcal{W}(f) | f : \Sigma \to \mathbb{R}^3 \text{ is a } C^2 - \text{immersion}\}.$$

As discussed in section 1.2.3, in the case of a non-orientable Σ, the integral is in fact calculated on the orientation cover of Σ. As lemma 1.2.24 explains, it makes no difference whether we talk of curvatures of Σ or those of its orientation cover.

Remark. It is clear, that the Willmore energy of a given C^2-immersion is finite as the integrand is continuous and the domain of integration is compact. Conventionally, there is a factor $\frac{1}{4}$ preceding the integral. The variant used here has technical advantages in the numerical context and can be found in [Rus, DDE05], for example. Many authors also use the expression

$$\int_\Sigma (H(f)^2 - K(f))\, d\mu_f$$

as a definition of the Willmore energy. By the theorem of Gauß-Bonnet 1.2.23, this is only a constant shift of the Willmore energy as defined above and does thus not affect critical point or flow theory.

Definition 2.2.2 (Minimal Willmore Surface). A C^2-immersion $f : \Sigma \to \mathbb{R}^3$ satisfying $\mathcal{W}(f) = \mathcal{W}(\Sigma)$ is called a *minimising Willmore surface.*

[1] cf. p. 222 in [Str96].

Lemma 2.2.3 (Invariance under Reparametrisation). *The Willmore energy of a C^2-immersion $f : \Sigma \to \mathbb{R}^3$ is invariant under reparametrisation, i. e. $\mathcal{W}(f \circ \phi) = \mathcal{W}(f)$ for all C^2-diffeomorphisms $\phi : \Sigma \to \Sigma$.*

Proof. Let f, ϕ be as in the lemma, let $g := g_f$, $\tilde{g} := g_{f\circ\phi}$ be the metrics induced on Σ by the immersions f and $f \circ \phi$, respectively. Let X, Y be any pair of continuous vector fields on Σ. Then by the chain rule, $\tilde{g}_p(X, Y) = \langle d(f \circ \phi)_p X, d(f \circ \phi)_p Y\rangle = \langle df_{\phi(p)} d\phi_p X, df_{\phi(p)} d\phi_p Y\rangle = g_{\phi(p)}(d\phi_p X, d\phi_p Y)$ which shows that ϕ is an isometry of $(\Sigma, \tilde{g})$ and (Σ, g). If we denote by $\nu : U \to \mathbb{R}^3$ a local unit normal field on $U \subset_o \Sigma$, then $\tilde{\nu} : \phi^{-1}(U) \to \mathbb{R}^3$ defined by $\tilde{\nu} := \nu \circ \phi$ is a local unit normal field, too, since for any continuous vector field X on $\phi^{-1}(U)$ we have $\langle \tilde{\nu}(p), d(f \circ \phi)_p X\rangle = \langle \nu(\phi(p)), df_{\phi(p)}(d\phi_p X)\rangle = 0$. Thus, the second fundamental form of Σ with respect to the immersion $f \circ \phi$ and the unit normal $\tilde{\nu}$ is given by $\tilde{h}(\tilde{X}, \tilde{Y}) = -\langle d\tilde{\nu}\tilde{X}, d(f \circ \phi)\tilde{Y}\rangle = -\langle d\nu_\phi \cdot d\phi\tilde{X}, df_\phi \cdot d\phi\tilde{Y}\rangle = h_\phi(X, Y)$ for all continuous vector fields $\tilde{X}, \tilde{Y}$ on $\phi^{-1}(U)$ and X, Y on U given by $X := d\phi\tilde{X}$, $Y = d\phi\tilde{Y}$. Let $p \in \phi^{-1}(U)$. If κ_1, κ_2 are the mean curvatures of (Σ, g) in $\phi(p)$ and $e_1, e_2 \in T_{\phi(p)}\Sigma$ are associated unit main curvature vectors, then setting $\tilde{e}_i := (d\phi_p)^{-1} e_i$ $(i = 1, 2)$, we have $\tilde{h}_p(\tilde{e}_i, \tilde{e}_j) = h_{\phi(p)}(e_1, e_j) = \kappa_i \delta_{ij}$ and thus the mean curvatures agree in corresponding points. In consequence, $\mathcal{H}(f \circ \phi) = \mathcal{H}(f) \circ \phi$ and the Willmore energy of the immersions f and $f \circ \phi$ of Σ into $\mathbb{R}^3$ agree. □

2.3 Conformal Invariance

The Willmore energy of an immersion f is obviously invariant under isometries M of $\mathbb{R}^3$ performed after the immersion, in symbols $\mathcal{W}(f) = \mathcal{W}(M \circ f)$. In the following, we will study its behaviour under conformal transformations of $\mathbb{R}^3$.

Definition 2.3.1 (Inversion at a Sphere). The *inversion at the sphere of radius r and centre c* is the map $C : \mathbb{R}^n \setminus \{c\} \to \mathbb{R}^n \setminus \{c\} : x \mapsto c + \frac{r^2(x-c)}{|x-c|^2}$.

Inversions are conformal mappings on their domains of definition. If $f : \Sigma \to \mathbb{R}^3$ is an immersion, $c \in f(\Sigma)$, and $C : \mathbb{R}^3 \setminus \{c\} \to \mathbb{R}^3 \setminus \{c\}$ is an inversion at a sphere with centre c and any radius, the map $C \circ f : \Sigma \setminus f^{-1}(c) \to \mathbb{R}^3$ is an immersion, but its domain of definition is not closed. Here, $f^{-1}(c) := \{p \in \Sigma \,|\, f(p) = c\}$. By compactness of Σ, the pre-image of c is a finite set, so that the integral for the Willmore energy can be defined although $\Sigma \setminus f^{-1}(c)$ is not closed. We will thus speak of the Willmore energy of the immersion $C \circ f$. We will not, though, include those immersions when taking the infimum in order to calculate $\mathcal{W}(\Sigma)$.

Before we come to proving the conformal invariance of $\mathcal{W}$, we cite a theorem that characterises all conformal transformations (i. e. automorphisms) of $\mathbb{R}^3$. A *similarity transform* of $\mathbb{R}^3$ is a bijective linear map $S : \mathbb{R}^3 \to \mathbb{R}^3$ that is a composite of isometries (with respect to the canonical metric on $\mathbb{R}^3$) and of *dilations*, i. e. linear maps of the form $S = \rho\,\mathrm{Id}_{\mathbb{R}^3}$ with $\rho \in \mathbb{R}, \rho > 0$.

Theorem 2.3.2 (Liouville's Conformality Theorem). [2] *Every conformal transformation of $\mathbb{R}^3$ is a composite of similarity transforms and inversions at spheres.*

Theorem 2.3.3 (Conformal Invariance of $\mathcal{W}$). [3] *Let* $\operatorname{card} A$ *denote the cardinality of a set A. The Willmore functional $\mathcal{W}$ transforms by*

$$\mathcal{W}(C \circ f) = \mathcal{W}(f) - 8\pi \operatorname{card} f^{-1}(\{c\}) \tag{2.2}$$

if C is a conformal transformation of $\mathbb{R}^3$. In particular, if C does not contain inversions at points lying on the surface $f(\Sigma)$, the energy is invariant under C. Note that $\operatorname{card} f^{-1}(\{c\})$ *is finite by compactness of Σ.*

Proof. As stated above, we can neglect isometries. By Liouville's conformality theorem, it suffices to treat dilations and the inversion at the sphere of radius 1 with centre in the origin. We will treat these cases separately. If Σ is non-orientable, we work with its orientation covering $\mathcal{P} : \tilde{\Sigma} \to \Sigma$, where $\tilde{\Sigma}$ is a closed, connected sufficiently smooth surface in its own right, immersed in $\mathbb{R}^3$ by $f \circ \mathcal{P}$. We then get $\mathcal{W}(C \circ f) = \frac{1}{2}\mathcal{W}(C \circ f \circ \mathcal{P}) = \frac{1}{2}(\mathcal{W}(f \circ \mathcal{P}) - 8\pi \operatorname{card}(f \circ \mathcal{P})^{-1}(\{c\})) = \mathcal{W}(f) - 8\pi \operatorname{card} f^{-1}(\{c\})$ recalling that $\mathcal{P}$ is a 2-sheeted covering. So, from now on, assume additionally that Σ is oriented.

Let $C : \mathbb{R}^3 \to \mathbb{R}^3 : x \to \rho x$ be a dilation, $\rho \neq 0$, and set $\hat{f} := C \circ f$. Then $d\hat{f} = \rho\, df$, so that the metric $\hat{g}$ of $\hat{f}$ satisfies $\hat{g} = \rho^2 g$. Therefore, $d\mu_{\hat{f}} = \sqrt{\det \hat{g}}\, d\lambda^2 = \rho^2 d\mu_f$. Since the mean curvature vector $\mathcal{H}(f)$ satisfies $\mathcal{H}(f) = \triangle_g f$ (cf. 1.2.22) we get the pointwise equality

$$\mathcal{H}(\hat{f}) = \triangle_{\hat{g}} \hat{f} = \frac{1}{\sqrt{\det \hat{g}}} \sum_{i,j=1}^{2} \partial_i(\hat{g}^{ij} \sqrt{\det \hat{g}}\, \partial_j \hat{f}) = \frac{1}{\rho\sqrt{\det g}} \sum_{i,j=1}^{2} \partial_i(g^{ij}\sqrt{\det g}\partial_j f) = \frac{1}{\rho}\mathcal{H}(f),$$

where (g^{ij}) and $(\hat{g}^{ij})$ denote the inverses of (g_{ij}) and $(\hat{g}_{ij})$, respectively. Combining these results, we get

$$\mathcal{W}(C \circ f) = \frac{1}{2}\int_\Sigma |\hat{\mathcal{H}}|^2\, d\mu_{\hat{f}} = \frac{1}{2}\int_\Sigma |\frac{1}{\rho}\mathcal{H}(f)|^2\, \rho^2\, d\mu_f = \frac{1}{2}\int_\Sigma |\mathcal{H}(f)|^2\, d\mu_f = \mathcal{W}(f).$$

It remains to show that 2.2 is valid for the inversion at the sphere of radius 1 with centre in the origin. Let $C : \mathbb{R}^3 \setminus \{0\} \to \mathbb{R}^3 \setminus \{0\} : x \mapsto \frac{x}{|x|^2}$ and $\hat{f} : \Sigma \setminus f^{-1}(0) \to \mathbb{R}^3 : p \mapsto C \circ f(p)$. Then we have for all $p \in \Sigma \setminus f^{-1}(0)$ and all $X, Y \in T_p\Sigma$

$$\begin{aligned}
d\hat{f}_p X &= \frac{1}{|f(p)|^2}\left(df_p X - \frac{2}{|f(p)|^2}\langle f(p), df_p X\rangle\, f(p)\right), \quad \text{and thus} \\
\hat{g}_p(X,Y) &= \frac{1}{|f(p)|^4}\langle df_p X - \frac{2}{|f(p)|^2}\langle f(p), df_p X\rangle\, f(p), df_p Y - \frac{2}{|f(p)|^2}\langle f(p), df_p Y\rangle\, f(p)\rangle \\
&= \frac{1}{|f(p)|^4}\left(g_p(X,Y) \pm \frac{4}{|f(p)|^2}\langle f(p), df_p X\rangle\langle f(p), df_p Y\rangle\right) \\
&= \frac{1}{|f(p)|^4}\, g_p(X,Y).
\end{aligned}$$

[2] cf. pp. 232, [SY94].
[3] cf. section 7.3, [Wil93] and pp. 557, [BK03].

In consequence, $d\mu_{\hat{f}} = \frac{1}{|f(p)|^4} d\mu_f$. Let $U \subset \Sigma \setminus f^{-1}(0)$ be an open orientable subset with $f|_U$ injective, ν a unit normal field on U with respect to g. Let $\hat{\nu}(p) := |f(p)|^2 \, dC|_{f(p)} \, \nu(p)$ for all $p \in U$. Then $\hat{\nu}$ is a unit normal field on U with respect to $\hat{g}$ as by conformality of C

$$\begin{aligned}
\langle \hat{\nu}(p), \hat{\nu}(p) \rangle &= |f(p)|^4 \, \langle dC|_{f(p)} \nu(p), dC|_{f(p)} \nu(p) \rangle \\
&= \langle \nu(p) - \frac{2}{|f(p)|^2} \langle \nu(p), f(p) \rangle \, f(p), \nu(p) - \frac{2}{|f(p)|^2} \langle \nu(p), f(p) \rangle \, f(p) \rangle \\
&= |\nu(p)|^2 \pm \frac{4}{|f(p)|^2} \langle \nu(p), f(p) \rangle^2 \\
&= 1, \quad \text{and} \\
\\
\langle \hat{\nu}(p), \partial_j \hat{f}(p) \rangle &= |f(p)|^2 \, \langle dC|_{f(p)} \nu(p), \partial_j \hat{f}(p) \rangle \\
&= |f(p)|^2 \, \langle dC|_{f(p)} \nu(p), dC|_{f(p)} \, \partial_j f(p) \rangle \\
&= 0,
\end{aligned}$$

for $j = 1, 2$. Let $h, \hat{h}$ denote the second fundamental forms of $f, \hat{f}$, respectively, $(h_{ij}), (\hat{h}_{ij})$ the according matrices with respect to some chart on U. Denote by (g_{ij}) the matrix of the first fundamental form g with respect to these coordinates. We calculate

$$\begin{aligned}
\hat{h}_{ij} &= \langle \hat{\nu}, \partial_i \partial_j \hat{f} \rangle \\
&= \langle \nu - \frac{2}{|f|^2} \langle \nu, f \rangle \, f, \partial_i \partial_j \hat{f} \rangle \\
&\overset{\text{chain rule}}{=} \frac{1}{|f|^2} \langle \nu, \partial_i \partial_j f \rangle - \frac{2}{|f|^4} g_{ij} \langle \nu, f \rangle - \frac{2}{|f|^4} \langle \nu, f \rangle \langle f, \partial_i \partial_j f \rangle \\
&\quad + \frac{8}{|f|^6} \langle f, \partial_i f \rangle \langle f, \partial_j f \rangle \langle \nu, f \rangle - \frac{2}{|f|^4} \langle \nu, f \rangle \langle f, \partial_i \partial_j f \rangle \\
&\quad + \frac{8}{|f|^6} \langle \nu, f \rangle \langle f, \partial_i f \rangle \langle f, \partial_j f \rangle + \frac{4}{|f|^4} \langle \nu, f \rangle \langle f, \partial_i \partial_j f \rangle \\
&\quad - \frac{16}{|f|^6} \langle \nu, f \rangle \langle f, \partial_i f \rangle \langle f, \partial_j f \rangle \\
&= \frac{1}{|f|^2} \langle \nu, \partial_i \partial_j f \rangle - \frac{2}{|f|^4} g_{ij} \langle \nu, f \rangle \\
&= \frac{1}{|f|^2} h_{ij} - \frac{2}{|f|^4} g_{ij} \langle \nu, f \rangle \\
\Rightarrow \quad \hat{h} &= \frac{1}{|f|^2} h - \frac{2}{|f|^4} \langle \nu, f \rangle g
\end{aligned}$$

Let κ_1, κ_2 be the eigenvalues of the Weingarten map L_p of f, i. e. the main curvatures of Σ, e_1, e_2 associated unit length directions. Then by quadratic form theory

$$\begin{aligned}\hat{h}(e_i, e_j) &= \frac{1}{|f|^2} h(e_i, e_j) - \frac{2}{|f|^4}\langle \nu, f\rangle g(e_i, e_j) \\ &= \frac{1}{|f|^2}\kappa_i \delta_{ij} - \frac{2}{|f|^4}\langle \nu, f\rangle \delta_{ij}.\end{aligned}$$

We see that $\hat{h}$ is diagonalised by e_1, e_2, too, so that unit main curvature directions of $\hat{f}$, $\hat{e_1}, \hat{e_2}$, are given by $\hat{e_i} = \frac{1}{\sqrt{\hat{g}(e_i,e_i)}} e_i = |f|^2 e_i$. The main curvatures $\hat{\kappa_1}, \hat{\kappa_2}$ of $\hat{f}$ are given by $\hat{\kappa_i} = \hat{h}(\hat{e_i}, \hat{e_i}) = |f|^4 \hat{h}(e_i, e_i) = |f|^4(\frac{\kappa_i}{|f|^2} - \frac{2}{|f|^4}\langle \nu, f\rangle) = |f|^2\kappa_i - 2\langle \nu, f\rangle$. Together with the transformation of the measures (s. above), we get (on U):

$$\begin{aligned}(\frac{1}{4}|\mathcal{H}(\hat{f})|^2 - K(\hat{f}))d\mu_{\hat{f}} &= ((\frac{\hat{\kappa_1} + \hat{\kappa_2}}{2})^2 - \hat{\kappa_1}\hat{\kappa_2})d\mu_{\hat{f}} \\ &= (|f|^2\frac{\kappa_1 - \kappa_2}{2})^2 \frac{1}{|f|^4} d\mu_f \\ &= ((\frac{\kappa_1 + \kappa_2}{2})^2 - \kappa_1\kappa_2)d\mu_f \\ &= (\frac{1}{4}|\mathcal{H}(f)|^2 - K(f))d\mu_f. \qquad (2.3)\end{aligned}$$

Let us assume for a moment that $f^{-1}(0) = \emptyset$.[4] Then we can integrate the above equality on all of Σ with the aid of a partition of unity and get by the Gauß-Bonnet theorem 1.2.23

$$\begin{aligned}\mathcal{W}(C \circ f) - 4\pi\chi(C(f(\Sigma))) &= \frac{1}{2}\int_\Sigma |\mathcal{H}(C \circ f)|^2 \, d\mu_{\hat{f}} - 2\int_\Sigma K(C \circ f)\, d\mu_{\hat{f}} \\ &= 2\int_\Sigma (\frac{1}{4}|\mathcal{H}(C \circ f)|^2 - K(C \circ f))\, d\mu_{\hat{f}} \\ &= 2\int_\Sigma (\frac{1}{4}|\mathcal{H}(f)|^2 - K(f))\, d\mu_f \\ &= \mathcal{W}(f) - 4\pi\chi(f(\Sigma)).\end{aligned}$$

Since C is a diffeomorphism of $\mathbb{R}^3 \setminus \{0\}$ and the Euler characteristic is a homeomorphic invariant, we get the desired result of $\mathcal{W}(C \circ f) = \mathcal{W}(f)$. Let us now return to the more general case where $f^{-1}(0)$ need not be empty. Clearly, g and $\hat{g}$ are conformally equivalent metrics on U, hence we can apply a formula for the sectional curvatures (cf. pp. 183, [SY94]) saying $K(\hat{f})\, d\mu_{\hat{f}} = K(f)\, d\mu_f + \triangle \log|f|^2\, d\mu_f$ which allows us to transform equation 2.3 to the pointwise equality

$$\frac{1}{2}|\mathcal{H}(\hat{f})|^2\, d\mu_{\hat{f}} = \frac{1}{2}|\mathcal{H}(f)|^2\, d\mu_f + 2\triangle \log|f|^2\, d\mu_f \qquad (2.4)$$

[4] This is somehow superfluous as this special case is included in the proof given below. As it is more, maybe, classical, we include it for clarity.

on $\Sigma \setminus f^{-1}(0)$. Due to the locality of the arguments we can assume without loss of generality that Σ is oriented. We plan to apply the divergence theorem to the integral of the above equality, where the domain of integration is Σ with disk holes around the pre-images of the origin, and then let the disk radii converge to zero.

Let $p \in f^{-1}(0)$. After performing a rigid motion M_p of $\mathbb{R}^3$ (which does not change the energy), we can assume by the implicit function theorem that f is locally given as the graph of a function $u := u_p : D_R(0) \to \mathbb{R}$ on $D_R(0) = \{z \in \mathbb{R}^2 \,|\, |z| < R\}$, satisfying $u(0) = 0$ and $du(0) = 0$, in symbols $\tilde{f} := \tilde{f}_p := M_p \circ f \circ \varphi_p^{-1} : D_R(0) \to \mathbb{R}^3 : z \mapsto (z, u_p(z))$. Again, we denote by $\tilde{g} := \tilde{g}_p$ the induced metric on the disk. For $0 < r < R$ let ∂D_r denote the circle about 0 with radius r in $\mathbb{R}^2$ and let $\eta : D_R(0) \setminus \{0\} \to TD_R(0) \simeq D_R(0) \times \mathbb{R}^2$ be the outward unit normal to ∂D_r with respect to $\tilde{g}$. For simplicity, we write $\eta(x) \in \mathbb{R}^2$ instead of $\eta(x) = (x, \tilde{\eta}(x)) \in D_R(0) \times \mathbb{R}^2$ for $x \in D_R(0)$. Let $G := (\tilde{g}_{ij})$ be the matrix of $\tilde{g}$ with respect to the canonical basis of $\mathbb{R}^2$. Let $r(z) := |z|$ for $z \in D_r(0)$, $e_r := \frac{z}{r}$, $e_\theta := Re_r$ with R a rotation about $\frac{\pi}{2}$ in the Euclidean metric. Then $\eta(z) = \frac{G^{-1}e_r}{\sqrt{\langle G^{-1}e_r, e_r\rangle}}(z)$ since the right hand side is orthogonal to e_θ [$\tilde{g}(G^{-1}e_r, e_\theta) = \langle G\, G^{-1}\, e_r, e_\theta\rangle = \langle e_r, R\, e_r\rangle = 0$] and normed by

$$\begin{aligned}
\tilde{g}\Big(\frac{G^{-1}e_r}{\sqrt{\langle G^{-1}e_r, e_r\rangle}}, \frac{G^{-1}e_r}{\sqrt{\langle G^{-1}e_r, e_r\rangle}}\Big) &= \frac{1}{\langle G^{-1}e_r, e_r\rangle}\tilde{g}(G^{-1}e_r, G^{-1}e_r) \\
&= \frac{1}{\langle G^{-1}e_r, e_r\rangle}\,\langle G\, G^{-1}e_r, G^{-1}e_r\rangle \\
&= 1.
\end{aligned}$$

For the divergence theorem, we have to calculate $\operatorname{grad}_{\tilde{g}} \log|\tilde{f}|^2$ in terms of u and G:

$$\begin{aligned}
\operatorname{grad}_{\tilde{g}} \log|\tilde{f}|^2(z) &= G^{-1}\, \operatorname{grad} \log(|z|^2 + |u(z)|^2) \\
&= \frac{2}{r}\,\frac{1}{1 + \frac{|u(z)|^2}{r^2}}\, G^{-1}\,(e_r + du(z)^t\,\frac{u(z)}{r})
\end{aligned}$$

The boundary term $B_p(r)$ at the circle ∂D_r appearing in the divergence theorem can thus be evaluated by the transformation formula ($l_{\tilde{g}}$ being the induced measure on ∂D_r)

$$\begin{aligned}
B_p(r) &= \int\limits_{\partial D_r} \tilde{g}(\operatorname{grad}_{\tilde{g}} \log|\tilde{f}|^2, \eta)(z)\, dl_{\tilde{g}}(z) \\
&= \int\limits_{\mathbb{S}^1} \tilde{g}(\operatorname{grad}_{\tilde{g}} \log|\tilde{f}|^2, \eta)(r\theta)\, \sqrt{\langle Ge_\theta, e_\theta\rangle}(r\theta)\, r d\theta \\
&= r\int\limits_{\mathbb{S}^1} \langle G \operatorname{grad}_{\tilde{g}} \log|\tilde{f}|^2, \eta\rangle(r\theta)\, \sqrt{\langle Ge_\theta, e_\theta\rangle}(r\theta)\, d\theta \\
&= 2\int\limits_{\mathbb{S}^1} \frac{1}{1 + \frac{|u(r\theta)|^2}{r^2}} \sqrt{\frac{\langle Ge_\theta, e_\theta\rangle}{\langle G^{-1}e_r, e_r\rangle}}(r\theta)\, \langle e_r + du^t\frac{u}{r}, G^{-1}e_r\rangle(r\theta)\, d\theta
\end{aligned}$$

Letting r tend to zero, we get (remembering $u(0) = du(0) = 0$, d^2u bounded)

$$\begin{aligned} |u(r\theta)|^2 &= |u(0)|^2 + 2\langle \partial_r u(0), u(0)\rangle r + \langle \partial_r^2 u(\xi\theta), u(\xi\theta)\rangle r^2 + \langle \partial_r u(\xi\theta), \partial_r u(\xi\theta)\rangle r^2 \\ &= r^2(\langle \partial_r^2 u(\xi\theta), u(\xi\theta)\rangle + \langle \partial_r u(\xi\theta), \partial_r u(\xi\theta)\rangle) \end{aligned}$$

with $\xi \in (0, r)$ by Taylor's theorem, so that the first factor in the integral tends to 1. Also, setting $\Gamma(t) := \mathrm{Id} + t\, du^t\, du$ for $t \in [0, 1]$, we know that the eigenvalues of $\Gamma^{-1}(t)$ are bounded above by 1. We can deduce with the main theorem of calculus and the chain rule that

$$\begin{aligned} |G^{-1} - \mathrm{Id}| &= |\int_0^1 \frac{d}{dt}\Gamma(t)^{-1}\, dt| \\ &= |\int_0^1 \Gamma(t)^{-1}\, \frac{d}{dt}\Gamma(t)\, \Gamma(t)^{-1}\, dt| \\ &\leq \int_0^1 |\Gamma(t)^{-1}|^2\, |du^t\, du|\, dt \\ &\leq |du|^2 \end{aligned}$$

whence $G(r\theta)$ and $G(r\theta)^{-1}$ uniformly tend to the identity as $r \to 0$ which cares for the second factor in $B_p(r)$. Then, by Cauchy-Schwarz's and by the triangle inequality, we get $|\langle du^t\, u, G^{-1}e_r\rangle| \leq |du|\, |u|\, |G^{-1}| \leq |du|\, |u|$. We conclude (using again $u(0) = du(0) = 0$)

$$\lim_{r\to 0} B(r) = \int_{\mathbb{S}^1} 2\, d\theta + \lim_{r\to 0} \int_{\mathbb{S}^1} \frac{2}{r}\langle du^t\, u, G^{-1}e_r\rangle(r\theta)\, d\theta = 4\pi.$$

Integrating equation 2.4 on $\Sigma_r := \Sigma \setminus \cup_{p\in f^{-1}(0)}\varphi_p(D_r(0))$ and using, as announced, the divergence theorem, we get

$$\mathcal{W}(C \circ f|_{\Sigma_r}) = \mathcal{W}(f|_{\Sigma_r}) - 2\sum_{p\in f^{-1}(0)} B_p(r)$$

and in the limit $r \to 0$

$$\mathcal{W}(C \circ f) = \mathcal{W}(f) - 2\sum_{p\in f^{-1}(0)} 4\pi = \mathcal{W}(f) - 8\pi\, \mathrm{card}(f^{-1}(0)).$$

□

The conformal invariance of the Willmore energy guarantees that a conformal image of a minimising Willmore surface is a minimising Willmore surface (as long as it is a C^2-immersion into $\mathbb{R}^3$). We can thus not expect to find unique minimising Willmore surfaces. Also, if we were interested in minimising sequences or in flows, we would have to secure the fixation of some normalisation parameters in order to get a chance of proving convergence. This will play a rôle in chapters 4 and 6.

M. Bauer and E. Kuwert([BK03]) take advantage of the reduction of the Willmore energy coming from the inversion at a sphere with centre on the surface when constructing higher genus minimising Willmore surfaces via a connected sum construction where one of the addends is inverted, cf. chapter 3.

2.4 Euler-Lagrange Equations

In the previous section, we have defined minimising Willmore surfaces. We would now like to define general Willmore surfaces as critical points of $\mathcal{W}$. The aim of this section is to prove the Fréchet-differentiability of $\mathcal{W}$, to calculate its first variation, and to characterise Willmore surfaces by the associated fourth order Euler-Lagrange equations. We will later describe how discrete Willmore surfaces can be constructed based on the notions introduced here, cf. chapter 3.

Theorem 2.4.1. [5] *Let Σ be a closed connected smooth surface. The Willmore functional $\mathcal{W}$ is C^1-Fréchet-differentiable on the open set $\{f \in C^4(\Sigma, \mathbb{R}^3) \,|\, f \text{ is an immersion}\}$. Its first variation is given by*

$$\delta\,\mathcal{W}(f)\phi = 2\int_\Sigma \left[\triangle_g H(f) + 2H(f)(H(f)^2 - K(f))\right] \langle \phi, \nu\rangle \, d\mu_f,$$

for all $\phi \in C^4(\Sigma, \mathbb{R}^3)$ with respect to any unit normal field[6] ν. $H(f)$ is the scalar mean curvature of f defined by $H(f) = \frac{1}{2}\langle \mathcal{H}(f), \nu\rangle$.

$f \in C^4(\Sigma, \mathbb{R}^3)$ is needed since $\mathcal{H}(f)$ already involves second order derivatives. Since Fréchet-differentiability is defined on normed spaces, we have to specify the norm on $C^4(\Sigma, \mathbb{R}^3)$ we are working with. As we will see, the specific norm does not play a key rôle in the proof of Fréchet-differentiability. We could, for example, choose $\|\cdot\|_{C^4}$. However, if we want to secure the C^1-differentiability of $\mathcal{W}$, it is crucial to use the C^4-norm in order to ensure that all the appearing curvature notions and the Laplace-Beltrami of the mean curvature are continuous. We could also use $H^{4,2}$ as the normed space where we test Fréchet-differentiability (with its natural norm). As in two dimensions this space (locally) embeds in C^2, cf. e. g. [Alt91, Wlo82], we would be able to derive a weak formulation. This would probably be more natural but lies beyond the scope of this text.

Proof. Again, if Σ is non-orientable, we work on its orientation cover. Lemma 1.2.24 and the definition preceding the lemma secure the carrying over of the result to Σ. Let us thus from now on assume that Σ is orientable. Let ν be a global unit normal field on Σ.

We will use proposition 2.1.3 and thus first check Gateaux-differentiability of $\mathcal{W}$. Let $U := \{f \in C^4(\Sigma, \mathbb{R}^3) \,|\, f \text{ is an immersion}\} \subset C^4(\Sigma, \mathbb{R}^3)$. Then U is open with respect to $\|.\|_{C^4}$ by the following argument showing that its complement in $C^4(\Sigma, \mathbb{R}^3)$ is closed.

[5] Parts of this proof originate in [Wil93].

[6] If Σ is non-orientable, we work on its orientation cover.

Suppose there was a sequence $(f_n)_{n\in\mathbb{N}}$ of $C^4(\Sigma,\mathbb{R}^3)$-mappings that are not immersions with limit $f \in U$. Let g be the Riemannian metric on Σ induced by f. Then there exist $p_n \in \Sigma$ and $X_n \in T_{p_n}\Sigma$ with $g_{p_n}(X_n, X_n) = 1$ that satisfy $df_{p_n}X_n = 0$. Since Σ is compact, the sequence $(p_n)_{n\in\mathbb{N}}$ converges to $p \in \Sigma$ without loss of generality and in particular, for every neighbourhood V of p in Σ there is a number n_V with $p_n \in V$ for all $n \geq n_V$. Let now (E_1, E_2) be a g-orthonormal frame on some neighbourhood V of p (cf. p. 24 in [Lee97] for definition and existence of orthonormal frames.), w. l. o. g. $n_V = 1$. As X_n has unit norm, it can be written as $X_n = \cos\alpha_n E_1(p_n) + \sin\alpha_n E_2(p_n)$ for all n, where $\alpha_n \in \mathbb{R}$. Let $X_n \in C^\infty(V)$ be the unit norm vector field given by $X_n(q) := \cos\alpha_n E_1(q) + \sin\alpha_n E_2(q)$ for all $q \in V$. Then $(X_n(p))_{n\in\mathbb{N}}$ is a bounded sequence in $(T_p\Sigma, g_p)$ and thus w. l. o. g. converges to a vector $X \in T_p\Sigma$ with $g_p(X, X) = 1$. Extend $X =: \cos\alpha E_1(p) + \sin\alpha E_2(p)$, $\alpha \in \mathbb{R}$, to a smooth vector field $X(q) := \cos\alpha E_1(q) + \sin\alpha E_2(q)$ on V. Then $Y := dfX : V \to T\mathbb{R}^3$ is a continuous vector field. Using $\|.\|_{g_q}$ as a symbol for the matrix norm on $T_q\Sigma$ induced by g_q and $|.|_{g_q}$ for the g_q-norm on $T_q\Sigma$, we have by linear algebra and by the triangle inequality

$$\begin{aligned} |df_pX| &\leq |df_pX(p) - df_{p_n}X(p_n)| + |df_{p_n}X(p_n) - df_{p_n}X_n(p_n)| + |df_{p_n}X_n - (df_n)_{p_n}X_n| \\ &\leq |Y(p) - Y(p_n)| + \|df_{p_n}\|_{g_p}|X(p_n) - X_n(p_n)|_{g_{p_n}} + \|df_{p_n} - (df_n)_{p_n}\|_{g_{p_n}}|X_n|_{g_{p_n}}. \end{aligned}$$

By continuity of Y, the first addend converges to zero. By C^4-convergence of (f_n), $\|df_{p_n}\|_{g_p}$ is bounded and $\|df_{p_n} - (df_n)_{p_n}\|_{g_{p_n}}$ converges to zero as $p_n \to p$. $|X_n|_{g_{p_n}} = 1$ is valid by construction, so the last addend vanishes, too. $|X(p_n) - X_n(p_n)|_{g_{p_n}} = |X(p) - X_n(p)|_{g_p} \to 0$ whence the right hand side of the above inequality converges to zero as $n \to \infty$. Thus, $df_pX = 0$ and f cannot be an immersion. We conclude that $\boldsymbol{U}$ **is open in** $\boldsymbol{C^4(\Sigma,\mathbb{R}^3)}$.

Let $\phi \in C^4(\Sigma,\mathbb{R}^3)$. We can globally write $\phi = \phi^\perp + \phi^T$ with $\phi^T \in df(T\Sigma)$, $\phi^\perp = \langle\phi,\nu\rangle\,\nu$. We will use $\delta := \frac{d}{d\varepsilon}|_{\varepsilon=0}$ as a shorthand and simplify our terms by Einstein's summing convention. By definition, we have $\delta\,\mathcal{W}(f)\phi = \frac{d}{d\varepsilon}\mathcal{W}(f+\varepsilon\phi)|_{\varepsilon=0}$ if this limit exists. By the implicit function theorem, we can locally write $\phi^T = df(X)$ with $X = X^l\partial_l$ a smooth vector field. We can choose a compact, orientable atlas $\{\psi_k : U_k \to \mathbb{R}^2\}_{k=1}^K$ satisfying $\phi^T = df(X_k)$ on U_k by lemma 1.2.3 with $X_k \in C^\infty(TU_k)$. Then $\phi = \phi^\perp + df(X_k)$ on U_k. Let $\{\eta_k\}$ be a partition of unity subordinate to $\{\psi_k\}$. We use the suggestive notation $.(\varepsilon)$ to mean $.(f+\varepsilon\phi)$. First of all, we discuss whether integration and differentiation can be interchanged. We have

$$\mathcal{W}(\varepsilon) = \sum_{k=1}^{K} \int_{\psi_k(U_k)} (\eta_k\,|\mathcal{H}(\varepsilon)|^2\,\sqrt{\det(g^{\psi_k}(\varepsilon))}) \circ \psi_k^{-1}\,d\lambda^2 \tag{2.5}$$

and use $\alpha_k(\varepsilon, x) := (\eta_k\,|\mathcal{H}(\varepsilon)|^2\,\sqrt{\det(g^{\psi_k}(\varepsilon))}) \circ \psi_k^{-1}(x)$ as a shorthand for the integrand, so that $\alpha_k : (-\rho,\rho)\times\psi_k(U_k) \to \mathbb{R}$ for all $k \in \{1,\dots K\}$, ρ being so small that $f \pm \varepsilon\phi \in U$ for all $\varepsilon \in (-\rho,\rho)$ (such a ρ exists by openness of U). For convenience, we will only explicitly refer to the k-dependency where it seems necessary. By a theorem on interchanging integration and differentiation, cf. [Els00], p. 147, we are allowed to do so if $\alpha(\varepsilon,\cdot) \in L^1(\psi(U))$ for all ε small enough [which is clear since α is continuous and the domain of integration can be extended to a compact set in $\mathbb{R}^2$ by choice of coordinates.], if additionally α can be partially differentiated with respect to ε for all $x \in \psi(U)$ and ε small enough $(*)$, and if

there is an almost everywhere non-negative $A \in L^1(\psi(U))$ with $|\frac{\partial \alpha}{\partial \varepsilon}(\varepsilon, x)| \leq A(x)$ almost everywhere in $\psi(U)$ and for all ε small enough $(**)$. Let us check whether α is partially differentiable with respect to ε.

Clearly, suppressing the dependency on the chart, for $i, j \in \{1, 2\}$, $g_{ij}(\varepsilon)$ is a quadratic polynomial in ε and thus smooth w. r. t. ε. Using $(g^{ij}) = (g_{ij})^{-1}$, it follows that g^{ij} is smooth w. r. t. ε for $i, j \in \{1, 2\}$, too, as the inverse of a matrix can be calculated via the determinant and the adjunct of this matrix which both smoothly depend on the matrix components by linear algebra. Also, if we choose $\nu(\varepsilon) := \frac{\partial_1(f+\varepsilon\phi)\times\partial_2(f+\varepsilon\phi)}{|\partial_1(f+\varepsilon\phi)\times\partial_2(f+\varepsilon\phi)|}$ as unit normal, then ν depends smoothly on ε as $f + \varepsilon\phi$ is an immersion and the numerator of the fraction is a polynomial in ε. This implies smooth dependency on ε of $h_{ij}(\varepsilon) = \langle \nu(\varepsilon), d^2(f + \varepsilon\phi)\rangle$ for $i, j \in \{1, 2\}$. Thus, $\alpha(\cdot, x)$ is smooth for every fixed $x \in \psi(U)$ and whence $(*)$ and $(**)$ are satisfied. We conclude that $\mathcal{W}(\varepsilon)$ is differentiable and that **we are allowed to interchange integration and differentiation**.

By the product rule and $\sum_{k=1}^{K} \eta_k \equiv 1$, we deduce from 2.5 that

$$\delta\,\mathcal{W}(f)\phi = \int_\Sigma \langle \mathcal{H}, \delta\mathcal{H}\rangle\, d\mu_f + \frac{1}{2}\sum_{k=1}^{K}\int_{U_k} \eta_k\, |\mathcal{H}|^2\, \delta(\sqrt{\det(g^{\psi_k})})\, d\lambda^2 \circ \psi_k, \tag{2.6}$$

where we have already shown that the derivatives on the right hand side exist. We will now calculate the derivatives δg_{ij}, $\delta\sqrt{\det g_{ij}}$, δg^{ij}, $\delta\nu$, δh_{ij}, and $\delta\mathcal{H}$ with the aid of the chain and product rules. Let ∇ denote the Levi-Cività connection[7] of (Σ, g), Γ^k_{ij} the associated Christoffel symbols.

- Using the equation $\nabla_i Y^j = \partial_i Y^j + \Gamma^j_{ik} Y^k$ for arbitrary local fields Y on Σ and the Gauß equations $\partial_i\partial_j f = \Gamma^m_{ij}\partial_m f + h_{ij}\nu$, we deduce $g_{ij}(\varepsilon) = \langle \partial_i f + \varepsilon\partial_i\phi, \partial_j f + \varepsilon\partial_j\phi\rangle = g_{ij} + \varepsilon(\langle \partial_i f, \partial_j\phi^\perp\rangle + \langle \partial_i\phi^\perp, \partial_j f\rangle + g_{il}\nabla_j X^l + g_{jl}\nabla_i X^l) + o(\varepsilon^2)$ and thus by definition of the second fundamental form $\delta g_{ij} = -2h_{ij}\langle \phi, \nu\rangle + g_{il}\nabla_j X^l + g_{jl}\nabla_i X^l$.

$\Rightarrow$ $\delta\sqrt{\det g} = \frac{1}{2} g^{ij}\delta g_{ij}\sqrt{\det g} = (-\langle \mathcal{H}, \phi\rangle + \operatorname{div}_g X)\sqrt{\det g}$ using $\operatorname{div}_g Y = \nabla_i Y^i$ for arbitrary Y.

- $g^{ij}g_{jk} = \delta^i_k$ implies $\delta g^{ij} = -g^{ik}(\delta g_{kl})g^{lj} = 2\langle \phi, \nu\rangle h^i_l g^{lj} - g^{kj}\nabla_k X^i - g^{il}\nabla_l X^j$, where (h^i_l) is the matrix of the Weingarten map L.

- Since $\nu(\varepsilon)$ is normed, $\langle \delta\nu, \nu\rangle = 0$, so that $\delta\nu = b^i\partial_i f$. We can determine the coefficients b^i by differentiating $\langle \nu(\varepsilon), \partial_j f + \varepsilon\partial_j\phi\rangle = 0$. We get $b^i = -g^{ij}(\partial_j\langle \phi, \nu\rangle + X^l h_{jl})$ and thus $\delta\nu = -g^{ij}\partial_j\langle \phi, \nu\rangle\partial_i f - h^i_l X^l\partial_i f$, using the Gauß equations.

- Using again the Gauß equations, the Weingarten equations $\partial_i\nu = h^j_i\partial_j f$, and the expression for $\delta\nu$ derived above, we can use the fact that $\nabla\langle \phi, \nu\rangle$ is a (0,1)-tensor field to see that $\delta h_{ij} = \nabla_i\nabla_j\langle \phi, \nu\rangle - \langle \phi, \nu\rangle h^k_i h_{jk} - h_{kl}X^l\Gamma^k_{ij} + \partial_i h_{jl}X^l + h_{il}\nabla_j X^l + h_{jl}\nabla_i X^l - h_{jl}\Gamma^l_{ik}X^k$.

[7] For the notions of Levi-Cività connection and associated Christoffel symbols as well as the equations used below, cf. for example [Lee97].

- Differentiating $h_{ij} = -\langle \partial_i \nu, \partial_j f\rangle$ shows that $\partial_i h_{jl} = \partial_l h_{ij} - \Gamma^k_{lj} h_{ik} + \Gamma^k_{ij} h_{lk}$ which leads to $\delta h_{ij} = \nabla_i \nabla_j \langle \phi, \nu\rangle - \langle \phi, \nu\rangle h^k_i h_{jk} + \partial_l h_{ij} X^l + h_{il} \nabla_j X^l + h_{jl} \nabla_i X^l - h_{jk} \Gamma^k_{il} X^l - h_{ik} \Gamma^k_{jl} X^l$.
- $\mathcal{H} = g^{ij} h_{ij} \nu$ locally, so $\delta \mathcal{H} = \delta(g^{ij}) h_{ij} \nu + g^{ij} \delta(h_{ij}) \nu + g^{ij} h_{ij} \delta\nu$. From the above and since $\triangle_g u = g^{ij} \nabla_i \nabla_j u$ for every smooth function u on Σ, we finally deduce that $\delta \mathcal{H} = \langle \phi, \nu\rangle h^i_l h^l_i \nu + \triangle_g \langle \phi, \nu\rangle \nu - 2 h^i_k \Gamma^k_{il} X^l \nu + \partial_l h_{ij} X^l g^{ij} \nu + g^{ij} h_{ij} \delta\nu$.

Elementary linear algebra shows $h^i_l h^l_i = \operatorname{trace}(L^2) = (\operatorname{trace} L)^2 - 2 \det L = |\mathcal{H}(f)|^2 - 2K(f)$. But remembering $H(f) = \frac{1}{2}\langle \mathcal{H}(f), \nu\rangle$ it is easy to see that $2\partial_l(H(f)) = -2 h^j_k \Gamma^j_{kl} + g^{ij} \partial_l h_{ij}$. We conclude $\langle \delta\mathcal{H}, \mathcal{H}\rangle = 2H(f)\left[(4H(f)^2 - 2K(f))\langle \phi, \nu\rangle + \triangle_g \langle \phi, \nu\rangle\right] + 4H(f)\partial_l H(f) X^l = 2H(f)\left[(4H(f)^2 - 2K(f))\langle \phi, \nu\rangle + \triangle_g \langle \phi, \nu\rangle\right] + 2g(\operatorname{grad}_g H(f)^2, X)$. By the above, the first integral in 2.6 can be evaluated by Green's identity[8] to

$$2 \int_\Sigma (4(H(f)^2 - 2K(f))H(f) + \triangle_g H(f))\langle \phi, \nu\rangle \, d\mu_f + 2 \sum_{k=1}^K \int_{U_k} \eta_k \, g(\operatorname{grad}_g H(f)^2, X) \, d\mu_f.$$

The second integral in 2.6 turns out to equal

$$-4 \int_\Sigma H(f)^3 \langle \phi, \nu\rangle \, d\mu_f - 2 \sum_{k=1}^K \int_{U_k} \eta_k \, g(\operatorname{grad}_g H(f)^2, X) \, d\mu_f$$

by the definition of the divergence and by integration by parts. Together, we get

$$\delta \mathcal{W}(f)\phi = 2 \int_\Sigma \left[\triangle_g H(f) + 2(H(f)^2 - K(f))\, H(f)\right] \langle \phi, \nu\rangle \, d\mu_f.$$

We have thus shown that **$\mathcal{W}$ is Gateaux-differentiable on the $\|.\|_{C^4(\Sigma,\mathbb{R}^3)}$-open set $U = \{f \in C^4(\Sigma, \mathbb{R}^3) \mid f$ is an immersion$\}$**.

Obviously, for every $f \in U$, $\delta \mathcal{W}(f)$ is a well-defined linear functional on $C^4(\Sigma, \mathbb{R}^3)$. We will now show that $\delta \mathcal{W}(f)$ is a continuous functional with respect to $\|.\|_{C^4}$ which gives us Fréchet-differentiability. This becomes trivial if we realise that by compactness of Σ,

$$|\delta \mathcal{W}(f)\phi| \le 2 \int_\Sigma |\triangle_g H(f) + 2(H(f)^2 - K(f))H(f)| \, d\mu_f \, \|\phi\|_{C^0} \le C \, \|\phi\|_{C^4}.$$

Finally, **$\mathcal{W}$ is C^1-Fréchet-differentiable on U** since $\delta \mathcal{W}(f)\phi$ is continuous on all of $U \subset_o C^4(\Sigma, \mathbb{R}^3)$ with respect to $\|.\|_{C^4}$ for fixed $\phi \in C^4(\Sigma, \mathbb{R}^3)$, cf. proposition 2.1.3. This proves our claim. □

Definition 2.4.2 (Willmore Surfaces). Let Σ be a closed smooth surface. A *Willmore surface* is an immersion $f \in C^4(\Sigma, \mathbb{R}^3)$ that is a *critical point of* $\mathcal{W}$, i. e. that satisfies $\delta\mathcal{W}(f) = 0$. By the fundamental lemma of the calculus of variations[9] (which is applicable as $\mathcal{W}$ is of class C^1), this is equivalent to f satisfying the *Euler-Lagrange equation*

$$\triangle_g H(f) + 2H(f)(H(f)^2 - K(f)) = 0. \tag{2.7}$$

[8] cf. pp. 44 in [Lee97].

[9] cf. p. 32 [BGH98] for a variant for integrals over $\Omega \subset \mathbb{R}^n$ which can be applied to our situation with the aid of a partition of unity.

Calculus of variations then tells us that every minimising Willmore surface is a Willmore surface (if it is of class C^4). We will give examples of Willmore surfaces of different topological types in the following section.

Remark. We only consider immersions into $\mathbb{R}^3$; it is also possible to study Willmore surfaces in arbitrary $\mathbb{R}^n$ but this lies beyond the scope of this text.

2.5 Examples

Let us calculate the energy of the round sphere immersion of $\mathbb{S}^2$ and of special immersions of the torus $\mathbb{T}^2$ into $\mathbb{R}^3$. For more examples and some results on minimising properties of the sphere and the Clifford torus, see chapter 3.

Proposition 2.5.1. *Every round sphere embedding $\iota : \mathbb{S}^2 \hookrightarrow \mathbb{R}^3$ is a Willmore surface. We have*

$$\mathcal{W}(\iota) = 8\pi.$$

Proof. Choose $\nu = \mathrm{id}_{\mathbb{S}^2}$ as unit normal field on $\mathbb{S}^2$. Let $\iota : \mathbb{S}^2 \hookrightarrow \mathbb{R}^3 : p \mapsto rp + c$ be a round sphere embedding of $\mathbb{S}^2$ into $\mathbb{R}^3$, with $r \in \mathbb{R}^+$ and $c \in \mathbb{R}^3$. It is then well-known that[10] $K(\iota) \equiv \frac{1}{r^2}$ and $H(\iota) \equiv \frac{1}{r}$ so that $\triangle_g H(\iota) + 2H(\iota)(H(\iota)^2 - K(\iota)) = 0$ on $\mathbb{S}^2$. We have thus shown that ι is a Willmore surface as it is of class C^4. To calculate the energy, we use polar coordinates on $\mathbb{S}^2$. Remember that by conformal invariance (theorem 2.3.3), the energy of any round sphere immersion into $\mathbb{R}^3$ must be the energy of the identity $\mathrm{id} : \mathbb{S}^2 \hookrightarrow \mathbb{R}^3$. As the image of polar coordinates differs from $\mathbb{S}^2$ only by a subset of area measure zero, we can deal with this one chart only. Polar coordinates are given by $\psi^{-1} : (-\frac{\pi}{2}, \frac{\pi}{2}) \times (0, 2\pi) \to \mathbb{R}^3 : (\theta, \varphi) \mapsto (\cos\theta\cos\varphi, \cos\theta\sin\varphi, \sin\theta)^t$.

We calculate the derivatives $\partial_\theta \psi^{-1}(\theta, \varphi) = (-\sin\theta\cos\varphi, -\sin\theta\sin\varphi, \cos\theta)^t$ and similarly $\partial_\varphi \psi^{-1}(\theta, \varphi) = (-\cos\theta\sin\varphi, -\cos\theta\cos\varphi, 0)^t$, so that $g^\psi_{\theta\theta}(\theta, \varphi) \equiv 1$, $g^\psi_{\varphi\varphi}(\theta, \varphi) = \cos^2\theta$ and the off-diagonal terms are zero. Whence by lemma 1.2.22 the mean curvature vector satisfies $\mathcal{H}(\mathrm{id}) \circ \psi^{-1} = (\triangle_g \mathrm{id}) \circ \psi^{-1} = -2\psi^{-1}$ so that $|\mathcal{H}(\mathrm{id}) \circ \psi^{-1}|^2 \equiv 4$ and the energy can be evaluated to $\mathcal{W}(\mathrm{id} : \mathbb{S}^2 \hookrightarrow \mathbb{R}^3) = \frac{1}{2}\int_{-\frac{\pi}{2}}^{\frac{\pi}{2}} \int_0^{2\pi} 4\sqrt{g^\psi_{\theta\theta} g^\psi_{\varphi\varphi}}\, d\varphi\, d\theta = 8\pi$. □

Next, we will discuss the energy of tori of revolution of constant circular cross-section. By conformal invariance, we can assume that the inner radius equals 1. The *torus of revolution of constant circular cross-section of radii* 1 *and* $R > 1$ is given by

$$T_R := \{(x^1, x^2, x^3) \in \mathbb{R}^3 |\, (R - \sqrt{(x^1)^2 + (x^2)^2})^2 + (x^3)^2 = 1\}$$

with differentiable structure and Riemannian metric induced by $\mathbb{R}^3$. The *Clifford torus*[11] is the torus satisfying $R = \sqrt{2}$, see the figure below.

[10] in any coordinates

[11] In fact, the Clifford torus is defined by $\frac{1}{\sqrt{2}}(\mathbb{S}^1 \times \mathbb{S}^1) \subset \mathbb{S}^3$. The embedding considered here then is the $\mathbb{S}^3$-stereographic projection of this into $\mathbb{R}^3$ (easy to verify by straightforward calculation). As stereographic projection is conformal, this does not change the energy.

Proposition 2.5.2. [12] *For the torus T_R, we have $\mathcal{W}(\mathrm{id} : T_R \hookrightarrow \mathbb{R}^3) = \frac{2\pi^2 R^2}{\sqrt{R^2-1}}$ and, in particular, $\mathcal{W}(\mathrm{id} : Cl \hookrightarrow \mathbb{R}^3) = 4\pi^2$. The Clifford torus has least energy among all tori of revolution of circular cross-section and is the only Willmore surface among them.*

Proof. We parametrise the upper half of the torus T_R by the adapted "flattening" coordinates $\psi^{-1} : (R-1, R+1) \times (0, 2\pi) \to \mathbb{R}^3 : (r, \theta) \mapsto (r\cos\theta, r\sin\theta, \sqrt{1-(R-r)^2}\,)^t$. We will calculate its Willmore integral and use the symmetry of the torus to calculate the Willmore energy as twice this value since the uncovered remainder has measure zero. We have $\partial_r \psi^{-1}(r,\theta) = (\cos\theta, \sin\theta, \frac{R-r}{\sqrt{1-(R-r)^2}})^t$, $\partial_\theta \psi^{-1}(r,\theta) = (-r\sin\theta, r\cos\theta, 0)^t$, and thus $g^\psi_{rr}(r,\theta) = \frac{1}{1-(R-r)^2}$, $g^\psi_{\theta\theta}(r,\theta) = r^2$ and the off-diagonal matrix elements are zero, so that $\sqrt{\det(g^\psi)} \circ \psi^{-1}(r,\theta) = \frac{r}{\sqrt{1-(R-r)^2}}$. By lemma 1.2.22, we deduce $\mathcal{H}(\mathrm{id}) \circ \psi^{-1}(r,\theta) = (\triangle_g \,\mathrm{id}) \circ \psi^{-1}(r,\theta) = (\cos\theta\,(-\frac{(R-r)^2}{r} + R - r), \sin\theta\,(-\frac{(R-r)^2}{r} + R - r), (R-2r)\,\frac{\sqrt{1-(R-r)^2}}{r})^t$ and whence get $|\mathcal{H}(\mathrm{id})|^2 \circ \psi^{-1}(r,\theta) = \frac{(R-2r)^2}{r^2}$. Thus,

$$
\begin{aligned}
\mathcal{W}(\mathrm{id} : T \hookrightarrow \mathbb{R}^3) &= 2\,\mathcal{W}(\psi^{-1}) = \int_{R-1}^{R+1}\int_0^{2\pi} \frac{(R-2r)^2}{r^2}\frac{r}{\sqrt{1-(R-r)^2}} d\theta dr \\
&= 2\pi \int_{R-1}^{R+1} \frac{(R-2r)^2}{r\sqrt{1-(R-r)^2}} dr \\
&= 2\pi(4\int_{R-1}^{R+1} \frac{r}{\sqrt{1-(R-r)^2}} dr - 4R\int_{R-1}^{R+1} \frac{1}{\sqrt{1-(R-r)^2}} dr \\
&\quad + R^2 \int_{R-1}^{R+1} \frac{1}{r\sqrt{1-(R-r)^2}} dr) \\
&= \frac{2\pi^2 R^2}{\sqrt{R^2-1}},
\end{aligned}
$$

where the integrals are evaluated with the aid of [BS70]. This gives $\mathcal{W}(Cl) = 4\pi^2$ (for $R = \sqrt{2}$). Since $R \mapsto \frac{2\pi^2 R^2}{\sqrt{R^2-1}}$ has a global minimum in at $R = \sqrt{2}$, we have proved the minimality of the Clifford torus. In the same coordinates, we have $H(\mathrm{id}) \circ \psi^{-1}(r,\theta) = \frac{1}{2}|\mathcal{H}(\mathrm{id})| \circ \psi^{-1}(r,\theta) = \frac{R-2r}{2r}$ where we have chosen the unit normal pointing to the outside. From the formulae we have derived for g^ψ, we get[13] $K(\mathrm{id}) \circ \psi^{-1}(r,\theta) = \frac{r-R}{r}$. The Laplace-Beltrami of $H(\mathrm{id})$ is $\triangle_g H(\mathrm{id}) \circ \psi^{-1}(r,\theta) = \frac{R}{2r^2}(1 + Rr - R^2)$ so that

$$
\triangle_g H(\mathrm{id}) + 2H(\mathrm{id})(H(\mathrm{id})^2 - K(\mathrm{id})) = \frac{2-R^2}{4r^3} R = 0 \quad \Leftrightarrow \quad R = \sqrt{2}
$$

on $(R-1, R+1) \times (0, 2\pi)$. The same is true on the lower half of the torus. On the two circles not covered by the flattening coordinates, the equality follows by continuity. Hence,

[12] The energy result is due to Willmore, cf. p.274 in [Wil93]; this proof is due to the author.
[13] cf. p. 37 in [Wil59].

the Clifford torus is a Willmore surface – the only one among the tori of revolution of constant circular cross-section. □

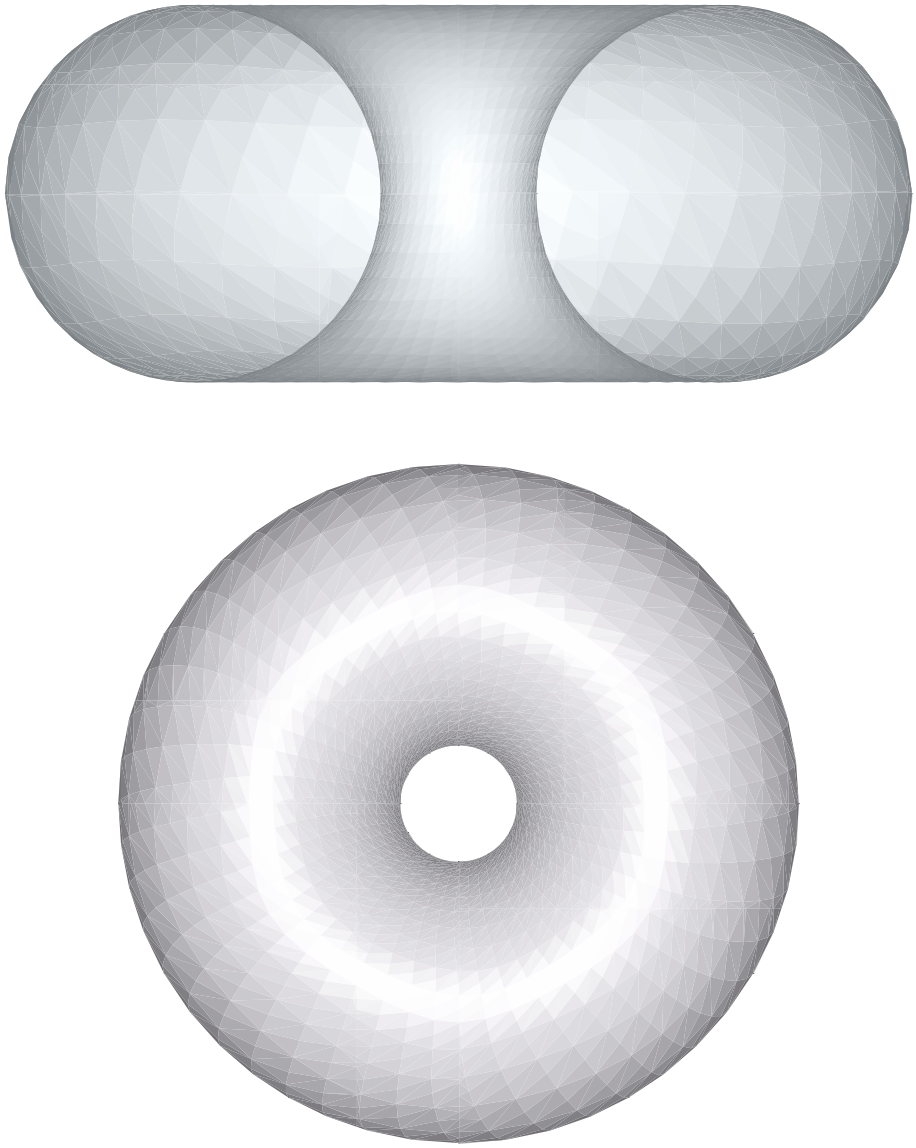

Figure 2.1: Clifford torus viewed from inside and from above.

3 Glueing Surfaces

In this chapter, we will develop an algorithm for glueing "discrete" surfaces together. The glueing scheme generates "discrete" (orientable) surfaces of any genus. These surfaces can then be used in any setting where one wishes to apply a numerical scheme – some kind of flow, for example – to a surface which cannot easily be discretised "by hand". We intend to use some glued surfaces as starting points for the gradient flow of the Willmore functional defined in chapter 2. The glueing procedure imitates a theoretical result of M. Bauer and E. Kuwert on the construction of minimisers of the Willmore energy, see chapter 4. As we will explained there, some glued surfaces might be good candidates for minimising the (discretised) Willmore energy and act as limit surfaces under the flow.

In the first section, we will give a short introduction into the theory of Willmore surfaces (see chapter 2 for the definition of Willmore surfaces). Our approach follows [BK03, PS87, Wil93]. In section 3.2, we will describe the glueing method and show several examples, in section 3.2.3 we will discuss some numerical details of the scheme.

3.1 Continuous Willmore Surfaces

First of all, we give a concise (and incomplete) overview[1] over some results on Willmore surfaces. By the surface classification theorem 1.2.15 and by lemma 2.2.3, it is clear that only the topological type (genus and orientability) influences the Willmore energy of a surface. We will thus concentrate on standard examples such as $\mathbb{S}^2$, $\mathbb{T}^2$ and $\mathbb{RP}^2$. We begin with $\mathbb{S}^2$: Its Willmore energy is $\mathcal{W}(\mathbb{S}^2) = 8\pi$ ([Wil65], see also proposition 2.5.1). This minimum is attained by all round-sphere immersions into $\mathbb{R}^3$ (recall the conformal invariance of $\mathcal{W}$, theorem 2.3.3) and only by those. All Willmore surfaces of the topological type of $\mathbb{S}^2$ have been classified by R. Bryant in [Bry84]. They have energy $8\pi n$ ($n \in \mathbb{N}$), but these critical values are not all attained. One famous example is the so-called *Willmore sphere* which is a self-intersecting immersion of energy 32π, see figure 3.1.

The situation for tori is far more complicated. T. J. Willmore proved in 1965 that the Clifford torus has minimal energy $4\pi^2$ among all tori of revolution of circular cross-section (see proposition 2.5.2 and the figures on p. 31). In 1970/71, K. Shiohama and A. Tagaki as well as T. J. Willmore showed that it has minimal energy among all tori embedded as tubes of constant cross-section. T. J. Willmore then conjectured that the Clifford torus (together with all its conformal transforms) is a minimiser for genus one orientable surfaces. L. Simon ([Sim86]) showed in 1986 that a minimiser of the topological type of the torus

[1] based on [PS87].

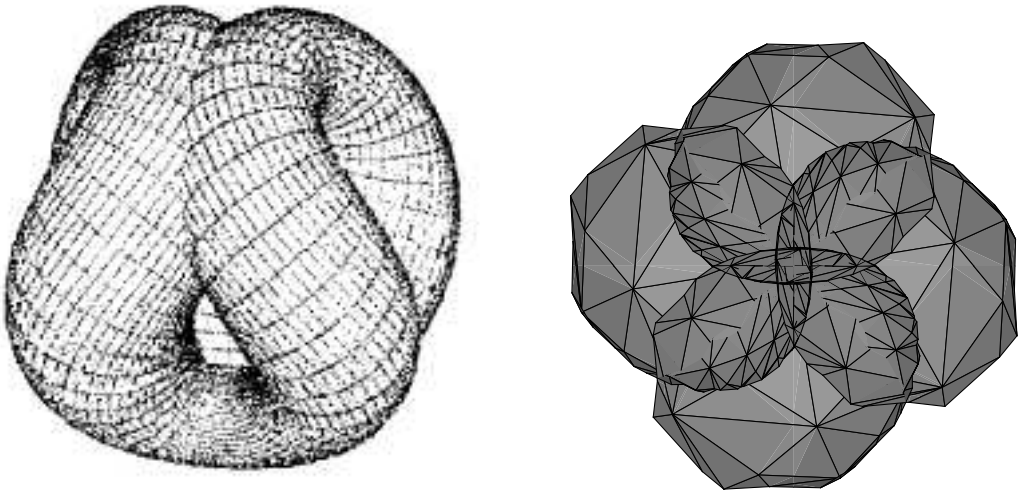

Figure 3.1: Willmore sphere ($n = 4$) – one figure is taken from [PS87], the second one has been constructed by G. Dziuk. It is cut in half

exists. In 2002, M. U. Schmidt [Sch02] presented a proof of this long-standing *Willmore Conjecture*[2].

P. Li & S. T. Yau [LY82] showed that $\mathcal{W}(\mathbb{RP}^2) \geq 24\pi$. Minimising Willmore surfaces have been identified by R. Bryant [Bry88] and R. Kusner [Kus]. They have energy 24π, indeed. R. Bryant classified all minimising Willmore surfaces of the topological type of $\mathbb{RP}^2$ in $\mathbb{R}^3$. One of these is known as *Boy's surface*, see figure 3.2.

Higher genus Willmore surfaces (and minimisers) are still an object of active research. Many examples of Willmore surfaces are stereographic projections of minimal surfaces in $\mathbb{S}^3$. The Clifford torus arises in this way, see section 2.5. However, by constructing counter-examples, U. Pinkall showed in [Pin85] that not all Willmore surfaces can be obtained in this way.

In [BK03], relying on a result obtained by L. Simon in [Sim93], M. Bauer and E. Kuwert proved existence of minimisers of all genera in the orientable case, see below. In their proof, they use a geometric connected sum construction which is the base for the discrete glueing procedure presented in this text.

[2] say M. Bauer and E. Kuwert in [BK03].

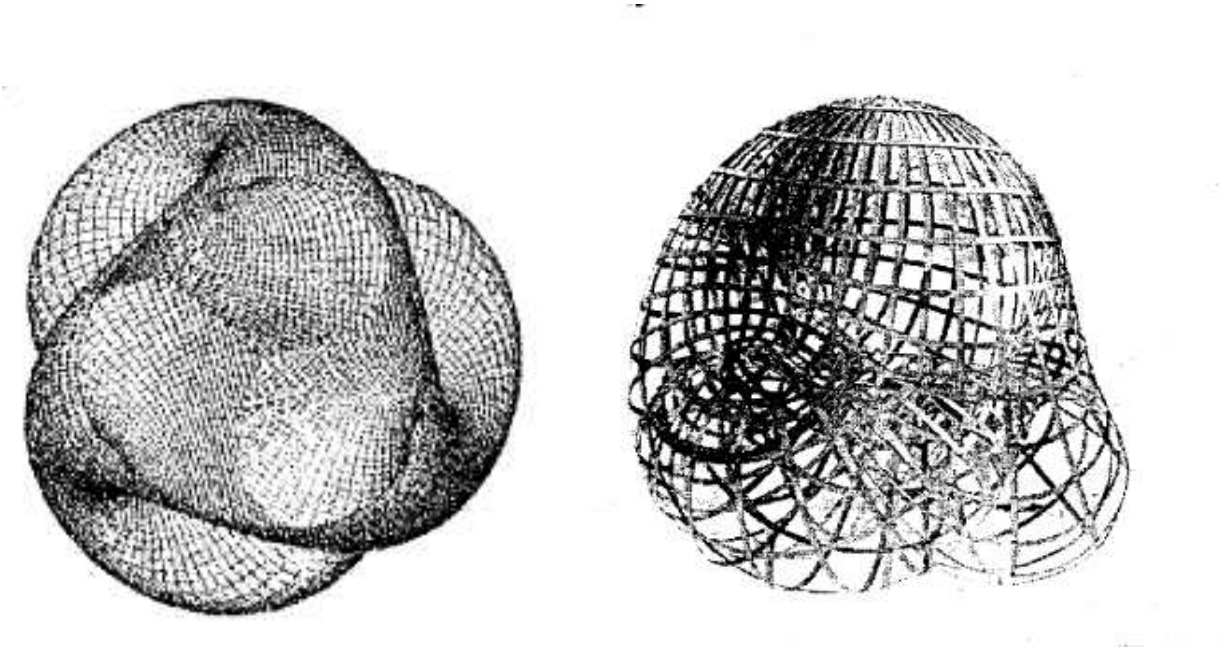

Figure 3.2: Boy's surface – one figure taken from [PS87], the other from [KP97] (Boy's surface in Oberwolfach)

3.1.1 Constructing Higher Genus Willmore Surfaces

All surfaces and immersions in this section are assumed to be smooth. M. Bauer and E. Kuwert showed in [BK03]

Theorem 3.1.1 (Existence of Willmore Surfaces of all Genera). *For any $g \in \mathbb{N}_0$, let $\beta_g := \mathcal{W}(\Sigma) = \inf\{\mathcal{W}(f) \mid f : \Sigma \to \mathbb{R}^3$ is an immersion$\}$, where Σ is a closed orientable surface of genus g. Then for any $g \in \mathbb{N}_0$, the infimum β_g is attained by an oriented, closed Willmore surface of genus g.*

The main idea of their paper lies in refining a theorem presented by L. Simon in 1993 ([Sim93]) using a geometric connected sum construction which will be sketched below. Simon's theorem says

Theorem 3.1.2 (Simon). *For any $g \in \mathbb{N}_0$, there is a partition $g = g_1 + \cdots + g_r$ with $g_i \geq 1$, such that the infima β_{g_i} are attained and*

$$\beta_g - 8\pi = \sum_{i=1}^{r} (\beta_{g_i} - 8\pi).$$

The connected sum theorem of M. Bauer and E. Kuwert says

Theorem 3.1.3 (Connected Sum Construction). *Let $f_i : \Sigma_i \to \mathbb{R}^3$, $i = 1, 2$ be two smoothly immersed closed surfaces. If neither f_1 nor f_2 is a round sphere (i. e. totally umbilic[3]), then there is an immersed surface $f : \Sigma \to \mathbb{R}^3$ with topological type of the connected sum $\Sigma_1 \# \Sigma_2$, such that*

$$\mathcal{W}(f) < \mathcal{W}(f_1) + \mathcal{W}(f_2) - 8\pi. \tag{3.1}$$

In the following, we will give a very rough sketch of the idea lying at the heart of the connected sum construction. We do this because the glueing scheme we will present in this chapter is inspired by theorem 3.1.3. Recall that by theorem 2.3.3, the energy of an immersed surface is reduced by the finite number $8\pi \operatorname{card} f^{-1}(c)$ when the surface is inverted at a sphere with centre c. Having this in mind, M. Bauer and E. Kuwert choose a *regular value* $c \in f_1(\Sigma_1)$ (i. e. a value having pre-image cardinality one) and invert f_1 at a sphere with centre c leading to an immersion $\hat{f}_1 : \Sigma_1 \setminus f^{-1}(c) \to \mathbb{R}^3$ with energy $\mathcal{W}(f_1) - 8\pi$ by theorem 2.3.3. Then, they cut out a "disk around infinity" (the "planar end" of $\hat{f}_1$) and scale down (and move) $\hat{f}_1$. Also, they cut a disk out of f_2 and scale up the result. The boundaries of the two disk-holes are joined by a biharmonic interpolation the energy of which is more than compensated by that of the two cut out disks so that the glued surface has both energy less than $\mathcal{W}(f_1) + \mathcal{W}(f_2) - 8\pi$ and is homeomorphic to $\Sigma_1 \# \Sigma_2$. For a more detailed insight, the reader is referred to [BK03]. The discrete glueing construction presented in this text relies upon this idea. One can thus hope to get "good approximations" to "numerical Willmore surfaces" with this procedure, see chapter 4.

3.2 Glueing Discrete Surfaces

In [DDE05], K. Deckelnick, G. Dziuk, and C. M. Elliott present an algorithm for the (discretised) Willmore flow relying on a trick of R. Rusu ([Rus]). This algorithm allows to study the flow behaviour of arbitrary orientable (discrete) surfaces "immersed" in $\mathbb{R}^3$, numerically. G. Dziuk has applied the scheme to surfaces parametrised over $\mathbb{S}^2$. The author has applied G. Dziuk's scheme to tori of revolution of circular cross-sections. The algorithm and the results obtained by the author are discussed in the following chapter.

As we were interested in the flow behaviour of higher genus surfaces, too, we have introduced a glueing scheme for discrete surfaces. The basic idea is to approximate the geometric connected sum construction presented above (very roughly). We intend to use the surfaces obtained in this manner as starting values for the (discretised) Willmore flow, see chapter 4. First of all, we will introduce the notion of "discrete surfaces" and of "discretised Willmore surfaces". Although those are continuous, we will call our customary (Willmore) surfaces "continuous" and mean this in contrast to "discrete/discretised". As we will only use the attribute "continuous" in order to make this distinction, no confusion should arise.

[3]For a definition of this notion, see [Wil93], for example.

Definition 3.2.1 (Discrete (Embedded) Surfaces). [4] A *triangle* T *in* $\mathbb{R}^3$ is the convex hull of three different points p_1, p_2, p_3. $p \in T$ is a *vertex of* T, if $p = p_i$ for $i \in \{1,2,3\}$, a subset $E \subset T$ is an *edge of* T, if $E = \operatorname{conv}\{p_i, p_j\}$ for $i \neq j \in \{1,2,3\}$. We say that a closed $C^{0,1}$-manifold $\Sigma \subset \mathbb{R}^3$ is *(regularly) triangulated* by a finite set of triangles $\mathcal{T} = \{T_1, \ldots, T_K\}$ if it satisfies

- $\Sigma = \cup_{T \in \mathcal{T}} T$
- If $T_i \cap T_j = \{p\}$ for any two different triangles $T_i, T_j \in \mathcal{T}$, then p is a vertex of both T_i and T_j.
- Otherwise, $T_i \cap T_j$ is an edge of both triangles.

If Σ is (regularly) triangulated by the *triangulation* or *mesh* $\mathcal{T}$, we call Σ a *discrete (embedded) surface (in* $\mathbb{R}^3$*)*. Let $\operatorname{diam} t$ denote the diameter of a triangle T. $h := \max_{T \in \mathcal{T}} \operatorname{diam} T$ is called the *mesh size* of $\mathcal{T} =: \mathcal{T}_h$. Vertices and edges of the triangles in the triangulation are also referred to as vertices and edges of the discrete surface. We usually omit the explicit reference to the triangulation $\mathcal{T}_h$ of Σ and write Σ_h to remind of it.

We say that T_i is a *neighbour* of T_j if they share a common edge (and are not identical). We also say that a vertex v_i is a *neighbour* of a different vertex v_j, if they belong to one and the same triangle. A map $f : \Sigma_h \to \mathbb{R}^n$ is called *piecewise linear*, if the restriction of f to each triangle, $f|_T$, is an affine-linear mapping. It is called *locally injective*, if each point $p \in \Sigma_h$ has a (topological) neighbourhood $U \subset \Sigma_h$ such that the restriction $f|_U$ is injective. f is called a *parametrisation* if it is continuous, piecewise linear, and locally injective. In that case, we say that $f(\Sigma_h)$ *is parametrised over* Σ_h or that $f(\Sigma_h)$ is a *deformation* of Σ_h.

Example. Figure 3.3 shows a discrete (embedded) surface, displayed by drawing its edges.

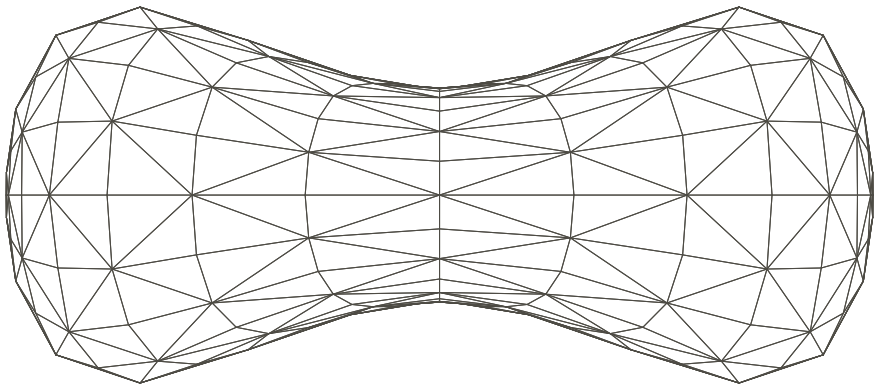

Figure 3.3: Discrete embedded dumbbell (cut in half) by G. Dziuk.

It is more difficult to define self-intersecting surfaces as the notion of an "immersion" is no longer defined in a merely continuous setting. Nevertheless, we need to give a definition of

[4] This definition is based on [Bra91, Rus].

"discrete immersed surfaces" since the Willmore flow may drive embedded surfaces to self-intersections, see chapter 4. We can, however, focus on orientable surfaces as we will only apply the glueing scheme and the (discretised) Willmore flow to orientable surfaces. We give a definition that is compatible with the glueing scheme and the (discretised) Willmore flow, see below and see chapter 4. Moreover, it respects the parametric formulation of the Willmore energy (see chapter 2) and of the Willmore flow, as well as the parametric approach chosen in the discretisation of this flow, see chapter 4.

Definition 3.2.2 (Discrete Immersed Surfaces). [5] A set $\tilde{\Sigma}_h \subset \mathbb{R}^3$ is called a *discrete immersed surface* if it is parametrised over a discrete embedded surface Σ_h, i. e. if there is a discrete embedded surface Σ_h and a continuous, locally injective, piecewise linear map $f : \Sigma_h \to \mathbb{R}^3$ with $f(\Sigma_h) = \tilde{\Sigma}_h$. If $\mathcal{T}_h$ denotes the triangulation of Σ_h, the set $\tilde{\mathcal{T}}_h := f(\mathcal{T}_h)$ is called a *triangulation* or *mesh* of $\tilde{\Sigma}$ and its mesh size, vertices, edges, neighbourhoods, and piecewise linear mappings are defined as above. If $\tilde{\Sigma}_h$ is a discrete immersed surface, we call the underlying discrete embedded surface Σ_h the *parametric domain of* $\tilde{\Sigma}_h$.

Note that $\tilde{\Sigma}_h$ is **not**, in general, a $C^{0,1}$-manifold as it might self-intersect. However, we treat it just as if it was one; for example, we ask whether it is homeomorphic to a given surface. This becomes meaningful if we "identify" $\tilde{\Sigma}_h$ with the underlying surface Σ_h when it comes to topological questions. Similarly, we understand a map $\tilde{x} : \tilde{\Sigma}_h \to \mathbb{R}$ as a map $x : \Sigma_h \to \mathbb{R}$ where $f \circ \tilde{x} = x$. Using this convention, any subset of $\mathbb{R}^3$ that is the image of a parametrisation of a discrete immersed surface is a discrete immersed surface. Any discrete embedded surface is a discrete immersed surface as the identity is clearly piecewise linear. From now on, we will not distinguish between the embedded and the immersed cases unless otherwise stated.

Examples. Figure 3.4 shows a discrete surface[6] that is not embedded. It is displayed by drawing its edges, figure 3.5 illuminates the notation in the vicinity of an edge.

We define

Definition 3.2.3 (Degeneration). Let $\tilde{\Sigma}_h \subset \mathbb{R}^3$ be the image of a discrete embedded surface Σ_h under a continuous piecewise linear map f. We say that the mesh of $\tilde{\Sigma}_h$ *degenerates* if f is not locally injective.

Remark. It follows from linear algebra that any continuous piecewise linear map defined on a discrete surface and having values in $\mathbb{R}$ or $\mathbb{R}^3$ is uniquely determined by its values on the vertices of the surface.

Definition 3.2.4 (Discretised (Willmore) Surfaces). We say that a discrete (embedded or immersed) surface Σ_h is the *discretisation of a surface* Σ immersed or embedded into $\mathbb{R}^3$ if it is an *interpolation* of Σ – i. e. if all vertices of Σ_h lie on Σ – and if it is homeomorphic to this surface. In particular, if Σ is embedded, we request that Σ_h is embedded, too. If Σ is a Willmore surface, then we call Σ_h a *discretised Willmore surface.*

[5] The author is not aware that this definition is explicitly used in any publication. It might be possible to improve or generalise this definition. However, all discrete immersed surfaces appearing in this text are of the kind defined here. Discrete immersed surfaces are also treated in [Rus, DDE05].

[6] It is a lengthy but straightforward calculation to see that this surface really is a discrete immersed surface. As we will not rely on this result, we do not show the calculation here.

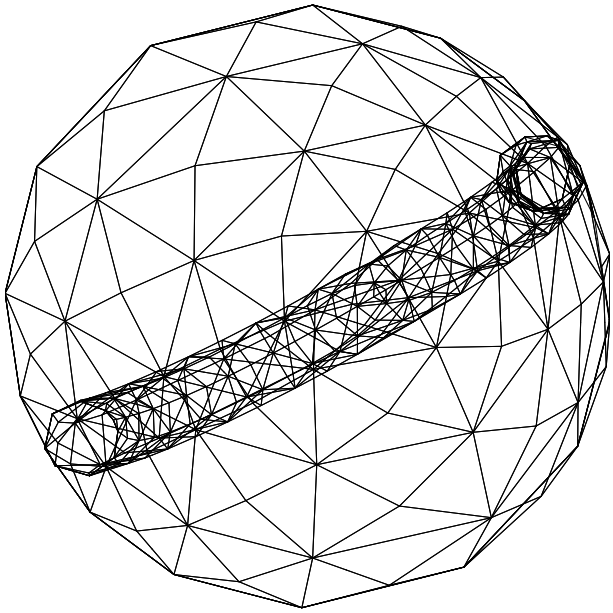

Figure 3.4: Discrete immersed surface (cut in half) by G. Dziuk. The cross-section of this surface is a circle with two loops on opposite sides.

In the literature, one also finds a notion of "discrete Willmore surfaces", see for example the paper [BS05] by A. I. Bobenko and P. Schröder. They use a completely different approach to get to a discrete version of Willmore energy, surfaces, and flow, by exploiting the conformal invariance of $\mathcal{W}$ to define a discrete conformally invariant Willmore energy W depending only on the angles of the discrete surface. A discrete Willmore surface then is a critical point (a solution of the Euler-Lagrange equations) of W, and their discrete Willmore flow is defined respectively. As we want to rely on Finite Element techniques, we will not follow them.

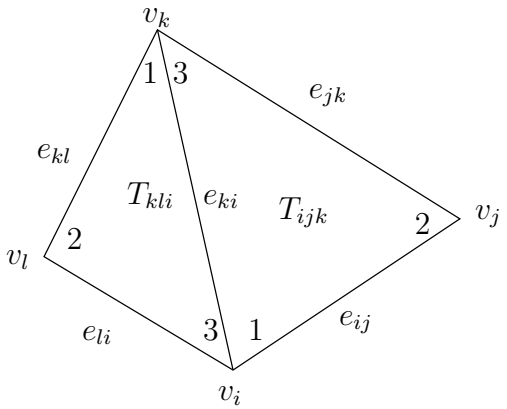

Figure 3.5: Notation for vertices, edges and triangles in the vicinity of an edge.

3.2.1 The Glueing Construction

In order to generate discretised surfaces of higher genera and good candidates for minimisers of the Willmore energy, we have developed a glueing scheme which we will now present. A rough version of the algorithm is included here, the complete[7] algorithm can be found in the appendix **??**. A few ideas are discussed to more detail in section 3.2.3. All discrete surfaces depicted in this chapter are displayed by drawing their edges if not otherwise stated. The discretised Willmore energy of a discrete surface is calculated in the following chapter.

The scheme is capable to glue together any two discrete surfaces from this list:

A round spheres, "crushed spheres" (see figure 3.6), a Willmore sphere as depicted in figure 3.1, the surfaces depicted in the figures 3.4 and 3.3, a ufo-like surface (see figure 3.7), and a further self-intersecting surface (see figure 3.8), all constructed by G. Dziuk

A' ellipsoids, see figure 3.10

B a dumbbell that has been constructed with the glueing scheme, itself see figure 3.9

C tori of revolution of circular cross-section, e. g. the Clifford torus, see figure 2.1

D any other triangulated surface

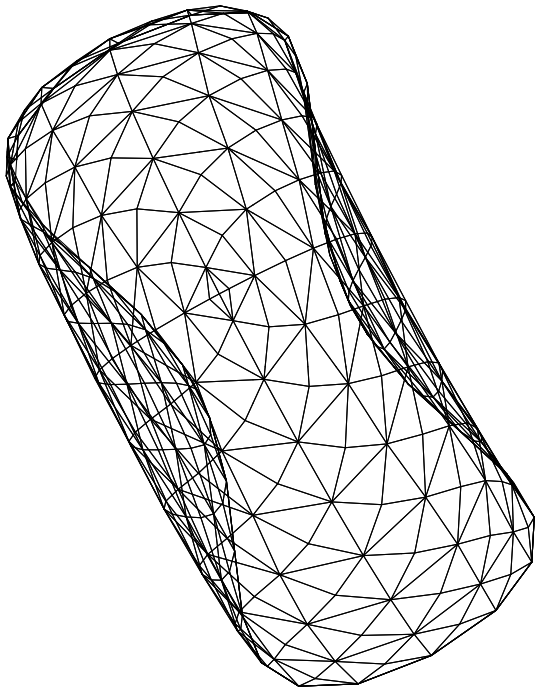

Figure 3.6: Crushed sphere by G. Dziuk.

[7] At least the new parts of it.

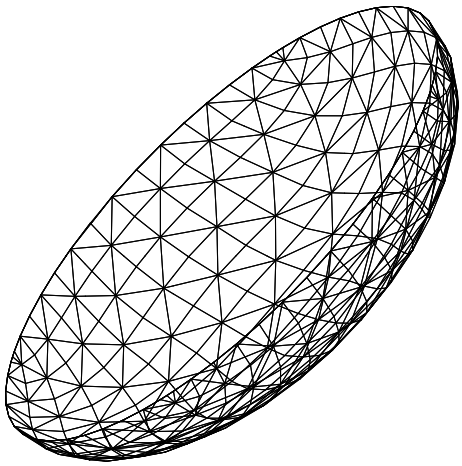

Figure 3.7: Ufo-like surface (cut in half) by G. Dziuk.

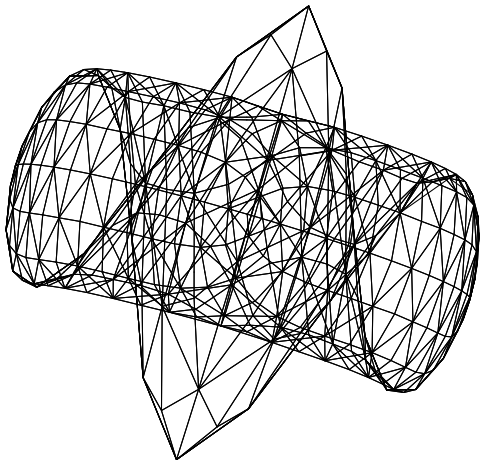

Figure 3.8: Self-intersecting surface (cut in half) by G. Dziuk.

The idea of the glueing scheme can be roughly described as follows: We load one discrete surface from the above list, refine it, if wished, and cut out one triangle of its refined triangulation. Afterwards, we refine the surface again but in a way that leaves the outer edges – the edges of the cut-out triangle – unchanged. Then we inscribe an equilateral hexagon into the hole and triangulate the remainder. This is followed by a parametrisation which takes the discrete surface to its final geometric form, e. g. to an ellipsoid (and by equilaterising the hexagon which might have changed in this process). Then we save it.

Now, we go through the same process with a second discrete surface from the above list. Additionally, the second surface can be inverted at a sphere with centre in the centre of mass of the hexagonal hole. The surface is then scaled such that both hexagons are congruent. The surfaces can now be joined directly or with a hexagonal cylinder in between. In the second case, this cylinder is now constructed. Finally, both surfaces are taken to

their final positions opposite of each other and rotated such that the outer normals to the hexagons cancel. They are glued by identifying the edges and vertices of the hexagons either directly or by means of the cylinder.

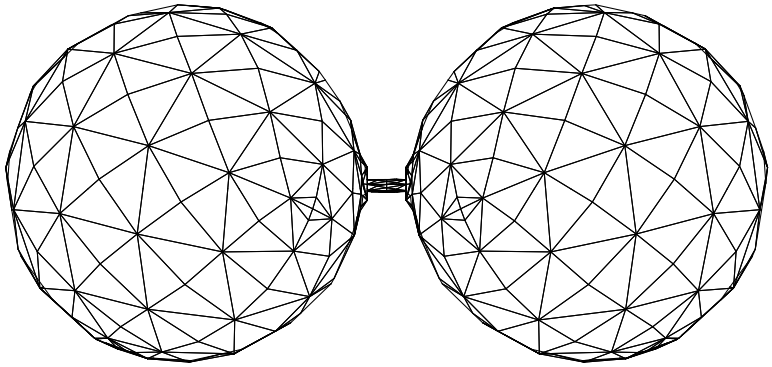

Figure 3.9: Glued dumbbell.

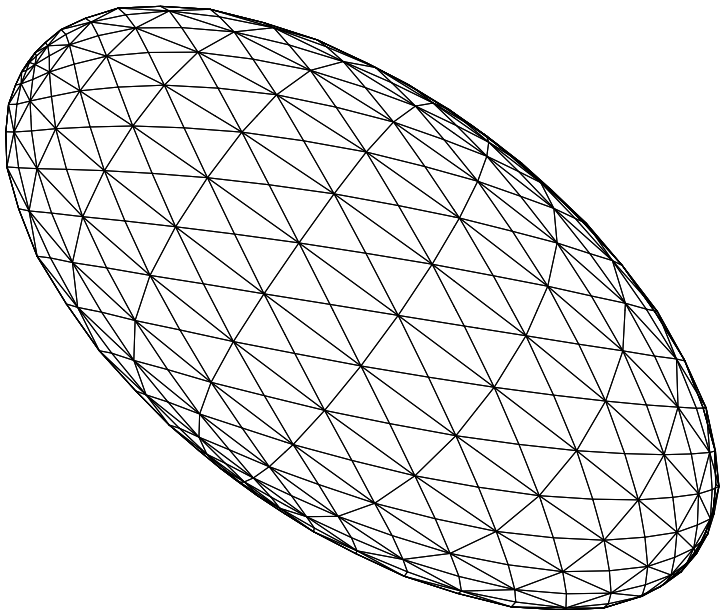

Figure 3.10: Ellipsoid.

3.2.2 The Glueing Algorithm

Having given a rough sketch of the ideas lying at the heart of the algorithm, we will now go into more detail. We will explain which options the user has when using the glueing program and which effect these options will have on the resulting surface. A flow chart of the program can be found on page 50. Most of the code is included in the appendix **??**, cf. pp. **??**.

(Input). The input for the program consists of a file `Input_glue` that specifies the values of a number of parameters. Some models are available, in particular the input files used for the results presented below. The documentation file `Input_glue.DOKU` explains all parameters and, if necessary, their possible values, see appendix **??**, p. **??**. As described above, the program allows to glue any two surfaces from the above list. In order to shorten the calculations in the case where both surfaces agree, we have introduced a parameter `samesurface` which can take the values `1` (different surfaces) and `0` (identical surfaces). If the second surface is supposed to be inverted at a sphere with centre close to the surface, the parameter `inverse` is set to `0`, otherwise, it is set to `1`. In the first case, we have to specify the radius `rad` of the inversion. If we wish to place a cylinder between the surfaces, we can do so by setting the parameter `withcyl` to `0` and specify a small number `adv` by which the cylinder shall be pushed out of the surface; otherwise, we set `withcyl` to `1`.

Now, we can begin with the specifications of the first surface. We can specify the number `ilz` of refinements the first surface will undergo before a hole is cut into it – this number implicitly determines the size of the hole –, the number `ilz2` of refinements it will undergo after the cutting out of the hole, the `genus` of the surface, and the number `ii1` of the triangle that is to be deleted. Then, we decide what kind of surface we wish to use. If we want to use a surface parametrised over the sphere as in items (A) or (A') in the above list, we set `projection` to `0`, `genus` to `0`, and choose a value for the parameter `surface`. Possible choices are `0` for the round sphere of radius one, `1` for the "crushed sphere" depicted in figure 3.6, `3` for the surface depicted in figure 3.4, `5` for the Willmore sphere, `6` for the dumbbell of figure 3.3, `7` for the ufo-like surface of figure 3.7, `8` for figure 3.8, and `9` for an ellipsoid as in figure 3.10. If we want to use a dumbbell that has been constructed with glueing scheme itself (see figure 3.9) we choose `genus` $= 0$, `projection` $= 2$. There is no need to assign a value to `surface` in that case. We can also choose to glue a torus. Then, we set `genus` $= 1$, `projection` $= 3$, and specify the outer and inner radii `r0, r1`. If we glue any other surface, we set `projection` to -1 and copy the data of the triangulation into a file called `triang.choose`.

Afterwards, we go through a similar process for the second surface. If the second surface is inverted, it is possible to refine the neighbourhood of the hole a certain number `ilz3` of times. Also, we can turn the second surface around the outer normal of the hole through any of the five angles that leave the regular hexagon invariant. The angle is specified by assigning a value $0, \ldots, 5$ to `rotangle`. Finally, we can smooth the glued surface with an iterative procedure called `discrete_mcf(mcf_freq, projection)` explained below, the frequency of which is decoded by `mcf_freq`.

(Output). The output of the glueing scheme consists of a triangulation for the glued surface saved in `triang.glued` and of a figure in GRAPE format saved as `GRAPE2309`.

Data Structure

In this paragraph, we describe the data structure[8] we use to represent the mesh of a discrete surface. A paper model of a macro dumbbell mesh can be found on page 49. A vertex of a surface mesh is called *inner* if it is a topologically inner point of the surface, otherwise it is called *outer*. A mesh is characterised by

- three integers `nt,ne,nv` that represent the number of triangles, edges, and vertices, respectively,
- by `3`×`nv` reals `x(1,i),x(2,i),x(3,i)` that represent the three Cartesian coordinates of the `i`-th vertex,
- by `nv` integers `itype(i)` that represent the type of the `i`-th vertex: `0` = inner vertex, `1` = outer vertex,
- by `3`×`nt` integers `itnode(1,i),itnode(2,i),itnode(3,i)` that represent the numbers of the vertices belonging to the `i`-th triangle
- by `3`×`nt` integers `itneig(1,i),itneig(2,i),itneig(3,i)` representing the numbers of the triangles neighbouring the `i`-th triangle, internally enumerated with their opposing vertices,
- and by `nt` integers `irefed(i)` defining the refinement edge of the `i`-th triangle, i. e. which edge with internal number 1, 2, or 3, enumerated with its opposing vertex, is supposed to be refined first.

Note that the data structure does not explicitly tell whether the surface it represents is embedded or not. Knowing that we only work with oriented surfaces, we can calculate the Euler characteristic of a given discrete surface from its triangulation by using the formula $\chi(\Sigma_h) = \texttt{nt} - \texttt{ne} + \texttt{nv}$ introduced in chapter 1. We should remark that not all possible values of this data structure represent discrete surfaces; choose the origin as the position of all vertices, for example. Also, for technical reasons, all triangles need to be consistently oriented.

Example. A non-refined spherical mesh would be saved as the list

8 12 6 | 1. 0. 0. 0 | 0. 1. 0. 0 | -1. 0. 0. 0 | 0. -1. 0. 0 | 0. 0. 1. 0 | 0. 0. -1. 0 | 1 2 5 | 2 3 5 | 3 4 5 | 4 1 5 | 2 1 6 | 3 2 6 | 4 3 6 | 1 4 6 | 2 4 5 | 3 1 6 | 4 2 7 | 1 3 8 | 8 6 1 | 5 7 2 | 6 8 3 | 7 5 4 | 3 | 3 | 3 | 3 | 3 | 3 | 3 | 3

that signifies that the mesh consists of 8 triangles, 12 edges, and 6 vertices. The first vertex has the coordinates $(1, 0, 0)^t$ and is inner, the second vertex has the coordinates $(0, 1, 0)^t$ and is also inner etc. The first triangle consists of the vertices with numbers 1, 2, and 5, the second of those with numbers 2, 3, and, 5, etc. All refinement edges have been set to

[8] This data structure was communicated to the author by G. Dziuk and M. Fried.

3, this does not affect the appearance of the surface, though. A figure of this octahedral mesh is shown below in figure 3.11.

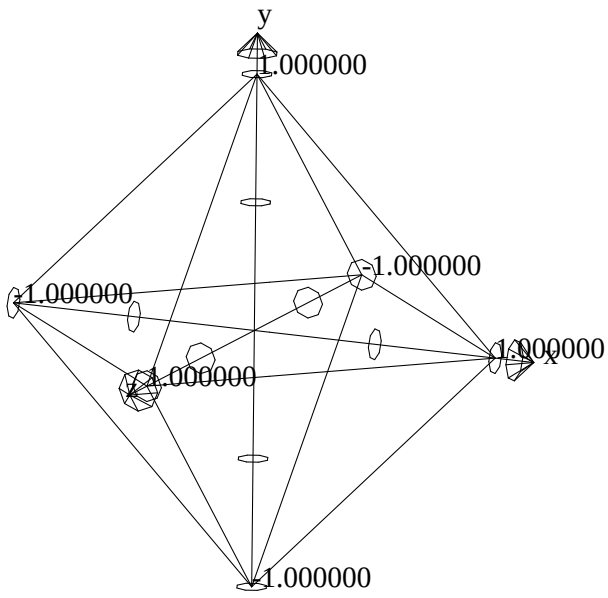

Figure 3.11: Octahedron with coordinate axes.

A continuous piecewise linear map from a discrete surface to $\mathbb{R}$ or $\mathbb{R}^3$ is represented by its values on the vertices, i. e. as a list of `nv` or $3\times$`nv` reals, respectively. This representation is justified by remark 3.2.

Structure of the Program

In this paragraph, we will describe the structure of the glueing program. A flow chart can be found on page 50. Some of the subroutines (macro triangulations, refining, ustart_glue, projecting, etc.) are discussed to more detail in section 3.2.3. Figures following the course of the algorithm can be found in section 3.3 below. The program works as follows:

- The parameters `samesurface, inverse, rad, withcyl`, and `adv` are read and tested for compatibility. For example, if one surface is inverted, a cylinder should not be used.

(1) The parameters for the first surface, namely `ilz, ilz2, genus, surface, ii1, projection, r0, r1` are read and tested for compatibility. `genus, surface, r0, r1, projection` are global variables, the others are local.

- The chosen macro-triangulation is read by the subroutine `macro_glue(projection)`. The prepared files are called `triang.sphere` (non-refined round sphere mesh by M. Fried; `projection` $= 0$), `triang.dumbbell` (refined glued dumbbell mesh constructed with the glueing scheme; `projection` $= 2$), `triang.torus` (non-refined

torus mesh; `projection` = 3), or `triang.choose` (any mesh the user has made available; `projection` = −1).

- The mesh is refined `ilz` times with a variant of M. Fried's and G. Dziuk's subroutine `refglobal_glue (ilz, neighs, projection)`. `neighs` is a zero vector at this point, `projection` determines to which surface the vertices shall be projected. If the surface is a torus, the mesh is improved by `discrete_mcf(5, 3)`, see below.

- A triangular hole is pierced into the surface with `pierce (ii1, which, neighs)`. The triangle with number `ii1` is deleted; `which` describes the vertices, `neighs` the neighbours of this triangle. The refinement edges of the neighbours of the hole are set such that they do not agree with the outer edges. See figure 3.17.

- The mesh is further refined `ilz2` times with the subroutine `refglobal_glue (ilz, neighs, projection)`. `neighs` is updated. As the refinement edges of the neighbours of the hole have not agreed with the outer edges in the step above, the hole keeps its triangular form. Again, we set the refinement edges of the neighbours of the hole such that they do not agree with the outer edges.

- We calculate the centre of mass, `mass`, of the three vertices neighbouring the hole (saved in `which`), the minimal distance of `mass` to these three vertices, `eps`, and `L` = 3 × `eps` in case a cylinder is to be glued between the surfaces. `L` represents half of the length of the cylinder, `eps` its radius. `eps, L` are global variables.

- Using the subroutine `trianglein (which, neighs, mass, eps)`, we first inscribe a smaller triangle into the hole and triangulate the remainder. Then, the inscribed triangle is equilaterised by `triangleequi (which, mass, prop)`. Inscribing a smaller triangle first ensures that the equilaterising process does not lead to overlapping edges, see below. `which, neighs, mass, eps` are updated. See figure 3.18 for the first part.

- We fit a regular hexagon into the triangle given by `which` in the subroutine `six (mass, which, neighs, sixneighs, intarray, surf)`. The centre of mass of the hole, `mass`, is updated. `sixneighs` takes over the rôle of `neighs`, i. e. marks the six neighbouring triangles of the hole. Similarly, the first six entries in the vector `intarray` take the rôle of `which` and save the numbers of the outer vertices. `surf` represents the number of the surface and is hence `1` in the present case, see figure 3.19.

- Now, we smooth the surface close to the hexagon by adding in three additional vertices by calling `smooth (neighs, sixneighs, projection, surf, inverse, 0)`. The new vertices will be projected onto the surface depending on the value of `projection`, see figure 3.20.

- In case we are working with a round sphere, this sphere will now be deformed to its final geometric form determined by `surface` via `ustart_glue()` by G. Dziuk, for example to an ellipsoid.

(2) We update the centre of mass of the hole called `mass`, update `eps, L` as radius and half of the length of the cylinder and then equilaterise the hexagon by appealing to `equilaterise (0, intarray, mass, eps)`. Again, we update `L`.

(3) In order to bring the surface to its nearly final glueing position, we translate the hole surface such that the centre of mass comes to lie at the origin. Then, we calculate the outer `normal` of the hexagon and rotate the surface about the origin so that the outer normal points in direction of the x_3-axis.

(4) We advance the cylinder by `adv` via `advance (intarray, adv, surf)` and translate the surface to its final position where the centre of mass of the hole lies at $(0, 0, -\mathtt{L} - \mathtt{eps} \times \mathtt{adv})^t$.

(5) Now, we save the mesh of the surface into a file called `triang.glued.1` (with the routine `write_glue (1)` by M. Fried), save a picture in GRAPE format in the file `GRAPE1` (with `movie (1)` by M. Fried and G. Dziuk), and save the coordinates of the six outer vertices with the aid of a matrix variable called `array`.

- Having finished with the first surface, we take care of the second one. If the variable `samesurface` $= 0$, we reflect the coordinate vectors of all vertices of the first surface at the x, y-plane through the origin (`reflect (point, vector)`). We re-orient all triangles with `orient()`. Then, we save the coordinates of the six outer vertices of the reflected surface to `array` and the internal numbers of these vertices to `intarray`. Again, we write the mesh into a file `triang.glued.3` and save a picture in GRAPE format to `GRAPE3`. We discard all superfluous information from `Input_glue`.

- If `samesurface` $= 1$, we set `surf` $= 2$ and go through all steps from (1) to (2) with the second surface.

- If `inverse` $= 0$, we invert the surface at the sphere with centre in the centre of mass of the hexagonal hole and radius `rad` by `invert (centre, rad)`. Afterwards, we re-orient the triangles with `orient()` and update the centre of mass.

- In any case, we rescale the second surface such that the regular hexagonal hole agrees in size with the one of the first surface (and such that the centre of mass of the hole remains invariant).

- Now, we go through steps (3) and (4). Then, we reflect the second surface at the x, y-plane so that it comes to lie opposite to the first one. We go through step (5) but save the information to the entries at the back of `array` and `intarray`, respectively.

- If `rotangle` takes a value of 1 through 5, we rearrange the coordinates saved in `array` and the internal vertex numbers saved in `intarray` in their order corresponding to the value of `rotangle`. The actual turning takes place in the step below.

- We rotate the second surface about the outer normal of the hexagonal hole with `turn (array)` so that both holes are mirror images of each other with respect to the x, y-plane through the origin.

- Having done so, we save the mesh of the second surface into a file called `triang.glued.3`, save a picture in GRAPE format in the file `GRAPE3`.

- If `withcyl` $= 0$, we use the subroutine `construct (array, intarray)` to construct a hexagonal cylinder that fits exactly between the hexagonal holes of the two surfaces. `array` and `intarray` provide the necessary information, the mid part of `intarray` is used to save the internal numbers of the outer vertices of the cylinder. The mesh of the cylinder is written to the file `triang.6cylinder`. We can hence treat the cylinder just as any other surface, load its mesh from `triang.6cylinder` with `macro_glue(1)`, and refine it twice (`refglobal_glue (2, neighs, 1)` with `neighs` $= 0$). Then, we save its mesh into a file called `triang.glued.2`, and save a picture in GRAPE format in the file `GRAPE2`, cf. figure 3.13.

- In any case, `mergesurfaces (intarray, withcyl, NSIX)` glues the surfaces together by identifying the corresponding vertices and adapting the neighbourhoods. `NSIX` represents the number of the last outer vertex of the second surface.

- A plausibility test is performed: we check whether the Euler characteristic[9] of the surface calculated from its genus agrees with the number `nt` $-$ `ne` $+$ `nv`.

- Finally, we use a smoothing method of G. Dziuk, `discrete_mcf (mcf_freq, -1)`, to smooth the mesh of the glued surface. The method consists of iteratively moving each vertex to the centre of mass of its neighbours with frequency `mcf_freq`. Then, the output is generated.

Having in mind our definition of discrete (immersed) surfaces, we have to justify why the glueing scheme generates data structures that really represent surfaces. All surfaces in the list on page 39 are indeed discrete surfaces. As the scheme allows the user to use his or her own data as an input, we have to make the assumption that those really are discrete surfaces. Further, we assume that the refinement process generates data belonging to a discrete surface if it starts with two discrete surfaces. Under these assumptions, the glueing scheme usually produces data belonging to a discrete surface by the following argument:

The piercing subroutine does not generate data representing a surface as surfaces are closed by definition in this text. We can argue that the data still represents a discrete "surface with boundary"[10]. This is not changed by the subroutine `trianglein(...)`. The subsequent equilaterising subroutine `triangleequi(...)` does not lead to degeneration, see section 3.2.3, below. Neither does the inscribing of a hexagon performed by `six(...)` nor the smoothing of the hexagon done by `smooth(...)`, see 3.2.3. The subroutine `ustart_glue()` performs a deformation of the surface and hence does not affect its non-degeneracy. The subroutine `equilaterise(...)` might cause degeneration but will not usually do so, see also section 3.2.3. After this, only bijective conformal mappings are applied "to the data" before it is glued – in fact, they are only applied to the vertices

[9] cf. p. 5.

[10] see [Lee03]; we will from now on consider those generalised surfaces as surfaces for notational simplicity.

and can thus be understood as locally injective, continuous piecewise linear mappings as discussed above.

The glueing or merging itself does obviously not cause any deformations in the case when the surfaces we are glueing do not intersect (in their final positions), see for example the dumbbell in figure 3.12 or the glued tori at the end of this section. If the surfaces do intersect (in their final positions), we have to name a discrete surface which acts as the parametric domain of the surface represented by the output data. We can do this as follows: by going over to the parametric domains of the input surfaces, we can assume that the surfaces we wish to glue are embedded. Leaving the glueing hexagon's edges where they are, we can deform both surfaces (or all three, if a cylinder is involved) in a manner that makes them disjoint. For example, scale up one of them and scale down the other. The resulting discrete embedded surface then acts as parametric domain for the discrete surface represented by the output data of the glueing scheme.

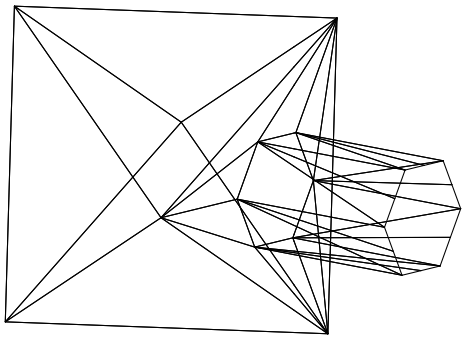

Figure 3.12: Non-refined dumbbell mesh viewed from the side and cut in half.

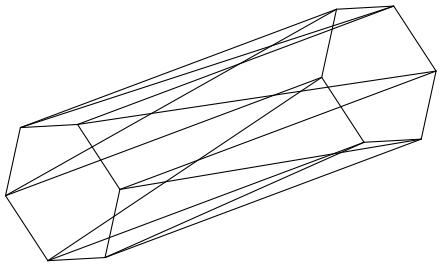

Figure 3.13: Non-refined cylinder mesh seen from the side.

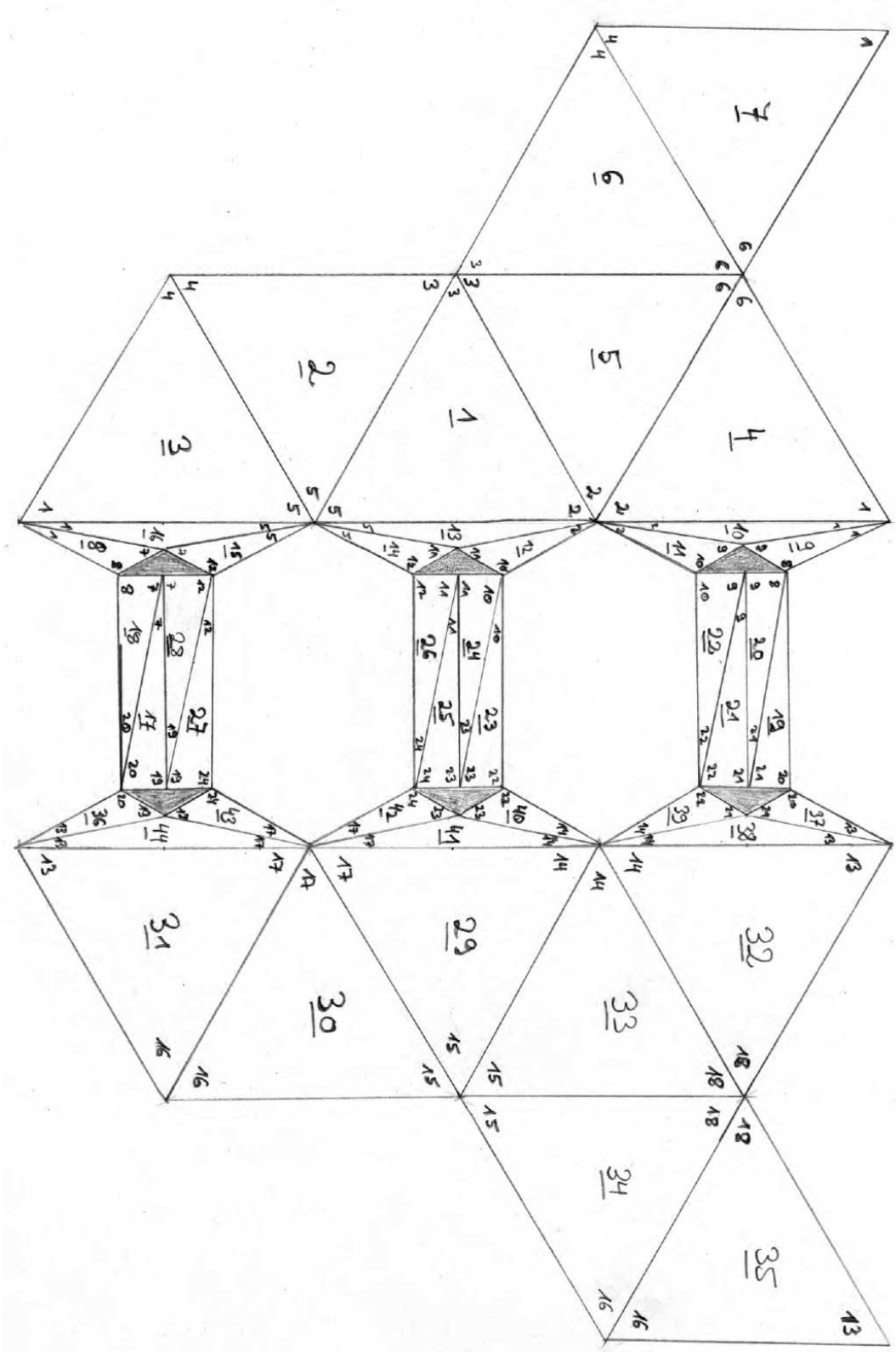

Figure 3.14: Dumbbell mesh paper model used as an aid for the implementation of the glueing scheme. Not exact. Please feel free to copy and glue together.

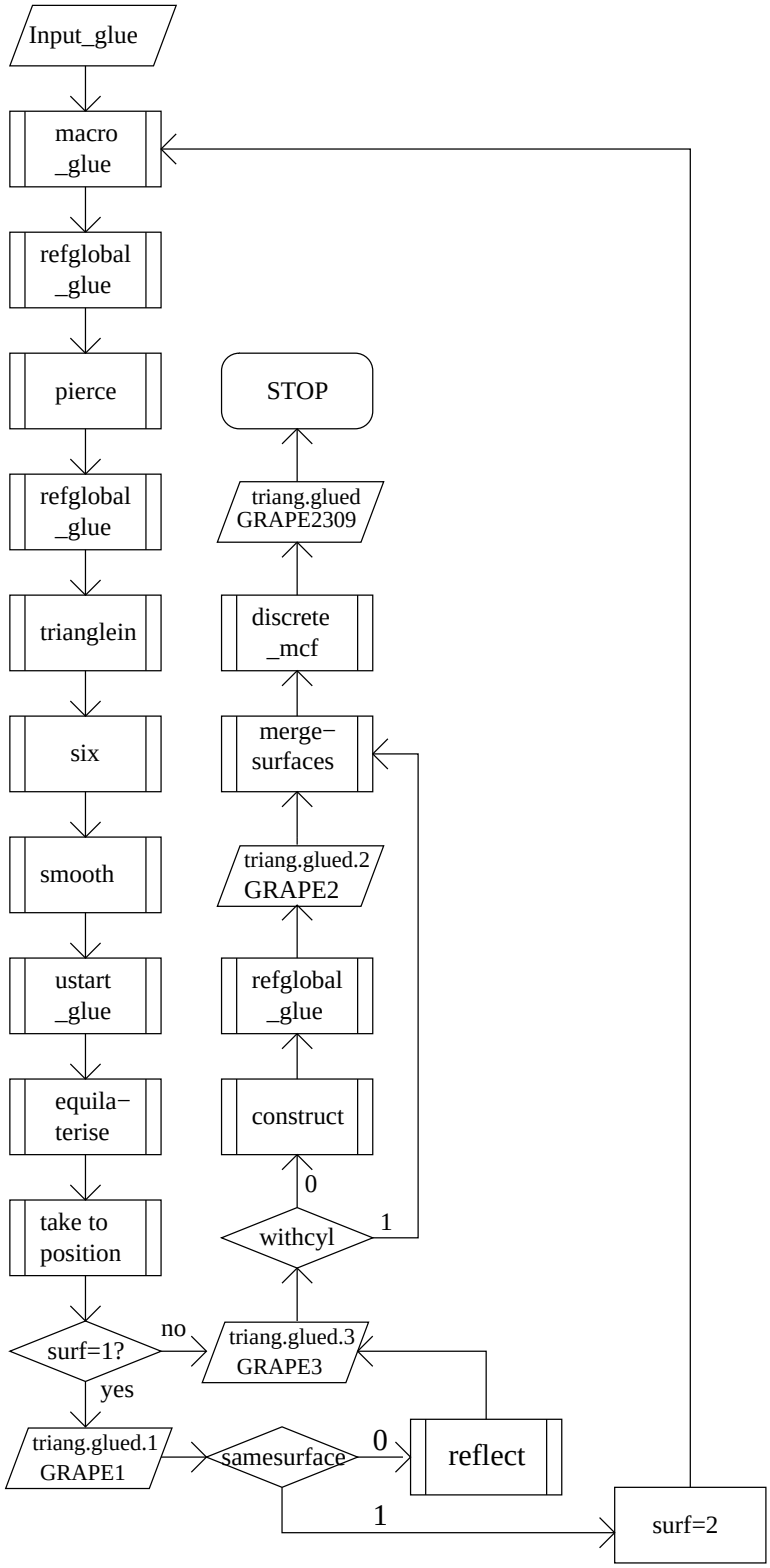

Figure 3.15: Flow chart for the glueing algorithm

3.2.3 Discrete Methods for Glueing

Having gone through the skeleton of the glueing method, we will subsequently discuss and justify some subroutines. The code of all these is included in the appendix.

Surface Representation

As we have described above, surface meshes are treated as specific data structures. These meshes allow to work with Finite Element Methods, see chapter 4. Starting with rather simple meshes, as for example an octahedral mesh as in figure 3.11 – we call these *macro meshes* or *macro triangulations* –, we get more complicated surfaces by applying parametrisations. This means that we do not need to find a new mesh for each different surface we would like to work with. Usually, we will refine[11] the mesh before we transform it. We use a standard refining procedure which we therefore do not explain here.

All surfaces listed under (A) and (A') on page 39 are such parametrisations over the round sphere mesh. The parametrisations are realised on data structure level by assigning new coordinates to all vertices. One can understand such a map as a continuous, locally injective, piecewise linear map by extending it linearly to the interiors of the triangles. For example, in the case of the "crushed sphere" depicted in figure 3.6, the new vertex coordinates are calculated by the rule $(\mathtt{x(1,i)}, \mathtt{x(2,i)}, \mathtt{x(3,i)})^t \mapsto (\mathtt{x(1,i)}, \mathtt{x(2,i)}, \frac{1}{2}\mathtt{x(3,i)})^t$ for all $\mathtt{i} = 1, \ldots, \mathtt{nt}$. This is the restriction of a linear transform of $\mathbb{R}^3$ and gives thus rise to a deformation of the round sphere mesh. In the glueing program, this deformation is applied by calling `ustart_glue()`.

The second basic mesh we work with is a toroidal mesh. Figures of it can be found on page 52. Any torus of revolution of a circular cross-section can easily be obtained from this torus by a deformation. When the radii of the torus are not "too different" from those used in the basic mesh, we can simply project[12] the mesh onto the surface with the prescribed radii. The third mesh also belongs to a topological sphere, it is a dumbbell mesh the author has constructed by the glueing scheme. A paper-model of a macro-version of this mesh can be found on page 49, a GRAPE picture of the macro-version is shown on page 48. When glueing with a cylinder we use a non-refined mesh of the form depicted in figure 3.13 and adapt the coordinates of the vertices.

Cutting Holes into Surfaces

Imitating the topological glueing construction, we glue two discrete surfaces together by cutting "small" topologically circular holes into both of them and identifying the boundaries of those holes. In order to prohibit the appearing of very acute angles in the case of glueing two round spheres, for example, we allow that this identification takes place with a cylinder between the surfaces.

[11] see also page 58 below for a discussion of the projection used when refining.
[12] see below for a discussion of the projection.

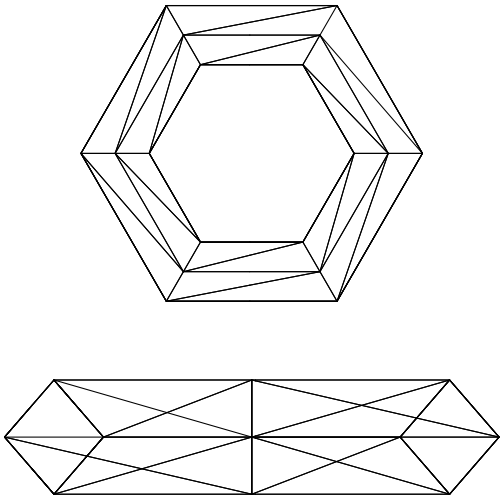

Figure 3.16: Non-refined torus mesh from above and from the side.

The easiest way to cut a hole into a triangulated surface the exact geometry of which might not be very well-known is to delete a triangle from the triangulation. The result is a discrete immersed or embedded surface that has a boundary consisting of three edges (at least, if the surface was closed before) – a topological circle. However, identification has not been convincing with triangles. Working without a cylinder, the glued surface usually seemed to have a "belt" around the glueing curve. This belt did not vanish when the Willmore flow was applied. On the other hand, working with a cylinder, a triangle did not allow the cylinder to become round when being refined. We have thus decided to glue via identification of higher order polygons inscribed into a triangular hole. Hexagons have provided the best results. The piercing procedure thus consists of cutting a triangular hole and inscribing a regular hexagon. The regularity of the hexagon allows to identify the boundaries of two pierced surfaces, straightforwardly.

On the data structure level, piercing consists of adapting the neighbourhood relations and the number `nt` of triangles of the mesh. The vertex numbers are not affected by the piercing procedure. In fact, we proceed as follows:

- save the numbers of the vertices of the deleted triangle to a vector `which`
- save the numbers of the neighbours of the hole to a vector `neigh`
- tell the neighbours of the hole that they lie on the border `itype` $= 1$
- adapt positions in the neighbour-list; the neighbours of the hole get negative neighbours in decreasing order
- adapt positions in the node-list; update `neighs` if necessary
- `nt`=`nt`-1
- make sure that no refinement edges are set to the border.

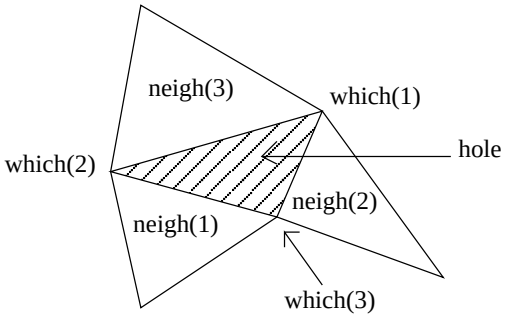

Figure 3.17: Triangular hole.

In general, the hole can have an irregular form. It can thus happen that very "ugly" triangles are produced when we inscribe a regular hexagon into the hole. It has proved convenient to inscribe a smaller equilateral triangle into the hole, inscribe a regular hexagonal hole into that, and refine its neighbourhood. The subroutine `trianglein(...)` inscribing a smaller triangle works along the following lines:

- set `NNTT`=`nt`
- calculate the centre of mass `mass` of the hole
- calculate the minimal distance `minprop` of `mass` to any of the hole's edges
- define three new vertices `x1, x2, x3` at distance $\frac{minprop}{2}$ of `mass`, `xi` lying on the line joining `mass` and the midpoint of the edge opposite of the `i`-th vertex, set their `itype` to `0`
- project these vertices to the surface[13]
- insert six new triangles around the hole, each joining either one of the new vertices with the edge of the same index or two of the new vertices with the old vertex saved in `which` having the same index
- set the neighbours of these new triangles as well as those of the former neighbours of the whole saved in `neigh`
- set the refinement edges of the new triangles such that the edges of the new hole are not affected
- update `which` and `neighs`
- update `nt`=`nt`+6, `ne`=`ne`+9, `nv`=`nv`+3
- refine the new triangles in pairs[14], update `neighs`
- improve the mesh with `discrete_mcf(mcf_freq, projection)`, see below
- equilaterise the hole with `triangleequi(...)`, see below

A sketch of the situation in the neighbourhood of the hole can be found on page 54.

[14] see below for a discussion of the projection
[14] with `refloc_glue(...)` by M. Fried.

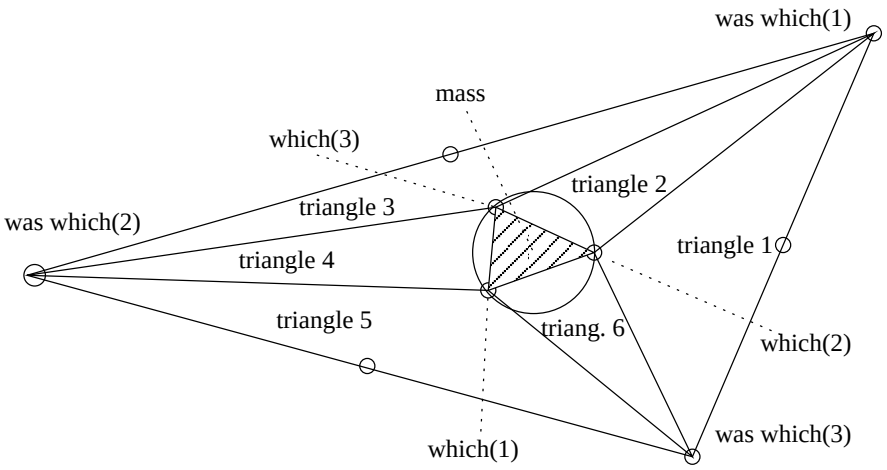

Figure 3.18: Inscribing a smaller triangle into a triangular hole – zoomed in on the hole.

As announced, the algorithm now equilaterises the triangular hole (see below) and inscribes a regular hexagon into this equilateral triangular hole. The geometric fact at the heart of this procedure is that the centre of mass separates the altitudes of an equilateral triangle in the ratio 1 : 2. Thus, the three points separating the part of the altitude that lies between the centre of mass and any vertex in the ratio 1 : 2 and the three points dividing the other part of the altitude in the ratio 2 : 1 all have the same distance from the centre of mass. Also they span a regular hexagon as the angle between two altitudes is $\frac{\pi}{3}$. The subroutine `six(mass, which, neighs, sixneighs, intarray, surf)` inscribes a regular hexagon with the vertices described above into the hole and fills the remainder with triangles as depicted in figure 3.19. The subroutine `smooth(...)` then refines the triangles around the hexagonal hole in order to adapt the mesh to the underlying surface it is supposed to approximate (although we should remark that the actual projection to the starting surface we have discussed above has not taken place yet), see figure 3.20. After the projection to the final geometric form, the hexagon needs to be taken back to its regular form. Nevertheless, it seemed easier to go through the steps in this order, as we can keep track of the well-definedness of the mesh and of its regularity since we know the exact "curvatures" of the non-projected surface – which is a sphere or a torus in most examples.

Let us now discuss the equilaterising strategies for triangles and hexagons. We begin with triangles (and the subroutine `triangleequi(which,mass,prop)`). We determine the biggest inner angle of the triangle and the shorter edge at this angle. We reduce the longer edge touching the biggest angle to the shorter edge's length. The triangle must now be isosceles. Now, we turn the formerly longer edge to the interior of the triangle until the angle reaches $\frac{\pi}{3}$ and obtain an equilateral triangle. As we have started by inscribing a small triangle into a larger one, the small having edge length at most a sixth of shortest altitude of the larger one, it is clear that the outside neighbourhood of this last is not affected by this equilaterising process. Also, only one vertex is moved in the equilaterising process. In the planar case we could argue that it remains in the convex hull of the neighbouring

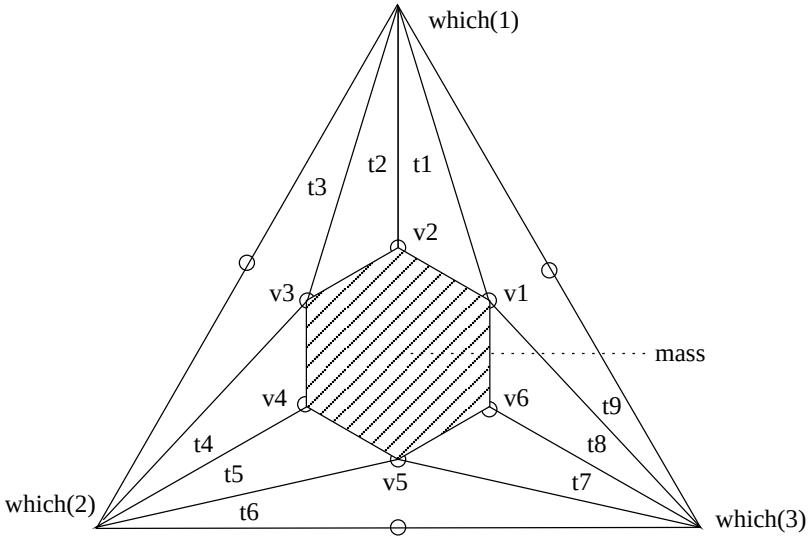

Figure 3.19: Inscribing a regular hexagon into an equilateral triangular hole. ti = i-th new triangle, vj = j-th new vertex, also called `sixneighs(j)`.

vertices so that the mesh does not overlap and hence still is well-defined. Arguing only in the neighbourhood of the moving point we find that by definition of discrete surfaces the interiors of triangles sharing a common point cannot overlap so that the mesh remains well-defined by Jordan's curve theorem. Inscribing a smaller triangle first thus ensures that the equilaterising process does not lead to overlapping edges. A sketch of the situation can be found on page 57.

We continue with the equilaterising method for hexagons. This method treats an irregular hexagon as split up into two triangles as in figure 3.22. Then both triangles are equilaterised individually. We shift one of them so that their respective centres of mass coincide and scale the larger one about this centre so that they agree in size. Subsequently, we turn one of them around the centre of mass to yield a regular hexagon. As we move four vertices in general, it can happen that the mesh is destroyed by this method. However, as we apply this method to a hexagon that is the projection onto a given surface of a regular hexagon, it will already be nearly regular in most cases so that the mesh remains non-overlapping.

Merging Surfaces

Having seen how the glueing scheme cuts regular hexagonal holes into surfaces, we will now discuss how such pierced surfaces are glued together by identifying the edges and vertices of the hole. In the topological setting, this means that we have cut out disks from two surfaces and now have to find a homeomorphism of the boundary circles. In the discrete setting, this homeomorphism will actually consist of a Euclidean motion and a dilation of one surface (at least if a cylinder is not involved). The algorithm is divided into two parts. The first step corresponds to effectuating the homeomorphism, the second one is to carry

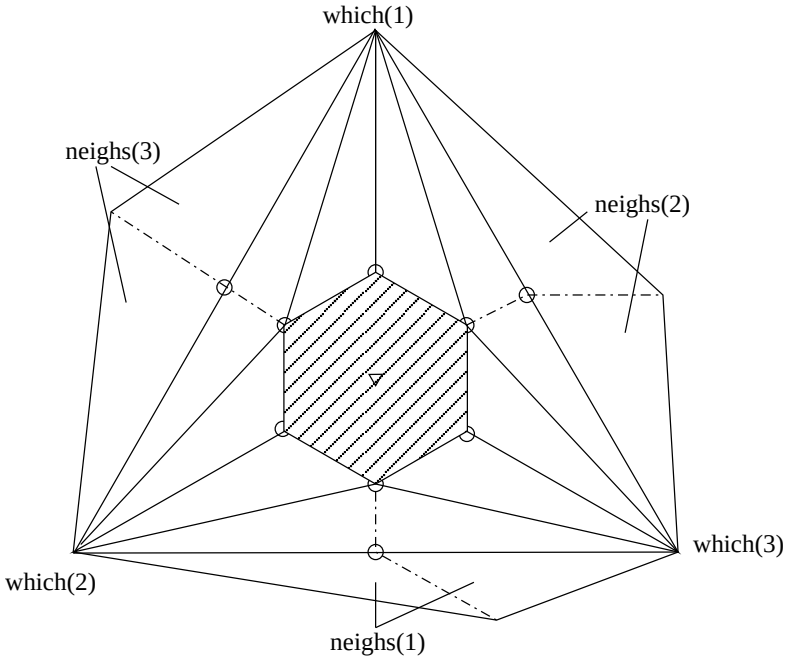

Figure 3.20: Smoothing around the hexagonal hole. The dashed lines are the new ones.

out the identification. We will only treat the variant without cylinder as the other one is very similar.

As both holes are regular hexagons, the homeomorphism can be chosen to be a composite of the following homeomorphisms. First dilate the surface having a larger hole about the centre of mass of the hole so that the hexagons are congruent. Secondly, move both surfaces in a way that the centres of mass of their holes coincide and the outer normals to their respective holes lie along the x_3-axis pointing in opposite directions. Thirdly, rotate one of them about the outer normal of its hole until the hexagons coincide. Now, we have to identify the vertices and the edges of the hexagons on data structure levels. In fact, to reach this goal, we define a new surface the mesh of which is represented by

- `nt` = number of triangles of the first surface (F) + number of triangles of the second surface (S)
- `ne` = number of edges of (F) + number of edges of (S) -6 (as twelve edges are identified in pairs)
- `nv` = number of vertices of (F) + number of vertices of (S) -6 (as twelve vertices are identified in pairs)

and by the merged lists of vertices, triangles, neighbours etc. When merging, we have to

- leave out those six coordinate triples belonging to the hexagon of (S) (the numbers of those had been saved in the vector `intarray`)

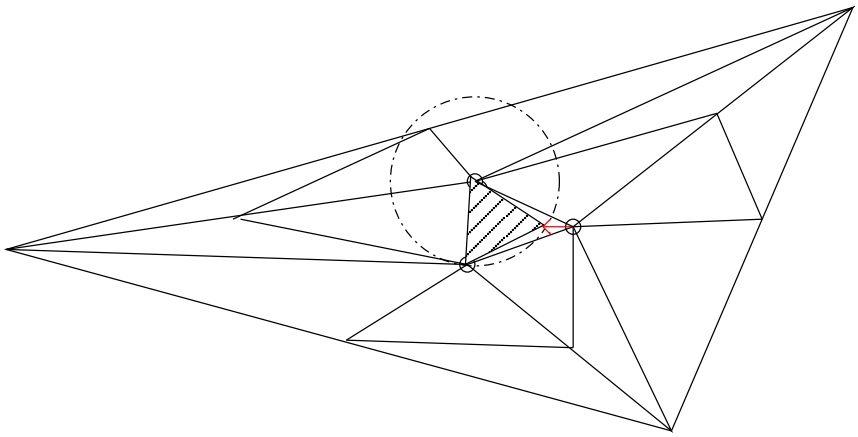

Figure 3.21: Sketch for the equilaterising of a triangle. The red arrow shows the movement of the vertex.

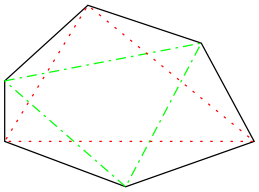

Figure 3.22: Two triangles combined to a hexagon.

- leave out the respective vertex types
- change the vertex types of the six hexagon vertices of (F) to `0`, i. e. to inner type (the numbers of those vertices had also been saved in the vector `intarray`)
- change the vertex numbers of triangles in (S) in the vicinity of the hole to the respective vertex numbers of (F) (the neighbours of the hole had been saved in the vector `sixneighs` and need not be calculated)
- change the neighbours of the neighbours of the hole in both (F) and (S) so that they neighbour each other adequately
- set the refinement edges of the neighbours of the hole such that the glueing edges are supposed to be refined.

This identification gives rise to a glued mesh representing the glued surface. If we know a projection formula for the glued surface as in the case of a dumbbell or of a round sphere pair where the second one is inverted, we can further refine the glued surface. In that case, setting the refinement edges to the glueing edges helps adapting the mesh in the glueing area.

Projection to Discrete Surfaces

Describing the glueing scheme we have often talked about the projection of a vertex onto a surface. This has no direct meaning as even arbitrary embedded discrete surfaces need not be the surface of a convex body and can hence induce sets of equidistance to different points of the surface. This happens for dumbbells, for example, cf. figure 3.23. Also, as the surfaces are not smooth, a closest point projection cannot always be calculated via outer normals to the surface. On the other hand, refining a surface mesh does not improve the mesh in what concerns its closeness to a given smooth surface if we do not project the new vertices onto the smooth surface. We have therefore decided to project as little as possible and, if "necessary", to project onto round spheres, tori, and dumbbells only as we have explicit formulae for these projections. This projection problem is the reason why we use our three standard models all through the glueing scheme and transform them to their final form at a very late point in the routine, namely after the surface has been equipped with a hexagonal hole.

The projection we use for the spherical case is $x \mapsto \frac{x}{|x|}$ where we use the Euclidean norm of $\mathbb{R}^3$. Here, we use that new vertices constructed in the refinement or in the piercing processes do not lie in the origin[15] but rather on the unrefined surface mesh. In the toroidal case with radii $r_0 > r_1$, we calculate the outer normal $N(x)$ to the torus of $x = (x_1, x_2, x_3)^t \in \mathbb{R}^3$ having the components

$$\begin{aligned} N_1(x) &= \frac{(1 - \frac{r_0}{\sqrt{x_1^2+x_2^2}})\, x_1}{\sqrt{(r_0 - \sqrt{x_1^2+x_2^2})^2 + x_3^2}}, \\ N_2(x) &= \frac{(1 - \frac{r_0}{\sqrt{x_1^2+x_2^2}})\, x_2}{\sqrt{(r_0 - \sqrt{x_1^2+x_2^2})^2 + x_3^2}}, \\ N_3(x) &= \frac{x_3}{\sqrt{(r_0 - \sqrt{x_1^2+x_2^2})^2 + x_3^2}} \end{aligned}$$

and then the projection onto the torus, $P(x) = x - (\sqrt{(r_0 - \sqrt{x_1^2+x_2^2})^2 + x_3^2} - r_1)\, N(x)$. In the case of the (glued) dumbbell, we have to deal with sets of equidistance. However, these sets only consist of several surfaces in $\mathbb{R}^3$ and have hence measure zero. It will thus very rarely happen that a point lying in one of the components of this set needs to be projected to the dumbbell. A cross-section of the dumbbell together with the set of equidistance can be found on page 59, a sketch of the surface on page 60. In this case, we project it to any point that is a closest point of it.

The dumbbell projection uses two symmetries of the dumbbell. The first symmetry is a rotational symmetry about the x_3-axis, the second one is a mirror symmetry about the x_1, x_2-plane. To utilise the first symmetry, we introduce the new variable $h(x) = \sqrt{x_1^2 + x_2^2}$. The projection can only be defined if $h(x) \neq 0$[16] and $x_3 \neq \pm(L+2)$ as it is not clear

[15] and not too close to it which is important numerically.
[16] or not too small, numerically speaking.

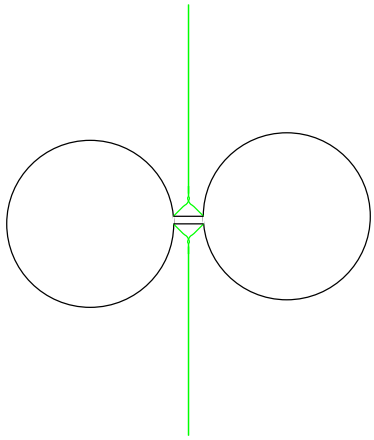

Figure 3.23: Sketch of cross-section of dumbbell with set of equidistance.

to where we should project in that case. This case, however will usually not happen as new vertices always lie on edges or inside triangles of the old mesh. In order to simplify the problem with the aid of the second symmetry, we always work with the absolute value of x_3. We use the variable *eps* as the radius of the cylinder and L as half its length (approximately, see below). In fact, we project onto a dumbbell with an (affine) linear interpolation between the spheres and the cylinder, see figure 3.24. The radius of the spheres is 1. We set *hsph* as the height of the meeting point of the linear interpolation and the sphere, and "elevation" as the elevation of the linear interpolation for $x_3 > 0$. The formulae are $hsph = \sqrt{1-(eps-1)^2}$ and $elevation = \frac{hsph-eps}{2eps}$. For each point $x = (x_1, x_2, x_3)^t \in \mathbb{R}^3$, we set $wside(x) = \text{sign}(x_3)$, where $\text{sign}(0) := 0$. We now calculate the minimal distances of x to each of the individual pieces constituting the dumbbell. We find $dcornl(x) = \sqrt{(h(x)-eps)^2 + (|x_3|-L+eps)^2}$, and similarly $dcornr(x) = \sqrt{(h(x)-hsph)^2 + (|x_3-L-eps|)^2}$, $dcyl(x) = |h(x)-eps|$ if $|x_3| \leq L-eps$ and $dcyl(x) = dcornl(x)$ otherwise, to be the distance of x to the lower (left) corner of the linear interpolation, to the higher (right) corner of the linear interpolation, and to the cylinder – by Pythagoras' theorem. In order to calculate the minimal distance to the linear interpolation, $dpol(x)$, we determine the squared distance of $(|x_3|, h(x))^t \in \mathbb{R}^+ \times \mathbb{R}^+$ to any point $(z, elevation\, z + elevation\, (L-eps) - eps)^t$ of the infinitely extended line which is the quadratic polynomial $d_x(z) = (elevation+1)\, z^2 - 2(|x_3| + h(x)\, elevation + elevation^2\, (L-eps) - elevation\, eps)\, z + (x_3^2 + h(x)^2 + (elevation\, (L-eps) - eps)^2)$. The minimal distance to the line then is the minimum of d_x, i. e. the root $z_0(x)$ of the first derivative of d_x. We find $z_0(x) = \frac{elevation^2\,(L-eps)+h(x)\,elevation+|x_3|-eps\,elevation}{1+elevation^2}$. We therefore determine the distance of x to the linear interpolation polynomial, $dpol(x)$, to equal the minimum of $dcornl(x)$, $dcornr(x)$ and, if $z_0(x) \in [L-eps, L+eps]$, of $\sqrt{(|x_3|-z_0)^2 + (h(x)-elevation\,(z_0-L+eps)-eps)^2}$. Finally, we find that the distance to the cut open sphere can be calculated as follows: set $eps_z(z) = \frac{hsph}{1-eps}\,(-|z|+L+1)$ – this describes the line joining the right corner of the linear interpolation map to the centre of the sphere – and then see that $dball(x) = dcornr(x)$ if $h(x) < eps_z(x_3)$ and $dball(x) = |\sqrt{h(x)^2 + (|x_3|-L-1)^2} - 1|$ otherwise.

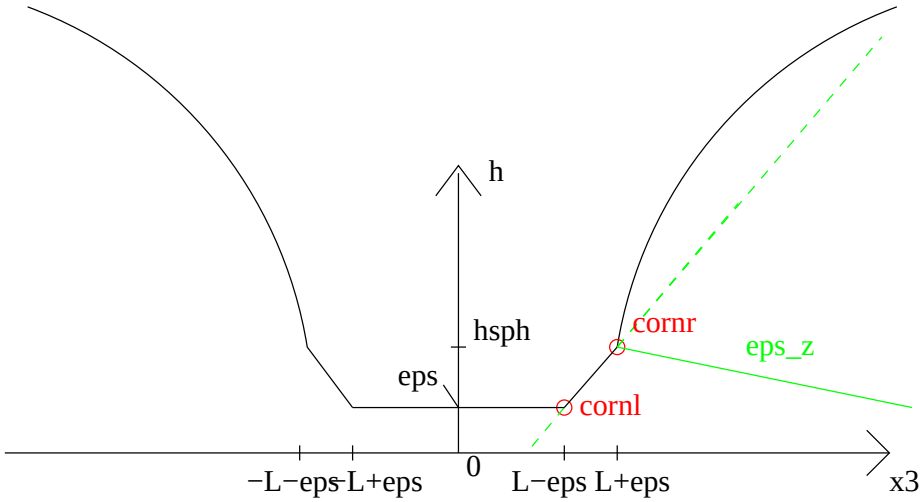

Figure 3.24: Cross-section of dumbbell with linear interpolation.

Having determined the distances of x to the individual pieces of the dumbbell, we compare these distances and set $mini(x)$ to their minimum and $miniwhich(x)$ to a number between 1 and 5, where 1 stands for minimal distance to the cylinder, 2 for minimal distance to the meeting point of the cylinder with the linear interpolation, 3 for minimal distance to the linear interpolation, 4 for minimal distance to the meeting point of the linear interpolation and the sphere, and 5 for minimal distance to the sphere. In critical cases (where two or more values agree) we proceed in the order: $1, 5, 3, 4, 2$ which means that in case $dcyl(x) = dball(x)$, $miniwhich(x)$ is set to 1 etc.

Then we project onto the respective part of the surface depending on $miniwhich(x)$. Remember that we project only in the case where $h(x) \neq 0$ if $x_3 \neq \pm(L+2)$. The projection onto the cylinder is given by $x \mapsto (\frac{eps\, x_1}{h(x)}, \frac{eps\, x_2}{h(x)}, x_3)^t$ (we can be sure that $|x_3| << L+2$ if we project onto the cylinder). We project to the left corner of the interpolation via $x \mapsto (\frac{eps\, x_1}{h(x)}, \frac{eps\, x_2}{h(x)}, (L - eps)\, wside(x))^t$ (again, $|x_3| << L+2$), and to the interpolation via $x \mapsto (\frac{r(x)\, x_1}{h(x)}, \frac{r(x)\, x_2}{h(x)}, z_0(x)\, wside(x))^t$, where $r = elevation\,(z_0(x) - L + eps) + eps$ (and again $|x_3| << L+2$). The projection to the right corner of the interpolation is given by the formula $x \mapsto (\frac{hsph\, x_1}{h(x)}, \frac{hsph\, x_2}{h(x)}, (L + eps)\, wside(x))^t$ (where again $|x_3| << L+2$). In the case of the sphere, we project via the orthogonal projection onto the sphere, namely by $x \mapsto (\frac{(x_1, x_2, x_3 - wside(x)\,(L+1))^t}{\sqrt{h(x)^2 + (|x_3| - (1+L))^2}}) + (0, 0, wside(x)\,(1+L))^t)$.

In fact, we also project onto a cylinder during the glueing process if we do not work with a dumbbell. This happens if a cylinder is glued in between two surfaces and this cylinder is refined. In that case, we use the canonical cylinder projection given by the formula $x = (x_1, x_2, x_3)^t \mapsto (eps\, \frac{x_1}{\sqrt{x_1^2 + x_2^2}}, eps\, \frac{x_2}{\sqrt{x_1^2 + x_2^2}}, x_3)^t$, where `eps` is the radius of the cylinder whenever $|x_3| \leq L$ when `L` is half the length of the cylinder.

Mesh Smoothing

We say that a mesh *is of low (high) quality* if the inner angles of the triangles in the mesh are (not) obtuse or acute. In his Willmore flow program, G. Dziuk measures mesh quality by measuring the minimal inner angle of all triangles contained in a given mesh (`winkel(...)`).

During the Willmore flow, but also in the glueing scheme, we can be confronted with low quality meshes. As we would like to apply the Willmore flow to the discrete surfaces discussed here, we have to consider methods that improve the mesh quality. We will present two options in this text. One of these is a local vertex displacement approach, the other is a global scheme using the concept of conformality. We will discuss the first one here and treat the second one in chapter 6.

In his Willmore flow scheme, G. Dziuk uses a local smoothing routine to improve the mesh quality. This method consists of iteratively moving each vertex to the centre of mass of its neighbours and to then project it back onto the given surface (in his case a round sphere). We understand that this technique is known as "Laplacian smoothing" in the literature[17]. In the glueing scheme, we apply this smoothing technique to round sphere, dumbbell, and torus meshes – by the name of `discrete_mcf(mcf_freq, projection)`[18]. As the vertices are not moved very far by this method, we only need to project points that lie very close to the surfaces so problems as described above will usually not arise. Tables showing the influence of this smoothing method onto a round sphere mesh and a torus mesh can be found on page 88.

However, we are also interested in smoothing the glued surfaces – for which we do not know an explicit projection. It turned out that the Laplacian smoothing technique delivers good results if we skip the projection of the vertices back to the surface. For example, if we call `discrete_mcf(mcf_freq, projection)` once or twice when glueing two surfaces with a cylinder, the glueing edges will get softer, see figure 3.25 below. A disadvantage of this smoothing method lies in the fact that the new vertices do not necessarily lie on the surface so that the mesh might not be a very good approximation to a given surface. In particular, the surface described by the mesh will shrink by an amount depending on the vertex density. This causes problems especially when the vertex density varies very strongly in the mesh as it is the case if an inverted surface is glued to a non-inverted one. It can then happen that the surface "shrinks" quickly where the mesh is coarse and virtually nothing changes where the mesh is dense, see figure 3.25.

[17] cf. p. 73 in [Hei03].
[18] "mcf" stands for "mean curvature flow".

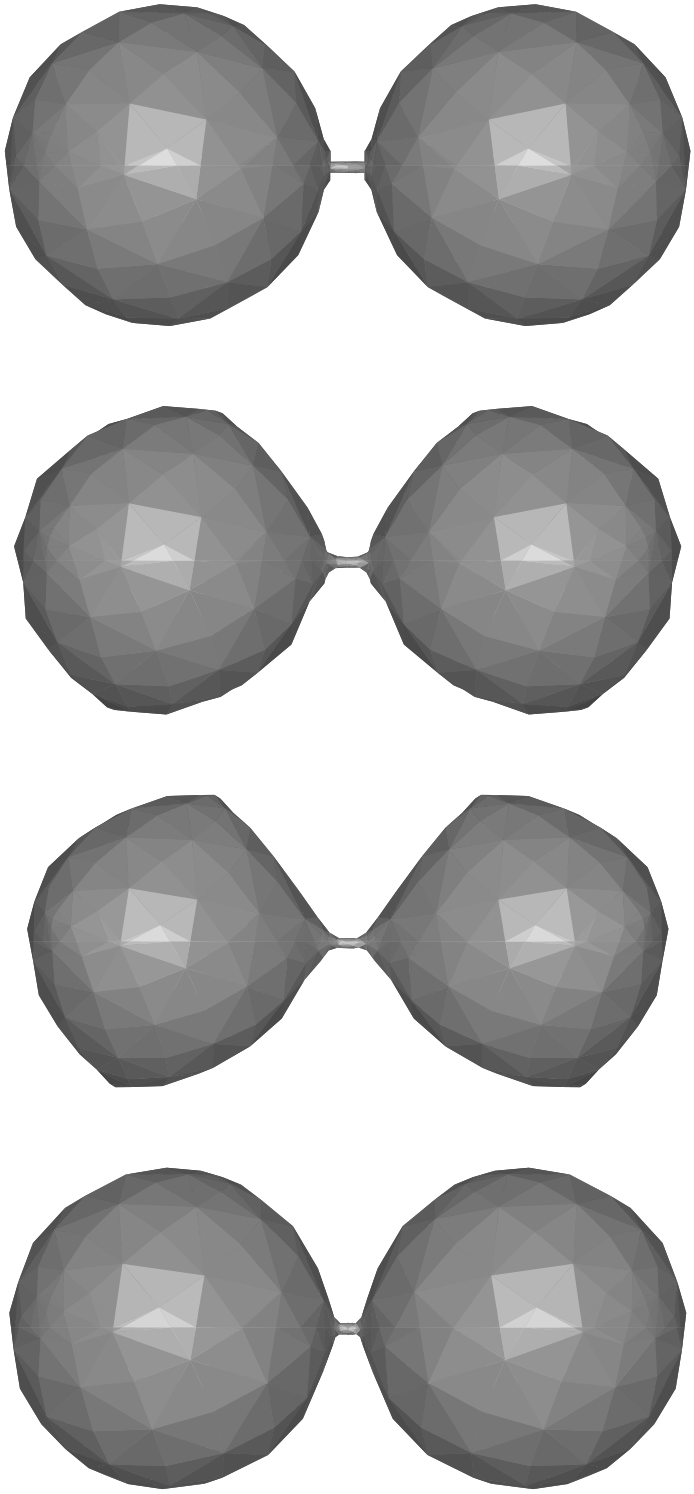

Figure 3.25: Dumbbell without and with Laplacian smoothing (once, twice without projection), twice with projection.

3.3 Results

Let us now have a look at the results of the glueing scheme. Figure 3.26 depicts a Clifford torus inverted at the centre of mass of a hexagonal hole. Figure 3.27 shows a cut open Willmore sphere with a round sphere glued to it at the inside. The parameters we have chosen are `samesurface` = 1, `inverse` = 1, `withcyl` = 0, `adv` = 0.0; for the Willmore sphere: `ilz` = 7, `ilz2` = 1, `genus` = 0, `surface` = 5, `ii1` = 1000, `projection` = 0; for the round sphere: `ilz` = 4, `ilz2` = 3, `genus` = 0, `surface` = 0, `ii1` = 1, `projection` = 0; for the glueing: `rotangle` = 0, and `mcf_freq` = 0. We also depict the glueing process with intermediate results; first we treat the glueing together of two tori with a cylinder in between. Afterwards, we depict the glueing together of one ellipsoid and one inverted ellipsoid.

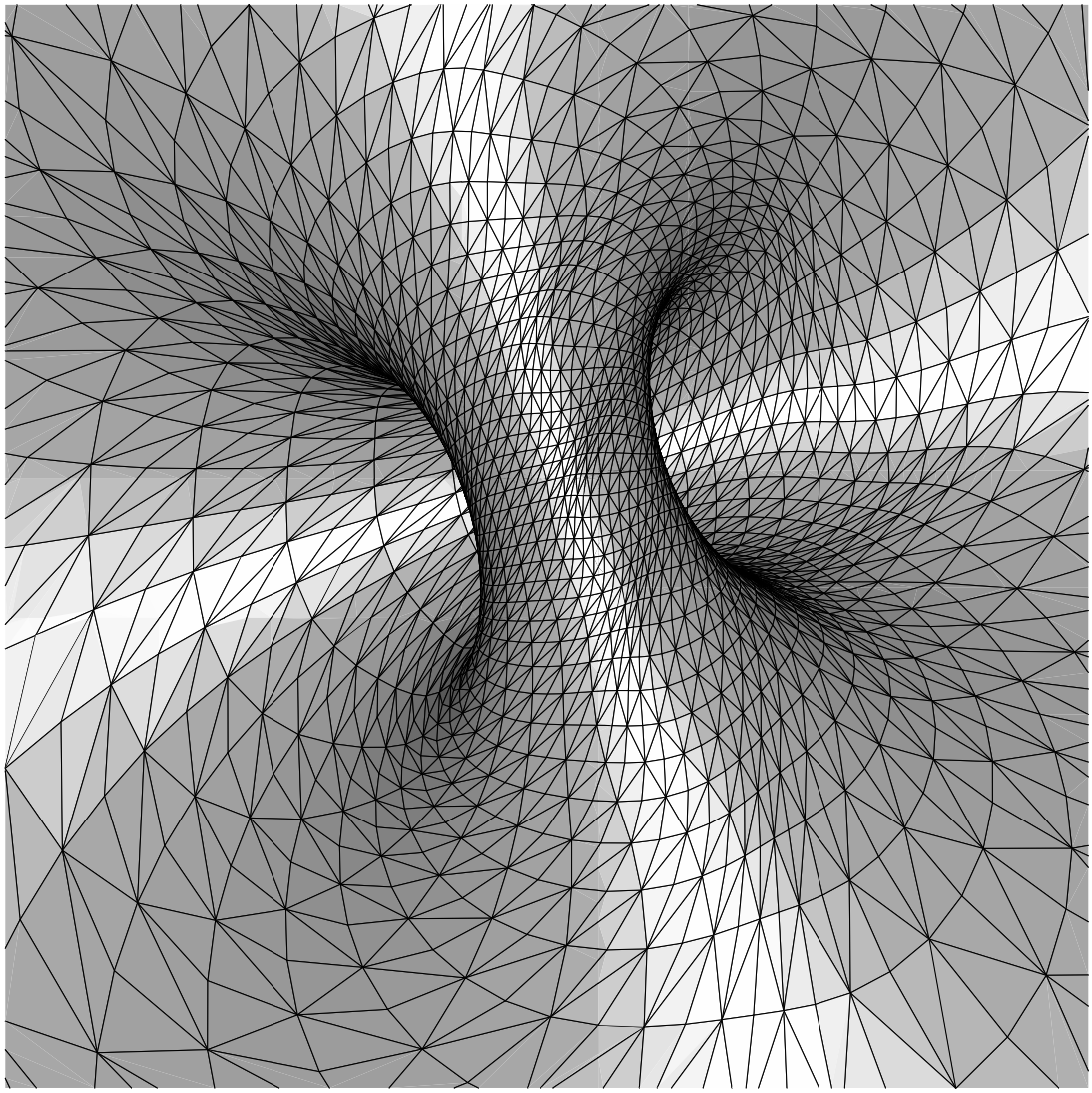

Figure 3.26: Inverted Clifford torus; only the interesting curved region is shown.

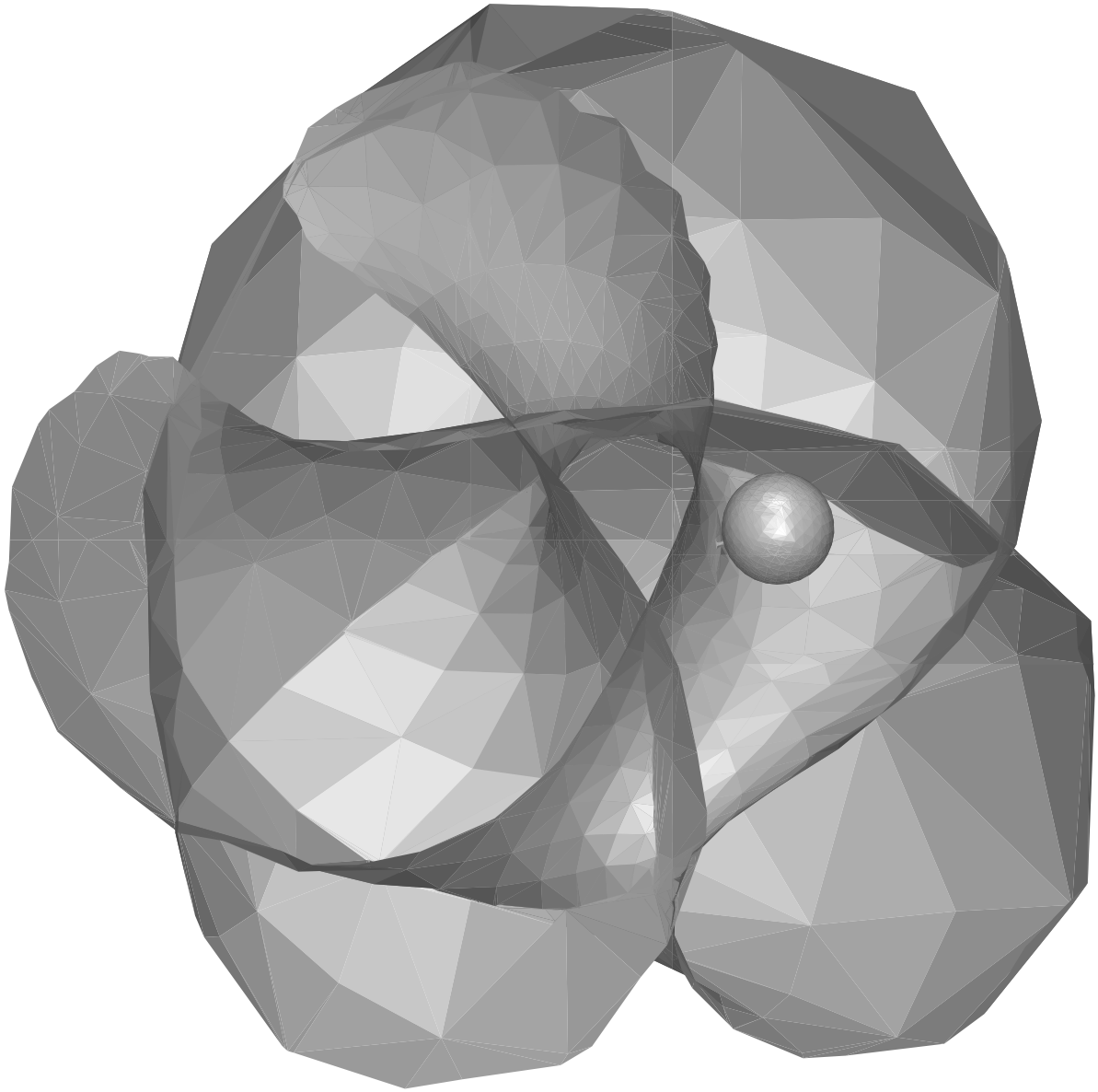

Figure 3.27: Willmore sphere with an inserted round sphere.

Glued Tori

The parameters chosen here are: `samesurface` = 0, `inverse` = 1, `withcyl` = 0, `adv` = 0.0, `ilz` = 5, `ilz2` = 2, `genus` = 1, `surface` = 0, `ii1` = 2, `projection` = 3, `r0` = 1.0, `r1` = 0.25, `rotangle` = 0, and `mcf_freq` = 0.

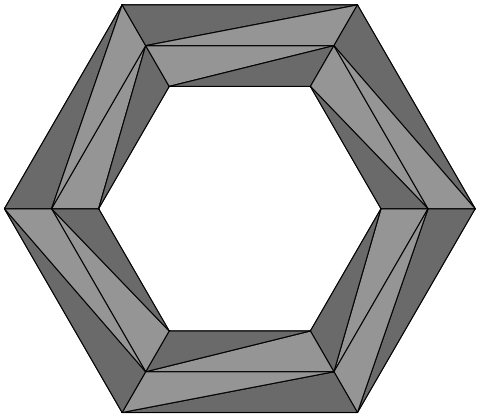

Figure 3.28: Macro triangulation used for the torus.

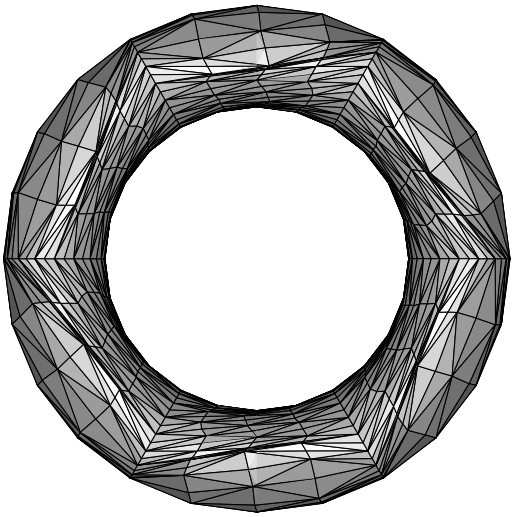

Figure 3.29: `ilz` times refined surface.

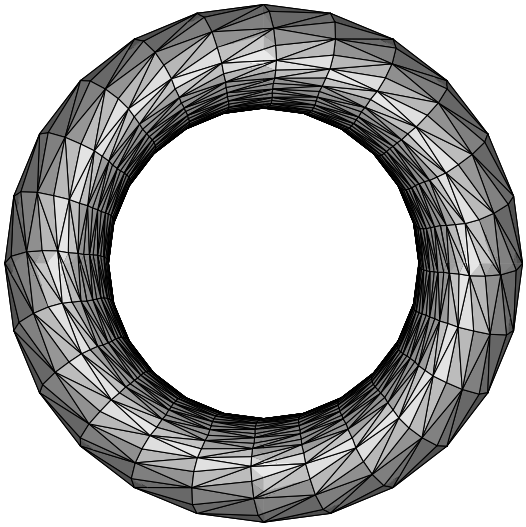

Figure 3.30: Improved mesh.

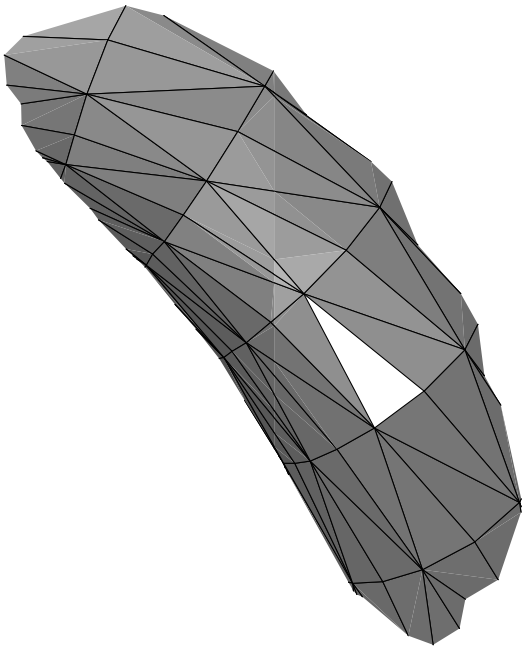

Figure 3.31: Pierced surface. Only small part depicted.

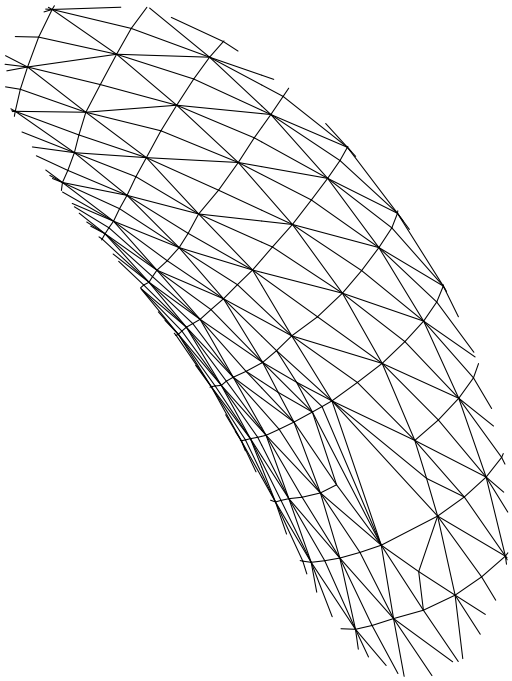

Figure 3.32: `ilz2` times refined pierced mesh. Only small part depicted.

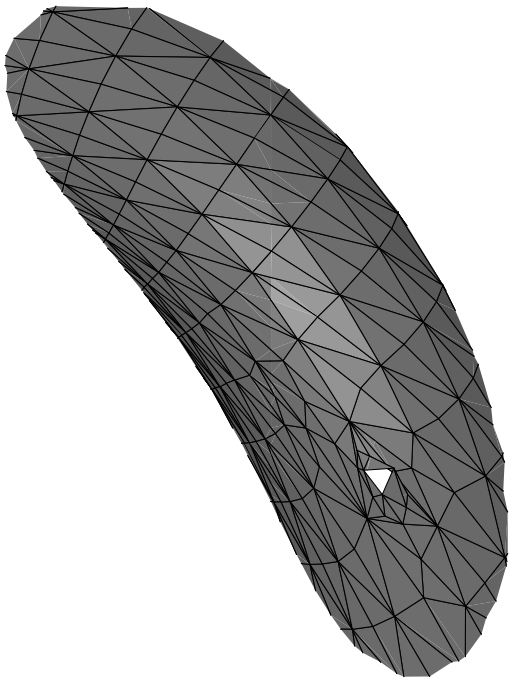

Figure 3.33: A smaller triangle has been inserted. Only small part depicted.

Figure 3.34: A hexagon has been inserted. Only small part depicted.

Figure 3.35: Neighbourhood of hexagon has been smoothed. Only small part depicted.

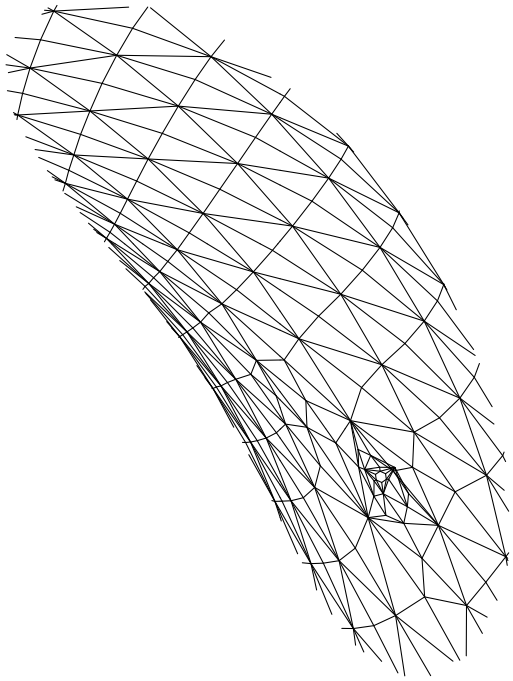

Figure 3.36: The same with mesh depicted. Only small part depicted.

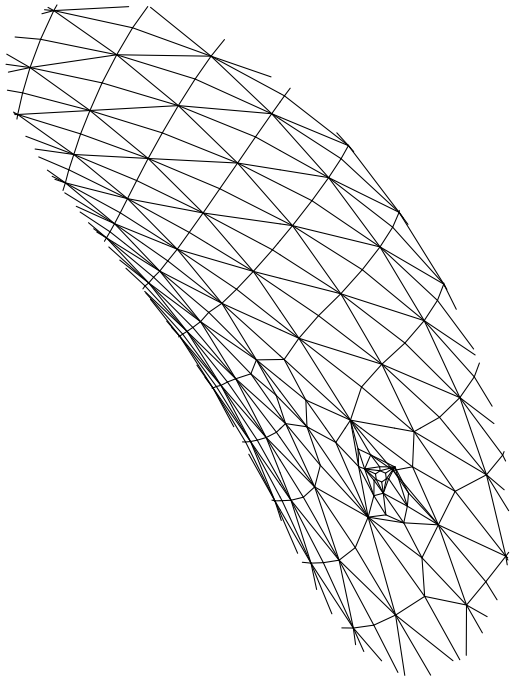

Figure 3.37: Mesh after `equilaterise(...)`. Only small part depicted.

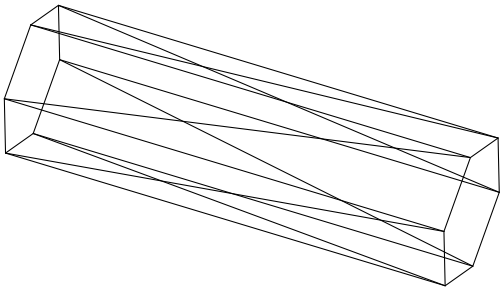

Figure 3.38: Macro triangulation used for the cylinder.

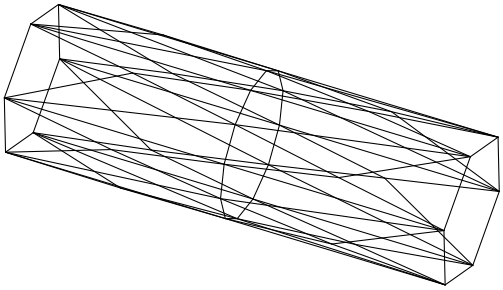

Figure 3.39: Refined cylinder mesh.

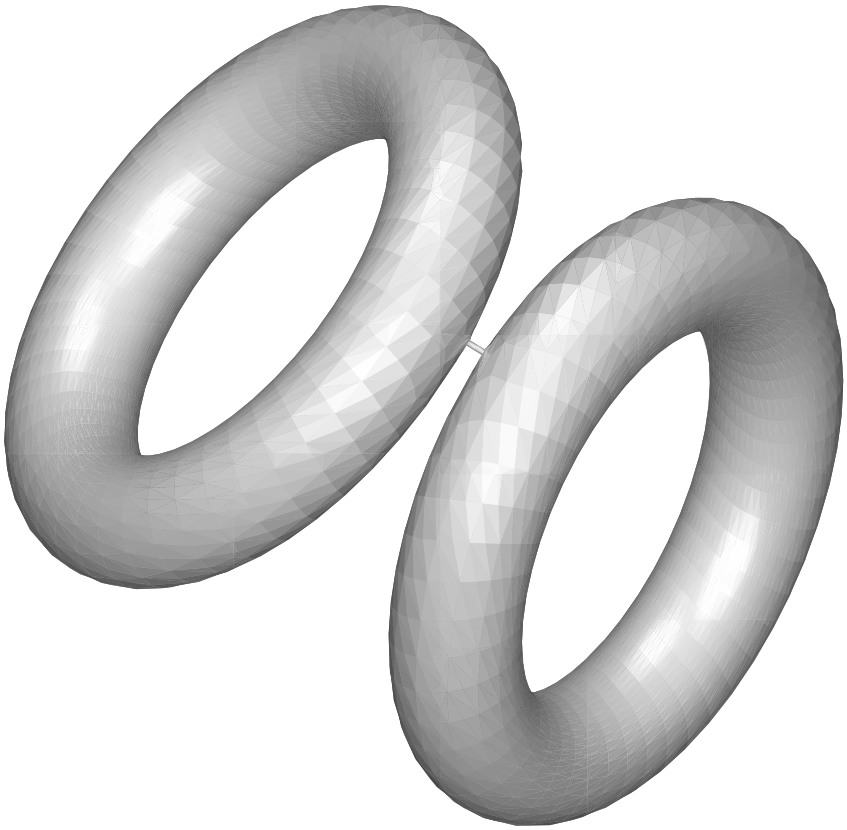

Figure 3.40: Glued surface.

Ellipsoid with Inserted Inverted Ellipsoid

The parameters chosen here are: `samesurface` = 1, `inverse` = 0, `rad` = 1.0, `withcyl` = 1; for the first surface: `ilz` = 5, `ilz2` = 2, `genus` = 0, `surface` = 9, `ii1` = 1, `projection` = 0; for the second surface: `ilz` = 5, `ilz2` = 2, `genus` = 0, `surface` = 9, `ii2` = 1, `projection` = 0, `ilz3` = 2 (refining about hexagonal hole), `rotangle` = 0, `mcf_freq` = 0.

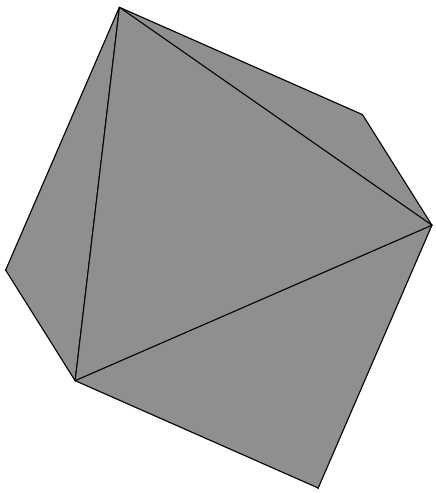

Figure 3.41: Macro triangulation used for the sphere.

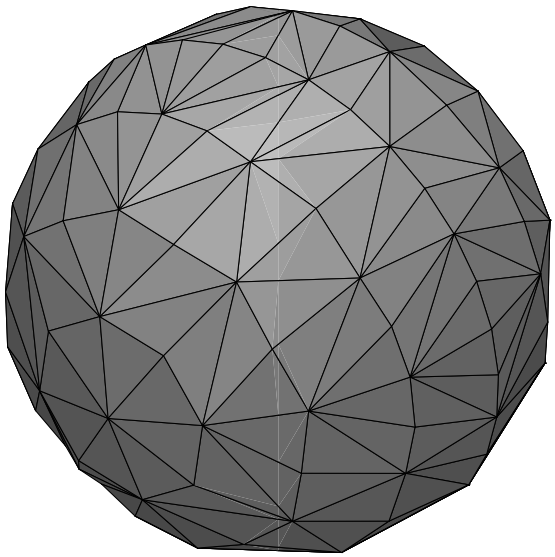

Figure 3.42: `ilz` times refined sphere.

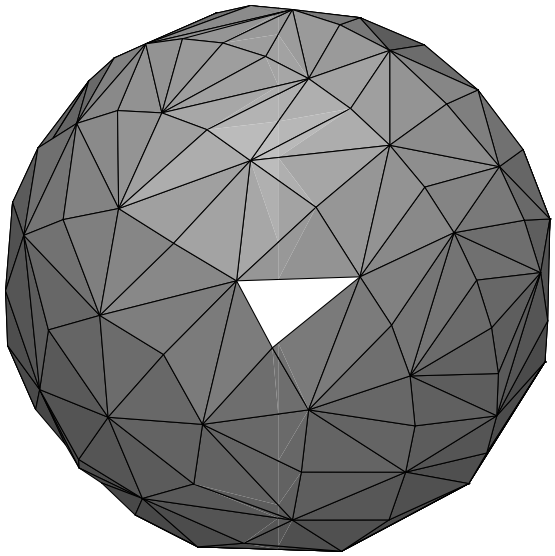

Figure 3.43: Pierced surface cut in half.

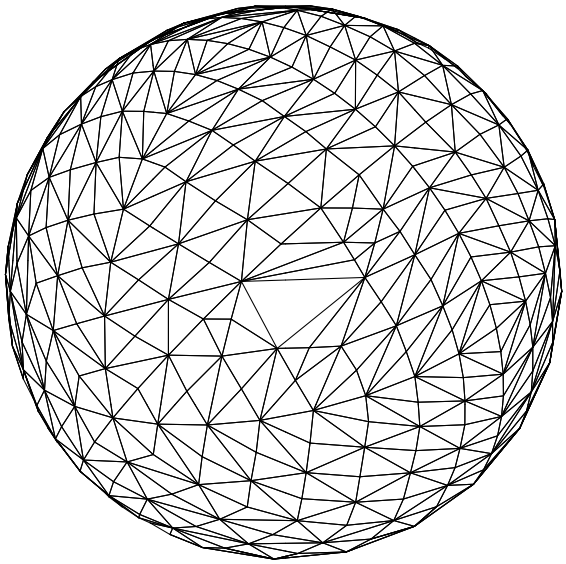

Figure 3.44: `ilz2` times refined pierced mesh. Cut in half.

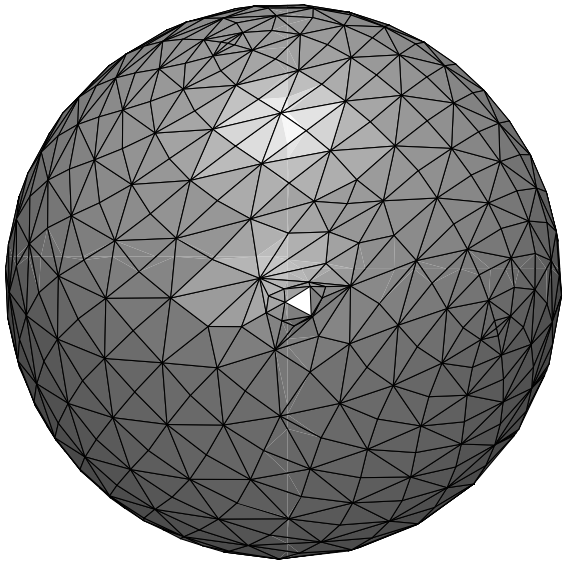

Figure 3.45: A smaller triangle has been inserted. Cut in half.

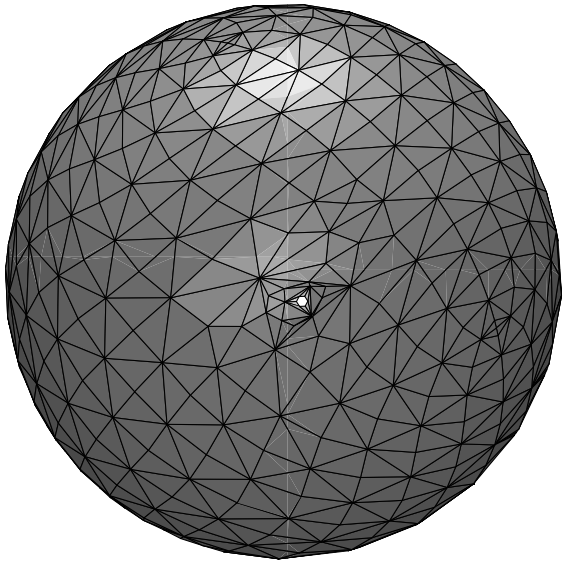

Figure 3.46: A hexagon has been inserted. Cut in half.

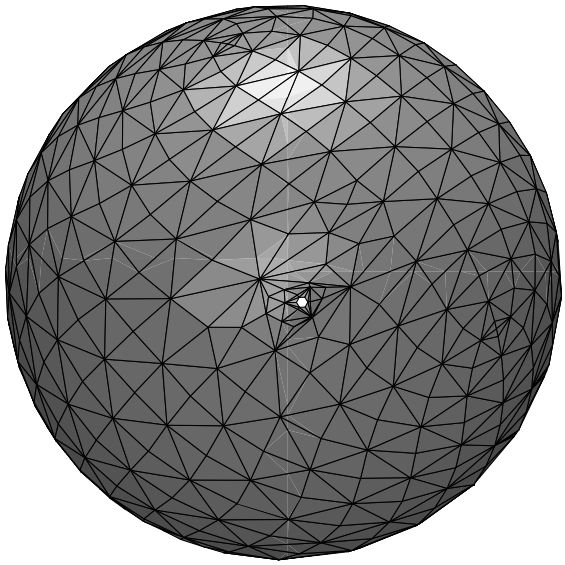

Figure 3.47: Neighbourhood of hexagon has been smoothed. Cut in half.

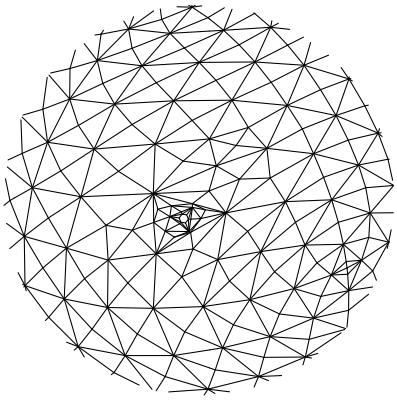

Figure 3.48: The same with mesh depicted. Only small part shown.

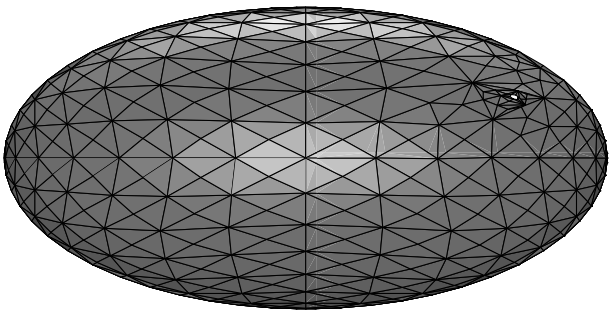

Figure 3.49: Final ellipsoidal form.

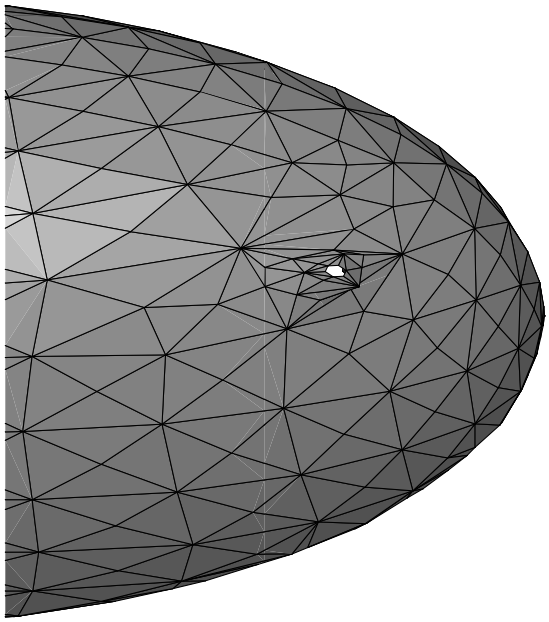

Figure 3.50: Final ellipsoidal form zoomed to the hole. Only part shown.

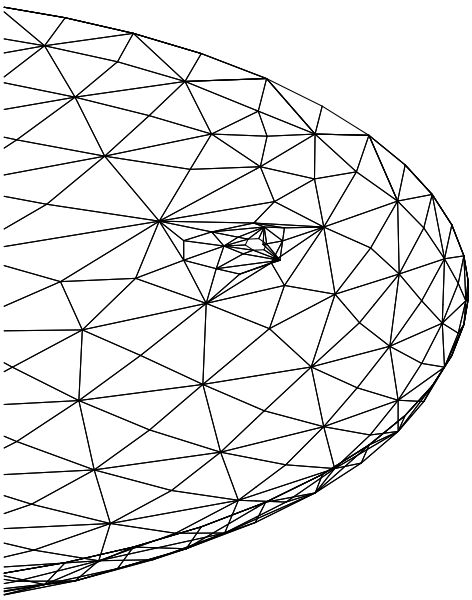

Figure 3.51: Final ellipsoidal mesh zoomed to the hole. Only part shown.

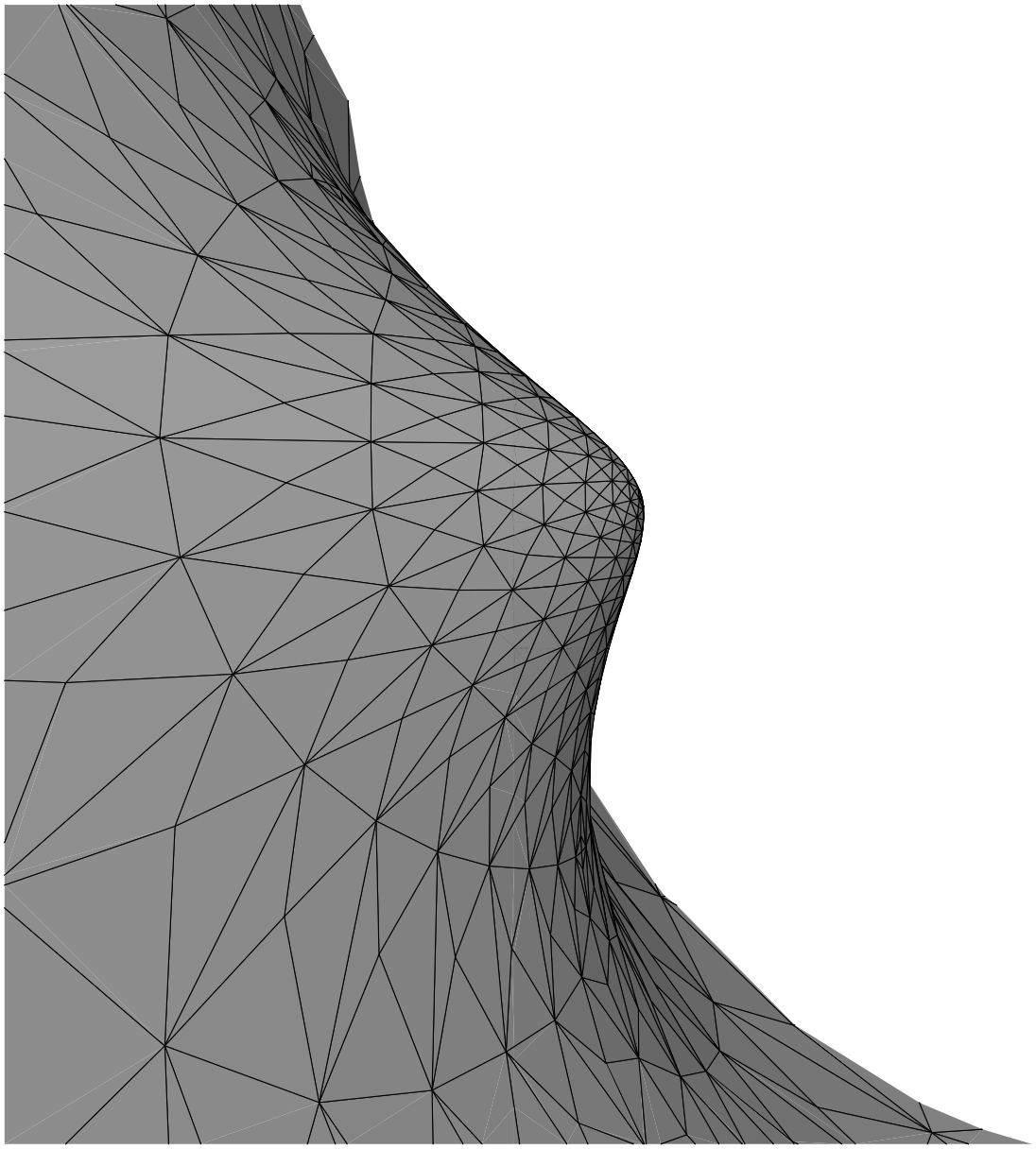

Figure 3.52: Ellipsoid inverted at a sphere with centre at the centre of mass of the hole. Only part shown.

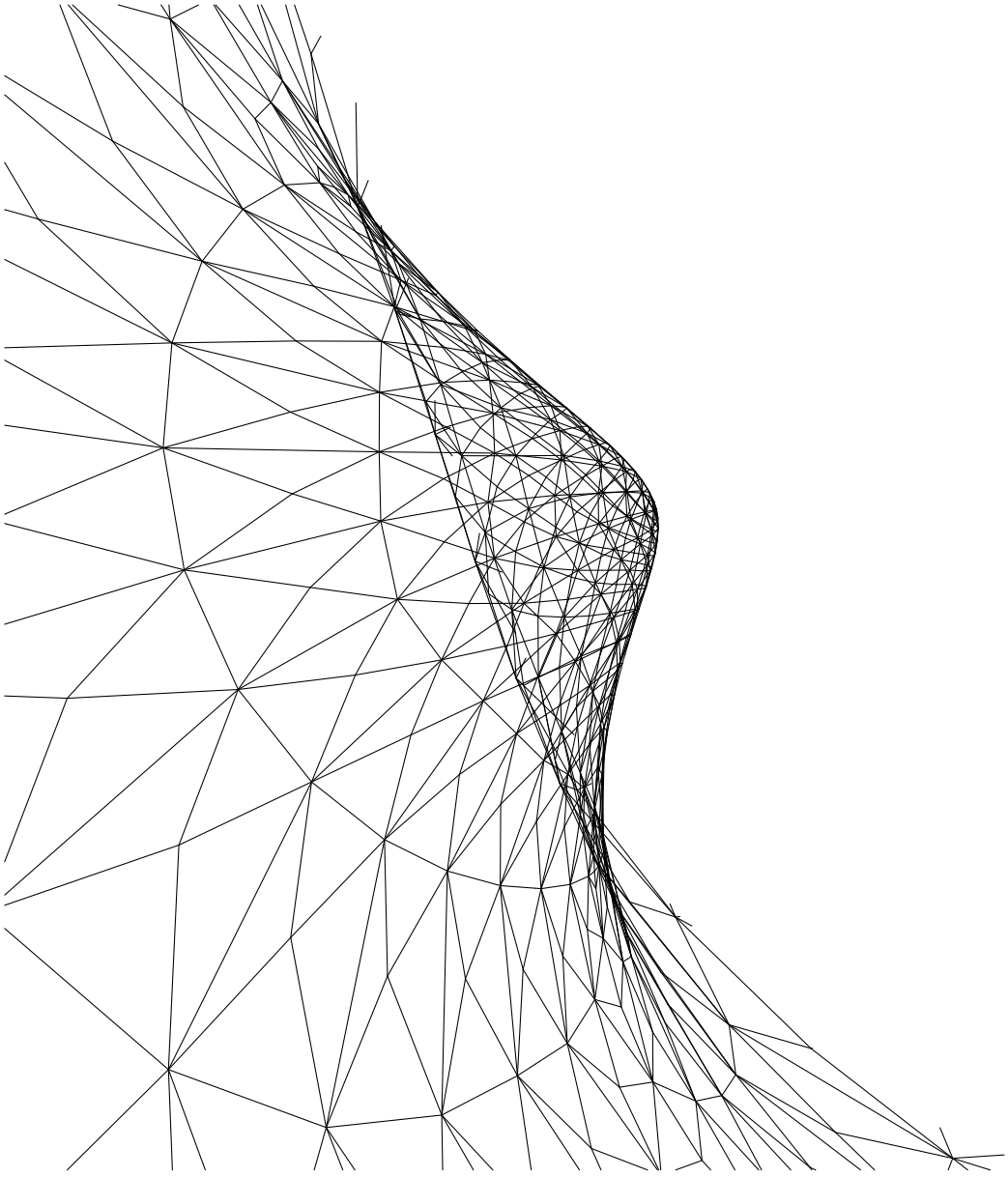

Figure 3.53: Ellipsoid mesh inverted at a sphere with centre at the centre of mass of the hole. Only part shown.

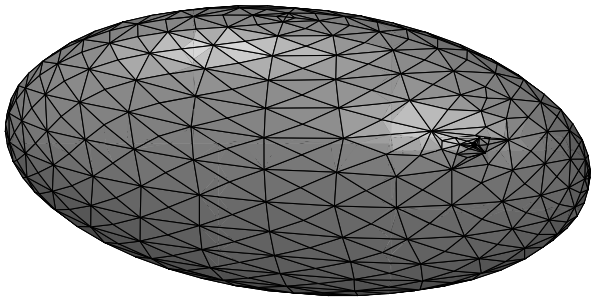

Figure 3.54: Glued surface.

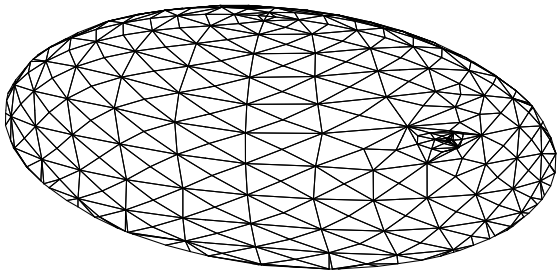

Figure 3.55: Glued mesh (cut in half).

3.4 Outlook

Let us now bring the discussion of the glueing scheme to an end with the question what generalisations of the scheme would be useful. So far, we are only able to glue surfaces in $\mathbb{R}^3$. As far as the author can see, there should be no obstacle to generalise the data structure and the algorithm to discrete surfaces in $\mathbb{R}^n$ as all properties used are internal to the surface except for one: we merge the surfaces by turning the outer normals of the holes such that they cancel. Outer normals to a surface are not well defined in an arbitrary surrounding $\mathbb{R}^n$ so we would have to be careful here and use that two plane hexagons always lie in a three dimensional subspace of $\mathbb{R}^n$. Apart from this, the generalisation to $\mathbb{R}^n$ should be straightforward.

Another kind of surfaces we could wish to glue together are non-orientable ones, especially some discrete version of $\mathbb{RP}^2$. This would be a more delicate change as the refining subroutines rely on a common orientation of the triangles in a surface mesh. It should, however, be possible to refine non-orientable surface meshes. This would allow to glue non-orientable surfaces with the glueing scheme as orientability is used nowhere else in the program.

Finally, having M. Bauer's and E. Kuwert's glueing result 3.1.1 in mind, it would be interesting to be able to glue two surfaces together not with a round cylinder but with a more complicated surface (of the same topology as the cylinder) in between.

4 Willmore Flow

In this chapter, we will give a very short introduction into the theory and the discretisation of the Willmore flow. We are mainly interested in this flow because it might allow to identify minimising Willmore surfaces, see below. Moreover, it might be possible to use the Willmore flow to prove existence, regularity, and other properties of minimising surfaces. Last but not least, the geometric evolution equation arising as the flow equation of the Willmore energy is interesting in its own right. The study of the Willmore flow has been initiated by E. Kuwert and R. Schätzle in 2002 ([KS02]). We begin with the definition of the (continuous) parametric Willmore flow (section 4.1). Then, we discuss a discretisation with Finite Element Methods presented by K. Deckelnick, G. Dziuk, and C. M. Elliott in [DDE05] (section 4.2), study some examples, and give an introduction to the mesh degeneration problem (section 4.3.1).

4.1 Continuous Willmore Flow

Recall that the Willmore energy $\mathcal{W}$ defined in section 2.2 is Fréchet differentiable on $C^4(\Sigma, \mathbb{R}^3)$ (theorem 2.4.1) and that its Fréchet derivative at $f \in C^4(\Sigma, \mathbb{R}^3)$ is denoted by $\delta\mathcal{W}(f)$. Before we can define the Willmore flow, we need the following lemma.

Lemma 4.1.1. *Let Σ be a closed, connected smooth surface. Let $L^2(\Sigma, \mathbb{R}^3)^*$ denote the normed dual of $L^2(\Sigma, \mathbb{R}^3)$ as defined in [Alt91]. Then the Fréchet derivative $\delta\mathcal{W}(f)$ of $\mathcal{W}$ at any C^4-immersion $f : \Sigma \to \mathbb{R}^3$ can be understood as a continuous linear functional on $L^2(\Sigma, \mathbb{R}^3)$, i. e. a member of $L^2(\Sigma, \mathbb{R}^3)^*$. There is a map $W(f) \in L^2(\Sigma, \mathbb{R}^3)$ satisfying $\delta\mathcal{W}(f)\phi = \langle W(f), \phi\rangle_{L^2(\Sigma,\mathbb{R}^3)}$ for all $\phi \in L^2(\Sigma, \mathbb{R}^3)$.*

Proof. Let $f \in C^4(\Sigma, \mathbb{R}^3)$ be an immersion, $\phi \in L^2(\Sigma, \mathbb{R}^3)$. Then

$$\delta\mathcal{W}(f)\phi := 2\int_\Sigma \left[\triangle_g H(f) + 2(H(f)^2 - K(f))\right]\langle\phi, \nu\rangle \, d\mu_f$$

is finite, since by Cauchy-Schwarz inequality

$$|\delta\mathcal{W}(f)\phi| \leq 2\|\triangle_g H(f) + 2(H(f)^2 - K(f))\|_{L^2(\Sigma,\mathbb{R}^3)}\|\phi\|_{L^2(\Sigma,\mathbb{R}^3)} =: C(f)\|\phi\|_{L^2(\Sigma,\mathbb{R}^3)}$$

where the constant $C(f)$ is finite by compactness of Σ and by the continuity of all involved curvature notions since f is of class C^4. We can also see from this inequality that $\delta\mathcal{W}(f)$ is continuous on $L^2(\Sigma, \mathbb{R}^3)$ which allows us to understand $\delta\mathcal{W}(f)$ as a member of $L^2(\Sigma, \mathbb{R}^3)^*$.

By the Riesz representation theorem[1], there is a function $W(f) \in L^2(\Sigma, \mathbb{R}^3)$ satisfying $\langle W(f), \phi \rangle_{L^2(\Sigma,\mathbb{R}^3)} = \delta \mathcal{W}(f)\phi$. We are done by theorem 2.4.1. □

The parametric Willmore flow is now defined as the L^2-gradient flow of the Willmore energy $\mathcal{W}$.

Definition 4.1.2 (L^2-Gradient of $\mathcal{W}$, Willmore Flow). [2] Let Σ be a closed, connected smooth surface. The Riesz representation $W(f) \in L^2(\Sigma, \mathbb{R}^3)$ of $\delta \mathcal{W}(f)$ (see lemma 4.1.1) is called the *L^2-gradient of $\mathcal{W}$* and is denoted by $W(f) = \operatorname{grad}_{L^2} \mathcal{W}(f)$. It follows from theorem 2.4.1 that $\operatorname{grad}_{L^2} \mathcal{W}(f) = 2(\triangle_g H(f) + 2(H(f)^2 - K(f))\, H(f))\nu$. By the *Willmore flow* or the *elastic flow*, we understand the fourth order geometric evolution equation

$$\partial_t f = -\operatorname{grad}_{L^2} \mathcal{W}(f) = -2(\triangle_g H(f) + 2(H(f)^2 - K(f))\, H(f))\nu \text{ on } \Sigma.$$

A solution of this flow equation is also referred to as a *Willmore flow*.

Remark. We recall that ν denotes any (local) unit normal field, $H(f)$ denotes the scalar mean curvature (depending on the choice of the normal field), and $K(f)$ denotes the Gauß curvature of the immersion f. $\triangle_g$ denotes the Laplace-Beltrami operator induced on Σ by the Riemannian metric g which arises as the pullback of the canonical metric on $\mathbb{R}^3$ via f.

We formulate the following initial value problem:

Problem 4.1.3 (Initial Value Problem (IVP)). [3] *To a given smooth, closed, and connected surface Σ smoothly immersed into $\mathbb{R}^3$ via $f_0 : \Sigma \to \mathbb{R}^3$ find a number $T > 0$ and a family $(f(t))_{t\in[0,T)}$ of smooth immersions $f(t) : \Sigma \to \mathbb{R}^3$ which describes the evolution of f_0 under the L^2-gradient flow of the Willmore energy and that satisfies $f(0) = f_0$. In other words, the family $(f(t))_{t\in[0,T)}$ shall satisfy*

$$\left.\begin{aligned} \partial_t f(t,p) &= -\operatorname{grad}_{L^2} \mathcal{W}(f(t))(p) \\ f(0,p) &= f_0(p) \end{aligned}\right\} \forall\, p \in \Sigma\, \forall\, t \in [0,T).$$

The interest in problem (IVP) (and the negative sign therein) stems from the idea of "steepest descent"[4]. This idea coming from $\mathbb{R}^n$ is based on the fact that the negative gradient of a sufficiently smooth map $w : \Omega \subset_o \mathbb{R}^n \to \mathbb{R}$ always points in the direction of steepest descent of the graph of w. Also, the "rest points" of a solution of the accompanying gradient flow are precisely the critical points of w. Similarly, Willmore surfaces are *stationary* for the Willmore flow, i. e. they satisfy $\operatorname{grad}_{L^2} \mathcal{W}(f) = 0$. We have seen in chapter 2 that all round spheres as well as the Clifford torus are Willmore surfaces so that the following corollary is immediate.

Corollary 4.1.4. *All round sphere immersions of $\mathbb{S}^2$ as well as the Clifford torus are stationary for the Willmore flow.*

[1] cf., for example, p. 145 in [Alt91].
[2] based on [KS02] and [Str96].
[3] cf. p.1 in [Rus].
[4] cf. pp. 76 in [Str96].

E. Kuwert and R. Schätzle ([KS02]) have proved short time existence of smooth solutions of the Willmore flow for any closed surface Σ immersed into an arbitrary $\mathbb{R}^n$ ($n \geq 3$) (*initial data*). Their discussion of the Willmore flow is characterised by the conformal invariance of the Willmore energy (see 2.3.3). G. Simonett ([Sim01]) has proved[5] long term existence of a solution of the Willmore flow with initial data close in $C^{2,\alpha}$ to a (round) sphere; furthermore, he showed that the solution gets spherical as $t \to \infty$. Similarly, E. Kuwert and R. Schätzle ([KS04]) have shown that any smooth initial immersion of a sphere into $\mathbb{R}^3$ with Willmore energy[6] less than 16π gives rise to an infinitely existing smooth Willmore flow that converges to the round sphere. U. F. Mayer and G. Simonett have shown in their paper [MS03] that the Willmore flow does in fact decrease the Willmore energy. More precisely, they have shown $\mathcal{W}(f(t)) \leq W(f_0)$ ($t \in [0,T]$) for any smooth immersed solution $f(t) : \Sigma \to \mathbb{R}^3$ of the Willmore flow with smooth initial data $f_0 : \Sigma \to \mathbb{R}^3$ and for any smooth orientable connected surface Σ.

Having these results in mind, we can hope to identify minimisers of the Willmore energy by studying long time behaviour of the Willmore flow on surfaces of higher genera. In particular, they let us hope to be able to get information on possible minimisers by studying the (discretised) Willmore flow numerically. But as U. F. Mayer and G. Simonett also remark in [MS03], their numerical simulations "seem to indicate that the Willmore flow can drive immersed surfaces to topological changes in finite time." It is not known to the author whether this effect has a theoretical equivalent. However, changes of topology cannot happen in the parametric approach we are using as the domain of the parametrisation fixes the topology – as long as the parametrisation gives rise to a (discrete) immersed surface and does not degenerate. We will now discuss a discretisation of the Willmore flow by Finite Element Methods.

4.2 Discretisation

In section 3.2, we have defined discrete embedded and immersed surfaces. We have also introduced the notion of discretised (Willmore) surfaces. In this section, we will discretise the Willmore energy with Finite Elements and give a concise overview over a discretised Willmore flow presented by K. Deckelnick, G. Dziuk, and C. M. Elliott. As we have noted above, one also finds a notion of "discrete Willmore energy" and "discrete Willmore flow" in the literature, see for example the paper [BS05] by A. I. Bobenko and P. Schröder.

When introducing immersed surfaces in section 3.2, we have succinctly stated that the Willmore flow can drive embedded surfaces to self-intersections. This fact has been proved by U. F. Mayer and G. Simonett ([MS03]). More precisely, they have shown that the Willmore flow can drive smooth orientable embedded (into $\mathbb{R}^3$) initial data to self-intersections in finite time. They have also reproduced this effect numerically[7].

[5] say E. Kuwert and R. Schätzle in [KS02].
[6] Note that they use a definition of the Willmore energy differing from ours by a factor $\frac{1}{2}$.
[7] says R. Rusu in [Rus].

For our study of the flow behaviour of the surfaces constructed by the glueing scheme, we have used a Finite Element Discretisation of the Willmore flow which is due to K. Deckelnick, G. Dziuk, and C. M. Elliott ([DDE05]) and relies on a trick by R. Rusu ([Rus]). Their approach is parametric. Other approaches as for example a level set method are also commonly used (cf. [Alb05], for example). The code of the discrete Willmore flow has been given to the author by G. Dziuk and contains pieces of code by M. Fried and A. Schmidt. We only give a very rough description of the scheme, here. A flow chart can be found on page 86. Convergence results of this scheme are not known to the author.

The continuous Willmore flow is of fourth order in space and of first order in time. The trick of R. Rusu consists of regarding the mean curvature vector and the "position vector" of the parametrisation as independent. This is called a "mixed method". She can thus transfer the single equation of fourth order into two coupled equations of second order in space, respectively. The time discretisation is semi-implicit and linearises the equations. Hence, this trick permits the use of piecewise linear Finite Elements for the space discretisation. Also, it induces a natural discretisation of the Willmore energy, see below.

The only space derivative operator appearing in the two new equations is the so-called "tangential gradient". It is defined by

Definition 4.2.1. [8] If $\Sigma \subset \mathbb{R}^3$ is a smooth embedded surface and U is an open neighbourhood of Σ in $\mathbb{R}^3$, the *tangential gradient* of a smooth map $f : U \to \mathbb{R}$ at a point $p \in \Sigma$ with normal $\nu(p) \in \mathbb{R}^3$ is defined as $\nabla_\Sigma f(p) := \operatorname{grad} f(p) - (\operatorname{grad} f(p) \cdot \nu(p))\nu(p)$. Here, $\operatorname{grad} f(p)$ denotes the usual gradient of f in p. The tangential gradient then is the projection of the gradient $\operatorname{grad} f(p)$ to the tangent plane of Σ at p. It only depends on the values of f on Σ.

Remark. The Gauß formula for Euclidean hypersurfaces[9] tells us that the tangential gradient of f agrees with the covariant derivative of f, ∇f, if f is sufficiently smooth.

From now on, we deviate slightly from the notation introduced in chapters 1 and 2 and work with the notation customary in the field of Finite Element Methods on surfaces. In particular, parametrisations are denoted by X, the mean curvature vector by Y, see below. Recall the definition of the Sobolev space H^1 on a $C^{0,1}$-surface (cf. chapter 1). The discretisation of problem 4.1.3 formulated by R. Rusu in [Rus] then reads[10]

Definition 4.2.2. Let Σ_h be a discrete surface[11], $\mathcal{T}_h$ its triangulation. The space

$$\mathcal{X}_h(\Sigma_h) := \{\phi \in C^0(\Sigma_h, \mathbb{R}^3) \,|\, \phi|_T \text{ is a linear polynomial for each } T \in \mathcal{T}_h\}$$

is called *Finite Element space* for Σ_h. We have $\mathcal{X}_h \subset H^1(\Sigma, \mathbb{R}^3)$ and $\dim \mathcal{X}_h < \infty$.

[8] cf. [Rus, GT70].

[9] cf. p. 140 in [Lee97].

[10] We vary slightly from R. Rusu's treatment as we have given a different definition of discrete immersed surfaces.

[11] If Σ_h is not embedded into $\mathbb{R}^3$, all following maps and spaces are meant to be defined on its parametric domain which is a discrete embedded surface.

Definition 4.2.3 (Discrete Position Vector, Discrete Curvature Vector). Let Σ_h be a discrete surface, $X \in \mathcal{X}_h(\Sigma_h)$ locally injective, i. e. a parametrisation. Then we call X the *(discrete) position vector* of the discrete surface $X(\Sigma_h)$. Let $d\mu_h$ denote the surface measure on Σ_h, let ":" denote the canonical inner product of 3×3-matrices. $Y \in \mathcal{X}_h(\Sigma_h)$ is called the *(discrete mean) curvature vector* for X if it satisfies the weak equivalent[12] of the identity $\triangle_g f = \mathcal{H}(f)$ proved in 1.2.22 or in other words if it satisfies

$$\int_{\Sigma_h} Y \cdot \psi \, d\mu_h + \int_{\Sigma_h} \nabla_{\Sigma_h} X : \nabla_{\Sigma_h} \psi \, d\mu_h = 0 \text{ for all } \psi \in \mathcal{X}_h(\Sigma_h).$$

The discrete mean curvature vector for a given position vector is unique by the fundamental lemma of the calculus of variations.

Problem 4.2.4 (Discretised Parametric Willmore Flow). *Let Σ_h^0 be a discrete surface. Let $X^0 \in \mathcal{X}_h(\Sigma_h^0)$ be the identity map on Σ_h^0, and let $Y^0 \in \mathcal{X}_h(\Sigma_h^0)$ be the curvature vector for X^0. Let $\tau > 0$ be a time step, $m_0 \in \mathbb{N}$. Denote by ν^0 the normal to Σ_h^0 (defined only and constant on the interiors of the triangles in the triangulation), and by μ_h^0 the surface measure on Σ_h^0. For $m = 0, 1, \ldots, m_0 - 1$, find functions $X^{m+1}, Y^{m+1} \in \mathcal{X}_h(\Sigma_h^m)$ such that*

- $\Sigma_h^{m+1} := X^{m+1}(\Sigma_h^m)$ *is a discrete surface ($\Leftrightarrow X^{m+1}$ is locally injective)*
- Y^{m+1} *is the curvature vector for* X^{m+1}
- ν^{m+1} *is the normal to* Σ_h^{m+1} *(defined only and constant on the interiors of the triangles in the triangulation),* μ_h^m *is the surface measure on* Σ_h^m
- *and such that for all* $\phi \in \mathcal{X}_h(\Sigma_h^m)$*, we have*

$$\begin{aligned} \frac{1}{\tau} \int_{\Sigma_h^m} (X^{m+1} - X^m) \cdot \phi \, d\mu_h^m + \frac{1}{2} \int_{\Sigma_h^m} |Y_h^m|^2 \nabla_{\Sigma_h^m} X^{m+1} : \nabla_{\Sigma_h^m} \phi \, d\mu_h^m \\ + \int_{\Sigma_h^m} \nabla_{\Sigma_h^m} Y^{m+1} : \nabla_{\Sigma_h^m} \phi - 2(\nu^m \nabla_{\Sigma_h^m} Y^{m+1}) \cdot (\nu^m \nabla_{\Sigma_h^m} \phi) \, d\mu_h^m &= 0. \end{aligned}$$

The discrete parametric Willmore flow is implemented by use of the canonical "nodal basis"[13] having nodes in the vertices only. In the following, we discuss the parameters and the output of the Willmore flow scheme.

(Input). The input for the program consists of a file `Input_will` that specifies the values of a number of parameters. The documentation file `Input_will.DOKU` explains all parameters and, if necessary, their possible values, see appendix **??**, p. **??**. We can specify the number `ilz` of refinements the surface will undergo before the flow is applied to it. As in the glueing scheme, we can specify its `genus`, the number `surface`, and the `projection` that is supposed to be used for the refinement and for the Laplacian smoothing. In case of a torus,

[12] cf. [Rus] for more information on the partial integration argument leading to this weak formulation.
[13] cf. p. 62 in [Bra91].

we can specify the torus radii `r0, r1`. Finally, we can determine whether a "conformal reparametrisation" is supposed to take place by setting `conformal` to 0 (yes) or 1 (no) – conformal reparametrisation will be discussed below. Also, we can specify the number `mcf_freq` of times the Laplacian smoothing scheme is applied to the surface before the discretised flow is applied. Last but not least, we can specify the time step `tau` by fixing an exponent `expo`. The time step will then be calculated from the mesh size[14] `h` by setting $\texttt{tau} = \texttt{h}^{\texttt{expo}}$. Other parameters are read from the file `ein`; as we have not changed those, we will not go into into detail. A few parameters are specified in the program, for example the frequency of the conformal reparametrisation.

(Output). The output of the Willmore flow scheme consists of images of the surface (produced with the subroutine `movie(...)`) and of its triangulations, both written down at certain steps of the iteration (specified internally with the variables `mmm` and `cut`, respectively). Also, a file called `Track.DOKU` is created to keep track of the process. It informs which surface the scheme works with, notes the level of refinement `ilz`, the time step `tau`, the envisaged hours of operation `finish`, the image and protocol frequency `mmm`, and the mesh writing frequency `cut`. Then, it states whether a conformal reparametrisation is undertaken. For each of the first ten steps of time, it notes the mesh regularity[15] measured by the subroutine `winkel(...)` and the discretised Willmore energy. The same is done in each `mmm`'th step.

The data structure used is the same one as in the glueing algorithm, see chapter 3. We give a short overview over the structure of the program; see the flow chart on the following page, too. The subroutines `refglobal_glue(...)`, `discrete_mcf(...)`, and `ustart_glue(...)` and all their subroutines are exactly those used in the glueing scheme. `macro_glue(...)` is slightly changed as it now allows to load the triangulation of a surface produced with the glueing scheme (saved in `triang.glued`). Some pieces of the chart are dashed; this indicates that we have not (yet) discussed the corresponding pieces of the code. The boxes containing the text "Prepare flow" and the box containing "adaptiv" stand for the discretised Willmore flow. The boxes named "Prepare harmonic" and "harmonic" describe the conformal reparametrisation and will be discussed in chapter 6.

[14] The mesh size `h` is calculated in the subroutine `gitter()` by G. Dziuk.

[15] Note that high numbers returned by `winkel(...)` correspond to low regularity and vice versa.

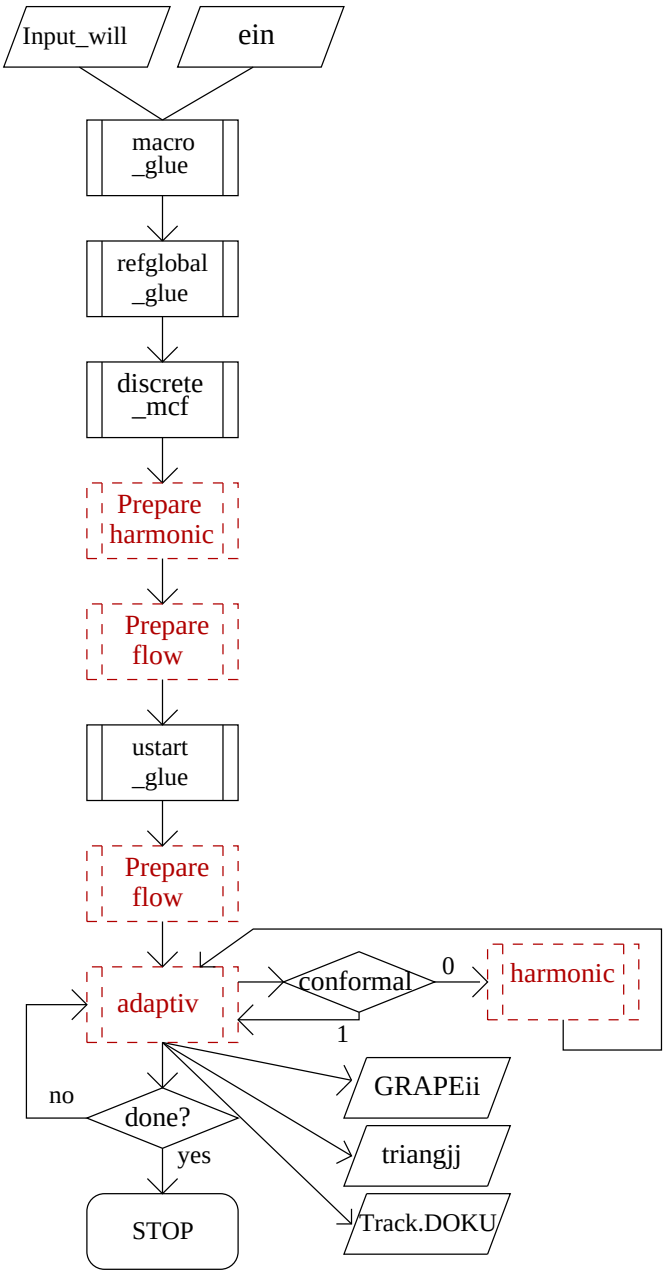

Figure 4.1: Flow Chart for the Willmore flow algorithm. The dashed pieces of the program have not (yet) been discussed.

4.2.1 Discretised Willmore Energy

In order to determine the Willmore energy of a glued surface, we have discretised the Willmore energy using the Finite Element spaces R. Rusu introduced for the discretisation of the Willmore flow. We use the subroutine `kruemmung()` of the implemented Willmore flow to determine the curvature vector of the surfaces; the subroutine calculating the Willmore energy is called `willenergy(Will)`.

Proposition 4.2.5 (Discretised Willmore Energy). [16] *Let Σ_h be a discrete surface, $\mathcal{T}_h$ its triangulation. Let Y be the curvature vector associated to the identity mapping $X : \Sigma_h \to \Sigma_h$ as described in definition 4.2.3. Recall that* `nv` *denotes the number of vertices in the triangulation. Let $y = (y_i)_{i=1,\dots,\mathtt{nv}}$ and $x = (x_i)_{i=1,\dots,\mathtt{nv}}$ be the respective coefficient vectors with respect to the nodal basis. The discretised Willmore energy is given by*

$$\mathcal{W}_h(x) = \frac{1}{12} \sum_{T \in \mathcal{T}_h} |T| \sum_{v_i \neq v_j \text{ are nodes of } T} H_{ij},$$

where $H_{ij} = y_i \cdot y_j$, and $|T|$ is the area of T.

Proof. Let $b = (b_1, b_2, b_3)$ be barycentric coordinates on the standard simplex T_0 and thus $b_1 + b_2 + b_3 = 1$. For any $T \in \mathcal{T}_h$, let $a^T = (a_1^T, a_2^T, a_3^T)$ denote the canonical $\mathbb{R}^3$-coordinates on T. Setting $Y^T(b) := Y(a^T(b))$, we have $|Y^T(b)|^2 = \sum_{r,s=1}^3 b_r b_s H_{i^T(r) i^T(s)}$ on $T \in \mathcal{T}_h$, where we denote the numbers of the vertices of T by $i^T(1), i^T(2), i^T(3)$. Thus, by the transformation formula, we get by symmetry of H

$$\begin{aligned}
\mathcal{W}_h(x) &= \frac{1}{2} \sum_{T \in \mathcal{T}_h} \int_T |Y(a)|^2 \, da \\
&= \frac{1}{2} \sum_{T \in \mathcal{T}_h} \frac{|T|}{|T_0|} \int_{T_0} |Y^T(b)|^2 \, db \\
&\overset{|T_0|=0.5}{=} \sum_{T \in \mathcal{T}_h} |T| \int_0^1 \int_0^{1-b_1} \sum_{r,s=1}^3 b_r b_s H_{i^T(r) i^T(s)} \, db_2 db_1 \\
&= \sum_{T \in \mathcal{T}_h} |T| \sum_{r,s=1}^3 H_{i^T(r) i^T(s)} \int_0^1 \int_0^{1-b_1} b_r b_s \, db_2 db_1 \\
&= \frac{1}{24} \sum_{T \in \mathcal{T}_h} |T| \sum_{r,s=1}^3 H_{i^T(r) i^T(s)} (1 + \delta_{rs}) \\
&= \frac{1}{12} \sum_{T \in \mathcal{T}_h} |T| \sum_{v_i \neq v_j \text{ are nodes of } T} H_{ij}
\end{aligned}$$

by calculating the integrals over all appearing quadratic polynomials. □

[16] cf. [Bra91] for the necessary definitions.

4.2.2 Examples

It seems that the discretised Willmore energy of some (discrete) surfaces depends very strongly on the regularity of this surface (measured by measuring the minimal angle in the mesh in subroutine `winkel(...)`). It is also influenced strongly by the Laplacian mesh-smoothing described in section 3.2 for some surfaces, especially for tori. The values for the eight times refined torus mesh with torus radii 1 and 0.25 are collected in table 4.2. For the eight times refined round sphere mesh, we get less variation – probably because the round sphere mesh is very regular by itself; the values are displayed in table 4.3. Note that the values of both the regularity and the discretised Willmore energy seem to become more or less stagnant after a few iterations of the Laplacian smoothing.

Using Laplacian smoothing without projecting back to the surface (as discussed in chapter 3 would change the surface and is thus not applicable. Neither does it yield better results in the sense that the energy remains more or less constant in case of the torus mesh.

`mcf_freq`	Willmore energy	regularity	`mcf_freq`	Willmore energy	regularity
0	1255.06	159.79	8	294.79	77.78
1	1869.16	504.99	9	285.57	72.38
2	553.77	162.81	10	279.50	67.19
3	722.36	2365.99	11	276.08	63.61
4	401.00	124.96	12	274.50	60.53
5	363.58	144.05	13	274.40	58.09
6	329.22	96.17	14	275.42	56.00
7	309.47	89.33	15	277.34	54.25

Figure 4.2: Rounded discretised Willmore energy and regularity of an eight times refined torus mesh, to which Laplacian smoothing is applied `mcf_freq` times.

`mcf_freq`	Willmore energy	regularity	`mcf_freq`	Willmore energy	regularity
0	29.31	10.25	8	26.54	8.73
1	28.27	15.80	9	26.47	8.72
2	27.46	9.84	10	26.41	8.70
3	27.22	10.09	11	26.35	8.68
4	27.00	9.24	12	26.30	8.66
5	26.85	9.05	13	26.26	8.64
6	26.72	8.76	14	26.22	8.62
7	26.63	8.75	15	26.18	8.60

Figure 4.3: Rounded discretised Willmore energy and regularity of an eight times refined round sphere mesh, to which Laplacian smoothing is applied `mcf_freq` times (with round sphere projection).

The (discretised) Willmore energy of some exemplary surfaces is listed in table 4.5. We have used the Laplacian smoothing method in order to achieve more or less stagnant regularities and stagnant discretised Willmore energies. The author has the impression that an energy increase takes place with higher refinement levels in all listed surfaces apart from the (non-glued) dumbbell and the (non-Clifford) torus. We explain this effect by the conjecture that further refined meshes realise more of the curvature of the curved surfaces they are interpolating. Also, the triangles of the triangulation become smaller so that the susceptibility to small variations increases.

The glued dumbbell shows a similar behaviour as the surfaces that arise as parametrised over the round sphere (apart from the deformed dumbbell). Neither its regularity nor its discretised Willmore energy depend strongly on the number of refinements or on the number of Laplacian smoothings applied to it. The glued ellipsoid cannot be refined in the scheme as there is no projection available for it. A Laplacian smoothing is also not feasible as it would need a projection, too. A non-projective Laplacian smoothing does severely change the geometric form as the mesh is much finer where the inverted ellipsoid has been inserted so that the main part of the ellipsoid shrinks and the inverted part remains more or less constant. The author assumes that the large value of the discretised Willmore energy of the glued ellipsoid is due to its low regularity.

The torus mesh (with radii 1 and 0.25) has a pattern after the refinement (see figure 4.4); this pattern vanishes with the Laplacian smoothing; the regularity and the discretised Willmore energy are lowered significantly. If we perform some hundreds of Laplacian smoothing iterations, we can still get to significantly lower discretised Willmore energy. The oscillation of the discretised Willmore energy with the number of refinements in the torus can maybe be explained by the fact that the refinement process alternately produces “good” triangles (with not very acute or obtuse angles) and “bad” triangles.

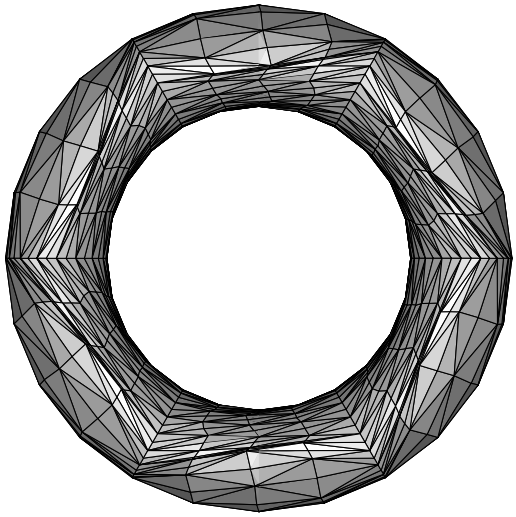

Figure 4.4: Torus mesh with pattern.

Surface (energy)	ilz	freq	W. energy	reg.	ilz	freq	W. energy	reg.
round sphere (25)	5	2	25	7	6	5	26	9
	7	2	26	7	8	9	26	9
	9	3	26	7	10	4	28	10
ellipsoid	5	3	34	13	6	4	36	10
	7	2	37	13	8	2	38	9
	9	4	38	14	10	3	39	9
glued ellip.	0	-	80	53				
dumbbell	5	3	41	18	6	4	41	13
	7	4	51	18	8	3	48	12
	9	5	57	22	10	4	51	12
glued dumb.	0	2	56	20	1	2	63	11
	2	4	66	13	3	4	73	14
Willm. sph. (101)	5	2	61	12	6	8	73	12
	7	3	86	8	8	6	95	9
	9	2	99	9	10	6	105	10
Cliff. torus (39)	5	5	45	17	6	5	46	15
	7	9	50	19	8	5	51	18
	9	19	56	22	10	4	55	20
torus (82)	5	5	81	21	6	$\simeq 7$	$\simeq 300$	$\simeq 70$
	7	10	85	22	8	$\simeq 10$	$\simeq 300$	$\simeq 70$
	9	$\simeq 15$	86	$\simeq 35$	10	$\simeq 40$	$\simeq 300$	$\simeq 60$

Figure 4.5: Rounded discretised Willmore energy and regularity of different discrete surfaces. `ilz` is the level of refinement, `freq`=`mcf_freq` is the number of iterations of the Laplacian smoothing we have applied. "ellipsoid" refers to the deformed ellipsoid mesh depicted in 3.10, "glued ellip." refers to the glued surface depicted in 3.54. "dumbbell" refers to the dumbbell mesh constructed by G. Dziuk, "glued dumb." refers to the mesh depicted in figure 3.9. "Willm. sph." refers to the mesh depicted in 3.1. "W." is a shorthand for "Willmore", "reg." for "regularity". The radii of "torus" are 1 and 0.25. "energy" stands for the theoretical Willmore energies that can be found in chapter 3.

4.3 Behaviour under the Flow

Let us have a look at the behaviour of different surfaces under the discretised Willmore flow. We begin with the ellipsoid depicted below. The chosen parameters are `ilz` $= 8$, `genus` $= 0$, `surface` $= 9$, `projection` $= 0$, `conformal` $= 1$, `mcf_freq` $= 0$, `expo` $= 3$. We depict the surface before the start of the iteration, after ten iterations, then after 100, 200, 300, 400, and 500 steps. As expected, the surface approximates a round sphere under the flow. The table below illustrates the behaviour of the Willmore energy under the Willmore flow: it decreases – which is consistent with the theoretical results. The same is true for the mesh regularity, at least at first.

step of the iteration	Willmore energy	regularity
1	40.03	10.03
2	35.84	9.68
3	35.12	9.60
4	34.63	9.54
5	34.23	9.49
6	33.89	9.44
7	33.60	9.40
8	33.33	9.37
9	33.09	9.34
10	32.86	9.31
100	26.69	10.02
200	25.10	11.18
300	24.84	12.17
400	24.81	13.31
500	24.80	14.70

Figure 4.6: Willmore energy under the Willmore flow for the ellipsoid.

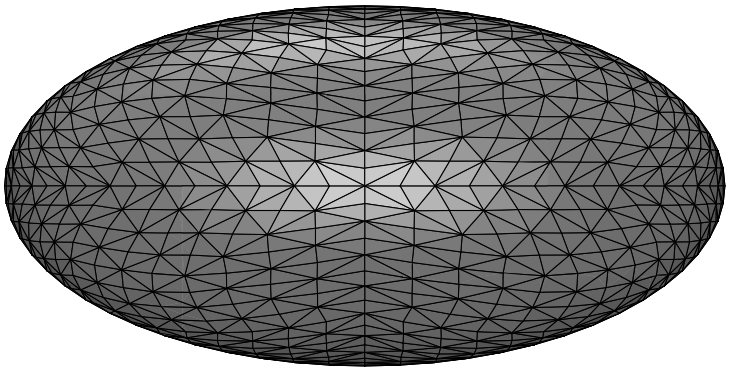

Figure 4.7: Before the iteration begins.

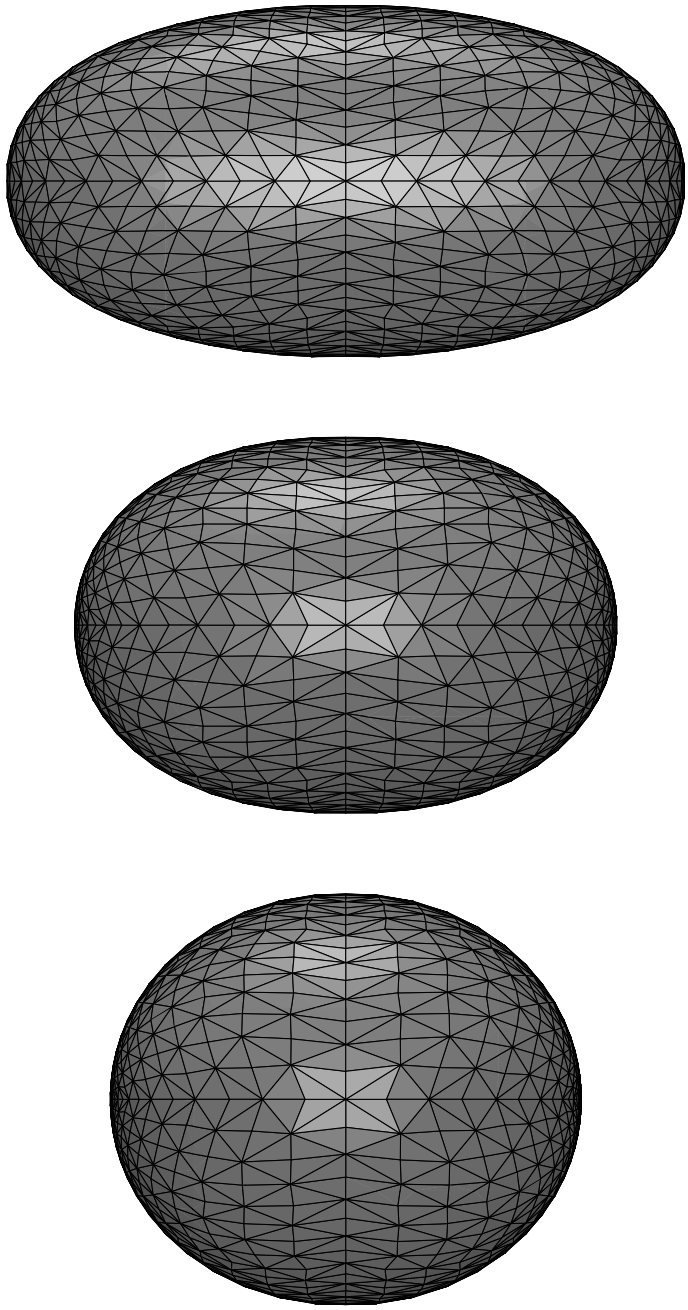

Figure 4.8: After 10, 100, and 200 steps of the iteration.

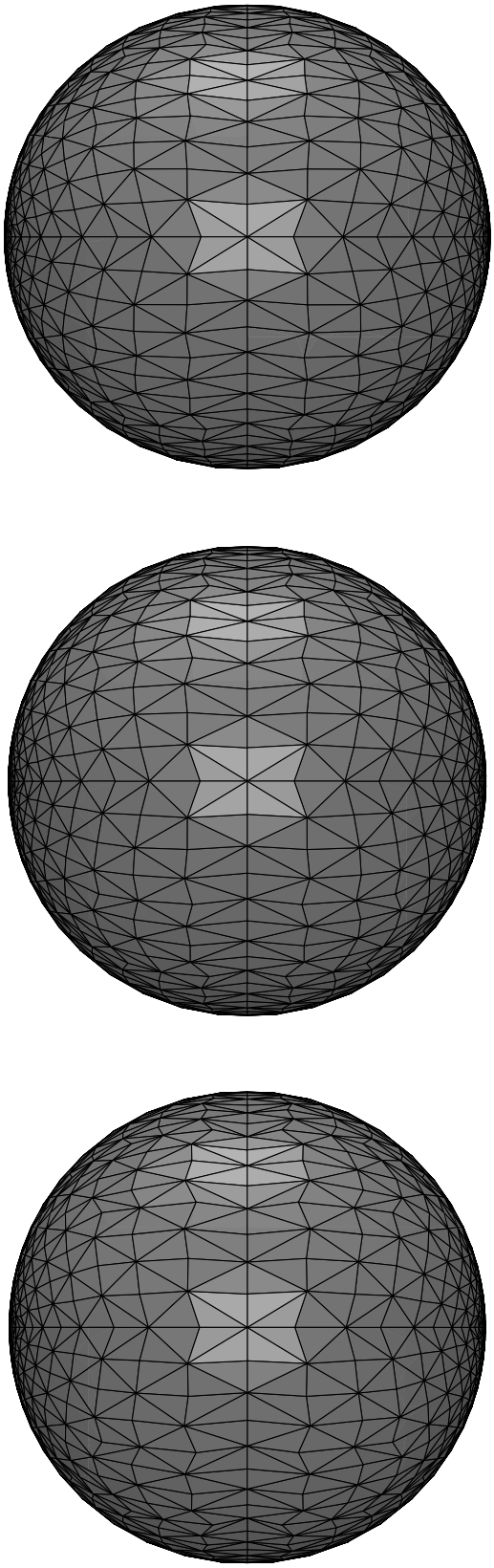

Figure 4.9: After 300, 400 and 500 steps of the iteration.

Now, we study the same situation for tori. The parameters for the following figures are chosen as `ilz` = 7, `genus` = 1, `projection` = 3, `r0` = 1, `r1` = 0.25, `conformal` = 1, `mcf_freq` = 10, and `expo` = 2. We depict the surface before the start of the iteration, after ten iterations, then after 20, 30, 40, 50, and 60 steps. Recalling that the Clifford torus is a minimiser for the Willmore energy we are not surprised that the torus approximates the Clifford torus under the Willmore flow. The Willmore energy also shows the expected behaviour as the table below illustrates.

step of the iteration	Willmore energy	regularity
1	84.64	22.33
2	76.30	22.33
3	74.02	20.38
4	72.03	19.83
5	70.26	19.35
6	68.66	18.93
7	67.21	18.55
8	65.88	18.22
9	64.66	17.91
10	63.53	17.63
20	55.45	15.78
30	50.51	14.90
40	47.09	14.46
50	44.61	14.15
60	42.79	13.92

Figure 4.10: The behaviour of the discretised Willmore energy under the Willmore flow for the torus.

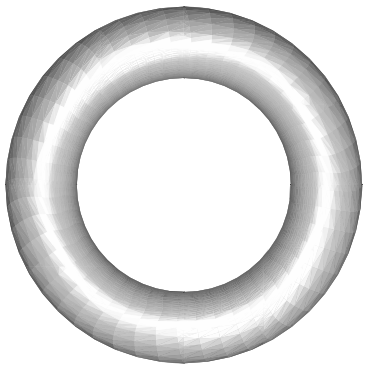

Figure 4.11: Before the iteration begins (this figure is scaled more than the following ones).

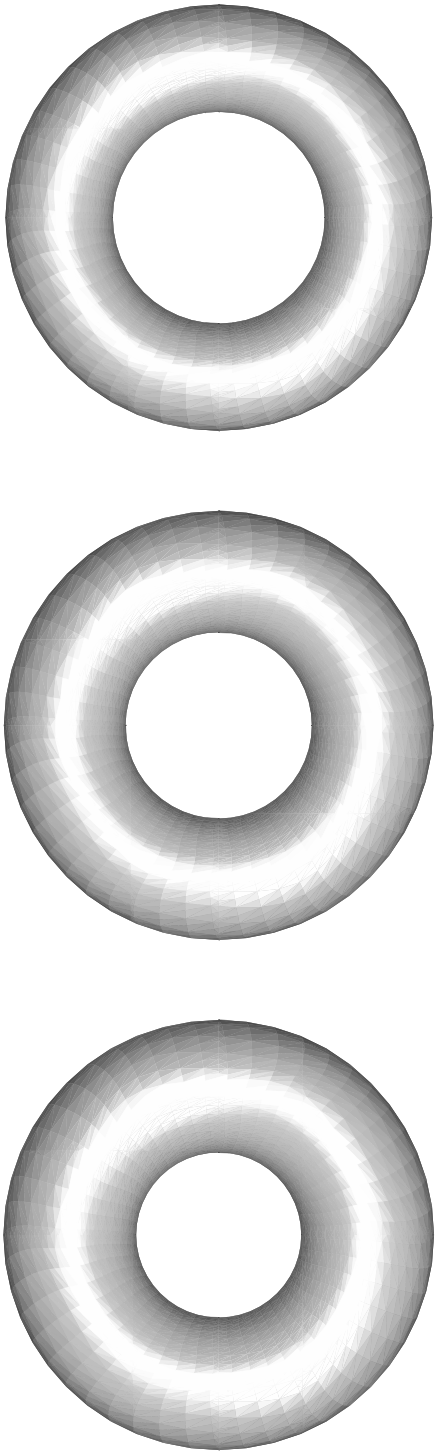

Figure 4.12: After 10, 20, and 30 steps of the iteration.

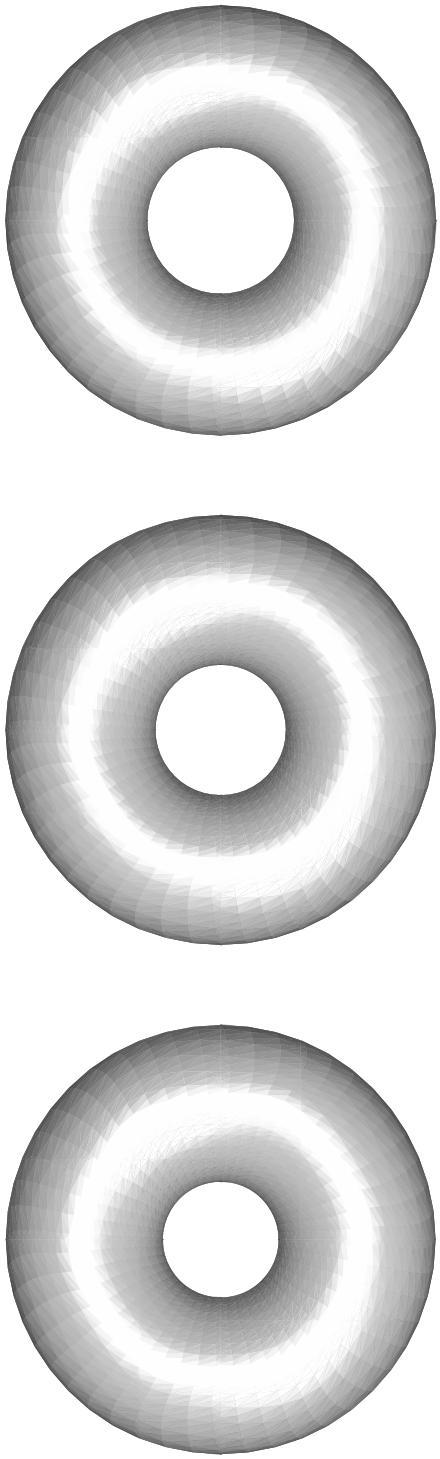

Figure 4.13: After 40, 50, and 60 steps of the iteration.

4.3.1 Mesh Degeneration

However, the "long time behaviour" of the surfaces, i. e. their behaviour under "many" iterations of the flow differs from the theory. The regularity explodes, the Willmore energy increases, too. This effect appears more quickly if we work with lower levels of refinement. We get the following data for the parameters listed above and the pictures on this and the following page.

step (ellipsoid)	W. energy	reg.	step (torus)	W.	reg.
600	24.80	21.06	170	39.33	33.39
700	24.81	64.81	210	39.33	149.62
740	24.86	269.81	240	217.44	763.81
796	25.18	6151.23	260	307.30	15296.05

Figure 4.14: Discretised Willmore energy after many iterations for ellipsoid and torus.

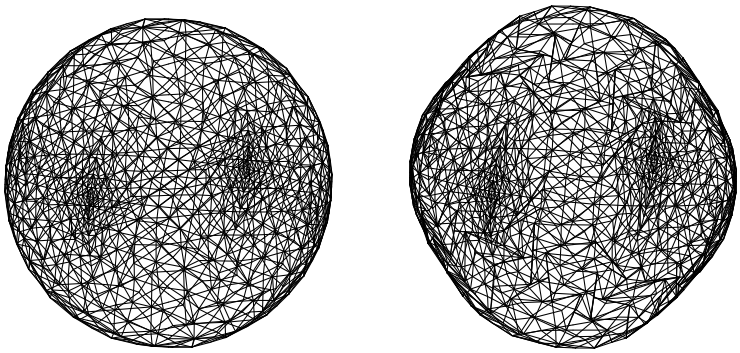

Figure 4.15: Ellipsoidal mesh after 600 and 796 steps of the iteration.

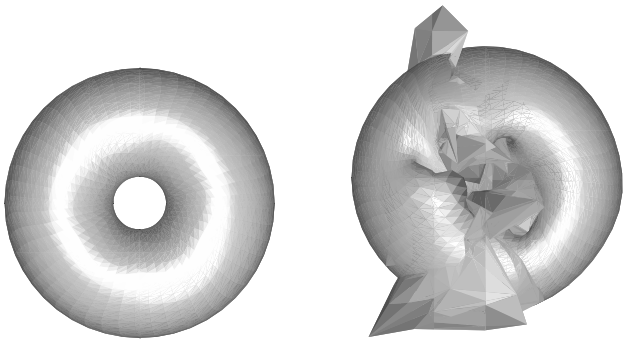

Figure 4.16: Torus after 210 and 240 steps of the iteration (figures are larger than those shown before.

Having seen the expected "short time behaviour" for the ellipsoid and for the toroidal mesh, we will now have a look at the effect of the Willmore flow on the glued dumbbell

mesh. The chosen parameters are `ilz` $= 2$, `genus` $= 0$, `projection` $= 2$, `conformal` $= 1$, `mcf_freq` $= 0$, and `expo` $= 5$. We depict the surface before the start of the iteration, after ten iterations, then after 20, 30, 40, 50, and 60 steps, respectively. In the first few steps, the neck of the dumbbell widens as we have expected because most of the curvature is "concentrated" there. Unfortunately, the mesh is destroyed much quicker as it is the case for the torus or the ellipsoid and we cannot study "long time behaviour", cf. figures 4.18 through 4.20.

U. Clarenz and G. Dziuk ([CD03]) have invented a trick for improving the mesh of a sphere that is parametrised over $\mathbb{S}^2$. Their method relies on "conformal reparametrisation". The theory behind this trick is presented in chapter 5, its discretisation and connection with the Willmore flow are discussed in chapter 6.

step	Willmore energy	regularity	step	Willmore energy	regularity
1	66.32	91.02	10	48.35	106.43
2	54.04	109.01	20	48.36	124.84
3	49.81	89.53	30	48.58	180.52
4	48.86	93.97	40	52.17	241.16
5	48.63	96.65	50	108.30	119.12
6	48.50	99.33			
7	48.44	101.04			
8	48.40	103.20			
9	48.37	104.56			

Figure 4.17: The behaviour of the Willmore energy under the flow for the glued dumbbell.

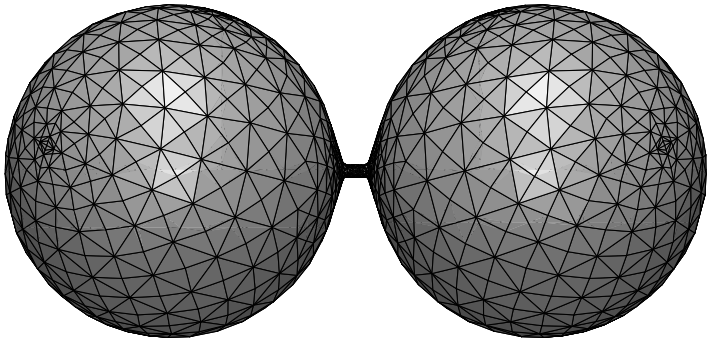

Figure 4.18: Before the iteration begins.

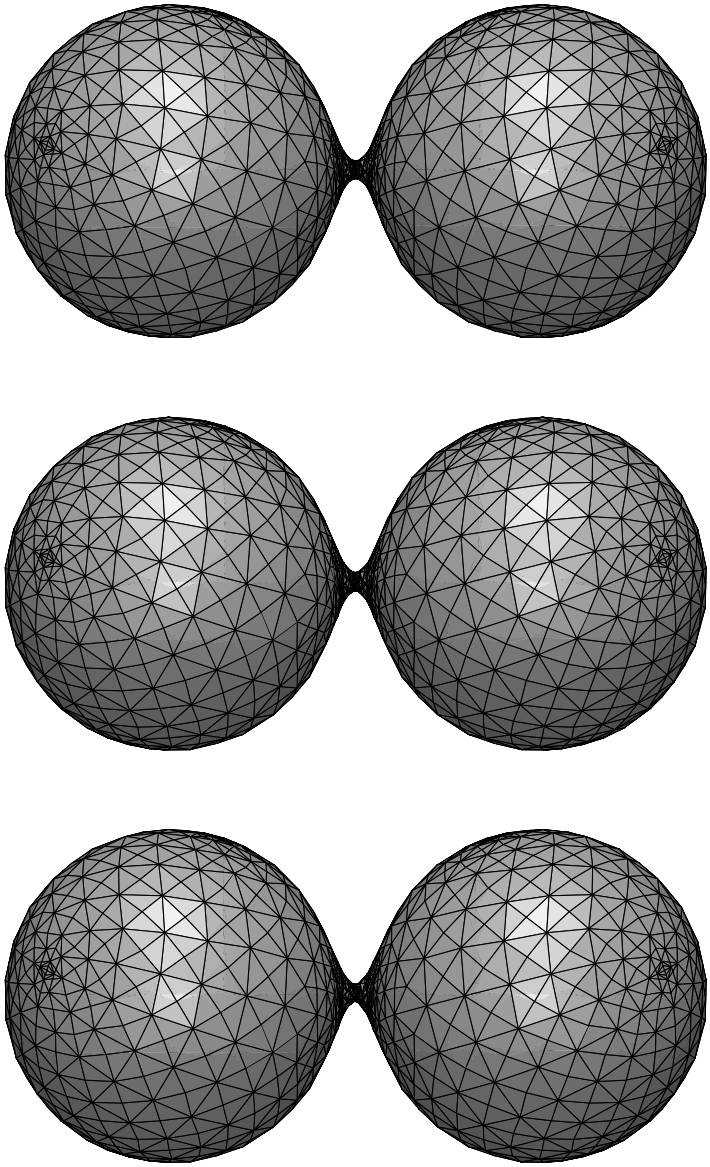

Figure 4.19: After 10, 20, and 30 steps of the iteration.

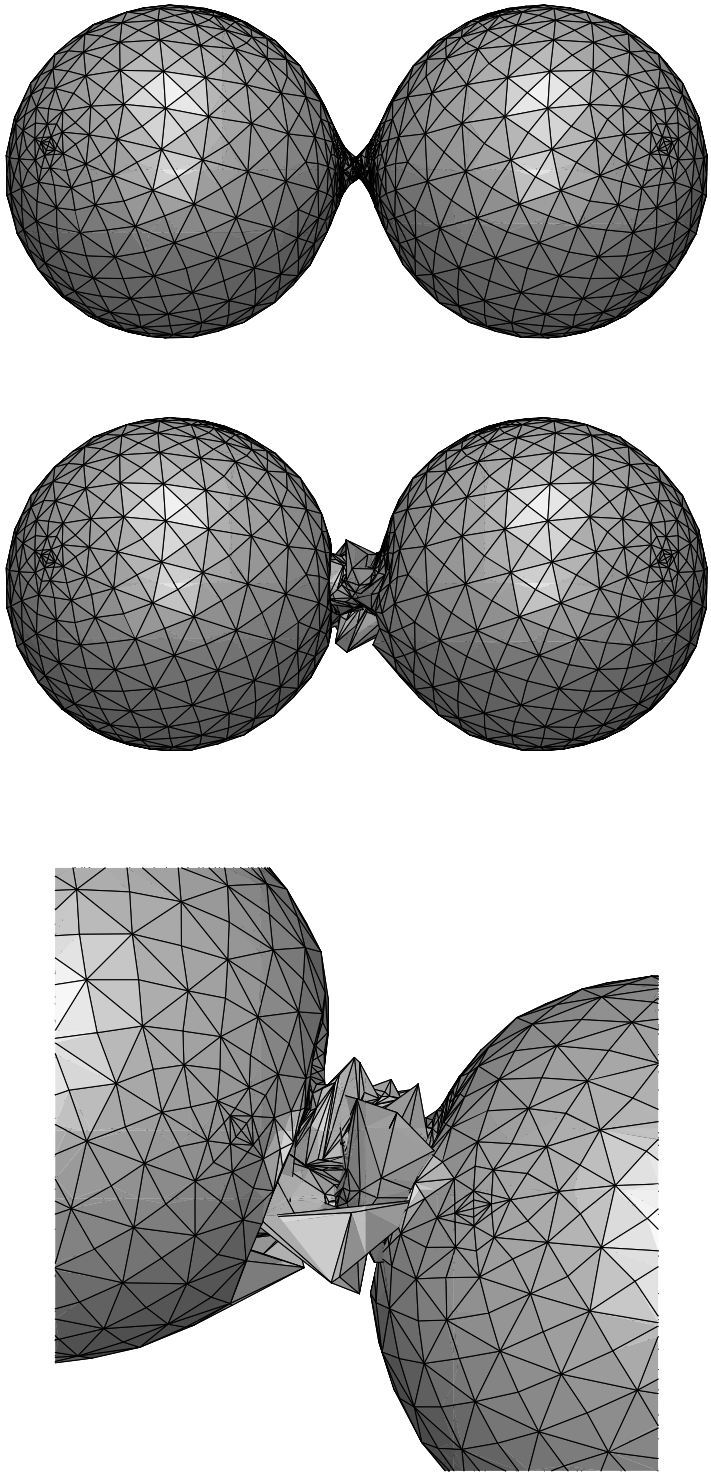

Figure 4.20: After 40 and 50 steps, and zoomed to the neck of the destroyed surface (after 60 iterations).

5 Conformal Parameters

In chapter 2, we have seen that conformality is a fundamental concept in the theory of Willmore surfaces. This is due to the conformal invariance of the Willmore functional (theorem 2.3.3). As announced in chapter 4, we can utilise this invariance to improve the mesh quality of deformed spheres – which we called the "conformality trick of U. Clarenz and G. Dziuk". In this chapter, we will describe the theoretical background of the conformality trick by proving an existence result for "global conformal parameters". The chapter is divided into four parts, namely an introduction, a proof of the existence result, a discussion of a similar proof by J. Jost, and, finally, a description of higher genus' phenomena. Chapter 6 will discuss the conformality trick, its conversion in the discrete setting, and the gained effects.

5.1 Introduction

It is well-known that a sphere with smooth Riemannian metric g can be conformally parametrised over $\mathbb{S}^2$ equipped with the canonical metric can – which means there is a conformal orientation-preserving diffeomorphism $h : (\mathbb{S}^2, \mathrm{can}) \to (\mathbb{S}^2, g)$, a *global conformal parameter*. To prove this, it suffices to combine the existence of isothermal coordinates (i. e. of local conformal parameters) with the uniformisation theorem[1]; the first can be reformulated to say that $\mathbb{S}^2$ is a *Riemann surface* and g is a conformal metric (see corollary 1.2.36), the second then states that every compact Riemann surface of genus 0 can be parametrised over the standard sphere by a *biholomorphic*[2] diffeomorphism h. By corollary 1.2.34, h is conformal.

Nevertheless, we wish to give a second, variational proof of the existence of global conformal parameters. We wish to do so because our proof makes the mesh-improving strategy chosen by U. Clarenz and G. Dziuk (the "conformality trick") plausible. At the same time, our proof constitutes a simplification of a variational proof given by J. Jost in [Jos90] (pp. 85). The first aspect is illuminated in chapter 6, the second will be discussed below (section 5.3). Our approach is guided by J. Jost's proof but presents some new ideas.

First of all, we state the existence theorem for global conformal parameters that we wish to prove. The definition of the Sobolev space H^1 and of h-compatible charts can be found

[1] cf. p.184 in [Jos91].
[2] both h and h^{-1} are holomorphic.

in chapter 1, the necessary explanations will be given below. J. Jost ([Jos90]) generalises this theorem by approximation techniques.

Theorem 5.1.1 (Existence of Global Conformal Parameters). *Let g be a Riemannian metric on $\mathbb{S}^2$ of class C^∞, let* can *denote the canonical metric on $\mathbb{S}^2$. Then, there exists a conformal, orientation-preserving diffeomorphism $h : (\mathbb{S}^2, \mathrm{can}) \to (\mathbb{S}^2, g)$ of class C^∞. Any two such diffeomorphisms differ by a preceding Möbius transform of $\mathbb{S}^2$, only. They are called* global conformal parameters.

Definition 5.1.2 (Möbius Transforms, Stereographic Charts). [3] A stereographic projection is a chart $\varphi : U_\varphi \to \mathbb{R}^2$ of $\mathbb{S}^2$ of the form $\varphi(p) = \frac{p - q(p\cdot q)}{1 - p\cdot q} \in E_q \cong \mathbb{R}^2$ where $q \in \mathbb{S}^2 \setminus U_\varphi$ and $E_q \subset \mathbb{R}^3$ is the plane with normal q through the origin. A *Möbius transform of* $\mathbb{S}^2$ is a diffeomorphism that has the form

$$z \mapsto \frac{az + b}{cz + d}$$

with respect to any one stereographic projection φ interpreted as $\varphi : \mathbb{S}^2 \to \mathbb{C} \cup \{\infty\}$, where $a, b, c, d \in \mathbb{C}$, $ad - bc \neq 0$.

Proposition 5.1.3. *Stereographic projections are conformal charts as defined in 1.2.28. Let $p_1, p_2, p_3 \in \mathbb{S}^2$, $q_1, q_2, q_3 \in \mathbb{S}^2$ satisfying $p_i \neq p_j$ and $q_i \neq q_j$ for $i \neq j \in \{1, 2, 3\}$. Then there is exactly one Möbius transform μ of $\mathbb{S}^2$ sending p_i to q_i, respectively. In particular, if $q_i = \sigma(p_i)$ $(i = 1, 2, 3)$ with respect to any orientation-preserving diffeomorphism σ, then μ is orientation-preserving. If $\mu : \mathbb{S}^2 \to \mathbb{S}^2$ is a smooth transform, then μ is a Möbius transform if and only if it is conformal with respect to the canonical metric* can *on $\mathbb{S}^2$.*

Before we prove the existence theorem, we sketch why it might become useful for mesh improvement (cf. chapters 4 and 6).

Remark. The global conformal parameters mentioned above are obtained as minimisers of a generalised Dirichlet energy E_g depending on the metric g. We roughly sketch the idea behind the conformality trick: Let $\Sigma_h \subset \mathbb{R}^3$ be a discrete surface. Try to find a "good" discretisation of $\mathbb{S}^2$, called $\mathbb{S}^2_h$, and a parametrisation $f : \Sigma_h \to \mathbb{S}^2_h$ (as defined in chapter 3) which is a homeomorphism and a minimiser of a discretised version of E_g (with respect to the "metric" induced on Σ_h by the canonical metric on $\mathbb{R}^3$).

Having found such a parametrisation f and a discretisation $\mathbb{S}^2_h$ of $\mathbb{S}^2$, we can pull back any mesh on $\mathbb{S}^2$ via f to yield a new mesh with vertices on Σ_h. Because of the "conformality" of f, the quality of the new mesh in terms of its interior angles equals the quality of the mesh chosen on $\mathbb{S}^2$. We then use this new triangulation as starting surface for the next steps of the iteration of the Willmore flow.

[3] The definition of Möbius transforms and the following proposition can be found in [Ahl66, Jos00, SY94], for example.

5.2 A Proof

In this section, we will give a variational proof of theorem 5.1.1. We will assume throughout that the metric g is of class C^∞. Many proofs, however, apply to continuous metrics, too. First of all, we will prove the uniqueness property.

Proof (Uniqueness). Let g be a Riemannian metric on $\mathbb{S}^2$. Suppose there are global conformal parameters $h, \tilde{h} : (\mathbb{S}^2, \mathrm{can}) \to (\mathbb{S}^2, g)$. As conformality carries over to composites, their composite $\mu := \tilde{h}^{-1} \circ h : (\mathbb{S}^2, \mathrm{can}) \to (\mathbb{S}^2, \mathrm{can})$ is a conformal diffeomorphism. Thus, by proposition 5.1.3, μ is a Möbius transform and $h = \tilde{h} \circ \mu$ which proves the uniqueness assertion of the theorem. □

Before we begin with the proof of theorem 5.1.1, we will make a few definitions and prove some lemmata. Fix three points $p_1, p_2, p_3 \in \mathbb{S}^2$, $p_i \neq p_j$ for $i \neq j \in \{1, 2, 3\}$.

Definition 5.2.1. Let $h : \mathbb{S}^2 \to \mathbb{S}^2$ be continuous. We say h *satisfies the three point condition (3P)* if $h(p_i) = p_i$ for $i \in \{1, 2, 3\}$. We call h *monotone* if the pre-images (under h) of connected sets are connected. If $h \in C^0 \cap H^{1,2}(S^2, S^2)$ (cf. proposition 1.3.6) we write $\det dh \geq 0$ ($\det dh > 0$) (and say h *has a non-negative (positive) Jacobian*), if its coordinate representations $\psi \circ h \circ \varphi^{-1} : \varphi(U_\varphi \cap h^{-1}(U_\psi)) \to \mathbb{R}^2$ satisfy $\det d(\psi \circ h \circ \varphi^{-1}) \geq 0$ (> 0) a. e. in all oriented charts $\psi : U_\psi \to \mathbb{R}^2$, $\varphi : U_\varphi \to \mathbb{R}^2$ of $\mathbb{S}^2$ with non-empty intersection $U_\varphi \cap h^{-1}(U_\psi)$.

We will take a variational approach in order to prove theorem 5.1.1. The class defined by

$$\mathcal{C} := \{h \in C^0 \cap H^{1,2}(\mathbb{S}^2, \mathbb{S}^2) \mid h \text{ is monotone and satisfies (3P) and } \det dh \geq 0\}$$

acts as the domain of definition of the functional E_g (a generalisation of the classical *Dirichlet energy*[4]) we will wish to minimise. Note that $\mathcal{C}$ is independent of the Riemannian metric g chosen on $\mathbb{S}^2$. A rough plan of the proof is given below. The following few lemmata collect some properties of $\mathcal{C}$.

I	E_g attains its minimum on $\mathcal{C}$.
II	Every minimiser $h : (\mathbb{S}^2, \mathrm{can}) \to (\mathbb{S}^2, g)$ of E_g in $\mathcal{C}$ is a conformal, orientation-preserving diffeomorphism.
√	Any such diffeomorphism is unique up to a preceding Möbius transform.

[4] For an introduction about Dirichlet energy cf. e. g. [Jos90].

Lemma 5.2.2.

$$\mathcal{C} \neq \emptyset, \text{ in particular } \mathrm{id}_{\mathbb{S}^2} \in \mathcal{C}$$

Proof. It is clear that $\mathrm{id}_{\mathbb{S}^2}$ lies in $C^0(\mathbb{S}^2, \mathbb{S}^2)$, is monotone, and satisfies (3P). Also, it has a positive Jacobian in the classical sense so that it has a non-negative Jacobian by chain rule. For any compact chart $\varphi : U \to \mathbb{R}^2$ of $\mathrm{id}_{\mathbb{S}^2}$, we have $\varphi \circ \mathrm{id}_{\mathbb{S}^2} \circ \varphi^{-1} \equiv \mathrm{id}_{\varphi(U)} \in H^1(\varphi(U))^2$ and thus $\mathrm{id}_{\mathbb{S}^2} \in \mathcal{C}$ by 1.3.6. □

Lemma 5.2.3. *If f is an orientation-preserving C^1-diffeomorphism of $\mathbb{S}^2$ that satisfies (3P), then*

$$h \in \mathcal{C} \Rightarrow h \circ f \in \mathcal{C}.$$

Proof. Let $h \in \mathcal{C}$, f as in the lemma. Then obviously $h \circ f \in C^0(\mathbb{S}^2, \mathbb{S}^2)$ is monotone and satisfies (3P). Let $\varphi : U_\varphi \to \mathbb{R}^2$, $\psi : U_\psi \to \mathbb{R}^2$ be compact oriented charts of $\mathbb{S}^2$ satisfying $(h \circ f)(U_\varphi) \subset U_\psi$ wlog. Define $\tilde{\varphi} := \varphi \circ f^{-1}$, then since f is an orientation-preserving diffeomorphism $\tilde{\varphi} : U_{\tilde{\varphi}} := f(U_\varphi) \to \mathbb{R}^2$ also is a compact oriented chart of $\mathbb{S}^2$ and satisfies $h(U_{\tilde{\varphi}}) \subset U_\psi$. We thus have $\psi \circ h \circ f \circ \varphi^{-1} = \psi \circ h \circ \tilde{\varphi}^{-1} \in H^1(\tilde{\varphi}(U_{\tilde{\varphi}}) = \varphi(U_\varphi), \mathbb{R}^2)$ so that lemma 1.3.3 tells us $h \circ f \in H^1(\mathbb{S}^2, \mathbb{S}^2)$. The same equation tells us that $h \circ f$ has a non-negative Jacobian and whence $h \circ f \in \mathcal{C}$. □

Lemma 5.2.4. *If $h \in C^0(\mathbb{S}^2, \mathbb{S}^2)$ is monotone and non-constant, then h is surjective. In particular, every $h \in \mathcal{C}$ is surjective.*

Proof. $\mathbb{S}^2$ is compact, h is continuous, so $h(\mathbb{S}^2)$ is compact. Suppose there were $p \in \mathbb{S}^2 \backslash h(\mathbb{S}^2)$ and let $q_1, q_2 \in h(\mathbb{S}^2)$ be different points (such points exist since h is non-constant). Then there are great circles through p and q_1, p and q_2, respectively, parametrised by arc length and denoted by $\gamma_i : [0, 2\pi] \to \mathbb{S}^2$ with $\gamma_i(\pi) = p$ for $i \in \{1, 2\}$. If γ_1, γ_2 describe the same great circle, we assume that $\gamma_1 = \gamma_2$. By compactness of $h(\mathbb{S}^2)$, there must be $t_1 \in [0, \pi)$ with $\gamma_1((t_1, \pi)) \subset \mathbb{S}^2 \setminus h(\mathbb{S}^2)$ and $\gamma_1(t_1) \in h(\mathbb{S}^2)$ as well as $t_2 \in (\pi, 2\pi)$ with $\gamma_1((\pi, t_2)) \subset \mathbb{S}^2 \setminus h(\mathbb{S}^2)$ and $\gamma_2(t_2) \in h(\mathbb{S}^2)$. As q_1, q_2 have been chosen to be distinct, we have $\gamma_1(t_1) \neq \gamma_2(t_2)$. Let $\gamma : [t_1, t_2] \to \mathbb{S}^2$, $\gamma := \gamma_1|_{[t_1,\pi]} * \gamma_2|_{[\pi,t_2]}$ which is well-defined due to $\gamma_i(\pi) = p$ $(i = 1, 2)$. Then γ is a curve in $\mathbb{S}^2 \setminus h(\mathbb{S}^2)$ with endpoints in $h(\mathbb{S}^2)$. Therefore, by monotonicity of h, $h^{-1}(\gamma([t_1, t_2])) \subset \mathbb{S}^2$ must be connected. On the other hand, $h^{-1}(\gamma([t_1, t_2])) = h^{-1}(\gamma(t_1)) \cup h^{-1}(\gamma(t_2))$. Since $h^{-1}(\gamma(t_1))$, $h^{-1}(\gamma(t_2))$ are closed, non-empty, and disjoint, this gives a contradiction. h must therefore be surjective. In particular, any $h \in \mathcal{C}$ satisfies (3P) and is henceforth non-constant. □

In the next lemmata, the metric g plays a rôle.

Lemma 5.2.5. [5] *Let $h \in C^0 \cap H^1(\mathbb{S}^2, \mathbb{S}^2)$, g any smooth Riemannian metric on $\mathbb{S}^2$. Let $d\,\mathrm{vol}_{\mathbb{S}^2}$ denote the Riemannian volume form on $\mathbb{S}^2$ with respect to* can. *We set*

$$E_g(h) := \frac{1}{2} \int_{\mathbb{S}^2} \langle dh, dh \rangle_{(T\mathbb{S}^2_{\mathrm{can}})^* \otimes h^{-1} T\mathbb{S}^2_g} d\,\mathrm{vol}_{\mathbb{S}^2},$$

where $\langle ., . \rangle_{(T\mathbb{S}^2_{\mathrm{can}})^* \otimes h^{-1} T\mathbb{S}^2_g}$ is the Riemannian metric on the bundle $(T\mathbb{S}^2)^* \otimes h^{-1} T\mathbb{S}^2$ induced by can *and the pullback of g via h. In this formula, $(T\mathbb{S}^2)^*$ denotes the cotangent bundle*

[5] The definition of E_g is based on pp. 401 in [Jos91].

of $\mathbb{S}^2$. $h^{-1}T\mathbb{S}^2$ *denotes the pullback of* $T\mathbb{S}^2$ *via* h. *Then the* energy E_g *is well-defined (i. e. independent of the chosen atlas), non-negative and finite. In particular, in local coordinates, the inner product can be calculated as*

$$\langle dh, dh\rangle_{(T\mathbb{S}^2_{\mathrm{can}})^*\otimes h^{-1}T\mathbb{S}^2_g} = \mathrm{can}^{\alpha\beta}\; g_{ij}\circ h\,\frac{\partial h^i}{\partial x^\alpha}\,\frac{\partial h^j}{\partial x^\beta}. \tag{5.1}$$

Proof. For $h \in C^1(\mathbb{S}^2,\mathbb{S}^2)$, all appearing bundles and the metrics thereon are clearly well-defined and the energy E_g is finite. Choosing h-compatible compact charts φ in the domain and ψ in the target by lemma 1.2.26, the inverses of which we denote by x^α and y^i, respectively, we have $dh = \frac{\partial h^i}{\partial x^\alpha}dx^\alpha \otimes \frac{\partial}{\partial y^i}$ and thus equation 5.1 applies. The right hand side is well-defined as a member of L^1 if $h \in C^0\cap H^1(\mathbb{S}^2,\mathbb{S}^2)$ by proposition 1.3.6 and by the Hölder inequality. Also, the right hand side term transforms in a way that leaves the energy integral unchanged – the calculation being the same as for C^1-maps (cf. p. 109 in [Alt91] and pp. 86 in [Jos91] (Sobolev sections)). We can thus define $\langle dh, dh\rangle_{(T\mathbb{S}^2_{\mathrm{can}})^*\otimes h^{-1}T\mathbb{S}^2_g}$ for $h \in C^0 \cap H^1(\mathbb{S}^2,\mathbb{S}^2)$ by using equality 5.1 as a definition. Using a partition of unity subordinate to the finite compact atlas in the domain of h, we deduce $0 \le E_g(h) < \infty$. □

Remark. We use $E := E_{\mathrm{can}}$ as a shorthand and call $E(h)$ the *Dirichlet energy* of h. We write $\mathcal{C}_K := \{h \in \mathcal{C} \,|\, E(h) \le K\}$ for $K > 0$. Again, note that $\mathcal{C}_K$ is independent of the metric g chosen on $\mathbb{S}^2$.

Lemma 5.2.6. *Let* g *be a smooth Riemannian metric on* $\mathbb{S}^2$. *Then there are constants* $m, M > 0$ *such that for all* $h \in C^0 \cap H^1(\mathbb{S}^2,\mathbb{S}^2)$, *we have*

$$mE(h) \le E_g(h) \le ME(h).$$

Proof. Let $\mathcal{B} = \{\varphi : U_\varphi \to \mathbb{R}^2\}$ be a finite compact atlas on $\mathbb{S}^2$ so that φ can be extended to an open set containing $\overline{U_\varphi}$ (exists by lemma 1.2.3). Then we can view $(g_{ij}) : \overline{U} \to \mathbb{R}^{2\times 2}$ and $(\mathrm{can}_{ij}) : \overline{U} \to \mathbb{R}^{2\times 2}$ as two continuous families of positive definite symmetric matrices (dropping the explicit reference to the charts for notational simplicity). By linear algebra, we know that for each $p \in \overline{U}$, there are two positive eigenvalues $\kappa_1(p), \kappa_2(p)$ of $(g_{ij})(p)$ and $\mu_1(p), \mu_2(p)$ of $(\mathrm{can}_{ij})(p)$, respectively, which are the roots of a quadratic equation the coefficients of which depend on p continuously. Since these roots must henceforth be continuous, the eigenvalues can be understood as continuous functions on $\overline{U}$ and do thus attain their minimal and maximal values in $\mathbb{R}^+$ by compactness of the domain. Let

$$m_{\mathcal{B}} := \min_{\varphi\in\mathcal{B}} \frac{\min\{\kappa_1^\varphi(p), \kappa_2^\varphi(p) \,|\, p \in \overline{U_\varphi}\}}{\max\{\mu_1^\varphi(p), \mu_2^\varphi(p) \,|\, p \in \overline{U_\varphi}\}} \quad \text{and} \quad M_{\mathcal{B}} := \max_{\varphi\in\mathcal{B}} \frac{\max\{\kappa_1^\varphi(p), \kappa_2^\varphi(p) \,|\, p \in \overline{U_\varphi}\}}{\min\{\mu_1^\varphi(p), \mu_2^\varphi(p) \,|\, p \in \overline{U_\varphi}\}},$$

then $0 < m_{\mathcal{B}}, M_{\mathcal{B}} < \infty$ only depend on the atlas chosen. We conclude by quadratic form calculus that in a chart $\varphi \in \mathcal{B}$, we have

$$m_{\mathcal{B}}\,\mathrm{can}^\varphi_{ij}\,X^iX^j \le g^\varphi_{ij}X^iX^j \le M_{\mathcal{B}}\,\mathrm{can}^\varphi_{ij}\,X^iX^j \tag{5.2}$$

for all vectors $X \in T\mathbb{S}^2$ ($p \in \overline{U}$). Let $h \in C^0 \cap H^1(\mathbb{S}^2,\mathbb{S}^2)$. Choose a finite compact stereographic atlas $\mathcal{A}$ in the domain of h which is h-compatible to $\mathcal{B}$ as in lemma 1.2.26.

Then we can write $\mathrm{can}^{\psi}_{\alpha\beta} = \rho^{\psi}\delta_{\alpha\beta}$, with $\rho^{\psi} : V_{\psi} \to \mathbb{R}^+$ continuous for all $\psi : V_{\psi} \to \mathbb{R}^2 \in \mathcal{A}$. We thus locally have by lemma 5.2.5

$$\begin{aligned} m_{\mathcal{B}}\langle dh, dh\rangle_{(T\mathbb{S}^2_{\mathrm{can}})^*\otimes h^{-1}T\mathbb{S}^2_{\mathrm{can}}} &= \frac{m_{\mathcal{B}}}{\rho^{\psi}} \sum_{\alpha=1}^{2} \mathrm{can}^{\varphi}_{ij} \circ h \, \frac{\partial h^i}{\partial x^{\alpha}} \frac{\partial h^j}{\partial x^{\alpha}} \\ &\overset{(5.2)}{\leq} \frac{1}{\rho^{\psi}} \sum_{\alpha=1}^{2} g^{\varphi}_{ij} \circ h \, \frac{\partial h^i}{\partial x^{\alpha}} \frac{\partial h^j}{\partial x^{\alpha}} \\ &= \langle dh, dh\rangle_{(T\mathbb{S}^2_{\mathrm{can}})^*\otimes h^{-1}T\mathbb{S}^2_{g}} \\ &\overset{(5.2)}{\leq} \frac{M_{\mathcal{B}}}{\rho^{\psi}} \sum_{\alpha=1}^{2} \mathrm{can}^{\varphi}_{ij} \circ h \, \frac{\partial h^i}{\partial x^{\alpha}} \frac{\partial h^j}{\partial x^{\alpha}} \\ &= M_{\mathcal{B}}\langle dh, dh\rangle_{(T\mathbb{S}^2_{\mathrm{can}})^*\otimes h^{-1}T\mathbb{S}^2_{\mathrm{can}}} \end{aligned}$$

almost everywhere, where $\varphi \in \mathcal{B}$ and (x^{α}) are the coordinates with respect to φ. Integrating this local inequality with the aid of a partition of unity, we get the desired result with constants $m_{\mathcal{B}}, M_{\mathcal{B}}$ depending on the atlas. However, as both E and E_g are independent of the atlas by lemma 5.2.5, the constants are universal. □

The generalised Dirichlet energy is conformally invariant in its domain just as the Willmore energy is in its image (see theorem 2.3.3). This explains the three point condition in the class $\mathcal{C}$.

Lemma 5.2.7. *Let $h \in C^0 \cap H^1(\mathbb{S}^2, \mathbb{S}^2)$, let $\mu : \mathbb{S}^2 \to \mathbb{S}^2$ a Möbius transform, let g be any smooth Riemannian metric on $\mathbb{S}^2$. Then*

$$E_g(h \circ \mu) = E_g(h).$$

Proof. Let $\varphi : U_{\varphi} \to \mathbb{R}^2$ and $\psi : U_{\psi} \to \mathbb{R}^2$ be $(h\circ\mu)$-compatible charts of $\mathbb{S}^2$ and such that φ is a stereographic projection (such charts exist by continuity of $h \circ \mu$). Then, denoting by (y^{α}) the local coordinates associated to the conformal chart $\tilde{\varphi} := \varphi \circ \mu^{-1} : \mu(U_{\varphi}) \to \mathbb{R}^2$ and by (x^{α}) those associated to φ, we locally have $\frac{\partial (h\circ\mu)^i}{\partial x^{\alpha}} = \frac{\partial h^i}{\partial y^{\gamma}} \circ \mu \, \frac{\partial \mu^{\gamma}}{\partial x^{\alpha}}$ by the Sobolev chain rule 1.1.7 and thus obtain in local coordinates (using proposition 5.1.3 and linear algebra)

$$\begin{aligned} \langle d(h\circ\mu), d(h\circ\mu)\rangle_{(T\mathbb{S}^2_{\mathrm{can}})^*\otimes(h\circ\mu)^{-1}T\mathbb{S}^2_{g}} &= \frac{1}{\lambda^{\varphi}} \delta^{\alpha\beta} \frac{\partial \mu^{\gamma}}{\partial x^{\alpha}} \frac{\partial \mu^{\rho}}{\partial x^{\beta}} \, (g^{\psi}_{ij} \circ h \, \frac{\partial h^i}{\partial y^{\gamma}} \frac{\partial h^j}{\partial y^{\rho}}) \circ \mu \\ &= \frac{1}{\lambda^{\varphi}} |\det(d\mu)| (\delta^{\gamma\rho} \, g^{\psi}_{ij} \circ h \, \frac{\partial h^i}{\partial y^{\gamma}} \frac{\partial h^j}{\partial y^{\rho}}) \circ \mu \\ &= \frac{\lambda^{\tilde{\varphi}} \circ \mu}{\lambda^{\varphi}} |\det(d\mu)| (\widetilde{\mathrm{can}}^{\gamma\rho} \, g^{\psi}_{ij} \circ h \, \frac{\partial h^i}{\partial y^{\gamma}} \frac{\partial h^j}{\partial y^{\rho}}) \circ \mu \\ &= \frac{\lambda^{\tilde{\varphi}} \circ \mu}{\lambda^{\varphi}} |\det(d\mu)| \, \langle dh, dh\rangle_{(T\mathbb{S}^2_{\mathrm{can}})^*\otimes h^{-1}T\mathbb{S}^2_{g}} \circ \mu \end{aligned}$$

almost everywhere with $\mathrm{can}^{\varphi}_{\alpha\beta} = \lambda^{\varphi}\delta_{\alpha\beta}$ and $\widetilde{\mathrm{can}}_{\alpha\beta} := \mathrm{can}^{\tilde{\varphi}}_{\alpha\beta} = \lambda^{\tilde{\varphi}}\delta_{\alpha\beta}$ by conformality of the charts. By the transformation formula for integrals and using $\sqrt{\det(\mathrm{can}^{\varphi})} = \lambda^{\varphi}$ as well as $\sqrt{\det(\widetilde{\mathrm{can}}^{\varphi})} \circ \mu = \lambda^{\tilde{\varphi}} \circ \mu$, we get the desired result of $E_g(h \circ \mu) = E_g(h)$. □

There are two ways of defining uniform convergence for sequences $(h_n)_{n\in\mathbb{N}} \subset C^0(\mathbb{S}^2,\mathbb{S}^2)$ to a limit $\in C^0(\mathbb{S}^2,\mathbb{S}^2)$. One consists of requesting that $\sup_{p\in\mathbb{S}^2} d_{\mathbb{S}^2}(h_n(p),h(p)) \to 0$ as $n\to\infty$ where $d_{\mathbb{S}^2}$ is the distance function induced by any Riemannian metric on $\mathbb{S}^2$; the other is to understand h_n, h as members of $C^0(\mathbb{S}^2,\mathbb{R}^3)$ and to request $\|h_n - h\|_{C^0(\mathbb{S}^2,\mathbb{R}^3)} \to 0$. As $\mathbb{S}^2$ is compact, both notions coincide. We will thus speak of uniform convergence without specifying the exact meaning.

Lemma 5.2.8. *Let g be a smooth Riemannian metric on $\mathbb{S}^2$, $K>0$. Then the functional $E_g : \mathcal{C}_K \to \mathbb{R}$ is* lower semi-continuous *with respect to uniform convergence, i. e. for any uniformly converging series $(h_n)_{n\in\mathbb{N}} \subset \mathcal{C}_K$ with limit $h\in\mathcal{C}_K$, we have*

$$E_g(h) \le \liminf_{n\to\infty} E_g(h_n).$$

We will give two different proofs of this lemma. One uses J. Nash's embedding theorem (cf. [Nas56, Gü89]), the other is more direct[6]. A third proof can be found on pp. 449 in [Jos91].

Proof (Using J. Nash's Embedding Theorem). By J. Nash's embedding theorem, $(\mathbb{S}^2,g)$ is isometrically embedded into some $\mathbb{R}^N$ via e. We can thus understand $e\circ\mathcal{C}$ as a subset of $H^1(\mathbb{S}^2,\mathbb{R}^N)$ by definition of $H^1(\mathbb{S}^2,\mathbb{S}^2)$. Let $(h_n)_{n\in\mathbb{N}}$ be a uniformly converging sequence in $\mathcal{C}_K$ with limit $h\in\mathcal{C}_K$, then $E(h_n)\le K$ by assumption. It is straightforward to see that $(e\circ h_n)$ converges uniformly in $C^0(\mathbb{S}^2,\mathbb{R}^N)$ to $e\circ h$. As, by lemma 5.2.6, there is a constant M with $E_g \le ME$ on $C^0\cap H^1(\mathbb{S}^2,\mathbb{S}^2)$, so we have $E_g(h_n)\le MK<\infty$ for all $n\in\mathbb{N}$. Also, according to our remark on page 15 and by J. Wloka[7],

$$\begin{aligned}
\|e\circ h_n\|^2_{H^1(\mathbb{S}^2,\mathbb{R}^N)} &= \int_{\mathbb{S}^2} |e\circ h_n|^2_{\mathbb{R}^N}\, d\,\mathrm{vol}_{\mathbb{S}^2} + 2E_g(h_n)\\
&\le \mathrm{vol}(\mathbb{S}^2)\ \sup_{p\in\mathbb{S}^2} |e(p)|^2_{\mathbb{R}^N} + 2E_g(h_n)\\
&\le \mathrm{vol}(\mathbb{S}^2)\ \sup_{p\in\mathbb{S}^2} |e(p)|^2_{\mathbb{R}^N} + 2MK < \infty,
\end{aligned}$$

so that $(e\circ h_n)_{n\in\mathbb{N}}$ is a bounded sequence in $H^1(\mathbb{S}^2,\mathbb{R}^N)$. From Hilbert space theory[8], it follows that $(e\circ h_n)_{n\in\mathbb{N}}$ has a $H^1(\mathbb{S}^2,\mathbb{R}^N)$-*weakly converging subsequence*[9] with limit $\tilde{h}\in H^1(\mathbb{S}^2,\mathbb{R}^N)$. We denote the subsequence by $(e\circ h_n)_{n\in\mathbb{N}}$, again. Uniform convergence implies strong and thus weak $L^2(\mathbb{S}^2,\mathbb{R}^N)$-convergence; also $H^1(\mathbb{S}^2,\mathbb{R}^N)$-weak convergence implies $L^2(\mathbb{S}^2,\mathbb{R}^N)$-weak convergence. Thus, we can deduce $e\circ h = \tilde{h}$ a. e. The norms then satisfy $\|e\circ h\|_{H^1(\mathbb{S}^2,\mathbb{R}^N)} \le \liminf_{n\to\infty}\|e\circ h_n\|_{H^1(\mathbb{S}^2,\mathbb{R}^N)}$ and thus $E_g(h)\le\liminf_{n\to\infty} E_g(h_n)$ which shows that $E_g:\mathcal{C}_K\to\mathbb{R}$ is lower semi-continuous. □

In order to replace J. Nash's embedding theorem, we prove the following elementary lemma that ensures that the properties of uniform convergence, being of class H^1, and being "energy bounded" carry over to local representations. We will frequently use this lemma in the proof of theorem 5.1.1.

[6] and allows for lower regularity (g need only be continuous).
[7] pp. 92 in [Wlo82].
[8] cf. e. g. [Alt91].
[9] cf. pp. 209 in [Alt91] for the definition of weak convergence and weak topology.

Lemma 5.2.9. *Let $h \in C^0 \cap H^1(\mathbb{S}^2, \mathbb{S}^2)$, let $\varphi : U \to \mathbb{R}^2, \psi : V \to \mathbb{R}^2$ be h-compatible compact charts of $\mathbb{S}^2$ such that V is contained in an open hemisphere. Let $u := \psi \circ h \circ \varphi^{-1}$. Then $u \in C^0 \cap H^1(\varphi(U), \mathbb{R}^2)$. Next, let $(h_n)_{n\in\mathbb{N}} \subset C^0 \cap H^1(\mathbb{S}^2, \mathbb{S}^2)$ be a sequence with $h_n(\overline{U}) \subset V$. If (h_n) is* energy bounded *(i. e. there is a constant $K > 0$ such that $E(h_n) \leq K$ for all $n \in \mathbb{N}$) then the sequence $(u_n)_{n\in\mathbb{N}}$ defined by $u_n := \psi \circ h_n \circ \varphi^{-1}$ has a $H^1(\varphi(U), \mathbb{R}^2)$-weakly converging subsequence with limit in $H^1(\varphi(U), \mathbb{R}^2)$. If (h_n) converges uniformly to h, then (u_n) converges uniformly to u. If (h_n) is energy bounded and converges uniformly to h, then a subsequence of (u_n) converges uniformly and weakly in $H^1(\varphi(U), \mathbb{R}^2)$ to u. Moreover, if $(h_n)_{n\in\mathbb{N}} \subset C^0(\mathbb{S}^2, \mathbb{S}^2)$ is any uniformly converging sequence with limit h, we can find finite compact sub-atlases of any given pair of atlases on $\mathbb{S}^2$ that are both h- and h_n-compatible for all $n \geq n_0$.*

Proof. u is well-defined as a member of $C^0(\varphi(U), \mathbb{R}^2)$ as φ and ψ are h-compatible. If we understand φ (and u with it) to be defined on some open set W containing $\overline{U}$ with $h(W) \subset V$ by compactness and h-compatibility, we can estimate the H^1-norm of u by $\|u\|^2_{H^1(\varphi(U),\mathbb{R}^2)} \leq \|\psi\|^2_{C^0(V,\mathbb{R}^2)} \operatorname{vol}(\varphi(U)) + 2E(u)$, where E denotes the classical Dirichlet energy of u. As in lemma 5.2.6, there is a universal constant $C > 0$ such that the inequality $\delta_{ij} X^i X^j \leq C \operatorname{can}^{\psi}_{ij} X^i X^j$ holds for all continuous vector fields X defined on a neighbourhood of $\overline{V}$. Therefore, we can calculate $E(u)$ by definition of u and compactness of all charts involved, and obtain

$$\begin{aligned}
E(u) &= \int_{\varphi(U)} |du|^2 \, dx^1 dx^2 \\
&= \int_{\varphi(U)} \delta^{\alpha\beta} \, \delta_{ij} \, \frac{\partial u^i}{\partial x^\alpha} \, \frac{\partial u^j}{\partial x^\beta} \, dx^1 dx^2 \\
&= \int_{\varphi(U)} \operatorname{can}^{\alpha\beta} \circ \varphi^{-1} \, \delta_{ij} \, \frac{\partial h^i}{\partial x^\alpha} \circ \varphi^{-1} \, \frac{\partial h^j}{\partial x^\beta} \circ \varphi^{-1} \, \sqrt{\det(\operatorname{can})} \circ \varphi^{-1} \, dx^1 dx^2 \\
&\leq C \int_{\varphi(U)} (\operatorname{can}^{\alpha\beta} \, \operatorname{can}^{\psi}_{ij} \circ h \, \frac{\partial h^i}{\partial x^\alpha} \, \frac{\partial h^j}{\partial x^\beta} \sqrt{\det(\operatorname{can})}) \circ \varphi^{-1} \, dx^1 dx^2 \\
&= C \int_U \langle dh, dh \rangle_{(T\mathbb{S}^2_{\text{can}})^* \otimes h^{-1} T\mathbb{S}^2_{\text{can}}} \, d \operatorname{vol}_{\mathbb{S}^2}
\end{aligned}$$

where (x^α) denotes the coordinates with respect to φ. Choose a pair of finite compact h-compatible atlases $\mathcal{A}, \mathcal{B}$ on $\mathbb{S}^2$ containing φ, ψ respectively with a partition of unity (η_l) subordinate to $\mathcal{A}$ satisfying $\eta \equiv 1$ on U. Then $E(u) \leq CE(h) < \infty$ by the above and thus $u \in C^0 \cap H^1(\varphi(U), \mathbb{R}^2)$.

Next, let $(h_n)_{n\in\mathbb{N}} \subset C^0 \cap H^1(\mathbb{S}^2, \mathbb{S}^2)$ be a sequence with $h_n(\overline{U}) \subset V$ that satisfies $E(h_n) \leq K$ for all $n \in \mathbb{N}$. Let $u_n := \psi \circ h_n \circ \varphi^{-1}$, then replacing u by u_n in the above calculation, we get $\|u_n\|^2_{H^1(\varphi(U),\mathbb{R}^2)} \leq \|\psi\|^2_{C^0(V,\mathbb{R}^2)} \operatorname{vol}(\varphi(U)) + 2C \int_U \langle dh_n, dh_n \rangle_{(T\mathbb{S}^2_{\text{can}})^* \otimes h^{-1} T\mathbb{S}^2_{\text{can}}} \, d \operatorname{vol}_{\mathbb{S}^2}$. As above, choosing any finite compact h_n-compatible pair of atlases $\mathcal{A}_n, \mathcal{B}_n$ on $\mathbb{S}^2$ containing φ, ψ, respectively, we derive $\|u_n\|^2_{H^1(\varphi(U),\mathbb{R}^2)} \leq \|\psi\|^2_{C^0(V,\mathbb{R}^2)} \operatorname{vol}(\varphi(U)) + 2CK$. Thus by Hilbert

space theory[10], there is a weakly $H^1(\varphi(U),\mathbb{R}^2)$-converging subsequence of (u_n) with limit in $H^1(\varphi(U),\mathbb{R}^2)$.

Let now $(h_n)_{n\in\mathbb{N}} \subset C^0 \cap H^1(\mathbb{S}^2,\mathbb{S}^2)$ be a sequence with $h_n(\overline{U}) \subset V$ and uniformly convergent to a limit $h \in C^0(\mathbb{S}^2,\mathbb{S}^2)$. We extend the chart ψ to an open neighbourhood $W := \{p \in \mathbb{R}^3 \,|\, |p| \in (0,2), \frac{p}{|p|} \in V\}$ of V in $\mathbb{R}^3$, such that $\psi : W \to \mathbb{R}^2$ is of class C^1 by setting $\psi(p) := \psi(\frac{p}{|p|})$ for $p \in W$. W contains all line segments connecting points of V since V is contained in an open hemisphere, so that we can apply the mean value theorem of calculus to ψ. For $x \in \varphi(U)$, this gives (since $h_n(\overline{U}) \subset V \subset W$)

$$|u_n(x) - u(x)| \leq \sup_{y\in W} \|d\psi(y)\| \, |h_n(\varphi^{-1}(x)) - h(\varphi^{-1}(x))| \leq \sup_{y\in W} \|d\psi(y)\| \, \|h_n - h\|_{C^0}$$

so that (u_n) converges uniformly to u as $n \to \infty$ on $\varphi(U)$. Let now, additionally, (h_n) be energy bounded and thus (u_n) have a weakly $H^1(\varphi(U),\mathbb{R}^2)$-converging subsequence with limit $\tilde{u} \in H^1(\varphi(U),\mathbb{R}^2)$. As both types of convergences imply weak $L^2(\varphi(U),\mathbb{R}^2)$-convergence, we have $u = \tilde{u}$ almost everywhere and thus $u \in C^0 \cap H^1(\varphi(U),\mathbb{R}^2)$.

Finally, let $(h_n)_{n\in\mathbb{N}} \subset C^0(\mathbb{S}^2,\mathbb{S}^2)$ be a uniformly converging sequence with limit h, $\mathcal{A},\mathcal{B}$ any given pair of finite atlases on $\mathbb{S}^2$. Let $\varepsilon > 0$. Then by lemma 1.2.3 and lemma 1.2.26, we can refine $\mathcal{A} = \{\varphi : U_\varphi \to \mathbb{R}^2\}$ and $\mathcal{B} = \{\psi : V_\psi \to \mathbb{R}^2\}$ such that they are finite, compact, and h-compatible and that all charts in $\mathcal{B}$ can be extended to ε-balls about their domains (i. e. to $B_\varepsilon(V_\psi)$). Then, by uniform convergence, there is an n_0 with $h_n(\overline{U_\varphi}) \subset B_\varepsilon(h(U_\varphi)) \subset B_\varepsilon(V_\psi)$ for all $n \geq n_0$. Hence the refined atlases are h_n-compatible for $n \geq n_0$. □

As differentiation is a local process, the chain and product rules described in proposition 1.1.7 carry over from the planar case to Sobolev functions on surfaces by the above lemma. We are now in a position to prove the lower semi-continuity of E_g (lemma 5.2.8) without relying on J. Nash's embedding theorem. Let g be a smooth Riemannian metric on $\mathbb{S}^2$, $K > 0$ such that $\mathcal{C}_K \neq \emptyset$ by lemma 5.2.2.

Proof (Not Using J. Nash's Embedding Theorem). Let $\varepsilon > 0$ and let $(h_n)_{n\in\mathbb{N}}$ be a uniformly converging sequence in $\mathcal{C}_K$ with limit $h \in \mathcal{C}_K$. Choose a pair of finite compact h- and h_n-compatible atlases $\mathcal{A} = \{\varphi_l : U_l \to \mathbb{R}^2\}_{l=1}^L, \mathcal{B} = \{\psi_l : V_l \to \mathbb{R}^2\}_{l=1}^L$ on $\mathbb{S}^2$, such that $\mathcal{A}$ consists of stereographic projections with the aid of lemma 5.2.9. Without loss of generality, counting charts in $\mathcal{B}$ several times if necessary, we can assume that $h(\overline{U}_l) \subset V_l$. Then by the same lemma, the functions $u_{n;l} := \psi_l \circ h_n \circ \varphi_l^{-1} : \varphi_l(U_l) \to \mathbb{R}^2$, $u_l := \psi_l \circ h \circ \varphi_l^{-1} : \varphi_l(U_l) \to \mathbb{R}^2$ lie in $C^0 \cap H^1(\varphi(U_l),\mathbb{R}^2)$ and $(u_{n;l})$ converges uniformly and weakly in $H^1(\varphi_l(U_l),\mathbb{R}^2)$ to u_l wlog. Collecting all results and notation, we use the symmetry and positive definiteness of $g_{ij}^l := g_{ij}^{\varphi_l}$ to get ((η_l) being a partition of unity subordinate to $\mathcal{A}$)

$$\begin{aligned} E_g(h_n) &= \sum_{l=1}^{L} \int\limits_{\varphi_l(U_l)} (\eta_l \circ \varphi_l^{-1})(g_{ij}^l \circ \psi_l^{-1} \circ u_{n;l})\, \delta^{\alpha\beta} \frac{\partial u_{n;l}^i}{\partial x^\alpha} \frac{\partial u_{n;l}^j}{\partial x^\beta}\, dx^1 dx^2 \\ &= \sum_{\alpha=1}^{2} \sum_{l=1}^{L} \int\limits_{\varphi_l(U_l)} (\eta_l \circ \varphi_l^{-1})(g_{ij}^l \circ \psi_l^{-1} \circ u_{n;l})\, (\frac{\partial u_{n;l}^i}{\partial x^\alpha})(\frac{\partial u_{n;l}^j}{\partial x^\alpha})\, dx^1 dx^2 \end{aligned}$$

[10] cf. e. g. [Alt91].

$$
\begin{aligned}
&\overset{\pm 0}{=} \sum_{\alpha=1}^{2}\sum_{l=1}^{L} \int\limits_{\varphi_l(U_l)} (\eta_l \circ \varphi_l^{-1})(g_{ij}^l \circ \psi_l^{-1} \circ u_{n;l}) \, (\frac{\partial u_l^i}{\partial x^\alpha})(\frac{\partial u_l^j}{\partial x^\alpha}) \, dx^1 dx^2 \\
&+ \sum_{\alpha=1}^{2}\sum_{l=1}^{L} \int\limits_{\varphi_l(U_l)} (\eta_l \circ \varphi_l^{-1})(g_{ij}^l \circ \psi_l^{-1} \circ u_{n;l}) \, (\frac{\partial (u_{n;l}-u_l)^i}{\partial x^\alpha})(\frac{\partial (u_{n;l}-u_l)^j}{\partial x^\alpha}) dx^1 dx^2 \\
&+ 2\sum_{\alpha=1}^{2}\sum_{l=1}^{L} \int\limits_{\varphi_l(U_l)} (\eta_l \circ \varphi_l^{-1}) \, (g_{ij}^l \circ \psi_l^{-1} \circ u_{n;l}) \, (\frac{\partial u_l^i}{\partial x^\alpha})(\frac{\partial (u_{n;l}-u_l)^j}{\partial x^\alpha}) \, dx^1 dx^2 \\
&\overset{\eta_l \geq 0}{\geq} \sum_{i,\alpha=1}^{2}\sum_{l=1}^{L} \int\limits_{\varphi_l(U_l)} (\eta_l \circ \varphi_l^{-1})(g_{ij}^l \circ \psi_l^{-1} \circ u_{n;l}) \, (\frac{\partial u_l^i}{\partial x^\alpha})(\frac{\partial u_l^j}{\partial x^\alpha}) \, dx^1 dx^2 \\
&+ 2\sum_{i,\alpha=1}^{2}\sum_{l=1}^{L} \int\limits_{\varphi_l(U_l)} (\eta_l \circ \varphi_l^{-1}) \, (g_{ij}^l \circ \psi_l^{-1} \circ u_{n;l}) \, (\frac{\partial u_l^i}{\partial x^\alpha})(\frac{\partial (u_{n;l}-u_l)^j}{\partial x^\alpha}) \, dx^1 dx^2
\end{aligned}
$$

where the first term on the right hand side converges to $E_g(h)$ since $(u_{n;l})$ converges uniformly to u_l and since $g_{ij}^l \circ \psi_l^{-1}$ is continuous. Finally, $(\frac{\partial (u_{n;l}-u_l)^j}{\partial x^\alpha})$ converges weakly to 0 in $L^2(\varphi_l(U_l), \mathbb{R}^2)$ and g_{ij}^l is bounded so that the second term vanishes as $n \to \infty$. We conclude $\liminf_{n\to\infty} E_g(h_n) \geq E_g(h)$ and are done. □

Lemma 5.2.10. *Let $G \subset \mathbb{R}^2$ be a bounded domain with smooth boundary, $u \in H^1(G, \mathbb{R}^2)$. Writing $u = (a, b)$ and taking (x, y) as coordinates in G, we have*

$$\int\limits_G \eta \, \det(da, db) \, dx \, dy = -\int\limits_G a \, \det(d\eta, db) \, dx \, dy \quad \text{for all } \eta \in C_0^\infty(G).$$

In particular, if $u_n \rightharpoonup u$ weakly in $H^1(G, \mathbb{R}^2)$ and uniformly in $C^0(G, \mathbb{R}^2)$, then

$$\int\limits_G \eta \, \det(du_n) \, dx \, dy \to \int\limits_G \eta \, \det(du) \, dx \, dy \quad \text{as } n \to \infty.$$

Proof. It is well-known that $C^\infty \cap H^1(G, \mathbb{R}^2)$ is dense in $H^1(G, \mathbb{R}^2)$ (cf. e. g. p. 56 in [Alt91]). We intend to lead an approximation argument. Thus, let $u \in C^\infty \cap H^1(G, \mathbb{R}^2)$, $u = (a, b)$, $\eta \in C_0^\infty(G)$. Then we have by definition of the wedge product, by the product rule for differential forms, by Stokes' theorem[11], and since η has compact support in G

$$
\begin{aligned}
\int\limits_G \eta \, \det(da, db) \, dxdy &= \int\limits_G \eta \, da \wedge db \\
&= \int\limits_G d(a\eta db) - \int\limits_G a \, d\eta \wedge db \\
&= 0 - \int\limits_G a \, \det(d\eta, db) \, dxdy
\end{aligned}
$$

[11] cf. p. 359 in [Lee03].

so that the postulated equation is valid for $u \in C^\infty \cap H^1(G;\mathbb{R}^2)$. Let now $u = (a,b)$ be as in the lemma. Then $\det(da, db) \in L^1(G)$ and $\det(d\eta, db) \in L^2(G)$ since $a, \partial_i a, \partial_i b \in L^2(G)$ by definition, so that both $\int_G \eta \det(da,db)\,dx\,dy$ and $\int_G a \det(d\eta, db)\,dx\,dy$ are finite. Let now $(u_n = (a_n, b_n))_{n\in\mathbb{N}}$ be a sequence in $C^\infty \cap H^1(G,\mathbb{R}^2)$ with (strong) H^1-limit u. Then clearly $\det(da_n, db_n) \to \det(da,db)$ in $L^1(G)$ and we can use Hölder inequality to see that

$$\begin{aligned} & |\int_G \eta \det(da,db)\,dxdy - \int_G \eta \det(da_n, db_n)\,dxdy| \\ \leq & \int_G |\eta||\det(da,db) - \det(da_n,db_n)|\,dxdy \\ \leq & \|\eta\|_{C^0(G)}\,\|\det(da,db) - \det(da_n,db_n)\|_{L^1(G)} \to 0. \end{aligned}$$

Moreover, we find that

$$\begin{aligned} & |\int_G a_n \det(d\eta, db_n)\,dxdy - \int_G a \det(d\eta,db)\,dxdy| \\ \overset{\pm 0}{=} & |\int_G (a_n - a)\det(d\eta,db_n) + a(\det(d\eta,db_n) - \det(d\eta,db))\,dxdy| \\ \leq & \|a - a_n\|_{L^2(G)}\,\|\det(d\eta,db_n)\|_{L^2(G)} \\ & + |\int_G (a\,\partial_x\eta)(\partial_y b_n - \partial_y b)\,dxdy| + |\int_G (a\,\partial_y\eta)(\partial_x b_n - \partial_x b)\,dxdy|. \end{aligned}$$

We have $\|\det(d\eta,db_n)\|^2_{L^2(G)} = \int_G |\partial_x\eta\partial_y b_n - \partial_y\eta\partial_x b_n|^2\,dx\,dy \leq 4\|d\eta\|^2_{C^0}\|db_n\|^2_{L^2} \leq C < \infty$ since $(b_n)_{n\in\mathbb{N}}$ converges [weakly] in $H^1(G)$ and thus its H^1-norm is bounded by Hilbert space theory. Consequently, the first addend in the above inequality converges to zero for $n \to \infty$ as (a_n) converges strongly to a in $L^2(G)$. We will now care for the second and third addends in the same inequality. As $a \in H^1(G)$, η is smooth, and G is bounded, both $a\,\partial_x\eta$ and $a\,\partial_y\eta$ lie in $L^2(G)$ so that the second and third term in the above inequality converge to 0 by [weak] convergence of $(b_n)_{n\in\mathbb{N}}$ to b in $H^1(G)$. As the brackets indicate, we can lead similar arguments if any sequence $(u_n)_{n\in\mathbb{N}} \subset H^1(G,\mathbb{R}^2), u_n = (a_n,b_n)$ converges uniformly and weakly in $H^1(G,\mathbb{R}^2)$ to $u \in H^1(G,\mathbb{R}^2), u = (a,b)$. Indeed, the first addend in the above inequality converges to zero as $\|\det(d\eta,db_n)\|^2_{L^2(G)} \leq C$ by weak convergence of (b_n), and by the uniform convergence of (a_n) to a on the bounded domain G. The second and third addends can be treated as above as only weak convergence was used there. This gives us the required results. □

Lemma 5.2.11 (Courant-Lebesgue). [12] *Let $G \subset \mathbb{R}^2$ be a disk, $u \in H^1(G,\mathbb{R}^n)$ with $E(u) \leq K$, $0 < \delta < 1$, $x \in G$. Then there exists some $r \in (\delta, \sqrt{\delta})$ for which $u|_{\partial B_r(x)\cap G}$ is (absolutely) continuous*[13] *and*

$$|u(x_1) - u(x_2)| \leq \sqrt{\frac{8\pi K}{\log(\frac{1}{\delta})}} \quad \text{for all } x_1, x_2 \in \partial B_r(x) \cap G.$$

[12] cf. [Jos90], p. 2.

[13] We need not be interested in the notion of absolute continuity here, for a definition cf. [Alt91], p. 60.

Now, we come back to the proof of theorem 5.1.1. First of all, we give a more detailed account of what we intend to do:

I E_g attains its minimum on $\mathcal{C}$.
- 1 $\mathcal{C}_K$ is equicontinuous for every $K > 0$.
- 2 $\mathcal{C}_K$ is closed with respect to uniform convergence.
- 3 Using Arzelá-Ascoli, (1) & (2) lead us to: $\mathcal{C}_K$ is (sequentially) compact in $C^0(\mathbb{S}^2, \mathbb{S}^2)$.
- 4 Let $(h_n)_{n\in\mathbb{N}}$ be a minimising sequence for E_g in $\mathcal{C}$, then by (3), there is a limit $h \in \mathcal{C}$ of a subsequence with respect to uniform convergence. By lower semi-continuity of E_g, it is immediate that h minimises E_g.

II Every minimiser $h : (\mathbb{S}^2, \mathrm{can}) \to (\mathbb{S}^2, g)$ of E_g in $\mathcal{C}$ is a conformal, orientation-preserving diffeomorphism.

$\surd$ Any such diffeomorphism is unique up to a preceding Möbius transform.

Note that (I1)-(I3) are independent of the metric chosen. The restriction to $\mathcal{C}_K$ is indeed necessary to get (sequential) uniform compactness:

Proposition 5.2.12. *E is unbounded on $\mathcal{C}$. $\mathcal{C}$ is not (sequentially) uniformly compact.*

Proof. Let $h_n : \mathbb{S}^2 \to \mathbb{S}^2$ be defined by

$$h_n(p) := (\cos(np^3)p^1 + \sin(np^3)p^2, -\sin(np^3)p^1 + \cos(np^3)p^2, p^3)^t$$

for $p = (p^1, p^2, p^3)^t \in \mathbb{R}^3$. Then h_n is clearly well-defined and smooth. h_n leaves the north pole and the south pole invariant. If we calculate the coordinate representations of h_n with respect to the north and the south pole stereographic projection restricted to become compact charts – they are each h_n-compatible with itself – we find that $h_n \in C^0 \cap H^1(\mathbb{S}^2, \mathbb{S}^2)$ by proposition 1.3.6 and that $\det d(\varphi_i \circ h_n \circ \varphi_i^{-1}) \equiv 1$, where i stands for either the north or the south pole projection. This means that h_n is a local diffeomorphism. Also, one can check that h_n is bijective so that it is an orientation-preserving diffeomorphism of $\mathbb{S}^2$. By 5.1.3, there is a Möbius transform μ_n such that $h_n \circ \mu_n$ satisfies (3P). Altogether, $h_n \circ \mu_n \in \mathcal{C}$ for all $n \in \mathbb{N}$. On the other hand, $E(h_n \circ \mu_n) = E(h_n)$ by lemma 5.2.7 and we can estimate (with $\theta_n(r) := n\frac{1-r^2}{1+r^2}$)

$$\begin{aligned} 2E(h_n) &= 2 \int\limits_{\{x\in\mathbb{R}^2 \,|\, |x|<1\}=:B_1(0)} (\rho_S \circ h_n \circ \varphi_S^{-1})((\frac{\partial h_n^1}{\partial x^1})^2 + (\frac{\partial h_n^2}{\partial x^2})^2)\, dx^1 dx^2 \\ &= 4 \int\limits_{B_1(0)} (\rho_S \circ h_n \circ \varphi_S^{-1}) \cos^2\theta_n(|x|)\, dx^1 dx^2 + \end{aligned}$$

$$
\begin{aligned}
&+16n \int\limits_{B_1(0)} (\rho_S \circ h_n \circ \varphi_S^{-1}) \frac{|x|^2}{(1+|x|^2)^2} \cos\theta_n(|x|) \sin\theta_n(|x|)\, dx^1 dx^2 \\
&+32n^2 \int\limits_{B_1(0)} (\rho_S \circ h_n \circ \varphi_S^{-1}) \frac{(x^1)^2}{(1+|x|^2)^4} (\sin\theta_n(|x|)x^1 - \cos\theta_n(|x|)x^2)^2\, dx^1 dx^2 \\
&+32n^2 \int\limits_{B_1(0)} (\rho_S \circ h_n \circ \varphi_S^{-1}) \frac{(x^2)^2}{(1+|x|^2)^4} (\sin\theta_n(|x|)x^2 + \cos\theta_n(|x|)x^1)^2\, dx^1 dx^2 \\
\overset{\text{elementary}}{\geq}\ & -8\pi n + 2 \min_{p^3>0} \rho_S(p)\, n^2 \int\limits_{B_1(0)} (\sin\theta_n(|x|)x^1 - \cos\theta_n(|x|)x^2)^2 (x^1)^2\, dx^1 dx^2 \\
+\ & 2 \min_{p^3>0} \rho_S(p)\, n^2 \int\limits_{B_1(0)} (\sin\theta_n(|x|)x^1 + \cos\theta_n(|x|)x^2)^2 (x^1)^2\, dx^1 dx^2 \\
\overset{\text{polar coord.}}{=}\ & -8\pi n + \min_{p^3>0} \rho_S(p)\, n^2 [2\pi \int\limits_0^1 \sin^2\theta_n(r) r^5\, dr + \frac{\pi}{6}] \\
\geq\ & -8\pi n + \frac{\pi}{6} n^2 \to \infty
\end{aligned}
$$

where ρ_S denotes the conformal factor of can and (x^i) the coordinates with respect to the south pole projection φ_S. Hence E is unbounded on $\mathcal{C}$. Also, for any $p \in \mathbb{S}^2$ and any $n > k \in \mathbb{N}$, we have $|h_n(p) - h_k(p)|^2 = 2(1-(p^3)^2)(1-\cos((n-k)p^3))$ and thus $\|h_n - h_k\|^2_{C^0(\mathbb{S}^2,\mathbb{R}^3)} \geq 0.1 > 0$ for all $n > k \in \mathbb{N}$ as $2(1-(\frac{\pi}{4})^2)(1-\cos((n-k)\frac{\pi}{4})) \geq 0.1$ for $n-k \not\equiv 0 \mod 8$ and $2(1-(\frac{1}{n-k})^2)(1-\cos(1)) \geq 0.1$ if $n-k \equiv 0 \mod 8, n-k \neq 8$ and $2(1-(\frac{1}{2})^2)(1-\cos(4)) \geq 0.1$ if $k+8=n$. Thus, $(h_n)_{n\in\mathbb{N}}$ does not contain a uniformly converging subsequence and $\mathcal{C}$ cannot be uniformly compact. □

Proof (of (I)). **(I1)** Let $K > 0$, wlog $\mathcal{C}_K \neq \emptyset$ (cf. lemma 5.2.2). Let $0 < \varepsilon < \min_{i\neq j}|p_i - p_j|$. An elementary calculation shows that there is a $\tilde{\delta} = \tilde{\delta}(\varepsilon, K) \in (0,1)$ with $(\frac{8\pi K}{\log(\frac{1}{\tilde{\delta}})})^{\frac{1}{2}} \leq \frac{\varepsilon}{4}$. Let $h \in \mathcal{C}_K$, $p \in \mathbb{S}^2$ with antipodal $\hat{p}$ such that $p, \hat{p} \notin \{p_1, p_2, p_3\}$. Let $\varphi : \mathbb{S}^2 \setminus \{p\} \to \mathbb{R}^2$ be the stereographic projection about p, $u := h \circ \varphi^{-1}$. Then $u \in C^0(\mathbb{R}^2, \mathbb{S}^2)$ is weakly differentiable and its energy satisfies $E(u) = \int_{\mathbb{R}^2} |du|^2\, dx^1 dx^2 = \int_{\mathbb{S}^2\setminus\{p\}} |dh|^2\, d\,\mathrm{vol}_{\mathbb{S}^2} = E(h) \leq K$. Let $x_0 \in \mathbb{R}^2$, $\delta := \min\{\tilde{\delta}, \frac{1}{4}\min_{i\neq j}|\varphi(p_i) - \varphi(p_j)|^2\}$. Let $D(x_0) := B_{\sqrt{\delta}}(x_0) \subset \mathbb{R}^2$ so that $u|_{D(x_0)} \in H^1(D(x_0), \mathbb{R}^3)$, since $D(x_0)$ is bounded, u has values in $\mathbb{S}^2$ and $E(u) \leq K < \infty$ as we have seen above. Since $\delta \in (0,1)$, we can apply the Courant-Lebesgue lemma 5.2.11 and get $r(x_0) \in (\delta, \sqrt{\delta})$ with $|u(x_1) - u(x_2)| \leq (\frac{8\pi K}{\log(\frac{1}{\delta})})^{\frac{1}{2}}$ for all $x_1, x_2 \in \partial B_{r(x_0)}(x_0)$. As we have chosen $\delta \leq \tilde{\delta}$ and $\tilde{\delta}$ such that $(\frac{8\pi K}{\log(\frac{1}{\tilde{\delta}})})^{\frac{1}{2}} \leq \frac{\varepsilon}{4}$ we can see that $|u(x_1) - u(x_2)| \leq \frac{\varepsilon}{4}$ for all $x_1, x_2 \in \partial B_{r(x_0)}(x_0)$.

Let now $z \in \partial B_{r(x_0)}(x_0)$, then $u(\partial B_{r(x_0)}(x_0)) \subset \overline{B_{\frac{\varepsilon}{4}}(u(z))} \subset B_{\frac{\varepsilon}{2}}(u(z))$. The open set $V(x_0) := \mathbb{S}^2 \setminus u(\partial B_{r(x_0)}(x_0))$ separates into open connected components. Precisely one of these components (=: $W(x_0)$) meets the connected set $\mathbb{S}^2 \setminus \overline{B_{\frac{\varepsilon}{2}}(u(z))} \subset V(x_0)$ which is non-empty by choice of ε. Also by choice of ε, $W(x_0)$ contains at least two different

p_i. As $h \in \mathcal{C}$, we know that $h^{-1}(W(x_0)) \subset \mathbb{S}^2$ is open and connected and contains at least two different p_i. We can "pierce" $h^{-1}(W(x_0))$ at p without losing these attributes, i. e. the set $h^{-1}(W(x_0)) \setminus \{p\}$ also is open and connected and contains at least two different p_i (remember that p was chosen different of all p_i). Now we can apply the diffeomorphism φ and get that $\varphi(h^{-1}(W(x_0)) \setminus \{p\}) = u^{-1}(W(x_0)) \subset \mathbb{R}^2$ also is open and connected and contains at least two different $\varphi(p_i)$. $u^{-1}(W(x_0)) \cap \partial B_{r(x_0)}(x_0) = \emptyset$ implies that the inclusion $u^{-1}(W(x_0)) \subset B_{r(x_0)}(x_0) \dot\cup (\mathbb{R}^2 \setminus \overline{B_{r(x_0)}(x_0)})$ holds. Thus, by connectedness, either $u^{-1}(W(x_0)) \subset B_{r(x_0)}(x_0)$ or $u^{-1}(W(x_0)) \subset \mathbb{R}^2 \setminus \overline{B_{r(x_0)}(x_0)}$. Since $r(x_0) < \sqrt{\delta} \leq \frac{1}{2}\min_{i\neq j}|\varphi(p_i) - \varphi(p_j)|$, at most one $\varphi(p_i)$ lies in $B_{r(x_0)}(x_0)$ so that $u^{-1}(W(x_0)) \subset \mathbb{R}^2 \setminus \overline{B_{r(x_0)}(x_0)}$. Since $\delta < r(x_0)$ and $\mathbb{S}^2 \setminus \overline{B_{\frac{\varepsilon}{2}}(u(z))} \subset W(x_0)$ we have $u(B_\delta(x_0)) \subset u(B_{r(x_0)}(x_0)) \subset \overline{B_{\frac{\varepsilon}{2}}(u(z))}$. Therefore,

$$\operatorname{diam} u(B_\delta(x_0)) \leq \varepsilon \quad \text{for all } x_0 \in \mathbb{R}^2.$$

Applying the same arguments to the stereographic projection $\hat\varphi$ about the antipodal $\hat p$ of p we get

$$\operatorname{diam} \hat u(B_{\hat\delta}(x_0)) \leq \varepsilon \quad \text{for all } x_0 \in \mathbb{R}^2,$$

where $\hat\delta := \min\{\tilde\delta, \frac{1}{4}\min_{i\neq j}|\hat\varphi(p_i) - \hat\varphi(p_j)|^2\}$ and $\hat u := h \circ \hat\varphi^{-1}$.

Let M be the maximal conformal factor of φ on $\mathbb{S}^2 \setminus B_{\frac{\pi}{4}}(p)$ (which equals the maximal conformal factor of $\hat\varphi$ on $\mathbb{S}^2 \setminus B_{\frac{\pi}{4}}(\hat p)$), $\rho := \min\{\frac{\delta}{M}, \frac{\hat\delta}{M}, \frac{\pi}{4}\}$, let $y \in \mathbb{S}^2$. Then one of the following cases is applicable:

- y lies in the closed upper hemisphere with respect to p (i. e. $y \in \overline{B_{\frac{\pi}{2}}(p)}$), thus $B_\rho(y) \cap B_{\frac{\pi}{4}}(\hat p) = \emptyset$ and $h(B_\rho(y)) = \hat u(\hat\varphi^{-1}(B_\rho(y))) \subset \hat u(B_{M\rho}(\hat\varphi(y))) \subset \hat u(B_{\hat\delta}(\hat\varphi(y)))$ and therefore
$$\operatorname{diam} h(B_\rho(y)) \leq \operatorname{diam} \hat u(B_{\hat\delta}(\hat\varphi(y))) \leq \varepsilon.$$

- y lies in the open lower hemisphere with respect to p (i. e. $y \in \mathbb{S}^2 \setminus \overline{B_{\frac{\pi}{2}}(p)}$), but then it lies in the upper hemisphere with respect to $\hat p$ and the same argument as above gives us
$$\operatorname{diam} h(B_\rho(y)) \leq \varepsilon.$$

As $y \in \mathbb{S}^2$ and ε were arbitrary and ρ was chosen independent of y, we conclude that $\mathcal{C}_K$ is equicontinuous. □

(I2) Now, we wish to show that $\mathcal{C}_K$ is closed with respect to uniform convergence. Let $K > 0$ again be such that $\mathcal{C}_K \neq \emptyset$ (by lemma 5.2.2). Let $(h_n)_{n\in\mathbb{N}} \subset \mathcal{C}_K$ be a uniformly converging sequence with limit $h \in C^0(\mathbb{S}^2, \mathbb{S}^2)$. Then obviously $\boldsymbol{h}$ **satisfies (3P)**. As in lemma 5.2.8, the inequality $\|h_n\|^2_{H^1(\mathbb{S}^2,\mathbb{R}^3)} = \|h_n\|^2_{L^2(\mathbb{S}^2,\mathbb{R}^3)} + 2E(h_n) \leq \operatorname{vol}(\mathbb{S}^2) + 2K$ implies the existence of a $H^1(\mathbb{S}^2, \mathbb{R}^3)$-weakly converging subsequence with limit $\tilde h \in H^1(\mathbb{S}^2, \mathbb{R}^3)$ by Hilbert space theory (cf. e. g. [Alt91, Wlo82]). Again, since both uniform and weak $H^1(\mathbb{S}^2, \mathbb{R}^3)$-convergence lead to weak $L^2(\mathbb{S}^2, \mathbb{R}^3)$-convergence individually, it is clear that $h = \tilde h$ almost everywhere and thus $\boldsymbol{h \in C^0 \cap H^1(\mathbb{S}^2, \mathbb{S}^2)}$. By lower semi-continuity of

the norm with respect to weak convergence, we also know that $\boldsymbol{E(h) \leq K}$. It remains to show that h has a non-negative determinant and is monotone.

Instead of directly checking the definition of $\det dh \geq 0$ we will prove the following simpler condition (*): for all $x \in \mathbb{S}^2$ there is an open neighbourhood $U_x \subset \mathbb{S}^2$, a compact oriented chart $\varphi_x : U_x \to \mathbb{R}^2$ of $\mathbb{S}^2$ as well as an oriented chart $\psi_x : V_x \to \mathbb{R}^2$ of $\mathbb{S}^2$ h-compatible to φ_x so that $\det d(\psi_x \circ h \circ \varphi_x^{-1}) \geq 0$ a. e. on $\varphi_x(U_x)$. By Sobolev chain rule (cf. 1.1.7), the multiplication property of the determinant, and the fact that finite unions of sets of measure zero have measure zero as well, it suffices to show (*).

So let $x \in \mathbb{S}^2$, $y \in \mathbb{S}^2$ with $h(x) \neq h(y)$ (remember that h is not constant by (3P)). Let φ_y be the stereographic projection of $\mathbb{S}^2$ about y, $\psi_{h(y)}$ the stereographic projection of $\mathbb{S}^2$ about $h(y)$. Let $0 < \varepsilon < \frac{1}{2}|h(x) - h(y)|$, $U_x := \mathbb{S}^2 \setminus h^{-1}(\overline{B_\varepsilon(h(y))}) = h^{-1}(\mathbb{S}^2 \setminus \overline{B_\varepsilon(h(y))})$, then U_x is open by continuity of h. Also, $x \in U_x$ and $y \notin U_x$ by choice of ε. Collecting our thoughts, we see that U_x is an open neighbourhood of x in $\mathbb{S}^2$. Let $V_x := B_\varepsilon(h(\overline{U_x}))$, then V_x is an open neighbourhood of $h(x)$ in $\mathbb{S}^2$ satisfying $h(\overline{U_x}) \subset V_x$. Again, $h(y) \notin \overline{V_x}$ by choice of ε and thus $\psi_x := \psi_{h(y)}|_{V_x}$ is a compact oriented chart of $\mathbb{S}^2$. Let $G_x \subset \varphi_x(U_x) \subset \mathbb{R}^2$ be a bounded open disk with centre $\varphi_x(x)$, then $\varphi_x := \varphi_y|_{\varphi_y^{-1}(G_x)}$, is a compact oriented chart of $\mathbb{S}^2$. Let $u := \psi_x \circ h \circ \varphi_x^{-1} : G_x \to \mathbb{R}^2$, $u_n := \psi_x \circ h_n \circ \varphi_x^{-1} : G_x \to \mathbb{R}^2$ (u_n is well-defined for $n \geq n_0$ since by uniform convergence $h_n(\varphi_x^{-1}(G_x)) \subset h_n(\overline{U_x}) \subset B_\varepsilon(h(\overline{U_x})) = V_x$; wlog $n_0 = 1$). We know that $\det du_n = \det d(\psi_x \circ h_n \circ \varphi_x^{-1}) \geq 0$ almost everywhere on G_x since h_n has a non-negative Jacobian by definition and since both charts involved are oriented. We want to show that $\det du \geq 0$ which implies (*), and therefore, as discussed above, $\det dh \geq 0$. We know from lemma 5.2.9 that $u_n \to u$ uniformly and wlog $u_n \rightharpoonup u$ in $H^1(G_x, \mathbb{R}^2)$ since (h_n) is energy-bounded. Let $\eta \in C_0^\infty(G_x)$ with $\eta \geq 0$ and let (s,t) denote the coordinates in G_x, then by lemma 5.2.10 we know that

$$\int_{G_x} \eta \det(du)\, ds\, dt = \lim_{n\to\infty} \int_{G_x} \eta \det(du_n)\, ds\, dt \geq 0.$$

The fundamental lemma of the calculus of variations (cf. p. 32 [BGH98]) then gives $\det du \geq 0$ almost everywhere on G_x and so we have shown (*). Thus, $\boldsymbol{\det dh \geq 0}$.

Last but not least, we will show that h is monotone. The first step consists of showing that h is surjective. By lemma 5.2.4, all h_n are surjective. Let now $y \in \mathbb{S}^2$, then by surjectivity of h_n there must be $x_n \in \mathbb{S}^2$ with $h_n(x_n) = y$. Since $\mathbb{S}^2$ is compact, a subsequence of $(x_n)_{n\in\mathbb{N}}$ converges to $x \in \mathbb{S}^2$. For this subsequence, we have by triangle inequality

$$|h(x) - y| \leq |h(x) - h_n(x)| + |h_n(x) - y| \leq \|h - h_n\|_{C^0} + |h_n(x) - h_n(x_n)|$$

where the first term converges to zero by uniform convergence and the second by equicontinuity of $\mathcal{C}_K$ (cf. (I1)). Thus, $h(x) = y$ and $\boldsymbol{h}$ **is surjective**. The second step will now be to show that the pre-images (under h) of connected sets are connected assuming that the pre-images of singletons are connected (which we will show in the last step). Let $A \neq \emptyset$ be a connected subset of $\mathbb{S}^2$ and suppose that $h^{-1}(A) = X \dot\cup Y$ with $X, Y \neq \emptyset$ relatively closed sets in $h^{-1}(A)$ with empty intersection. By continuity and surjectivity of h as well as compactness of $\mathbb{S}^2$, $h(X)$ and $h(Y)$ are non-empty relatively closed sets in A satisfying

$h(X) \cup h(Y) = A$ so that their intersection cannot be empty since A was assumed to be connected. Let $a \in h(X) \cap h(Y)$, then $h^{-1}(a) = (h^{-1}(a) \cap X) \dot{\cup} (h^{-1}(a) \cap Y)$ where $h^{-1}(a) \cap X \neq \emptyset$ and $h^{-1}(a) \cap Y \neq \emptyset$ are relatively closed, which is a contradiction to $h^{-1}(a)$ being closed and connected.

The last step is – as announced – to show that the pre-images of singletons are connected. Let $a \in \mathbb{S}^2$. By uniform convergence we know that for all $\varepsilon > 0$ there is a number $n_0 \in \mathbb{N}$ such that for all $n \geq n_0$ we have $h^{-1}(a) \subset h_n^{-1}(B_\varepsilon(a))$. We use this property to define a strictly increasing sequence $(n_k)_{k\in\mathbb{N}}$ inductively: Choosing $\varepsilon = 1$, there is $n_1 \in \mathbb{N}$ such that $h^{-1}(a) \subset h_n^{-1}(B_1(a))$ for all $n \geq n_1$. If $n_1, \ldots, n_{k-1}$ have been defined, there is $n_k > n_{k-1}$ such that $h^{-1}(a) \subset h_n^{-1}(B_{\frac{1}{k}}(a))$ for all $n \geq n_k$ (choosing $\varepsilon = \frac{1}{k}$). Now $(h_{n_k})_{k\in\mathbb{N}}$ is a subsequence of $(h_n)_{n\in\mathbb{N}}$ (which we will denote by $(h_k)_{k\in\mathbb{N}}$ in the sequel). Suppose that $h^{-1}(a) = X \dot{\cup} Y$, where $X, Y \subset \mathbb{S}^2$ are non-empty, compact sets with empty intersection (remember that h is continuous). Let $\delta := \frac{1}{2}d(X,Y) > 0$. Set $X^\delta := B_\delta(X)$, $Y^\delta := B_\delta(Y)$, then we know that $X^\delta \cap Y^\delta = \emptyset$. Let $Z := \mathbb{S}^2 \backslash (X^\delta \cup Y^\delta)$, then Z is compact. By construction, both $h_k^{-1}(B_{\frac{1}{k}}(a)) \cap X^\delta$ and $h_k^{-1}(B_{\frac{1}{k}}(a)) \cap Y^\delta$ are open and non-empty for all $k \in \mathbb{N}$. By monotonicity of h_k and connectedness of balls, we deduce that $h_k^{-1}(B_{\frac{1}{k}}(a)) \cap Z \neq \emptyset$ for $k \in \mathbb{N}$. Let henceforth $x_k \in h_k^{-1}(B_{\frac{1}{k}}(a)) \cap Z$. By compactness of Z there is a subsequence of $(x_k)_{k\in\mathbb{N}}$ with limit $x \in Z$ (we denote this subsequence by $(x_k)_{k\in\mathbb{N}}$). Let now $\varepsilon > 0$, then by equicontinuity of $\mathcal{C}_K$ (cf. (I1)) there must be $\rho > 0$ with $\operatorname{diam}(\tilde{h}(B_\rho(x))) \leq \frac{\varepsilon}{3}$ for all $\tilde{h} \in \mathcal{C}_K$. Let now $k_0 \in \mathbb{N}$ be such that $d(x, x_k) < \rho$, $\|h_k - h\|_{C^0} \leq \frac{\varepsilon}{3}$ (uniform convergence) and $\frac{1}{k} \leq \frac{\varepsilon}{3}$ for all $k \geq k_0$. Then by triangle inequality

$$|h(x) - a| \leq |h(x) - h_k(x)| + |h_k(x) - h_k(x_k)| + |h_k(x_k) - a| \leq \varepsilon$$

by construction. Thus $h(x) = a$, which is a contradiction to $x \in Z$ since the set $Z \cap h^{-1}(a)$ has been chosen to be empty. So, all three steps together guarantee that ***h* is monotone**. Collecting all bold face information, we see that $h \in \mathcal{C}_K$. We have now shown that $\mathcal{C}_K$ is closed with respect to uniform convergence. □

(I3) Let $K > 0$ such that $\mathcal{C}_K \neq \emptyset$, cf. lemma 5.2.2. Then for any $h \in \mathcal{C}_K$, we have $\|h\|_{C^0(\mathbb{S}^2,\mathbb{R}^3)} = 1$ and thus by (I1) and (I2), $\mathcal{C}_K$ is equicontinuous, closed, and uniformly bounded in $C^0(\mathbb{S}^2, \mathbb{R}^3)$ so that by the theorem of Arzelá-Ascoli (cf. [Alt91], p. 93) $\mathcal{C}_K$ is (sequentially) compact with respect to uniform convergence. □

(I4) Since $\mathcal{C} \neq \emptyset$ by lemma 5.2.2, there is a minimising sequence $(h_n)_{n\in\mathbb{N}}$ for E_g in $\mathcal{C}$, and thus there is a constant $\tilde{K} > 0$ with $E_g(h_n) \leq \tilde{K}$ for all $n \in \mathbb{N}$. By lemma 5.2.6, there is a constant $m > 0$ with $E(h_n) \leq \frac{1}{m}E_g(h_n) \leq \frac{\tilde{K}}{m} < \infty$ for all $n \in \mathbb{N}$. Then with $K := \frac{\tilde{K}}{m}$ and (I3), there is a limit $h \in \mathcal{C}_K$ of a subsequence of (h_n) with respect to uniform convergence. By lower semi-continuity of E_g, cf. lemma 5.2.8, it is immediate that h minimises E_g. □

Taking together (I1)-(I4), we have shown that E_g attains its minimum on $\mathcal{C}$ and are thus done with (I). □

Corollary 5.2.13. *If g is a smooth Riemannian metric on $\mathbb{S}^2$, $h \in C^0(\mathbb{S}^2, \mathbb{S}^2)$, then there is a pair of finite, h-compatible, compact, oriented C^∞-atlases on $\mathbb{S}^2$ the first of which is conformal with respect to* can*, the second to g.*

Proof. Follows from lemma 1.2.3 and lemma 1.2.26. □

Definition 5.2.14 (Variation of the Independent Variables). [14] Let X be a smooth, Y a C^1-manifold, $\mathcal{D} \subset C^0(X, Y)$. We say that a function $h \in \mathcal{D}$ is *stationary with respect to variation of the independent variables for a functional* $\mathcal{F} : \mathcal{D} \to \mathbb{R}$, if for every pair of h-compatible atlases $\mathcal{A} = \{\varphi_k : U_k \to \mathbb{R}^n\}_{k=1}^K$ of X and $\mathcal{B}$ of Y and every smooth family of diffeomorphisms $\sigma_t : X \to X$ $(t \in (-\varepsilon, \varepsilon))$ with $\sigma_0 = \mathrm{id}_X$, and $\sigma_t \equiv \mathrm{id}_X$ outside some compact set $W \subset U_l$ with non-empty interior $(l \in \{1, \ldots, K\})$ satisfying $W \cap U_k = \emptyset$ for $k \neq l, k \in \{1, \ldots, K\}$, we have $h \circ \sigma_t \in \mathcal{D}$ for all $t \in (-\varepsilon, \varepsilon)$ and

$$\frac{d}{dt}|_{t=0} \mathcal{F}(h \circ \sigma_t) = 0.$$

In particular, the derivative on the left hand side shall exist.

Remark. Variation of the independent variables is very similar to differentiation of the functional (cf. chapter 2), only that we consider tangential instead of linear variations in some ambient space. Whence, this notion permits us to not embed $(\mathbb{S}^2, g)$.

The following is a plan for the remaining proof:

- ✓ E_g attains its minimum on $\mathcal{C}$.
- II Every minimiser $h : (\mathbb{S}^2, \mathrm{can}) \to (\mathbb{S}^2, g)$ of E_g in $\mathcal{C}$ is a smooth, conformal, orientation-preserving diffeomorphism.
  - 1 Every such minimiser is stationary with respect to variation of the independent variables for $E_g : \tilde{\mathcal{C}} \to \mathbb{R}$, with $\tilde{\mathcal{C}} := \{h \circ \mu \,|\, h \in \mathcal{C}, \mu \text{ Möbius transform}\}$.
  - 2 Every $h \in C^0 \cap H^1(\mathbb{S}^2, \mathbb{S}^2)$ that is stationary with respect to variation of the independent variables for E_g is holomorphic and consequently smooth and conformal.
  - 3 Every such minimiser is a smooth orientation-preserving diffeomorphism.
- ✓ Any such diffeomorphism is unique up to a preceding Möbius transform.

Proof (of (II)). [15] Let g be a smooth metric on $\mathbb{S}^2$. We will use theorem 1.2.29, i. e. rely on the existence of isothermal coordinates/ conformal charts with respect to g. Set $\tilde{\mathcal{C}} := \{h \circ \mu \,|\, h \in \mathcal{C}, \mu \text{ Möbius transform}\}$.

[14] Cf. p. 15 in [Jos90].

[15] Regularity of (weakly) harmonic energy-minimisers was established by C. E. B. Morrey in 1948, see [Har97].

(II1) Let $h \in \mathcal{C}$ be a minimiser of E_g. Choose a compact, conformal, h-compatible pair of atlases $\mathcal{A} = (\varphi_k : U_k \to \mathbb{R}^2)_{k=1}^K$, $\mathcal{B} = (\psi_k : V_k \to \mathbb{R}^2)_{k=1}^K$ on $\mathbb{S}^2$ as in corollary 5.2.13 subordinate to the given pair of atlases[16]. Let $(\eta_k)_{k=1}^K$ be a partition of unity subordinate to $\mathcal{A}$. By definition of variation of the independent variables 5.2.14, it suffices to show the following property (*): for any $l \in \{1, \dots, K\}$ and any smooth family of diffeomorphisms $\sigma_t : \mathbb{S}^2 \to \mathbb{S}^2$, $t \in (-\varepsilon, \varepsilon)$, with $\sigma_0 \equiv \mathrm{id}_{\mathbb{S}^2}$ and $\sigma_t \equiv \mathrm{id}_{\mathbb{S}^2}$ outside some compact set $W \subset U_l$ with non-empty interior, we have $h \circ \sigma_t^{-1} \in \tilde{\mathcal{C}}$ and $\frac{d}{dt}|_{t=0} E_g(h \circ \sigma_t^{-1}) = 0$. This variation of the definition is admissible since the inverse family to any such family satisfies all the required criteria as well.

By proposition 5.1.3, for every $t \in (-\varepsilon, \varepsilon)$, there is a Möbius transform μ_t of $\mathbb{S}^2$ such that $\sigma_t^{-1} \circ \mu_t$ satisfies (3P)[17]. It is clear that σ_t is orientation-preserving since $\sigma_0 = \mathrm{id}_{\mathbb{S}^2}$ is. Thus, by the same proposition, μ_t is orientation-preserving. Using lemma 5.2.3 we deduce that $h \circ \sigma_t^{-1} \circ \mu_t \in \mathcal{C}$ and hence $h \circ \sigma_t^{-1} \in \tilde{\mathcal{C}}$. As h is a minimiser of E_g, we have $E_g(h \circ \sigma_t^{-1}) = E_g(h \circ \sigma_t^{-1} \circ \mu_t) \geq E_g(h)$ by lemma 5.2.7. The function $E_g(h \circ \sigma_t^{-1}) : (-\varepsilon, \varepsilon) \to \mathbb{R} : t \mapsto E_g(h \circ \sigma_t^{-1})$ thus has a minimum at $t = 0$. We will now show that it is differentiable at $t = 0$ and thus $\frac{d}{dt}|_{t=0} E_g(h \circ \sigma_t^{-1}) = 0$ whence h has been shown to be stationary with respect to the variation of independent variables on $\tilde{\mathcal{C}}$.

Denoting the coordinates with respect to φ_k by (x^α) and using $\mathrm{can}^{\alpha\beta}\sqrt{\det(\mathrm{can})} = \delta^{\alpha\beta}$, $g_{ij}^{\psi_k} = \rho_k \delta_{ij}$ by our choice of coordinates, we get by the transformation formula for integrals with the new variable $y = \varphi_k \circ \sigma_t^{-1} \circ \varphi_k^{-1}(x)$ ($\varphi_k \circ \sigma_t^{-1} \circ \varphi_k^{-1}(\varphi_k(U_k)) = \varphi_k(U_k)$ by construction)

$$
\begin{aligned}
& 2E_g(h \circ \sigma_t^{-1}) \\
= & \sum_{k=1}^{K} \sum_{\alpha,i=1}^{2} \int_{\varphi_k(U_k)} (\eta_k \cdot \rho_k \circ h \circ \sigma_t^{-1}) \circ \varphi_k^{-1} \left(\frac{\partial(\psi_k^i \circ h \circ \sigma_t^{-1} \circ \varphi_k^{-1})}{\partial x^\alpha}\right)^2 dx^1 dx^2 \\
= & \sum_{k=1}^{K} \int_{\varphi_k(U_k)} (\eta_k \circ \sigma_t \circ \varphi_k^{-1}) \{ \sum_{i=1}^{2} (\rho_k \circ h \circ \varphi_k^{-1}) \frac{\partial(\psi_k^i \circ h \circ \varphi_k^{-1})}{\partial y^\beta} \frac{\partial(\psi_k^i \circ h \circ \varphi_k^{-1})}{\partial y^\gamma} \} \\
& \qquad \times \sum_{\alpha=1}^{2} \left(\frac{\partial(\varphi_k^\beta \circ \sigma_t^{-1} \circ \varphi_k^{-1})}{\partial x^\alpha} \frac{\partial(\varphi_k^\gamma \circ \sigma_t^{-1} \circ \varphi_k^{-1})}{\partial x^\alpha} \right)|_{\varphi_k \circ \sigma_t \circ \varphi_k^{-1}} \det d(\varphi_k \circ \sigma_t \circ \varphi_k^{-1}) dy^1 dy^2
\end{aligned}
$$

where we have used the chain rule to calculate the partial derivatives. Note that the domains of the integrals are not changed by this transformation due to the choice of the family σ_t. Use $f_k(t, y)$ as a shorthand for the integrand in the above equation where $t \in (-\varepsilon, \varepsilon), y \in \varphi_k(U_k)$. Then $f_k : (-\varepsilon, \varepsilon) \times \varphi_k(U_k) \to \mathbb{R}$ is measurable. By the rules for interchanging integral and differentiation (cf. e. g. p. 147 in [Els00]), it suffices to show that $f_k(t, \cdot) \in L^1(\varphi_k(U_k))$ for all $t \in (-\varepsilon, \varepsilon)$, that the partial derivatives $\frac{\partial f_k}{\partial t}$ exist for all $y \in \varphi_k(U_k)$ and all $t \in (-\varepsilon, \varepsilon)$, and that there is a a. e. positive function $F_k \in L^1(\varphi_k(U_k))$

[16] again counting charts in $\mathcal{B}$ several times, if necessary.
[17] μ_t need not be continuous with respect to t.

which bounds the absolute values of these partial derivatives for $t \in (-\frac{\varepsilon}{2}, \frac{\varepsilon}{2})$. We will thus proceed to check these three conditions.

First of all, it is obvious that $f_k \geq 0$ is measurable and thus $f_k(t,\cdot) \in L^1(\varphi_k(U_k))$ for all t since the energy of $h \circ \sigma_t^{-1}$ is finite for all t. Secondly, it is only necessary to derivate the terms outside the braces respectively, which are smooth with respect to t, as the terms in the braces are independent of t, so the partial t-derivatives of f_k exist for all k, $y \in \varphi_k(U_k)$, and $t \in (-\varepsilon, \varepsilon)$. Thirdly, let $k \neq l$. For $y \in \varphi_k(U_k)$, $f_k(t,y) = f_k(0,y)$ for all t since $\sigma_t \equiv \mathrm{id}_{\mathbb{S}^2}$ outside W and $W \cap U_k = \emptyset$, so that $\frac{\partial f_k}{\partial t}(t,y) = 0 =: F_k(y)$ for all $t \in (-\varepsilon, \varepsilon)$ and $y \in \varphi_k(U_k)$. The same is true for $k = l$ and $y \in U_l \setminus W$. Let now $k = l$. Then, the partial t-derivatives we calculate by product rule are all bounded by continuity of ρ_l and compactness of the atlas, and thus there are constants $C^{\beta\gamma} > 0$ such that in $[-\frac{\varepsilon}{2}, \frac{\varepsilon}{2}] \times \varphi_l(W)$, we have

$$|\frac{\partial f_l}{\partial t}(t,y)| \leq C^{\beta\gamma} \sum_{\alpha,i=1}^{2} (\frac{\partial(\psi_l^i \circ h \circ \varphi_l^{-1})}{\partial y^\beta})(\frac{\partial(\psi_l^i \circ h \circ \varphi_l^{-1})}{\partial y^\gamma})(y) =: F_l(y)$$

whence $0 \leq F_k \in L^1(\varphi_k(U_k))$ for all k. As discussed above, we can now interchange integration and differentiation and obtain

$$\frac{d}{dt} E_g(h \circ \sigma_t^{-1})|_{t=0} = \sum_{k=1}^{K} \int\limits_{\varphi_k(U_k)} \frac{\partial f_k}{\partial t}(0,y)\, dy^1 dy^2 = \int\limits_{\varphi_l(W)} \frac{\partial f_l}{\partial t}(0,y)\, dy^1 dy^2,$$

so in particular this derivative exists. We thus see that ***h* is stationary with respect to the variation of independent variables for E_g** and are done with (II1). □

(II2) We have to show that every $h \in C^0 \cap H^1(\mathbb{S}^2, \mathbb{S}^2)$ which is stationary with respect to variation of the independent variables for E_g is smooth and conformal. To this end, let $h \in C^0 \cap H^1(\mathbb{S}^2, \mathbb{S}^2)$, let $\mathcal{A} = (\varphi_k : U_k \to \mathbb{C})_{k=1}^K$, $\mathcal{B} = (\psi_k : V_k \to \mathbb{C})_{k=1}^K$ be a compact, conformal, oriented h-compatible pair of atlases on $\mathbb{S}^2$ as in corollary 5.2.13[18]. Denote the conformal factor of g by ρ_k as above. Fix $l \in \{1, \ldots, K\}$, $p \in U_l \subset \mathbb{S}^2$. Let $(\eta_k)_{k=1}^K$ be a partition of unity subordinate to $\mathcal{A}$ with $\eta_l \equiv 1$ on a closed neighbourhood W of p with $W \subset U_l$. Let σ_t be a smooth family of diffeomorphisms such that $\sigma_t \equiv \mathrm{id}_{\mathbb{S}^2}$ outside W, $\sigma_0 \equiv \mathrm{id}_{\mathbb{S}^2}$ as in definition 5.2.14 (such a family always exists as it arises as the flow of any smooth vector field with support in W). As h is stationary for E_g, we have $h \circ \sigma_t^{-1} \in \tilde{\mathcal{C}}$ and $\frac{d}{dt}|_{t=0} E_g(h \circ \sigma_t^{-1}) = 0$ by (II1). Using the abbreviations $f = f_l$ and $u := \psi_l \circ h \circ \varphi_l^{-1}$ as above, $\chi := \frac{\partial(\varphi_l \circ \sigma_t^{-1} \circ \varphi_l^{-1})}{\partial t}|_{t=0}$, and (x^α) as coordinates belonging to φ_l, we have on W (with $\eta_l \equiv 1$ on W and the usual rules for differentiation, as well as $\varphi_l \circ \varphi_l^{-1} = \mathrm{id}_{\varphi_l(U_l)}$)

$$\frac{\partial f}{\partial t}(0,\cdot) = \sum_{i,\alpha=1}^{2} (\rho_l \circ h \circ \varphi_l^{-1}) \frac{\partial u^i}{\partial x^\beta} \frac{\partial u^i}{\partial x^\gamma} \times \left[\frac{\partial \chi^\beta}{\partial x^\alpha} \delta_\alpha^\gamma + \delta_\alpha^\beta \frac{\partial \chi^\gamma}{\partial x^\alpha} - \delta_\alpha^\beta \delta_\alpha^\gamma (\frac{\partial \chi^1}{\partial x^1} + \frac{\partial \chi^2}{\partial x^2}) \right]$$

[18] again counting charts in $\mathcal{B}$ several times, if necessary.

$$= \sum_{i=1}^{2}(\rho_l \circ h \circ \varphi_l^{-1})\left[(\frac{\partial\chi^1}{\partial x^1} - \frac{\partial\chi^2}{\partial x^2})((\frac{\partial u^i}{\partial x^1})^2 - (\frac{\partial u^i}{\partial x^2})^2) + 2\frac{\partial\chi^1}{\partial x^2}\frac{\partial u^i}{\partial x^1}\frac{\partial u^i}{\partial x^2} + 2\frac{\partial\chi^2}{\partial x^1}\frac{\partial u^i}{\partial x^1}\frac{\partial u^i}{\partial x^2}\right]$$
$$= (\frac{\partial\chi^1}{\partial x^1} - \frac{\partial\chi^2}{\partial x^2})(|\frac{\partial u}{\partial x^1}|_g^2 - |\frac{\partial u}{\partial x^2}|_g^2) + 2(\frac{\partial\chi^1}{\partial x^2} + \frac{\partial\chi^2}{\partial x^1})(\langle\frac{\partial u}{\partial x^1}, \frac{\partial u}{\partial x^2}\rangle_g),$$

where $|.|_g$ and $\langle .,.\rangle_g$ denote the norm and inner product induced by g, respectively. Setting $\phi : \varphi_l(\operatorname{int} W) \to \mathbb{C}$, $\phi(x^1, x^2) := |\frac{\partial u}{\partial x^1}|_g^2 - |\frac{\partial u}{\partial x^2}|_g^2 - 2i\langle\frac{\partial u}{\partial x^1}, \frac{\partial u}{\partial x^2}\rangle_g$, this reads

$$\frac{\partial f}{\partial t}(0,x) = \phi^1(\frac{\partial\chi^1}{\partial x^1} - \frac{\partial\chi^2}{\partial x^2}) - \phi^2(\frac{\partial\chi^1}{\partial x^2} + \frac{\partial\chi^2}{\partial x^1})$$

for all $x \in \varphi_l(\operatorname{int} W)$, where ϕ^1, ϕ^2 denote the real and imaginary part of ϕ, respectively. Thus

$$\begin{aligned} 0 &\overset{\text{(II1)}}{=} \frac{d}{dt}|_{t=0} E_g(h \circ \sigma_t^{-1}) \\ &\overset{\text{as in (II1)}}{=} \int\limits_{\varphi_l(\operatorname{int} W)} \frac{\partial f}{\partial t}(0,x)\, dx^1 dx^2 \\ &= \int\limits_{\varphi_l(\operatorname{int} W)} \{\phi^1(\frac{\partial\chi^1}{\partial x^1} - \frac{\partial\chi^2}{\partial x^2}) - \phi^2(\frac{\partial\chi^1}{\partial x^2} + \frac{\partial\chi^2}{\partial x^1})\}\, dx^1 dx^2. \end{aligned} \tag{5.3}$$

Remember that χ was defined by $\chi := \frac{\partial(\varphi_l \circ \sigma_t^{-1} \circ \varphi_l^{-1})}{\partial t}|_{t=0}$. Since we can understand any map $\chi = (\chi^1, \chi^2) \in C_0^\infty(\varphi_l(\operatorname{int} W), \mathbb{R}^2)$ as being a tangent vector field to $\mathbb{R}^2$ and then use its flow σ_t to vary the independent variables, we are allowed to choose $\chi^1, \chi^2 \in C_0^\infty(\varphi_l(\operatorname{int} W), \mathbb{R})$ in equation 5.3. Choosing first $\chi := \chi^1$ and $\chi^2 \equiv 0$ and then $\chi := \chi^2$, $\chi^1 \equiv 0$, we get both

$$\begin{aligned} 0 &= \int\limits_{\varphi_l(\operatorname{int} W)} \{\phi^1 \frac{\partial\chi}{\partial x^1} - \phi^2 \frac{\partial\chi}{\partial x^2}\}\, dx^1 dx^2 \quad \text{and} \\ 0 &= \int\limits_{\varphi_l(\operatorname{int} W)} \{\phi^1 \frac{\partial\chi}{\partial x^2} + \phi^2 \frac{\partial\chi}{\partial x^1}\}\, dx^1 dx^2 \end{aligned}$$

for all $\chi \in C_0^\infty(\varphi_l(\operatorname{int} W))$. This means that $\phi : \varphi_l(\operatorname{int} W) \to \mathbb{C}$ is *weakly holomorphic*[19]. Also, as l and p were arbitrary, $\mathbb{S}^2$ is covered by finitely many such sets W_m with $\varphi_m(\operatorname{int} W_m)$ being the domains of maps $u_m = \varphi_m \circ h \circ \varphi_m^{-1}$ and maps $\phi_m : \varphi_m(\operatorname{int} W_m) \to \mathbb{C}$ by compactness with $W_m \subset U_m$. Refine the atlas $\mathcal{A}$ on $(\mathbb{S}^2, \text{can})$ such that the sets $\operatorname{int} W_m$ are domains of definitions of charts $\varphi_m : \operatorname{int} W_m \to \mathbb{C}$. It follows from regularity theory of the Cauchy-Riemann equations that all ϕ_m are holomorphic and of class C^∞ on their respective domains, cf. e. g. pp. 18 in [Kuw98]. Also, we quote from [Jos91], pp. 407, that the transformation behaviour of the holomorphic maps ϕ_m allows us to understand them as the coefficients of a holomorphic quadratic differential, $\phi = \phi_m dz^2$, $z = x^1 + ix^2$ being the complex coordinate with respect to φ_m, $dz := d(x^1) + i\, d(x^2)$, $dz^2 := dz \otimes dz$. By

[19] cf. e. g. [Kuw98] for more details on this notion.

lemma 8.2.4 in [Jos91], ϕ must vanish as its domain of definition is $\mathbb{S}^2$ (and consequently $\phi_m \equiv 0$ on $\varphi_m(\operatorname{int} W_m)$).

We know from lemma 5.2.9 that $u_m \in C^0 \cap H^1(\varphi_m(\operatorname{int} W_m), \mathbb{C})$. Thus, using complex notation[20] and suppressing the index m, $\frac{\partial u}{\partial z} := \frac{1}{2}(\frac{\partial u}{\partial x^1} - i\frac{\partial u}{\partial x^2})$ and $\frac{\partial u}{\partial \overline{z}} := \frac{1}{2}(\frac{\partial u}{\partial x^1} + i\frac{\partial u}{\partial x^2})$, it is easy to see that $\phi = \rho \circ \varphi^{-1}\,(|\frac{\partial u}{\partial x}|^2 - |\frac{\partial u}{\partial y}|^2 - 2i\langle \frac{\partial u}{\partial x}, \frac{\partial u}{\partial y}\rangle) = 4\rho \circ \varphi^{-1}\,\frac{\partial u}{\partial z}\,\overline{\frac{\partial u}{\partial \overline{z}}}$ a. e. on $\varphi(\operatorname{int} W)$ (remembering that ρ denotes the conformal factor of g on $\operatorname{int} W$). Also, we can calculate the Jacobian of u by $|\frac{\partial u}{\partial z}|^2 - |\frac{\partial u}{\partial \overline{z}}|^2 = \frac{1}{4}((\frac{\partial u^1}{\partial x} + \frac{\partial u^2}{\partial y})^2 + (\frac{\partial u^2}{\partial x} - \frac{\partial u^1}{\partial y})^2 - (\frac{\partial u^1}{\partial x} - \frac{\partial u^2}{\partial y})^2 - (\frac{\partial u^2}{\partial x} + \frac{\partial u^1}{\partial y})^2) = \frac{\partial u^1}{\partial x}\frac{\partial u^2}{\partial y} - \frac{\partial u^2}{\partial x}\frac{\partial u^1}{\partial y} = \det(du)$ a. e. on $\varphi(\operatorname{int} W)$. As $\phi \equiv 0$ on $\varphi(\operatorname{int} W)$ and $\det du \geq 0$ a. e. since $h \in \mathcal{C}$ and the involved charts are oriented, we have $\frac{\partial u}{\partial z}(z) = 0$ or $\frac{\partial u}{\partial \overline{z}}(z) = 0$ for almost all $z \in \varphi(\operatorname{int} W)$ (since $\rho \neq 0$) and $|\frac{\partial u}{\partial z}|^2 \geq |\frac{\partial u}{\partial \overline{z}}|^2$ so that

$$\frac{\partial u_m}{\partial \overline{z}} = 0 \text{ a. e. on } \varphi_m(\operatorname{int} W_m).$$

Multiplying this equation by $\chi \in C_0^\infty(\varphi_m(\operatorname{int} W_m))$ and integrating over $\varphi_m(\operatorname{int} W_m)$, this means that u_m is weakly holomorphic. As above, this guarantees u_m to be holomorphic and of class C^∞. This implies in particular that ***h* is holomorphic and smooth**. By definition of ϕ_m and $\phi_m \equiv 0$ on $\varphi_m(\operatorname{int} W_m)$, we deduce that u_m must be conformal. Using lemma 8.2.2 in J. Jost's book (p. 408) and remembering that by choice of our atlas on $(\mathbb{S}^2, g)$, the metric g is conformal, we conclude that ***h* is indeed conformal**. □

(II3) It remains to show that every minimiser $h \in \mathcal{C}$ of E_g is an orientation-preserving diffeomorphism. For this, let $h \in \mathcal{C}$ be a minimiser of E_g. Then by (II1), h is stationary with respect to the variation of independent variables of E_g on $\tilde{\mathcal{C}}$. By (II2), h is a holomorphic, conformal map of class C^∞. We know that ***h* is surjective** as it is monotone, cf. lemma 5.2.4. Also by monotonicity, every point has a connected pre-image. But h is holomorphic, so the pre-image of each $q \in \mathbb{S}^2$ must consist of isolated points for the following reason: let $p \in h^{-1}(q)$. Then there are h-compatible conformal charts $\varphi : U_\varphi \to \mathbb{R}^2$, $\psi : U_\psi \to \mathbb{R}^2$ with $p \in U_\varphi$ and $\varphi(p) = 0$. $u : \varphi(U_\varphi) \to \mathbb{C}$ defined by $u(z) := \psi \circ h \circ \varphi^{-1}(z) - \psi(q)$ has a zero at 0. Complex analysis[21] then tells us that there either is a neighbourhood $G \subset \varphi(U_\varphi)$ of 0 in which 0 is the only zero of u or $u \equiv 0$ on its domain. $u \equiv 0$ implies $h|_{U_\varphi} \equiv q$. As h is non-constant, we can choose U_φ big enough that $h|_{U_\varphi} \not\equiv q$. Thus, $p = \varphi^{-1}(0)$ is the only pre-image of q under h in $\varphi^{-1}(G)$ so that the pre-image of q has shown to consist of isolated points. As $h^{-1}(q)$ is connected by monotonicity, ***h* is injective and thus a homeomorphism** as $\mathbb{S}^2$ is compact and Hausdorff. It now suffices to show that the Jacobian determinant $\det dh$ is strictly positive, since then we are in a position to use the inverse function theorem which tells us that h is a diffeomorphism onto its image $\mathbb{S}^2$. From $\det dh > 0$ we can also derive that h is orientation-preserving. Let us thus check whether $\det dh > 0$ everywhere.

Let $p \in \mathbb{S}^2$, ψ, φ as above with $q := h(p)$. Then by the above, $u(z) = z^n a(z)$ on G with some $n \in \mathbb{N}$ and $a : G \to \mathbb{C}$ holomorphic and $a(z) \neq 0$ for all $z \in G$. u is injective with h, so it follows from complex analysis[22] that $n = 1$. Whence by product rule and continuity,

[20] cf. the same chapter in [Jos91] as above.
[21] cf. pp. 127 in [Ahl66].
[22] cf.theorem 11, p. 131 in [Ahl66].

$|\frac{\partial u}{\partial z}| = |z\frac{\partial a}{\partial z} + a(z)| > 0$ on a neighbourhood of $z = 0$ since $|\frac{\partial u}{\partial z}|(0) = |a(0)| > 0$. Hence $\det d(\psi \circ h \circ \varphi^{-1}) = \det du = |\frac{\partial u}{\partial z}|^2 > 0$ locally. Thus $\mathbf{\det dh > 0}$ and consequently $\boldsymbol{h}$ **is a smooth orientation-preserving diffeomorphism**. □

We have thus shown that for g of class C^∞, **every minimiser $\boldsymbol{h \in \mathcal{C}}$ of $\boldsymbol{E_g}$ in $\boldsymbol{\mathcal{C}}$ is a conformal, orientation-preserving diffeomorphism of class $\boldsymbol{C^\infty}$** and are finally done with (II). □

Corollary 5.2.15. *The global conformal parameters corresponding to a smooth Riemannian metric g on $\mathbb{S}^2$ can be found by minimising E_g on the class $\mathcal{C}$ defined above.*

5.3 A Different Proof

As noted above, we have used J. Jost's proof of theorem 5.1.1 as a guideline for our proof. But our proof differs from J. Jost's in three main aspects. The first difference lies in the class chosen as domain for the functional we wish to minimise. Secondly, we simplified J. Jost's argument for "$\det dh \geq 0$" (see lemmata 3.1.3 and 3.1.4 in [Jos90]) with a partial integration argument. Finally, using isothermal coordinates, we do not need the Hartman-Wintner lemma and the lemma of Heinz to ensure bijectivity and the non-vanishing of the Jacobian. We will now discuss these differences going into detail. In order to make the two approaches comparable, we present J. Jost's work in our notation.

The Domain of E_g

Our proof of theorem 5.1.1 was divided into three main parts: existence of minimisers of E_g in $\mathcal{C}$, proof of the fact that these minimisers are conformal diffeomorphisms, and uniqueness. J. Jost equally carries out these steps. However, he chooses a different class as the domain of variation of E_g. The path he follows is to define a class

$$\mathcal{D} := \{h \in C^0(\mathbb{S}^2, \mathbb{S}^2) \mid h \text{ is an orientation-preserving diffeomorphism and satisfies (3P)}\}$$

and to henceforth work with its "closure" $\overline{\mathcal{D}}$ "with respect to weak H^1 and uniform convergence".[23] We understand that "closure of $\mathcal{D}$ w. r. t. weak $H^{1,2}$ and uniform convergence"

[23] This is, at least, how we understand his definition which seemingly contains a type-set error. Literally, he writes on page 87: "We choose three different points z_1, z_2, z_3, in $\mathbb{S}^2$ and three different points p_1, p_2, p_3 in Σ [Σ is a differentiable surface homeomorphic to $\mathbb{S}^2$ with continuous metric (g_{ij}) i. e. a surface diffeomorphic to $\mathbb{S}^2$ – the author]. Let $\mathcal{D}$ be the class of all diffeomorphisms $v : \mathbb{S}^2 \to \Sigma$ satisfying $E(v) = \frac{1}{2}\int g_{ij}(v(z))(v^i_x v^j_x + v^i_y v^j_y)\,dx\,dy$ (3.1.5) and let $\overline{\mathcal{D}}$ be the closure of $\mathcal{D}$ w. r. t. weak $H^{1,2}$ and uniform convergence." Note that what J. Jost denotes by E is E_g in our notation. We assume that he understands the three point normalisation $h(z_i) = p_i$ for $i = 1, 2, 3$ to be included instead of the void condition $E(v) = \frac{1}{2}\int g_{ij}(v(z))(v^i_x v^j_x + v^i_y v^j_y)\,dx\,dy$. This hypothesis is strengthened by his reference to (3.1.5) on the same page: "Moreover, if we have a sequence $(w_n)_{n\in\mathbb{N}}$ in the uniform and weak closure of the class of diffeomorphisms between Σ and $\mathbb{S}^2$, but not necessarily satisfying (3.1.5), then we still have $E(v) \leq E(w)$ (3.1.7) since the normalisation (3.1.5) can always be achieved by composing w_n with a Möbius transformation, i. e. conformal automorphism of $\mathbb{S}^2$, without changing

signifies that $\overline{\mathcal{D}}$ is supposed to be the closure of $\mathcal{D}$ with respect to the uniform and the weak H^1 topology at the same time; i. e. in the topology generated by the intersections of sets that are open with respect to uniform convergence and those that are open in the weak H^1-topology.

It is clear that J. Jost's class $\mathcal{D}$ is contained in our class $\mathcal{C}$. With the aid of Jost's lemma (3.1.4) and the fact that any $h \in \overline{\mathcal{D}}$ can be uniformly approximated by a sequence in $\mathcal{D}$, it can be shown that $\overline{\mathcal{D}}$ is also contained in $\mathcal{C}$. We preferred to use the class $\mathcal{C}$ as domain of E_g as we found it easier to deal with, see below. Nevertheless, some arguments work as for $\mathcal{C}$. These include e. g. lemma 5.2.2 (non-emptyness of the class), all statements on $C^0 \cap H^1(\mathbb{S}^2, \mathbb{S}^2)$, e. g. lemma 5.2.6 ($E_g$ and E are "equivalent"), lemma 5.2.7 (Möbius transforms leave the energy invariant), 5.2.8 (E_g is lower semi-continuous) and finally proposition 5.2.12 (the energy is unbounded on $\mathcal{D}$).

Non-Negative Jacobian

All maps in class $\mathcal{C}$ have a non-negative Jacobian. We use this property to ensure both orientation preservedness and diffeomorphy of the minimiser of E_g, see (II3). It carries over to uniform and weak H^1-limits by lemma 5.2.10 which relies on a partial integration argument. J. Jost also works with the notion of a non-negative Jacobian but he proves a stronger result, namely that non-negativity of the Jacobian carries over to uniform limits (see lemma (3.1.3) and (3.1.4) in [Jos90])[24]. We understand that he needs this stronger result in order to show that the members of his minimising class $\overline{\mathcal{D}}$ have a non-negative Jacobian. He uses the notion of a winding number and a formula relating this number to the Jacobian as well as some approximation arguments in the proof of (3.1.4).

Thus, we can profit from using the class $\mathcal{C}$ as simpler arguments for the non-negativity of the Jacobian become available.

Diffeomorphy

First of all, we review our proof of diffeomorphy of the minimisers ((II2), (II3)). We prove (weak) holomorphy of minimisers of E_g in $\mathcal{C}$ with the aid of isothermal coordinates and deduce smoothness and conformality. Surjectivity is immediate, injectivity follows from monotonicity and holomorphy, again expressed in isothermal coordinates. The (non-negative) Jacobian of a minimiser cannot vanish since the minimiser is holomorphic

$E(w_n)$ [...]." Also, he uses the three-point normalisation when applying the Courant-Lebesgue lemma (p. 87). In our language, this can be expressed as (3P) since we can identify Σ with $\mathbb{S}^2$. As, on p. 90, he assumes that $J(v_n) := \det dv_n$ has the same sign for all $n \in \mathbb{N}$ – where $(v_n)_{n\in\mathbb{N}} \subset \mathcal{D}$ is a sequence that approximates a minimiser $v \in \overline{\mathcal{D}}$ uniformly and weakly in $H^{1,2}$ – we have included the condition of "orientation-preserving" in the definition of $\mathcal{D}$.

[24] Again, we assume that the condition that the sequence converges weakly in H^1 is a type-set error as J. Jost does not use this condition on the one hand and cannot straightforwardly secure it for a minimising sequence on the other hand.

and injective (see (II3)) and whence it is a (orientation-preserving, conformal) diffeomorphism.

J. Jost proceeds differently to show that (conformal, harmonic, holomorphic, and smooth) minimisers are indeed diffeomorphisms. He gets surjectivity from the fact that any map in $\overline{\mathcal{D}}$ is the uniform limit of a sequence of diffeomorphsims in $\mathcal{D}$. He shows that any minimiser in $\overline{\mathcal{D}}$ is injective by appealing to the Hartman-Wintner lemma[25]. Finally, he deduces the strict positiveness of the Jacobian by the lemma of Heinz[26].

The differences described in this paragraph do not arise as a consequence of the choice of classes. In fact, they are owed to the use of isothermal coordinates which transfers the problem to a standard complex analysis setting.

5.4 Higher Genus Surfaces

In the first part of this chapter, we have seen that two Riemannian metrics on the sphere are always conformally equivalent in the sense that there is a conformal diffeomorphism between them. This statement does not apply to surfaces of higher genera. Indeed, even for the torus there is more than one conformal equivalence class, i. e. there exist two smooth metrics on $\mathbb{T}^2$ that are not conformally equivalent[27].

[25] cf. p. 70 in [Jos90].
[26] cf. p. 78 in [Jos90].
[27] cf. pp. 75 in [Jos00].

6 Mesh Improvement

At the end of chapter 4, we have seen that the discretised Willmore flow drives the mesh of a discrete surface to degeneration. This effect has equally appeared for glued surfaces and for conventionally constructed surfaces. We will now describe the "conformality trick" introduced by U. Clarenz and G. Dziuk in [CD03] as a strategy for mesh improvement for topological spheres and study its applicability to discrete glued surfaces. We will only go into detail where differences between glued surfaces and surfaces parametrised over $\mathbb{S}^2$ arise.

6.1 The Conformality Trick

As we have shown in chapter 5, every smooth Riemannian metric g on $\mathbb{S}^2$ is conformally equivalent to the canonical metric can. If we could find a numerical equivalent of a conformal diffeomorphism between a discrete spherical surface Σ_h (that is given to us as a step of iteration in the discretised Willmore flow) and a fixed discrete sphere the mesh of which has a high quality, then we could use this "discrete conformal diffeomorphism" in order to transfer the "good" mesh to Σ_h. This idea is the basis for the conformality trick.

In the smooth setting, the global conformal parameters that realise the conformal equivalence have been identified as the minimisers of the generalised Dirichlet energy E_g in the class $\mathcal{C} = \{h \in C^0 \cap H^{1,2}(\mathbb{S}^2, \mathbb{S}^2) \,|\, h \text{ is monotone and satisfies (3P) and } \det dh \geq 0\}$ – a result that can be exploited numerically. We define

Definition 6.1.1 (Harmonic Maps). [1] A map $h \in C^\infty(\mathbb{S}^2, \mathbb{S}^2)$ is called *harmonic* with respect to the canonical metric can in the domain and a smooth Riemannian metric g on $\mathbb{S}^2$ in the image if it is a solution of the Euler-Lagrange equations of the generalised Dirichlet energy E_g.

Corollary 6.1.2. *Let g be a smooth Riemannian metric on $\mathbb{S}^2$. Any minimiser of E_g in $\mathcal{C}$ and hence any global conformal parameter $h : (\mathbb{S}^2, \text{can}) \to (\mathbb{S}^2, g)$ is harmonic.*

Proof. The first claim follows from theorem 5.1.1 as holomorphic maps are automatically harmonic on Riemann surfaces (see [Jos91]). Let $h : (\mathbb{S}^2, \text{can}) \to (\mathbb{S}^2, g)$ be any global conformal parameter and let $\tilde{h}$ be a minimiser of E_g. Then by the uniqueness statement of theorem 5.1.1, the composition $\mu := h^{-1} \circ \tilde{h}$ is a conformal automorphism of $\mathbb{S}^2$ and hence

[1] cf. p. 403 in [Jos91] or p. 2 in [SY94].

a Möbius transform by proposition 5.1.3. But this implies $E_g(h) = E_g(h \circ \mu) = E_g(\tilde{h})$ by lemma 5.2.7 so that h must be a minimiser of E_g, too. □

The converse is also valid:

Theorem 6.1.3. [2] *Let g be a smooth Riemannian metric on $\mathbb{S}^2$ and suppose there is a harmonic diffeomorphism $h : (\mathbb{S}^2, \mathrm{can}) \to (\mathbb{S}^2, g)$. Then h is conformal.*

We now give a new interpretation to our result 5.1.1. Let Σ be any smooth surface diffeomorphic to $\mathbb{S}^2$ and immersed into $\mathbb{R}^3$, let g be the smooth Riemannian metric induced on Σ by the canonical metric of $\mathbb{R}^3$. Then we can restate the theorem to say that Σ *can be globally conformally parametrised over* $\mathbb{S}^2$ which means that there is a conformal orientation-preserving diffeomorphism $h : (\mathbb{S}^2, \mathrm{can}) \to (\Sigma, g)$. [Let $\tilde{g}$ be the smooth Riemannian metric induced on $\mathbb{S}^2$ via the given diffeomorphism $f : \mathbb{S}^2 \to \Sigma$. Then theorem 5.1.1 states that there exists a conformal orientation-preserving diffeomorphism $\tilde{h} : (\mathbb{S}^2, \mathrm{can}) \to (\mathbb{S}^2, \tilde{g})$. Setting $h := f \circ \tilde{h}$ proves the claim.]

For the following, we adapt our notions and notations to the discrete setting as introduced in the chapters 3 and 4. For example, if $f : \Sigma \to \mathbb{R}^3$ is an immersion, we "identify" Σ and its image under f. In this language[3], the trick of U. Clarenz and G. Dziuk consists of the following idea:

Problem 6.1.4 (Mesh Improvement Problem I). [4] *Let Σ be a smooth surface immersed into $\mathbb{R}^3$. Let $\nabla_\Sigma X$ denote the tangential gradient*[5] *of X and let $\triangle_\Sigma$ denote the induced Laplace operator, i. e. $\triangle_\Sigma X := \nabla_\Sigma \cdot \nabla_\Sigma X$. Find a conformal diffeomorphism $X : \Sigma \to \mathbb{S}^2$, i. e. a diffeomorphism satisfying the non-linear elliptic system*

$$-\triangle_\Sigma X = |\nabla_\Sigma X|^2 X, \quad |X| = 1 \text{ on } \Sigma.$$

Remark. It is important for the discretisation that the conformal diffeomorphism maps onto the round sphere equipped with the canonical metric and does not start there as it did in chapter 5, see below. This implies that we cannot minimise E_g but need to minimise some "dual" energy E^g where the rôles of g and can are interchanged. But as we have reinterpreted theorem 5.1.1 to apply to arbitrary smooth surfaces the metric of which is induced by an immersion into $\mathbb{R}^3$, it is possible[6] to work with the energy

$$E_\Sigma(X) := \frac{1}{2} \int_\Sigma |\nabla_\Sigma X|^2 \, d\mu_\Sigma,$$

where μ_Σ denotes the measure induced by the immersion, and ∇_Σ is defined as above. The critical points of E_Σ are then obtained by differentiating $\varepsilon \mapsto \int_\Sigma |\nabla_\Sigma \frac{X+\varepsilon Y}{|X+\varepsilon Y|}|^2 \, d\mu$ where $Y \in C^0 \cap H^1(\Sigma, \mathbb{R}^3)$ (cf. [CD03]).

[2] This is due to J. Eells and J. C. Wood, [Eel92], say U. Clarenz and G. Dziuk in [CD03].

[3] These notions and notations are sloppy; in case Σ is not embedded, we would have to be more careful in order to be precise. As no confusion arises, we prefer to follow [CD03].

[4] cf. [CD03].

[5] as introduced on page 83.

[6] cf. [CD03, SY94].

We would like to solve the mesh improvement problem by minimising E_Σ, but first we have to define a class where we minimise on. Although it does not depend on g and could thus be used as the domain of E_Σ, the class $\mathcal{C}$ is not perfectly appropriate for discretisation purposes as the conditions of three point normalisation and monotonicity are not linear. The class used in [CD03] replaces[7] the three point condition by an integral condition (ICM) that also "fixes the Möbius group" of $\mathbb{S}^2$. The advantage of this integral condition is that it is linear and thus easily discretisable. Secondly, it does not request the property of non-negative Jacobian.

The class used as a starting point for the discretisation is

$$\mathcal{C}(\Sigma) := \{X \in C^0 \cap H^1(\Sigma, \mathbb{R}^3) \,|\, |X(p)| = 1 \,\forall\, p \in \Sigma \text{ and } X \text{ satisfies (ICM)}\}.$$

Let us reformulate the mesh improvement problem as a minimiser problem:

Problem 6.1.5 (Mesh Improvement Problem II). [8] *Let Σ be a smooth surface immersed into $\mathbb{R}^3$. Find a minimiser of E_Σ in $\mathcal{C}(\Sigma)$.*

In [CD03], it is not discussed whether E_Σ really attains its minimum on $\mathcal{C}(\Sigma)$. However, making small adaptions, it should follow from our proof of theorem 5.1.1 that such a minimiser is a harmonic/conformal diffeomorphism.

6.1.1 Discretisation and Implementation

Let $\Sigma_h \subset \mathbb{R}^3$ be a discrete surface. Recall the definition of the finite element space $\mathcal{X}_h(\Sigma_h)$ given in chapter 4. According to [CD03], the integral condition can be discretised with linear Finite Elements to a condition $(\text{ICM})_h$. Let $\mathtt{nv}$ denote the number of vertices of Σ_h; let v_i, $i \in \{1, \dots \mathtt{nv}\}$, denote the vertices of Σ_h. U. Clarenz and G. Dziuk introduce the discrete class

$$\mathcal{C}_h(\Sigma_h) := \{X \in \mathcal{X}_h(\Sigma_h) \,|\, |X(v_i)| = 1 \,\forall i \in \{1, \dots, \mathtt{nv}\}, X \text{ satisfies } (\text{ICM})_h\}.$$

They discretise the energy by $E_h(X) := \frac{1}{2}\int_{\Sigma_h} |\nabla_{\Sigma_h} X|^2 d\mu_h$ for $X \in \mathcal{X}_h(\Sigma_h)$ and formulate the discretised mesh improvement problem

Problem 6.1.6 (Discretised Mesh Improving Problem I). *Let $\Sigma_h \subset \mathbb{R}^3$ be discrete surface homeomorphic to the sphere. Also, let $\mathbb{S}^2_h$ be a given discretisation of $\mathbb{S}^2$. Find an injective map $X \in \mathcal{C}_h(\Sigma_h)$ which is a minimiser of the generalised Dirichlet energy E_h. The discrete surface $\tilde{\Sigma}_h$ defined by $\tilde{\Sigma}_h := X^{-1}(\mathbb{S}^2_h)$ is then used as starting point for the following iterations of the discretised Willmore flow. The vertices of $\tilde{\Sigma}_h$ lie on Σ_h.*

[7] In fact, their integral condition allows for rotations by π. This does not influence the discretised scheme as the steps of the iteration are small.

[8] cf. [CD03].

The side conditions $|X(v_i)|^2 = 1$ for all $i \in \{1, \ldots, \mathtt{nv}\}$ are reformulated as non-linear integral conditions $(\mathrm{ICS2})_h$ with the aid of a real-valued continuous piecewise linear Lagrange multiplier λ. The linear integral conditions $(\mathrm{ICM})_h$ that fix the Möbius group are realised by six real Lagrange multipliers ρ. Before we formulate the final version of the mesh improvement problem, let us agree on some notation. Let the real-valued piecewise linear Finite Element space be denoted by

$$\mathcal{V}_h(\Sigma_h) := \{\lambda \in C^0(\Sigma_h, \mathbb{R}) \mid \lambda|_T \text{ is linear for every } T \in \mathcal{T}_h\}.$$

Recall that $\mathcal{X}_h(\Sigma_h) = \mathcal{V}_h(\Sigma_h)^3$. Also, let $M_h : \mathcal{X}_h(\Sigma_h) \to \mathbb{R}$ be a linear operator chosen such that $M_h(X) = 0$ if and only if X satisfies the integral conditions $(\mathrm{ICM})_h$.

U. Clarenz and G. Dziuk introduce an energy $F_h : \mathcal{X}_h(\Sigma_h) \times \mathcal{V}_h(\Sigma_h) \times \mathbb{R}^6 \to \mathbb{R}$,

$$F_h(X, \lambda, \rho) := E_h(X) + \frac{1}{2} \int_{\Sigma_h} \lambda(|X|^2 - 1) + \rho \cdot M_h(X) \, d\mu_h$$

that additively combines the energy E_h with terms corresponding to the integral conditions $(\mathrm{ICS2})_h$ and $(\mathrm{ICM})_h$, respectively. A solution of problem 6.1.6 then consists of a parametrisation $X \in \mathcal{X}_h(\Sigma_h)$, Lagrange parameters $\lambda \in \mathcal{V}_h(\Sigma_h)$ and $\rho \in \mathbb{R}^6$ such that (X, λ, ρ) satisfies the Euler-Lagrange equations of F_h. We quote without proof

Problem 6.1.7 (Discrete Mesh Improvement Problem II). *Let $\Sigma_h \subset \mathbb{R}^3$ be a discrete surface homeomorphic to the sphere. Also, let $\mathbb{S}_h^2$ be a given discretisation of $\mathbb{S}^2$. Find an injective map $X \in \mathcal{C}_h(\Sigma_h)$ and Lagrange parameters $\lambda \in \mathcal{V}_h(\Sigma_h)$, $\rho \in \mathbb{R}^6$ such that*

$$\int_{\Sigma_h} \nabla_{\Sigma_h} X : \nabla_{\Sigma_h} Y \, d\mu_h + \int_{\Sigma_h} \lambda X \cdot Y \, d\mu_h + \rho \cdot M_h(Y) = 0 \quad \forall Y \in \mathcal{X}_h(\Sigma_h) \tag{6.1}$$

$$\int_{\Sigma_h} \kappa(|X|^2 - 1) \, d\mu_h = 0 \quad \forall \kappa \in \mathcal{V}_h(\Sigma_h) \tag{6.2}$$

$$M_h(X) = 0. \tag{6.3}$$

The discrete surface $\tilde{\Sigma}_h$ defined by $\tilde{\Sigma}_h := X^{-1}(\mathbb{S}_h^2)$ is then used as starting point for the following iterations of the discretised Willmore flow. The vertices of $\tilde{\Sigma}_h$ lie on Σ_h.

In their mesh improvement algorithm, it is assumed that the given surface Σ_h is explicitly parametrised over a discretisation $(\mathbb{S}_h^2)^0$ of $\mathbb{S}^2$. Denote this parametrisation by $U : \mathbb{S}_h^2 \to \Sigma_h$. As for the implementation of the discretised Willmore flow, the nodal basis of $\mathcal{X}_h(\Sigma_h)$ is used. A simplified Newton method[9] is used to reduce the problem to a linear equation. As starting point for the Newton method, X^0 is chosen to be the inverse[10] of the parametrisation U, λ^0 and ρ^0 are chosen equal to zero. The linear equation is then iteratively solved by the method of conjugate gradients (CG)[11]. The flow chart on page 133 illustrates the procedure.

[9] cf. [CD03, Sto79]. In fact, the author has used a damped Newton method as this has proved more convenient for the glued surfaces, see below.

[10] Recall that we have understood an immersed surface as parametrised over an embedded one. Mappings etc. are then defined on the embedded parametric domain.

[11] cf. [CD03, Sto79].

Problem 6.1.8 (Discretised Mesh Improvement Algorithm). *Let Σ_h be a discrete surface parametrised over a sphere. Let $X^0 = U^{-1} \in \mathcal{C}_h(\Sigma_h)$, $\lambda^0 = 0 \in \mathcal{V}_h(\Sigma_h)$, and $\rho^0 = 0 \in \mathbb{R}^6$. Let $\varepsilon > 0$ be a tolerance and let $m_0 \in \mathbb{N}$.*

Denote by μ_h the surface measure and by ∇_{Σ_h} the tangential gradient on Σ_h. For each $m = 0, 1, \ldots, m_0 - 1$, find $X^{m+1} \in \mathcal{X}_h(\Sigma_h)$, $\lambda^{m+1} \in \mathcal{V}_h(\Sigma_h)$, and $\rho^{m+1} \in \mathbb{R}^6$ that solve the linear system

$$\begin{aligned}
&\int_{\Sigma_h} \nabla_{\Sigma_h} X^{m+1} : \nabla_{\Sigma_h} Y \, d\mu_h + \int_{\Sigma_h} \lambda^m X^{m+1} \cdot Y \, d\mu_h \\
&\qquad + \int_{\Sigma_h} \lambda^{m+1} X^m \cdot Y \, d\mu_h + \rho^{m+1} \cdot M_h(Y) \;=\; 0 \qquad \forall\, Y \in \mathcal{X}_h(\Sigma_h) \\
&\qquad\qquad \int_{\Sigma_h} \kappa X^{m+1} \cdot X^m \, d\mu_h \;=\; \frac{1}{2} \int_{\Sigma_h} \kappa (|X^m|^2 - 1) \, d\mu_h \quad \forall\, \kappa \in \mathcal{V}_h(\Sigma_h) \\
&\qquad\qquad\qquad M_h(X^{m+1}) \;=\; 0.
\end{aligned}$$

If X^{m+1} is locally injective[12] ($\Leftrightarrow (\mathbb{S}_h^2)^{m+1} := X^{m+1}(\Sigma_h^m)$ is a discretisation of $\mathbb{S}^2$) and if the L^2-error $\|X^{m+1} - X^m\|_{L^2(\Sigma_h, \mathbb{R}^3)} + \|\lambda^{m+1} - \lambda^m\|_{L^2(\Sigma_h, \mathbb{R})} + |\rho^{m+1} - \rho^m| > \varepsilon$, continue with the next iteration. If X^{m+1} is locally injective and if the L^2-error lies below ε for m_1, then set $\tilde{\Sigma}_h := (X^{m_1})^{-1}((\mathbb{S}_h^2)^{m_1})$ and let $\tilde{U} : (\mathbb{S}_h^2)^{m_1} \to \tilde{\Sigma}_h$ be the parametrisation with which the Willmore flow is continued.

6.1.2 Examples

Let us first have a look at the behaviour of the deformed ellipsoid under the discretised Willmore flow with mesh improvement by the conformality trick. The chosen parameters are `ilz` $= 8$, `genus` $= 0$, `surface` $= 9$, `projection` $= 0$, `conformal` $= 0$, also `mcf_freq` $= 0$ and `expo` $= 3$. The mesh improvement is carried out every sixth iteration. As expected, the surface approximates a round sphere under the flow as it did without mesh improvement. This time, however, the mesh does not degenerate and the scheme does not stop before the final time `final` $= 1$ is reached. This is equivalent to approximately 13400 iterations. We depict the surface before the start of the iteration, and after 10, 100, 1000, and 10000 steps. The table below illustrates the behaviour of the Willmore energy and of the mesh regularity. The Willmore energy and the mesh regularity behave under the mesh improvement as listed in the table on page 131. The data and figures indicate that the conformality trick works well for discrete surfaces parametrised over the round sphere.

Although, theoretically, conformal reparametrisation does not leaves the Willmore energy invariant, we get changes, numerically, see table 6.3. Changes in the Willmore energy occurring because of the mesh improvement are probably due to two factors: the first (small)

[12] If X^{m+1} is not locally injective, it cannot be inverted and a new parametrisation over the sphere is not available.

effect is that the iterative Newton and CG schemes do not find exact solutions to problem 6.1.7; the second is that the surface changes under the reparametrisation. The vertices of the reparametrised surface lie on the old surface, but if the old mesh is not very "good", features can be lost. The author supposes that this is what happened to the ellipsoid after five iterations, cf. the table and the figures on page 132 below – which would explain the sharp edges of the surface after ten iterations, see figure 6.1. The author further assumes that these sharp edges are smoothed out by the Willmore flow in the following iterations. The quality of the mesh does not change very much through the six steps that lie between two mesh improvements; this can be seen at the number of iterations the Newton scheme needs to converge (i. e. to reduce the L^2-error so that it is smaller than ε), cf. figure 6.6. Please note that the surfaces on page 132 are scaled down more than the others for display purposes.

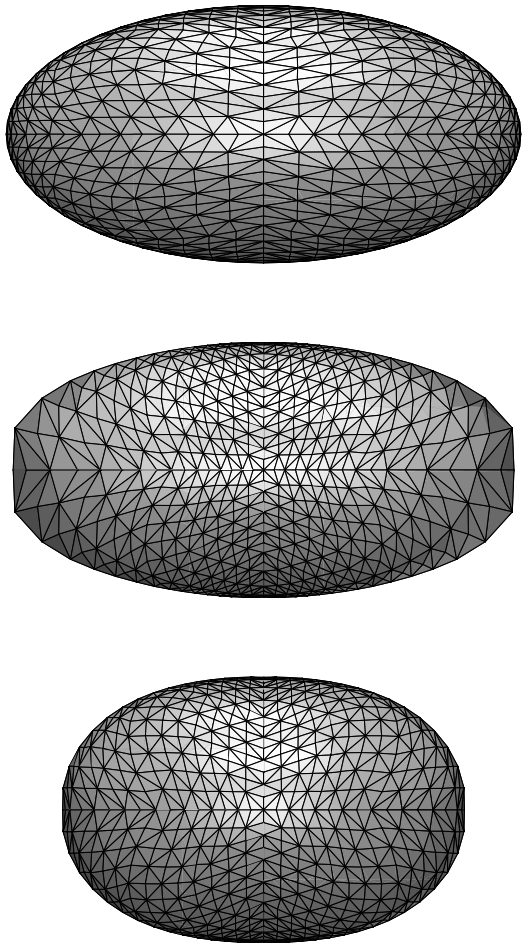

Figure 6.1: Before the iteration, after 10, and 100 steps of the iteration with mesh improvement.

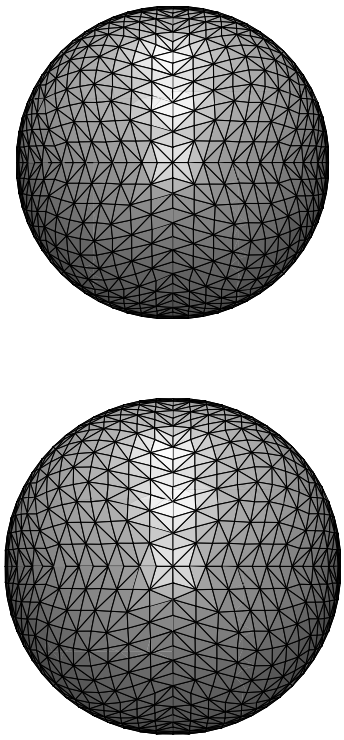

Figure 6.2: After 1000, and 10000 steps of the iteration with mesh improvement.

step	W. energy	reg.	without mesh improvement: W. energy	reg.
1	40.03	10.03	40.03	10.03
10	31.78	11.62	32.86	9.31
100	27.03	10.44	26.69	10.02
1000	24.92	10.41	-	-
10000	24.92	10.40	-	-

Figure 6.3: Willmore energy and regularity under the flow with mesh improvement.

after step	W. energy before	reg. before	W. energy after	reg. after
6	33.89	9.44	50.42	10.96
12	31.44	11.99	32.25	10.99
18	30.98	11.41	31.18	10.92
24	30.66	11.22	30.81	10.78
30	30.36	11.06	30.47	10.71
36	30.06	10.92	30.14	10.71
42	29.77	10.81	29.84	10.69

Figure 6.4: Willmore energy and regularity under the mesh improvement.

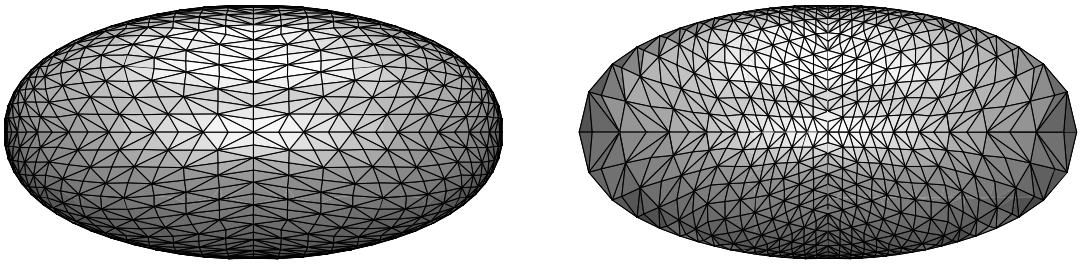

Figure 6.5: Mesh improvement after the fifth iteration: before and after improvement.

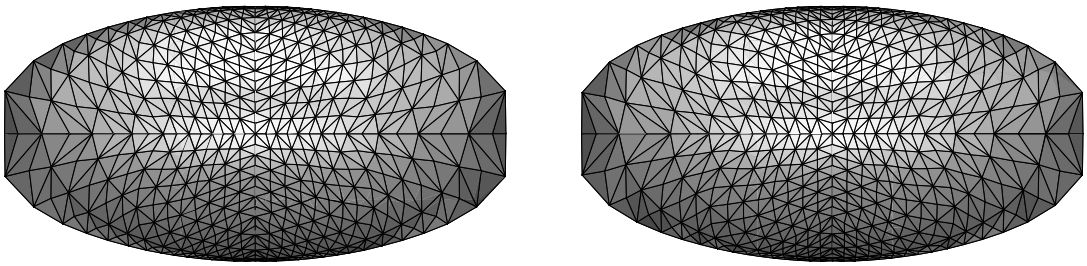

Figure 6.6: Mesh improvement after the eleventh iteration: before and after improvement.

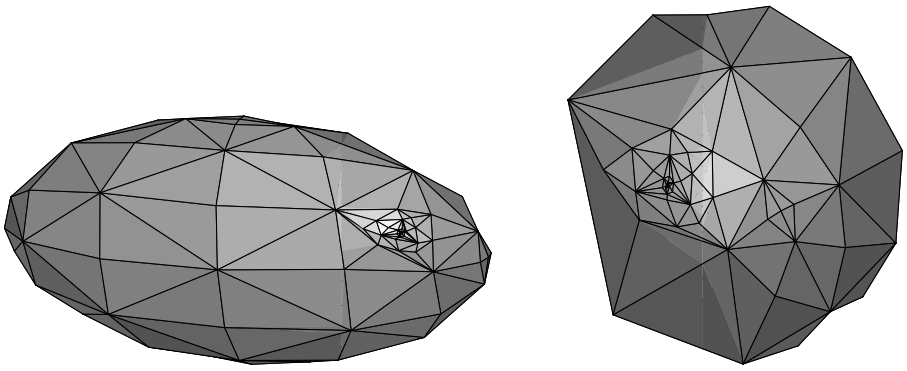

Figure 6.7: Mesh of a glued ellipsoid and the corresponding round sphere mesh as described in the text.

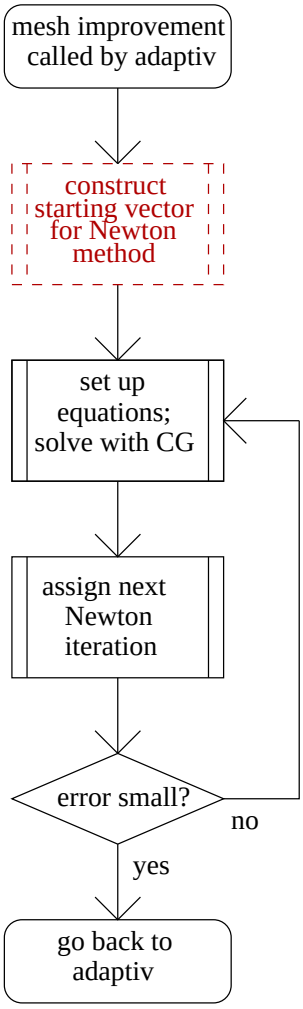

Figure 6.8: Flow Chart for the mesh improvement algorithm. The light coloured pieces of the program have not been discussed.

6.2 Glued Surfaces and the Conformality Trick

For topological spheres that are the output of the glueing procedure, the conformality trick is not applicable without changes as they are not explicitly parametrised over a round sphere mesh by construction. This means that we cannot easily determine a starting point for the Newton method. As the Newton method is fairly sensitive to the starting point and the energy F_h and the class $\mathcal{C}_h(\Sigma_h)$ we are minimising on are not easy to understand, this has forced us to investigate on how to find a starting point from where the Newton method converges. First of all, we have replaced the Newton method by a damped Newton method, see section 6.2. Then, we have tried several techniques for calculating a discretisation $(\mathbb{S}^2_h)^0$ of $\mathbb{S}^2$ and a parametrisation $U : (\mathbb{S}^2_h)^0 \to \Sigma_h$ for two exemplary surfaces: for surfaces of the type of the glued ellipsoid described in section 3.3 and for surfaces similar to the glued dumbbell depicted in figure 3.9. The parameters chosen for the glueing of the dumbbell are: `samesurface` $=$ `withcyl` $= 0$, `ilz` $= 3$, `ilz2` $= 1$, `genus` $=$ `surface` $= 0$, finally `ii1` $= 1$, `projection` $=$ `rotangle` $=$ `mcf_freq` $= 0$.

For some embedded surfaces such as the glued ellipsoid, for example, it is straightforward to calculate a discretisation of $\mathbb{S}^2$ by simply projecting all vertices of the surface onto $\mathbb{S}^2$ via $x \mapsto \frac{x}{|x|}$. This gives a mesh the vertices of which lie on $\mathbb{S}^2$ at least if its centroid[13] lies in the origin. A similar strategy can be applied to the glued dumbbell (in subroutine `round()`); the vertices can be projected via $x = (x_1, x_2, x_3)^t \mapsto (\frac{x_1}{\sqrt{1-(x_3^2/L^2)}}, \frac{x_2}{\sqrt{1-(x_3^2/L^2)}}, \frac{x_3}{L+2})^t$, where L is the length of the cylinder and 1 is the radius of the spheres in the dumbbell. However, the resulting meshes discretising $\mathbb{S}^2$ are of a very low quality, see page 132 above.

We have tried to improve this mesh with Laplacian smoothing (both with and without round sphere projection) but without success. Neither the usual nor the damped Newton method converge with this starting point, not even for very low levels of refinement. For glued dumbells, the situation is a little better. Although the damped Newton method does not converge with a starting point constructed as above – even not for low levels of refinements – we were able to construct a finer mesh on the dumbbell and a parametrisation over $\mathbb{S}^2$ which constitutes a suitable starting point. We have done this as follows:

Having in mind the hugely different sizes of the triangles in the pictures above and below, we have written subroutines `reksurf_s(order, last, divided)` and `surf_s(i, divid, avarea)` that iteratively subdivide all triangles having larger size than thirty percent of the "average size" `avarea` of a triangle on the sphere. The average size of a triangle is calculated as `avarea` $= \frac{\mathrm{vol}(\mathbb{S}^2)}{\mathtt{nt}}$. The refinement process is encoded into the vectors `order` and `divided` so that we can afterwards refine the dumbbell mesh analogously. This is realised in the subroutine `refsurf_recursive(order, last)`. All the above subroutines are called by the subroutine `xgood_mesh()`. For a glued dumbbell being constructed from

[13] or centre of mass

two four times refined spheres, the damped Newton method converges. However, the resulting new mesh does not approximate the initial glued dumbbell very well, see the figure below.

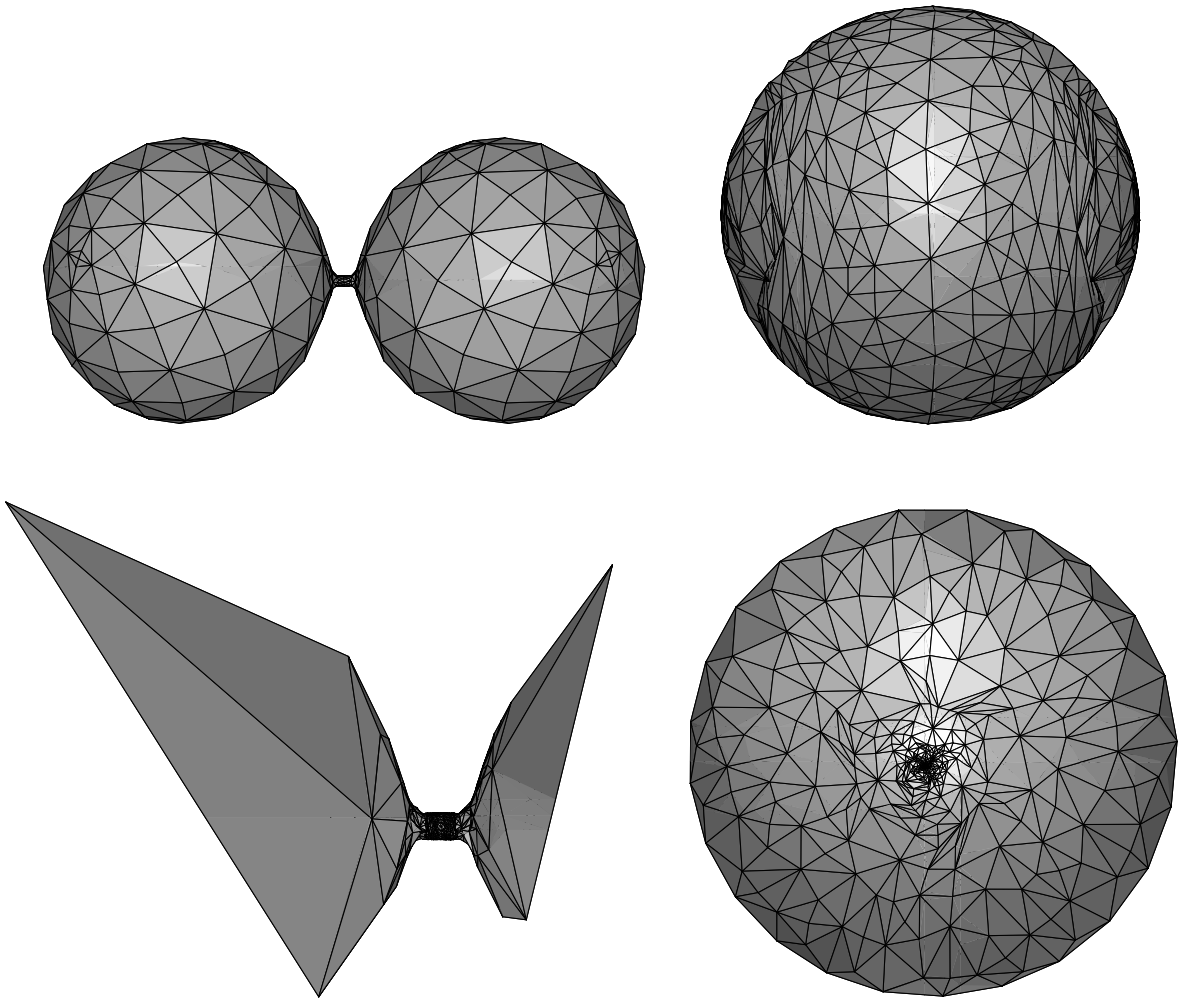

Figure 6.9: top: a glued dumbbell (left) – surface C, the round sphere mesh before the mesh improvement; bottom: the round sphere mesh after the mesh improvement (right) – surface B, and the new "dumbbell mesh" after the mesh improvement (left) – surface A. (The surfaces are scaled differently for display.)

We can see in this figure that the mesh concentrates where the curvature is concentrated and does not grep the spherical parts of the dumbbell shape. We tried to remedy this deficiency by further refining the surfaces. The idea is the following: subdivide some triangles of the surface that is the output of the mesh improvement, "surface A", chosen for their "non-niceness" (see below), then imitate these refinements in the discretised round sphere mesh having been calculated by the mesh improvement algorithm, "surface B" (with a subroutine `reksurf_s(...)` similar to `reksurf(...)`). Finally, imitate these refinements again in the dumbbell mesh we took as starting point for the mesh improvement algorithm, "surface C". This procedure ensures that surface C is parametrised over surface B. Also,

it allows us to decide whether a specific triangle should be refined by only considering the shapes of the triangles in A. We have developed three methods to decide which triangle shall be subdivided. Inspired by figure 6.9, we compare the area of all triangles with a characteristic area and subdivide large triangles; also, we compare the length of every edge with a typical length and subdivide the triangles having long edges in a way that these edges are refined; and thirdly, we try to smooth the tips at both ends of surface A by subdividing triangles that have large "outer angles". By "outer angles", we understand the angles between the normal of the triangle under consideration and the normal of each of its neighbours, respectively.

As before, we save the information needed for an imitation of the refinement to the vectors `order, last, divided`, and `dividedge`. We rely on the refinement subroutines `rekref_glue(...)` and `refel_glue(...)` which we have also used for the glueing scheme. We do not go into detail, the code is included in the appendix. A flow chart is shown on page 138.

area We decide to subdivide a triangle if it is larger than a characteristic size in the surface – this size is calculated as `avarea` $= 0.5($`minarea` $+ 0.5$`maxarea`$)$, `minarea, maxarea` are the minimal and maximal sizes of triangles in the mesh. For this, we use the subroutines `reksurf(order, last, divided, dividedge)`, `surf(i, divid, avarea, edg)`, and `minmaxsurf(minarea, maxarea)`. The first subroutine simulates a recursive call and controls the refinement process. We iteratively compare the triangles' sizes with the number `avarea` several times. The number `avarea` is adapted in each loop. The second subroutine calculates the minimal and maximal area a triangle in the mesh of surface A has and the third one then prepares and executes the subdivision of this triangle (and the neighbour thereof).

edges Similarly, we iteratively subdivide all triangles that have "untypical" edge lengths. We choose those triangles for subdivision that have particularly long edges. We use the subroutine `rekedge(order, last, divided, dividedge)` as simulator for a recursive call and as controller and the subroutine `minmaxedge(minedge, maxedge)` to calculate the minimal and maximal edge length of the mesh. We define a characteristic length `avedge` $= 0.5($`minedge` $+ 0.5$`maxedge`$)$. `maxedglength(i, edg, divid, avedge)` then subdivides all triangles that have an edge longer than fifty percent of `avedge` in a way that reduces the length of this long edge.

angles Finally, we use `outsideangle(order, last, divided, dividedge)` and `angle(i, edg, divid, maxangle)` to iteratively subdivide all triangles with outer angles of a size larger than $\frac{\pi}{10}$.

All these subroutines are collected in the subroutine `improve_mesh()`. The resulting dumbbell mesh and the corresponding round sphere mesh (stemming from the mesh depicted in figure 6.9) are depicted in figure 6.10.

Now, we apply the mesh improvement scheme again, this time with the refined surface constructed above as starting point. As parametric domain, we use the refined round sphere mesh constructed in `improve_mesh()`. The following method is controlled by `nicer_mesh()`.

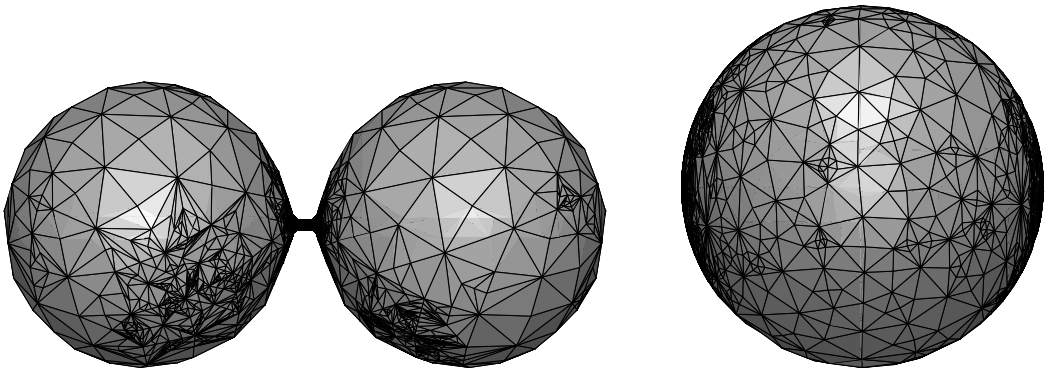

Figure 6.10: Refined glued dumbbell – surface C, refined round sphere mesh – surface B.

First, we determine some technical neighbouring information; we need to know for each vertex to which triangles it belongs. This is executed in the subroutine `neighbouring(...)`, the information is saved to its parameters. Then we perform the mesh improvement relying on the conformality trick. Usually, this would mean that we construct the output dumbbell mesh by pulling back the round sphere mesh we have started with via the parametrisation as described above. This time, however, we construct a new discretisation of the round sphere and pull this one back. The advantage is that we can construct a very regular mesh on $\mathbb{S}^2$ without respecting the structure of the mesh on the dumbbell (such as its number of vertices etc.) so that the new mesh on the dumbbell will hopefully adapt very well to the curvature of the dumbbell but still grep all characteristic features. The new mesh is constructed in the subroutine `sphere(...)`, the mesh is pulled back by `pullback(...)`. This variant of mesh improvement is executed by the subroutine `harmonicmap_nice(...)`. All methods that we have described are controlled by `parameter_mesh(...)`. A flow chart is shown on page 138. The output "dumbbell" surface after `parameter_mesh(...)` is depicted below.

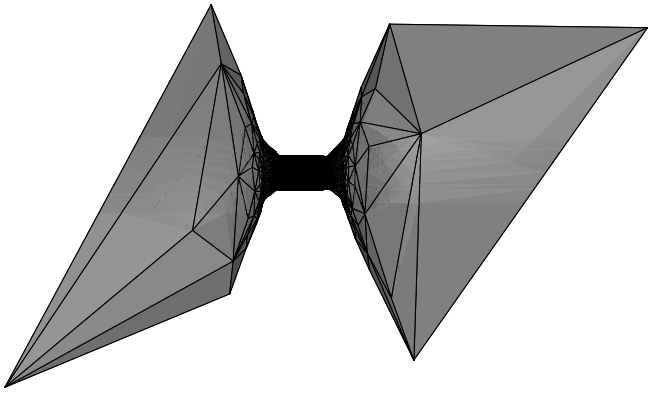

Figure 6.11: After parameter_mesh: new glued dumbbell.

We conclude that more specific methods need to be developed in order to improve the mesh of a glued dumbbell. The same is true even more for glued ellipsoids. The imitated

refinement method did not work for glued ellipsoids at all, as their mesh is very fine in the region where the inverted ellipsoid has been inserted. We could therefore not find a starting point from which the Newton method converged.

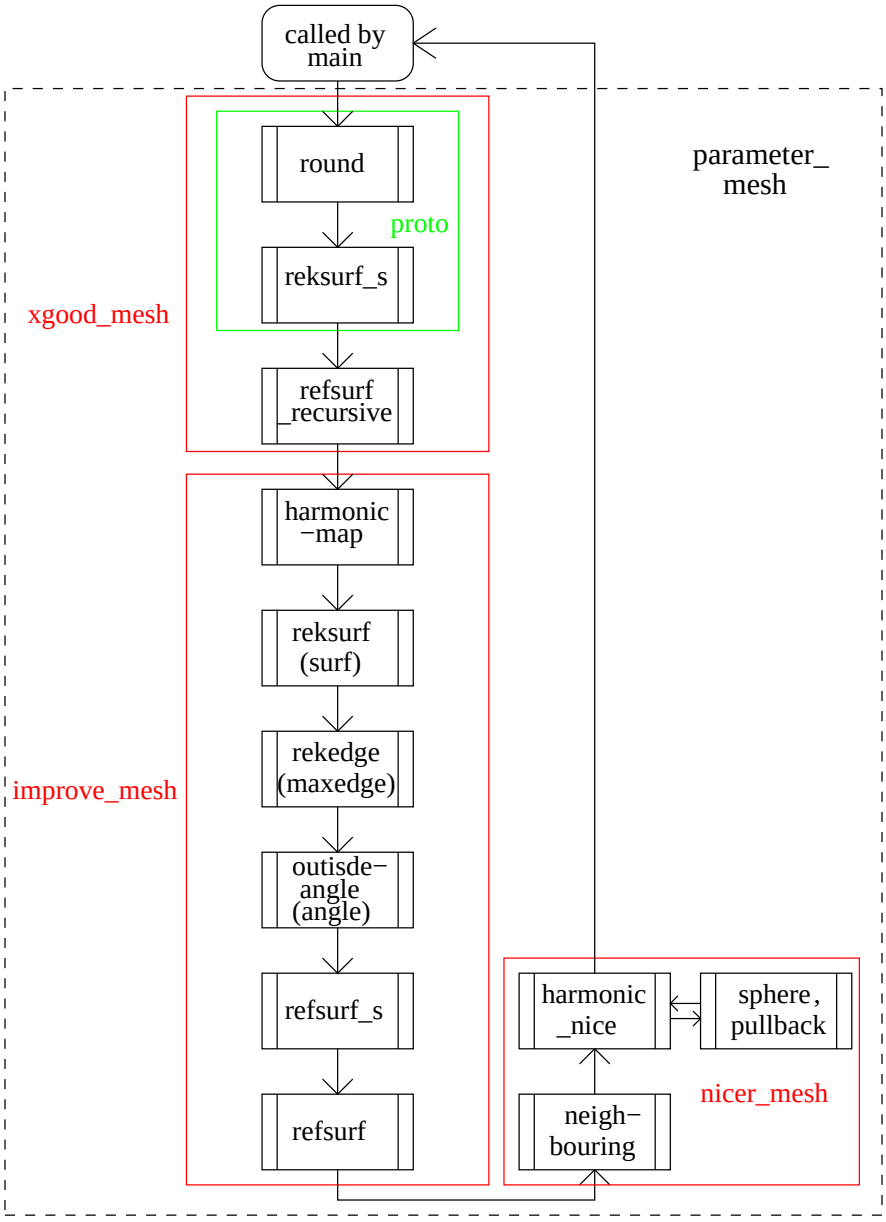

Figure 6.12: Flow Chart for the construction of a starting parametrisation for the glued dumbbell.

Damped Newton Methods

Instead of the Newton method used by U. Clarenz and G. Dziuk, we work with a damped Newton method as described in [Sto79,Dzi91]. We do so to secure that the scheme does not lead "very far away" of the minimum of the energy F_h. Instead of using the conventional rule

$$z^{m+1} = z^m - (f'(x^m))^{-1} f(x^m)$$

where $f = (F_h)'$ and $z = (X, \lambda, \rho)$, we use the modified version

$$z^{m+1} = z^m - t^m (f'(z^m))^{-1} f(z^m),$$

where $t^m \in (0, 1]$ is chosen as follows. Set $\sigma = 0.5$. For $m = 0, 1, \ldots$ iteratively choose the smallest number $q^m \in \mathbb{N}_0$ that satisfies $|f(z^m - t^m (f'(x^m))^{-1} f(x^m))| \leq (1 - \sigma t^m)|f(z^m)|$ with $t^m := 2^{-q^m}$. For convergence results, we refer to [Sto79, Dzi88].

6.3 Conclusions

In chapters 2 and 4 we have introduced the Willmore energy and flow. We have sketched how the continuous setting can be transfered to a discretised scheme and have studied the discretised Willmore energy of discrete surfaces and their behaviour under the discretised Willmore flow. In chapter 3, we have presented a glueing scheme for discrete surfaces. We have subsequently studied the behaviour of glued surfaces under the Willmore flow and their Willmore energies. At the end of chapter 4, we have described a mesh degeneration phenomenon that appears in the application of the discretised Willmore flow.

In this chapter, we have seen that discrete surfaces that are given as parametrisations over $\mathbb{S}^2$ are susceptible to mesh improvements with the conformality trick of U. Clarenz and G. Dziuk. This trick relies on the theory presented in chapter 5. We have further seen that this trick cannot be generalised straightforwardly to higher genus surfaces since two surfaces of the same genus $g > 0$ need not be conformally equivalent. As we have no indication that the Willmore flow should preserve the conformal type of a given surface, a conformality trick would have to be established more carefully. Carsten Eilks[14] has communicated to the author that he has constructed a conformality trick for tori relying on affine linear mappings. X. Gu and S.-T. Yau[15] have taken a different approach than U. Clarenz and G. Dziuk and were able to calculate global conformal parametrisations of surfaces of arbitrary non-zero genera.

Finally, we have explained why the conformality trick of U. Clarenz and G. Dziuk is difficult to apply to glued surfaces homeomorphic to $\mathbb{S}^2$. The reason for this was twofold. For most glued surfaces, a suitable starting vector for the Newton method used in the conformality trick could not be found. We have shown exemplarily how this deficiency can be partially remedied for a glued dumbbell.

[14] Institut für Angewandte Mathematik, Albert-Ludwigs-Universität Freiburg, the work is unpublished.
[15] cf. [GY02, GY03].

Bibliography

[Ahl66] L. Ahlfors. *Complex Analysis*. McGraw-Hill, 2 edition, 1966.

[Aki82] J. E. Akin. *Application and Implementation of Finite Elements Methods*. Computational Mathematics and Applications. Academic Press, 1982.

[Alb05] T. Albrecht. Impainting with the mumford-shah-euler image model. Master's thesis, Universität Freiburg, 2005.

[Alt91] H. W. Alt. *Lineare Funktionalanalysis*. Springer, 3 edition, 1991.

[Beh95] Lintz Behara, Fritsch, editor. *The Theorem of Gauß-Bonnet in Complex Analysis*, Symposia Gaussiana. de Gruyter, 1995.

[BGH98] G. Buttazzo, M. Giaquinta, and S. Hildebrandt. *One-dimensional variational problems: an introduction*. Clarendon Press, Oxford, 1998.

[BK03] M. Bauer and E. Kuwert. Existence of minimizing willmore surfaces of prescribed genus. *IMRN*, 10:553–576, 2003.

[Bla29] W. Blaschke. *Vorlesungen über Differentialgeometrie III*. Springer, 1929.

[Blo97] E. D. Bloch. *A first course in Geometric Topology and Differential Topology*. Birkhäuser, 1997.

[Bra91] D. Braess. *Finite Elemente*. Lehrbuch. Springer, 1991.

[Bry84] R. Bryant. A duality theorem for willmore surfaces. *J. Diff. Geom.*, 20:25–53, 1984.

[Bry88] R. Bryant. Surfaces in conformal geometry. in preparation, 1988.

[BS70] I. N. Bronstein and K. A. Semendjajew. *Taschenbuch der Mathematik*. Verlag Harri Deutsch, 10 edition, 1970.

[BS05] A. I. Bobenko and P. Schröder. Discrete willmore flow. In M. Desbrun and H. Pottman, editors, *Eurographics Symposium on Geometry Processing*, 2005.

[Can70] P. B. Canham. The minimum energy of bending as a possible explanation of the biconcave shape of the human red blood cell. *Journal of Theoretical Biology*, 26(1):61–81, 1970.

[CD03] U. Clarenz and G. Dziuk. Numerical methods for the conformal parametrization of surfaces. Lecture at Newton Institute, Cambridge, 2003.

[CDD+04] U. Clarenz, U. Diewald, G. Dziuk, M. Rumpf, and R. Rusu. A finite element method for surface restoration with smooth boundary conditions. *Computer Aided Geometric Design*, 21(5):427–445, 2004.

[dC83] M. P. do Carmo. *Differentialgeometrie von Kurven und Flächen.* Aufbaukurs Mathematik. vieweg studium, 1983.

[dC94] M. P. do Carmo. *Differential Forms and Applications.* Universitext. Springer, 1994.

[DD95] K. Deckelnick and G. Dziuk. Convergence of a finite element method for non-parametric mean curvature flow. *Numer. Math.*, 72:197–222, 1995.

[DDE05] K. Deckelnick, G. Dziuk, and C. M. Elliott. Computation of geometric partial differential equations and mean curvature flow. *Acta Numerica*, pages 139–232, 2005.

[DH02] P. Deuflhard and A. Hohmann. *Numerische Mathematik I.* de Gruyter, 3 edition, 2002.

[Dzi88] G. Dziuk. Finite elements for the beltrami operator on arbitrary surfaces. In S. Hildebrandt and R. Leis, editors, *Partial differential equations and calculus of variations*, pages 42–155. Springer, 1988.

[Dzi91] G. Dziuk. Numerik i, 1990/91. Mathematisches Institut Universität Freiburg.

[Eel92] J. Eells. *Selected Papers of J. Eells and Collaborators*, chapter Harmonic Maps. World Scientific, 1992.

[EG92] L. C. Evans and R. F. Gariepy. *Measure Theory and Fine Properties of Functions.* CRC Press, 1992.

[Els00] J. Elstrodt. *Maß- und Integrationstheorie.* Springer, 3. edition, 2000.

[GKM86] D. Gromoll, W. Klingenberg, and D. Meyer. *Riemannsche Geometrie im Großen.* Lecture Notes in Mathematics. Springer, 1986.

[GT70] D. Gilbarg and N. S. Trudinger. *Equations of Mean Curvature Type.* Springer, 2 edition, 1970.

[GY02] X. Gu and S. T. Yau. Computing conformal structures of surfaces. *Comm. Inf. Syst.*, 2(2):121–146, 2002.

[GY03] X. Gu and S. T. Yau. Global conformal surface reparametrisation. *Eurographics Symposion on Geometry processing*, pages 127–138, 2003.

[Gü89] M. Günther. Zum einbettungssatz von j. nash. *Math. Nachr.*, 144:165–187, 1989.

[Har97] R. M. Hardt. Singularities of harmonic maps. *Bulletin of the AMS*, 34(1):15–34, 1997.

[Hei91] M. Heisterkamp. *FORTRAN 90.* BI Wissenschaftsverlag, 1991.

[Hei03] C. J. Heine. *Comptutations of form and stability of rotating drops with finite elements.* PhD thesis, RWTH Aachen, 2003.

[Hel73] W. Helfrich. Elastic properties of lipid bilayers: Theory and possible experiments. *Zeitschrift für Naturforschung*, C 28(1):693–703, 1973.

[Hél04] F. Hélein. A weierstrass representation for willmore surfaces. In C. K. Anand, P. Baird, E.Loubeau, and J.C. Wood, editors, *Harmonic morphisms, harmonic maps and related topics*, volume 413 of *Research Notes in Mathematics.* Chapman and Hall/CRC, 2004.

[Heu92] H. Heuser. *Funktionalanalysis.* Teubner, 1992.

[Hir91] M. Hirsch. *Differential Topology.* Graduate Texts in Mathematics. Springer, 1991.

[Hut91] J. Hutchinson. Computing conformal maps and minimal surfaces. In G. Dziuk, G. Huisken, and J. Hutchinson, editors, *Proc. CMS*, volume 26, pages 140–161, 1991.

[Jos90] J. Jost. *Two-dimensional geometric variational problems.* pure and applied mathematics. Wiley-Interscience, 1990.

[Jos91] J. Jost. *Riemannian Geometry and Geometric Analysis.* Universitext. Springer, 1991.

[Jos00] J. Jost. *Compact Riemann Surfaces, An intorduction to Contemporary Mathematics.* Universitext. Springer, zweite edition, 2000.

[(Jr80] H. Blaine Lawson (Jr.). *Lectures on Minimal Submanifolds*, volume 1. Publish or Perish, 1980.

[KP88] R. S. Kulkarni and U. Pinkall, editors. *Conformal Geometry.* Aspekte der Mathematik. Vieweg, 1988.

[KP97] H. Karcher and U. Pinkall. Die boyesche fläche in oberwolfach. *DMV-Mitteilungen*, 1, 1997.

[KS02] E. Kuwert and R. Schätzle. Gradient flow for the willmore functional. *Comm. Anal. Geom.*, 10(2):307–339, 2002.

[KS04] E. Kuwert and R. Schätzle. Removability of point singularities of willmore surfaces. *Annals of Mathematics*, 160:315–359, 2004.

[Kus] R. Kusner. Conformal geometry and complete minimal surfaces. preprint.

[Kus89] R. Kusner. Comparison surfaces for the willmore problem. *Pacific Journal of Math.*, 138(2):317ff, 1989.

[Kus95] R. Kusner. Esimates for the biharmonic energy on unbounded planar domains, and the existence of surfaces of every genus that minimize the squared-mean-curvature integral. *Elliptic and Parabolic Methods in Geometry*, 1995.

[Kuw98] E. Kuwert. Einführung in die theorie der minimalflächen, 1998. Mathematisches Institut Universität Freiburg.

[Law70] H. B. Lawson. Complete minimal surfaces in $\mathbb{S}^3$. *Annal. of Math.*, 92:335–374, 1970.

[Lee97] J. M. Lee. *Riemannian Manifolds, An Introduction to Curvature.* Graduate Texts in Mathematics. Springer, 1997.

[Lee03] J. M. Lee. *Introduction to Smooth Manifolds.* Graduate Texts in Mathematics. Springer, 2003.

[LH92] J. M. Sullivan L. Hsu, R. Kusner. Minimizing the squared mean curvature integral for surfaces in space forms. *Experimental Maths.*, 1:191–207, 1992.

[LY82] P. Li and S. T. Yau. A new conformal invariant and its applications to the willmore conjecture and the first eigenvalue of compact surfaces. *Invent. Math.*, 69:269–291, 1982.

[MS03] U. F. Mayer and G. Simonett. Self-intersections for the willmore flow. *Nonlinear Differential Equations Appl.*, 55:341–348, 2003.

[Nas56] J. Nash. The imbedding problem for riemannian manifolds. *Ann. of Math.*, 63:20–63, 1956.

[Pin85] U. Pinkall. Hopf tori in $\mathbb{S}^3$. *Invent. Math.*, 81:379–86, 1985.

[PS87] U. Pinkall and I. Sterling. Willmore surfaces. *Math. Intelligencer*, 9:38–43, 1987.

[Rad25] T. Radó. Über den begriff der riemannschen fläche. *Acta Litt. Sci. Szeged*, 2:101–121, 1925.

[Rud99] W. Rudin. *Reelle und Komplexe Analysis.* Oldenbourg, 1999.

[Rus] R. Rusu. An algorithm for the elastic flow of surfaces. Universität Freiburg.

[Sch69] J. T. Schwartz. *Nonlinear Functional Analysis.* Gordon & Breach, New York, 1969.

[Sch96] A. Schmidt. Computation of three dimensional dendrites with finite elements. *Comp. Phys.*, 125:293–312, 1996.

[Sch02] M. U. Schmidt. A proof of the willmore-conjecture. Preprint No. 546, 2002.

[Sim83] L. Simon. *Lectures on Geometric Measure Theory*, volume 3 of *Centre for Mathematical Analysis.* Australian National University, 1983.

[Sim86] L. Simon. Existence of willmore surfaces. In *Proceedings of the Centre for Math. founds.*, volume 10, pages 187–216, Canberra, 1986.

[Sim93] L. Simon. Existence of surfaces minimizing the willmore functional. *Comm. Anal. Geom.*, 1(2):281–326, 1993.

[Sim01] G. Simonett. The willmore flow near spheres. *Differential Integral Equations*, 14:1005–1014, 2001.

[Soe04] W. Soergel. Topologie und kategorientheorie. lecture notes, 2004.

[ST80] H. Seifert and W. Threlfall. *A textbook of Topology.* Academic Press, 1980.

[Sto79] J. Stoer. *Einführung in die Numerische Mathematik I, II.* Springer, 3 edition, 1979.

[Str96] M. Struwe. *Variational Methods; Applications to Nonlinear Partial Differential Equations and Hamiltonian Systems.* Springer, 2 edition, 1996.

[SY94] R. Schoen and S. T. Yau. *Lectures on Differential Geometry.* Conference Proceedings and Lecture Notes in Geometry and Topology. Intern. Press., Mass., 1994.

[Wil59] T. J. Willmore. *An Introduction to Differential Geometry.* Oxford Clarendon Press, 1959.

[Wil65] T. J. Willmore. Note on embedded surfaces. *Ann. Stiint. Univ. "Al. I. Cuza", Iasi. Ia. Mat.*, pages 493–6, 1965.

[Wil82] T. J. Willmore. *Total Curvature in Riemannian Geometry.* Wiley, 1982.

[Wil91] T. J. Willmore. A survey on willmore immersions. In F. Dillen and L. Verstraelen, editors, *Geometry and Topology of Submanifolds, IV*, pages 11–16, Leuven, 1991. World Scientific.

[Wil93] T. J. Willmore. *Riemannian Geometry.* Oxford Science Publications, 1993.

[Wlo82] J. Wloka. *Partielle Differentialgleichungen.* B. G. Teubner, Stuttgart, 1982.

Index

List of Symbols

List of Figures